UNIVERSITY OF OKLAHOMA

GRADUATE COLLEGE

CATALYST EVOLUTION VIA DYNAMIC COMBINATORIAL CHEMISTRY

A DISSERTATION

SUBMITTED TO THE GRADUATE FACULTY

In partial fulfillment of the requirements for the

Degree of

DOCTOR OF PHILOSOPHY

By

MASAOMI MATSUMOTO

Norman, Oklahoma

2010

CATALYST EVOLUTION VIA DYNAMIC COMBINATORIAL CHEMISTRY


A DISSERTATION APPROVED FOR THE
DEPARTMENT OF CHEMISTRY AND BIOCHEMISTRY



BY



_____
Dr. Kenneth M. Nicholas, Chair


_____
Dr. Ronald L. Halterman


_____
Dr. George Richter-Addo


_____
Dr. Richard W. Taylor


_____
Dr. Michael H. Engel

ACKNOWLEDGMENTS

TABLE OF CONTENTS

# LIST OF TABLES

LIST OF FIGURES

ABSTRACT

Dynamic combinatorial chemistry (DCC) is a combinatorial method of synthesis utilizing complex mixtures under thermodynamic control, called dynamic combinatorial libraries (DCL). The addition of a template molecule which preferentially stabilizes one species in the complex mixture perturbs the equilibrium, amplifying that species. Although DCC is a promising method for exploring complex chemical space, it is underexplored as a method for discovering new catalysts. Here we discuss some approaches to applying DCC to the development of catalysts. In order to explore the possibility of incorporating the powerful ligand and general base characteristics of imidazole into a DCL, histidine-derived pseudopeptide monomers suitable for acid-catalyzed hydrazone-exchange-based DCC were produced. DCLs of histidine-derived pseudopeptide oligomers were produced and characterized. Although attempts at eliciting templating behavior were unsuccessful, a cyclic dimer of the histidine-derived building block was found to catalyze the hydrolysis of *p*-nitrophenylacetate with a tenfold greater rate enhancement than 4-methylimidazole. Dynamic libraries of Schiff-base zinc complexes were used to explore templating with transition state analogs (TSA). It was discovered that addition of phosphonate and trifluoromethylketone TSAs to equilibrating mixtures of zinc Schiff-base complexes amplifies the best catalysts for the hydrolysis of picolinate esters. A promising lead into the kinetic resolution of picolinate esters by chiral zinc Schiff-base catalysts was discovered. Efforts are under way to explore the dynamic combinatorial chemistry of enantioselective catalysts for kinetic resolution using this system.

# 1. DYNAMIC COMBINATORIAL CHEMISTRY AND CATALYST EVOLUTION

## 1.1 Molecular Evolution

The design and synthesis of receptors and supramolecular catalysts is still a challenging task for synthetic chemistry. Due to the extremely long development cycle for design, synthesis and testing, even relatively simple receptors will require large investments of time and resources to produce *de novo*. This has effectively set a limit to the complexity of receptors and catalysts that can feasibly be constructed. A potential solution to this problem is to utilize methods that take advantage of *molecular evolution*, which is a loosely defined phenomenon encompassing such varied methods as molecular imprinted polymers (MIP), catalytic antibodies (abzymes), and dynamic combinatorial chemistry (DCC). The key concept in these methods is that a small target molecule is used to transfer structural information to the large receptor molecule.

Recent developments in seemingly disparate fields of chemistry, including catalytic antibodies, molecular imprinted polymers and dynamic combinatorial libraries (DCL) constitute a single conceptual approach to chemical problems. This approach, termed Molecular Evolution,[1] is the study of the response of a chemical system to the application of a selection stimulus. Rather than rationally designing candidate molecules which are subsequently screened for desired characteristics, a chemical system (immunologic response, templated polymerization, or DCL) is constructed, then challenged with a template molecule. The response of the chemical system to the template (production of abzyme, MIP, or DCL amplification) returns information about the structural features necessary to elicit the desired characteristics (binding, catalysis,

biological activity). The focus of rational design is shifted away from the candidate

molecules and to the overall experimental design of the selection experiment.

### 1.1.1 Catalytic antibodies
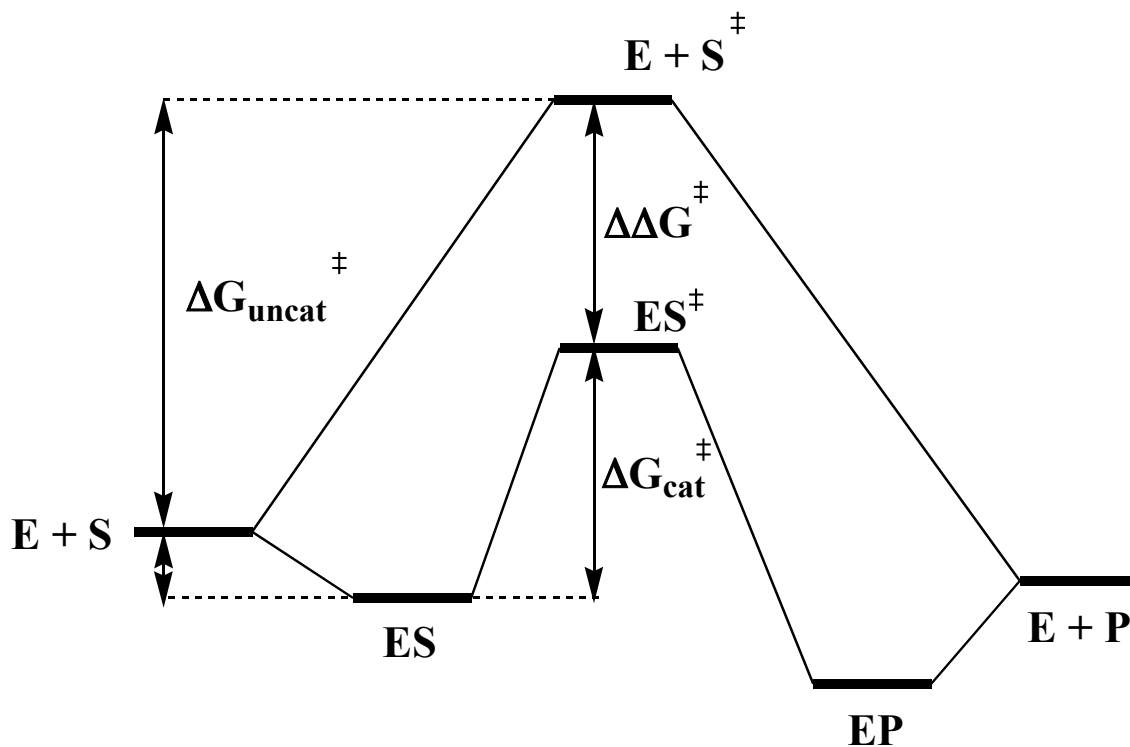


**Figure 1.** Jencks' diagram depicting schematized energy levels for enzyme-catalyzed

(lower pathway) and uncatalyzed (upper pathway) reactions. In this model, $\Delta\Delta G^{\ddagger}$, the

difference between free energy of activation for the catalyzed and uncatalyzed reactions,

corresponds to the binding energy of the enzyme-transition state complex minus the

binding energy of the enzyme-substrate complex.

Pauling's and Jencks' postulate that enzymes are receptors for the activated

complex of the catalyzed reaction[2,3] is the foundation of the transition-state analog

(TSA)-mediated evolutionary approach to catalysis. (Figure 1) In this model of enzyme

catalysis, the catalytic power of the enzyme comes primarily from its ability to bind and stabilize the transition state ('activated complex') of the reaction. In other words, the enzyme is a receptor for a transition state. Any species that preferentially stabilized the transition state of a reaction over the substrate will lower the activation barrier and should, in theory, behave as a catalyst. In practice, the use of evolutionary methods to elicit catalysis can be traced back to catalytic antibodies, as envisioned by Jencks[3] in 1969 and realized independently by Lerner and Schultz in 1986[4-6]:

"If complementarity between the active site and the transition state contributes significantly to enzymatic catalysis, it should be possible to synthesize an enzyme by constructing such an active site. One way to do this is to prepare an antibody to a haptenic group which resembles the transition state of a given reaction. The combining sites of such antibodies should be complementary to the transition state and should cause an acceleration by forcing bound substrates to resemble the transition state."

William P. Jencks,  **Catalysis in Chemistry and Enzymology**, 1969.

In this approach, a transition-state analog tethered to a protein is used as a hapten to elicit an immune response in a live animal. Antibodies generated in the immunologic response are harvested and screened for hapten binding. Some of these antibodies will have enhanced catalytic activity for the reaction that the TSA represents.

The first accounts of catalytic antibodies were reported independently by Schultz[4,5] and Lerner[6] in 1986. Lerner et al. used phosphonate TSA **1** to elicit antibodies

that catalyzed the hydrolysis of analogous activated subtrates **2** and **3** (Figure 2). The antibody also exhibited substrate selectivity toward unactivated substrates **4** and **5**, while showing no catalytic activity toward **6, 7** or **8**, in which function groups R and R' are missing or switched. The catalytic antibody exhibited saturation kinetics, and was inhibited competitively by **9**. The antibody exhibited a $k_{cat}/k_{uncat}$ for substrate **4** of 960.
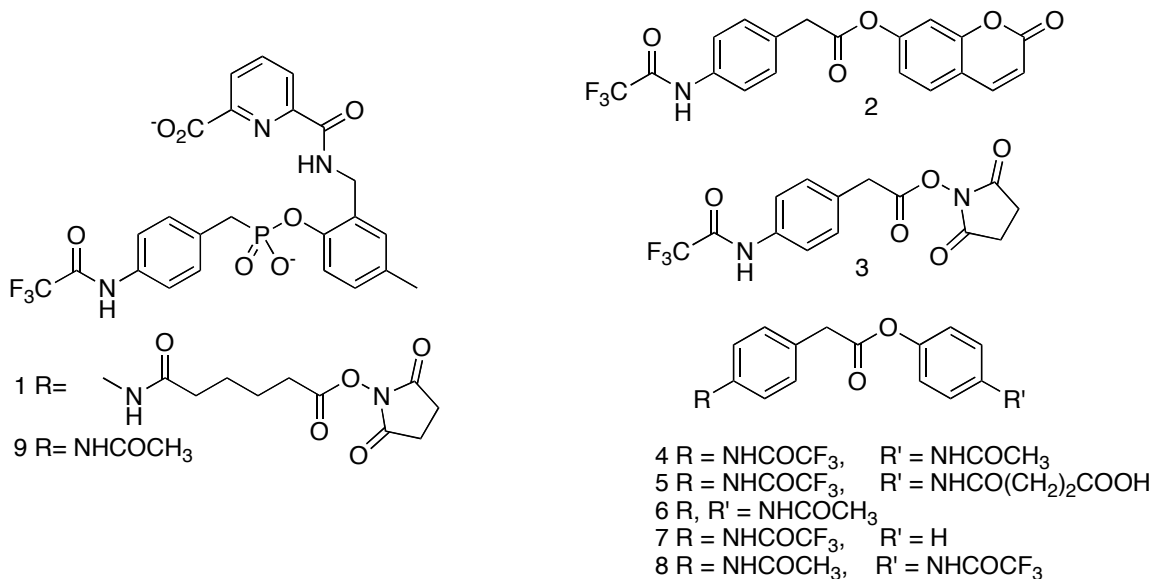


**Figure 2.** TSA hapten **1** and substrates **2** – **8** from Lerner's catalytic antibody study.

Schultz reported that an immunoglobulin that bound phosphate ester TSA **10** displayed enhanced catalysis of the hydrolysis of nitrophenylcarbonate substrate **11**.[4] (Figure 3) This catalytic antibody showed substrate specificity for the cationic choline-derived substrate **11**. Schultz then demonstrated that an antibody with catalytic specifity for substrate **13** could be elicited by hapten **12**.[5] The antibody thus elicited diplayed a $k_{cat}/k_{uncat}$ for substrate **13** of 810.

4
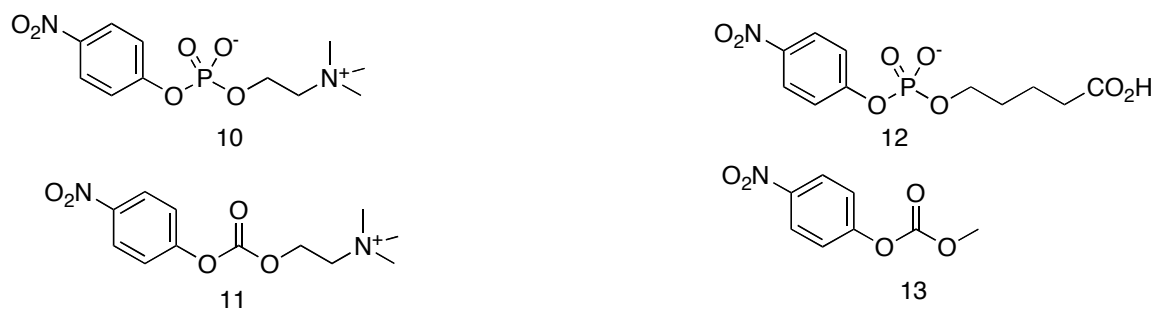
**Figure 3.** TSA guest **10** and substrate **11** for immunoglobulin, and TSA hapten **12** and substrate **13** for catalytic antibody from Schultz's study.

Since then reports of TSA-hapten induced catalytic antibodies have proliferated, producing catalysts for various reactions including amide hydrolysis, cycloadditions, and aldol additions.[7]

Janda reported the elicitation of a catalytic antibody by a mercury-containing metallo-hapten.[8] Antibody 38G2 was elicited by hapten **14**, (Figure 4) which simulates the transition state of an ester hydrolysis assisted by mercuric ion. Antibody 38G2 was found to hydrolyze ester **15** with $k_{cat}/k_{uncat}$ of 300. The catalytic activity of this antibody was found to be dependent on the presence of mercuric ion as the metallo-cofactor. This work represents a unique entry into catalytic antibodies, in which a metallo-TSA was used to elicit metallo-cofactor-dependent catalysis.
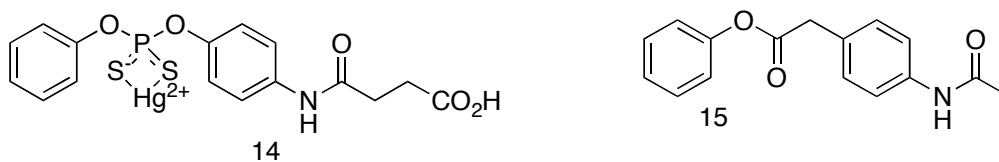


**Figure 4.** Janda's hapten and substrate for eliciting a mercuric ion cofactor-dependent metallo-catalytic antibody.

Fujii demonstrated that for a series of esterolytic catalytic antibodies elicited by phosphonate haptens, there is a reasonable correlation between catalytic activity (log $k_{cat}/k_{uncat}$) and TSA binding characteristics (log $K_m/K_i$).[9,10] On a plot of log $k_{cat}/k_{uncat}$ vs. log $K_m/K_i$, (Figure 5) five of the six antibodies tested lie on a line with slope 0.924 and r of 0.95. One of the six (7C8) is not on the line, suggesting that this catalytic antibody deviates from the rest in the mechanism of its action. This suggests that on the whole, there is a general correlation between transition-state analog stabilization and catalytic activity given that the TSA is sufficiently accurate and mechanistically relevant to the particular catalyst . Such observations do much to reinforce the hypothesis that transition-state stabilization translates into enhanced catalytic rate in enzyme-like catalysts.
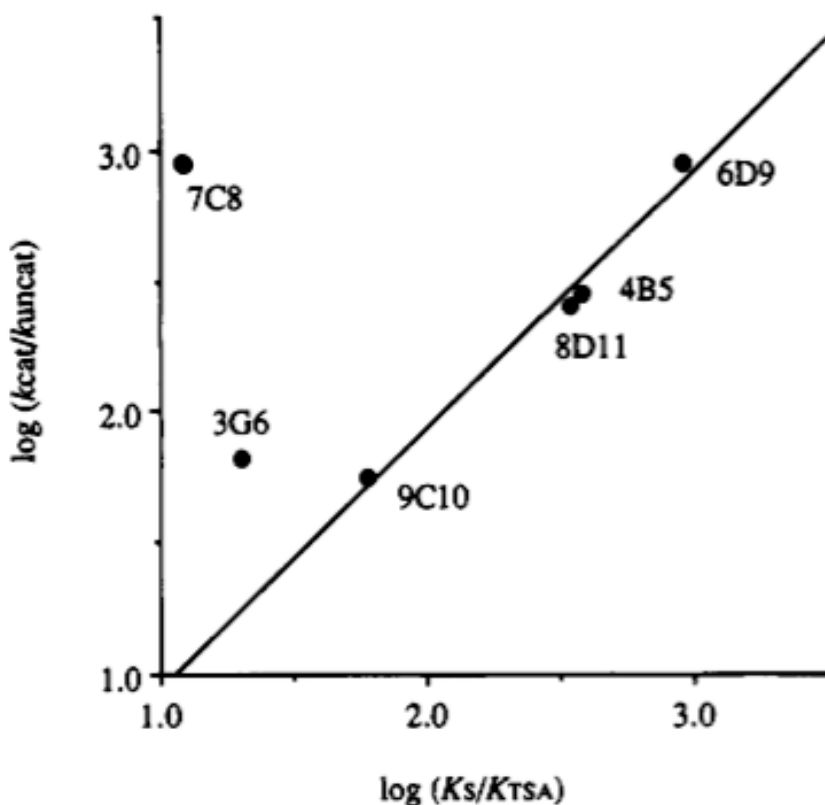


**Figure 5.** Correlation between TSA-binding and catalysis in a library of catalytic antibodies. Fujii, et al.[9]

**1.1.2 Catalytic Molecular Imprinted Polymers**

In a conceptually related but chemically distinct approach, polymers can be synthesized under molecular imprinting conditions.[11] The polymer is made up of building blocks which include functionalized monomers designed to interact with the template molecule. In catalyst MIPs, the template is a TSA, and the monomers are selected so that interactions with the TSA will be relevant to catalysis. The polymerization is kinetically controlled, and the resulting polymer must be treated to remove the template molecule, producing vacancies which are analogous to active sites in enzymes. The resulting MIP catalyzes the reaction whose transition state the TSA emulates. The heterogenous character of the active sites produced in this way can hinder the study of such systems.

In one of the first accounts of TSA-imprinted MIP, Mosbach showed that *p*-nitrophenylmethylphosphonate (**16**)-imprinted polymer containing imidazole-functionalized monomer (Figure 6) catalyzed the hydrolysis of *p*-nitrophenylacetate (NPA) (**17**).[12] The polymer consisted of 4(5)-vinylimidazole (**18**), 1,4-dibromobutane (**19**), and cobaltous ion. The polymer produced in the presence of TSA **16** was found to be 60% more active than the control polymer, which was produced without TSA. Further, the catalytic activity of the imprinted polymer was inhibited by **16**.
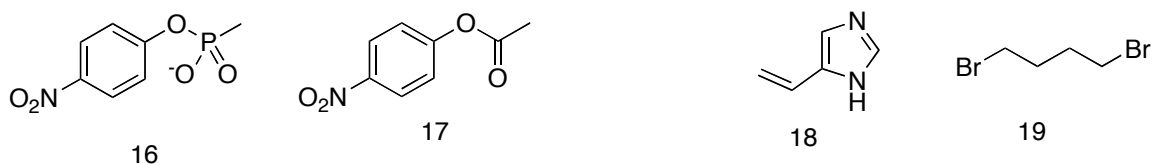


**Figure 6.** TSA template **16**, substrate **17**, and monomers **18** and **19** from Mosbach's early example of catalytic metallo-MIP.

In an example of a metal-free MIP catalyst, TSA **20** was used to imprint a water-soluble polymer.[13] (Figure 7) The polymer was constructed by radical polymerization of L-histidine methyl ester derivative **22** and monomers **23**, **24**, and **25**. The resulting histidine-functionalized polymer was found to hydrolyze amino ester substrate **21** with a $k_{cat}/k_{uncat}$ of 5.78. Substrate selectivity was demonstrated for **21** over alanine and phenylalanine derivatives ($k_{cat}/k_{uncat}$ = 2.21 and 1.79, respectively). An enantiospecificity of 12.4 is reported; $k_{cat}/k_{uncat}$ for Z-D-Leu-PNP is 0.95. Curiously, no unimprinted control polymer is reported in this work.
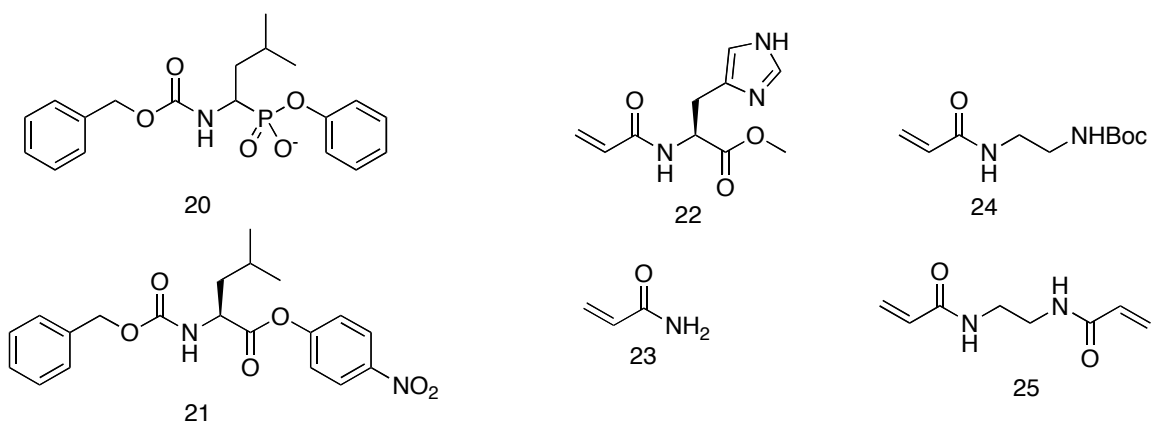


**Figure 7.** TSA template **20**, substrate **21**, and monomers for a catalytic MIP.

Mosbach et al. used cobaltous ion, vinylpyridine monomers and a diketone template to generate a MIP class-II aldolase mimic.[14] (Figure 8) Template **26** was used to imprint a cobaltous ion-containing polymer consisting of styrene **27**, divinylbenzene **28**, and 4-vinylpyridine **29**. The resulting MIP catalyzed the aldol condensation of acetophenone **30** and benzaldehyde **31** to form chalcone **32** with eightfold rate enhancement with respect to the solution reaction with cobaltous ion. Templating is

thought to occur through coordination of **26** with cobaltous ion-pyridine complex (**33**). Template **26** was shown to inhibit the reaction.
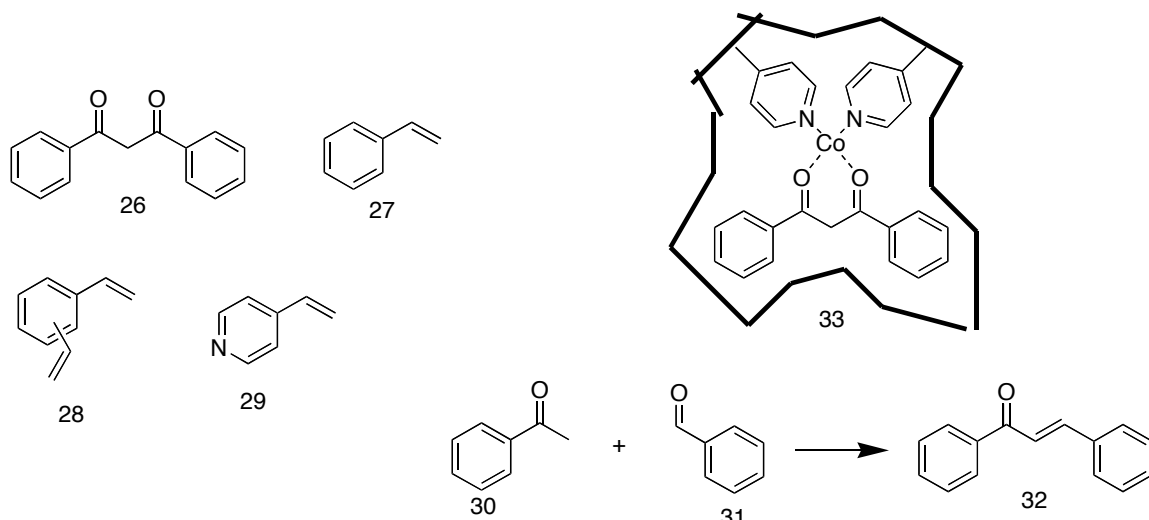


**Figure 8.** Mosbach's MIP Class-II Aldolase mimic.

In an extremely sophisticated entry into the field of metallo-MIP, Severin introduced a phosphonate-TSA template into an imprinted polymer containing a ruthenium-($\eta^6$-arene) complex.[15,16] (Figure 9) TSA **34** was designed to simulate the simultaneous transfer of a hydride and proton in the ruthenium mediated hydrogenation, via a tetrahedral transition state for hydride transfer to the carbonyl carbon and hydrogen bonding of the carbonyl oxygen to the acidic amine proton. Upon removal of the TSA template, the resulting MIP was catalytically active for the transfer hydrogenation of benzophenone with a TOF of 51.4 h$^{-1}$. The non-TSA-imprinted (control) polymer with equivalent amount of ruthenium complex exhibited a TOF of 16.5 h$^{-1}$. The catalytic MIP was selective for ketones with a similar steric profile to the TSA. Substrates with bulkier groups or long alkyl chains were not accepted by the catalyst.

9
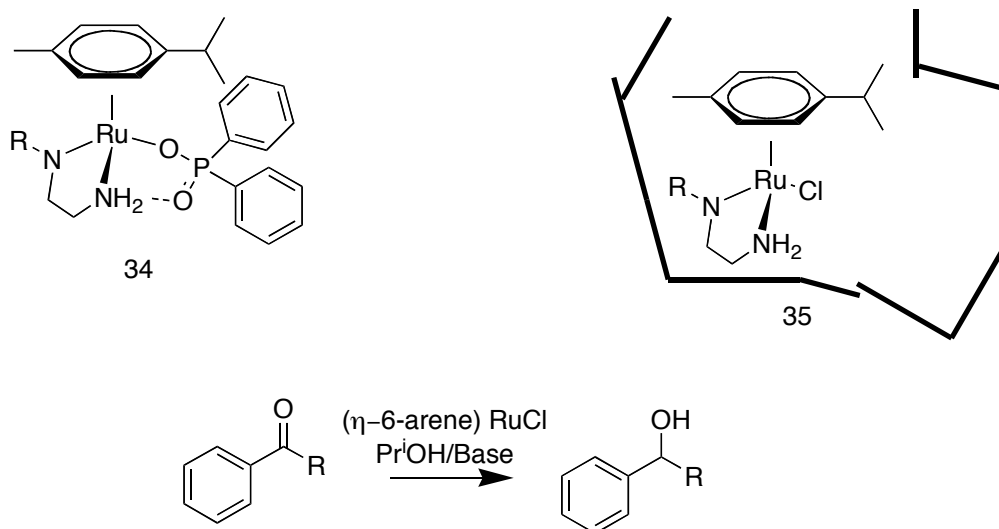
**Figure 9.** Severin's molecular imprinted polymer hydrogenation catalyst **35**, and the metal complex TSA used to imprint it.

Wulff used copper and zinc complex-derived functional monomers and a phosphate ester TSA to elicit metal ion catalyzed hydrolytic catalysis relevant to carboxypeptidase A.[17,18] (Figure 10) A triamine ligand/amidinium functionalized monomer **39** was prepared which is capable of binding a metal ion in proximity to a guanidinium function, in mimicry of the active site of carboxypeptidase A. Phosphate ester TSA **36** simulates the tetrahedral transition state for nucleophilic attack of hydroxide on a carbonate. The TSA phosphate can hydrogen bond to the amidinium group of the reactive monomer, and the pyridyl nitrogen can bind the metal-triamine complex. These interactions of the TSA with monomers simulate the mode of transition state stabilization. The reactive monomer was polymerized together with EDMA (ethylenedimethacrylate) using radical polymerization conditions in acetonitrile/DMSO. The imprinted polymers showed catalytic activity 50 to 80 times higher than the unimprinted control polymer. The copper-MIP catalyzes the hydrolysis of pyridyl

carbonate **37** with $k_{cat}/k_{uncat}$ 75700. The zinc-MIP catalyzes the hydrolysis of diphenylcarbonate **38** withy $k_{cat}/k_{uncat}$ of 6900. These represent the highest rate accelerations to date using a MIP catalyst.
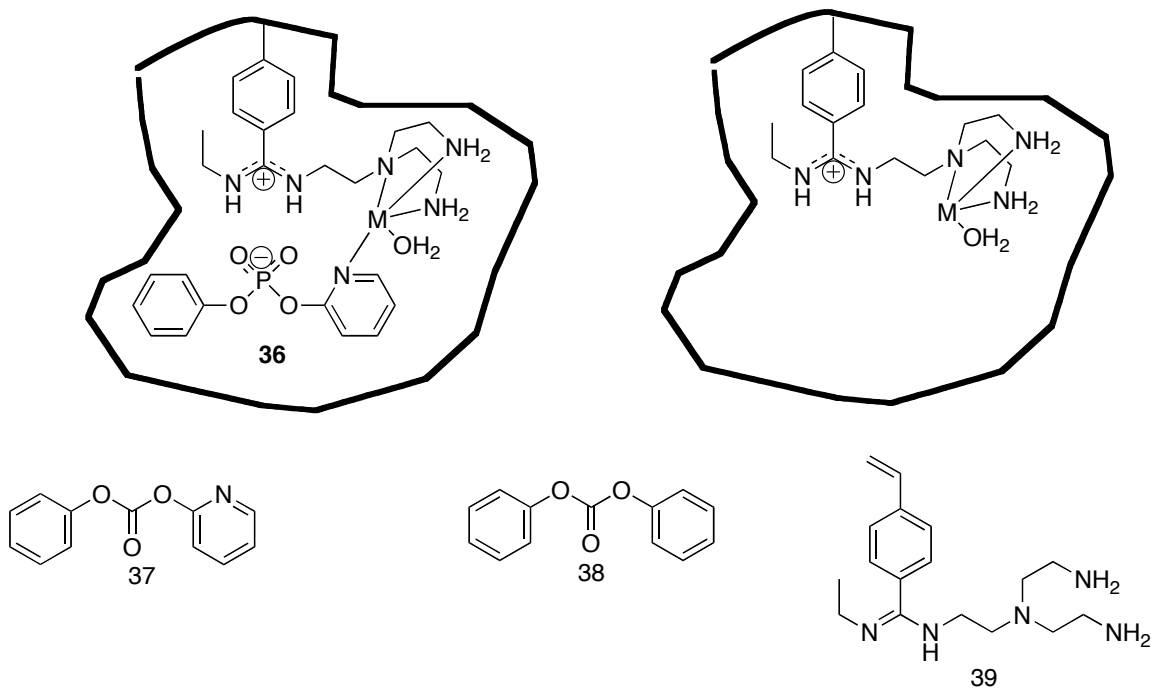


**Figure 10.** Wulff's MIP carboxypeptidase A model.

## 1.2 Dynamic Combinatorial Chemistry and Catalysis

Dynamic combinatorial chemistry (DCC) is combinatorial chemistry under thermodynamic control.[19] In conventional or *static* combinatorial chemistry, a library of structurally varied compounds is synthesized, and then screened by a chemical or biological process to assess the individual library members for affinity, catalysis, enzyme inhibition, or biological activity. In dynamic combinatorial chemistry, the virtual library (Lehn), i.e. the set of possible combinations of building blocks exists not as a synthesized library but as a mixture in dynamic equilibrium with building blocks. (Figure 11) The application of an external stimulus to this mixture, termed a DCL (dynamic combinatorial

library) may shift the equilibrium to favor a specific product or building block. This may be due to interactions between the stimulus, termed the *template*, and a member of the library. If the template preferentially removes a product from the DCL, by LaChatelier's principle, the DCL will "respond" to the perturbation in the position of the equilibrium by producing more of that product. This event is termed *"amplification"*. In effect, DCC combines the synthesis and screening steps appropriate for a conventional combinatorial library into one step and combines all the parallel syntheses into one mixed synthesis. Therefore, it represents a conceptually new and powerful methodology for the discovery of molecules with specific functional characteristics, such as receptors, inhibitors, drugs, and catalysts. Several excellent reviews exist on the subject of DCL.[19-24]

The essential requirement for DCC is the *reversibility* of the exchange reaction, i.e., the presence of a chemical bond that can be formed and broken under mild reaction conditions. Two further requirements for successful templating are that the exchange reaction should be orthogonal to template binding chemistry, and that the monomers should be capable of interacting in some way with the template. A fourth practical requirement is that there should be some way to analyze the mixtures that will be formed. Often, a method for stopping the exchange reaction, although not necessary, will facilitate the analysis.

A DCC approach to catalyst evolution remains relatively underexplored. As of this writing, only three research papers on this topic exist. The first two are from Sanders et al., DCL utilizing cyclic disulfide oligomers constructed from aromatic building blocks, and the third is our work, detailed in Chapter 3. The general concept is this: a DCL is constructed and challenged with a transition state analog (TSA). The perturbation

of the DCL equilibrium by the presence of the TSA is detected by comparing the templated library to a control library. Species which are amplified or attenuated are identified, and the amplification factor is quantified. The catalytic activity of the library members is assayed to determine what relationship exists between catalysis and amplification.
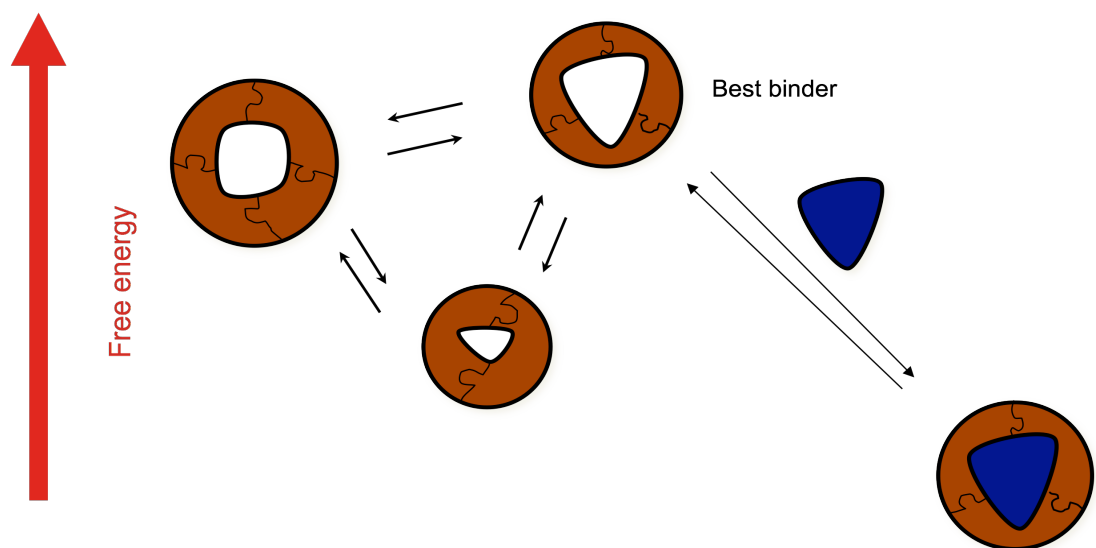


**Figure 11.** A schematic representation of template-mediated perturbation of equilibrium in a DCL.

## 1.2.1 Exchange reactions in DCC

The list of reversible *covalent* reactions for DCL is unfortunately rather short.[19] By far the most often used of these reactions are imine exchange, disulfide exchange and hydrazone exchange. (Figure 12) Although these reactions by no means represent the entire possible range of available exchange chemistries for DCL, they constitute a preponderance of the DCL literature. Hydrazones are the imine-like condensation product

of a hydrazide or hydrazine and aldehyde. Hydrazone exchange is usually catalyzed by a Brönsted acid. Under neutral or basic conditions, the reaction is extremely slow. An advantage of the hydrazone linkage is that the equilibrium for hydrazone formation lies very far to the product side, even in water. However, the necessity of an acid catalyst (in practice, excess acid is used), can interfere with some recognition processes. In disulfide exchange, thiols are placed in an alkaline solution and exposed to atmospheric dioxygen. The resulting dithiols undergo reversible exchange reactions with thiolate building blocks. Exchange can be shut down by adjusting the alkalinity of the solution to neutral.

a) Imine exchange

$$R_1 \diagup\hspace{-0.3em}N\diagdown R_2 \;+\; R_3\diagup\hspace{-0.3em}N\diagdown R_4 \;\rightleftharpoons\; R_1\diagup\hspace{-0.3em}N\diagdown R_4 \;+\; R_3\diagup\hspace{-0.3em}N\diagdown R_2$$
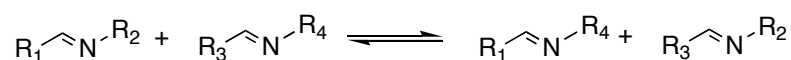
b) Hydrazone exchange



c) Disulfide exchange

$$R_1\diagdown S \cdot S \cdot R_2 \;+\; R_3\diagdown S \cdot S \cdot R_4 \;\rightleftharpoons\; R_1\diagdown S \cdot S \cdot R_4 \;+\; R_3\diagdown S \cdot S \cdot R_2$$
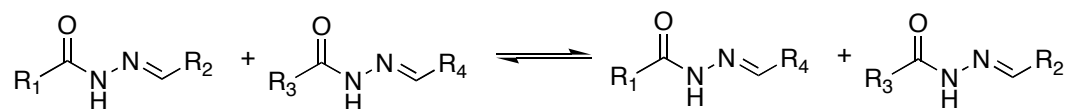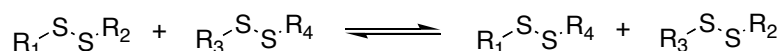
**Figure 12.** Generalized schemes for three common exchange reactions in DCL. Note that disulfide exchange is a topologically different exchange process from a) and b), since the $R_1R_1$, $R_2R_2$, $R_3R_3$, and $R_4R_4$ products are also possible.

Imine exchange is by far the oldest known reversible linkage for DCL. Its advantages are that the linkage is very labile under mild conditions, and produces a good donor atom for coordinating a metal ion. The equilibrium for imine condensation, though dependent on the electronic character of the aldehyde and amine, is not favorable under aqueous conditions.[25] The imine linkage remains somewhat labile under almost all

conditions, making DCL mixture analysis and isolation very difficult. Techniques for "freezing" library composition by reduction preceding analysis must be used.

## 1.2.2 Examples of DCL in which small-molecules are "cast" by complexation to an enzyme target

Lehn has termed the templated formation of receptors "molding", and the templated formation of inhibitors or substrates "casting", by analogy to macroscopic processes.[26] In "casting," information about the structure of an enzyme active site is transmitted to a library of small molecule ligands under thermodynamic control. Lehn demonstrated that imine exchange could be utilized to equilibrate a library of small molecule inhibitors of carbonic anhydrase in the presence of target enzyme.[27] (Figure 13) The monomers consisted of four amines (**40a-d**) and three aldehydes (**40.1-40.3**) Sodium cyanoborohydride reduction was used to "fix" the composition of the library so that it could be analyzed by RP-HPLC. When compared to the control library, a population shift was observed which included the amplified species **40.3c**, which is structurally most similar to known carbonic anhydrase inhibitor **41**.
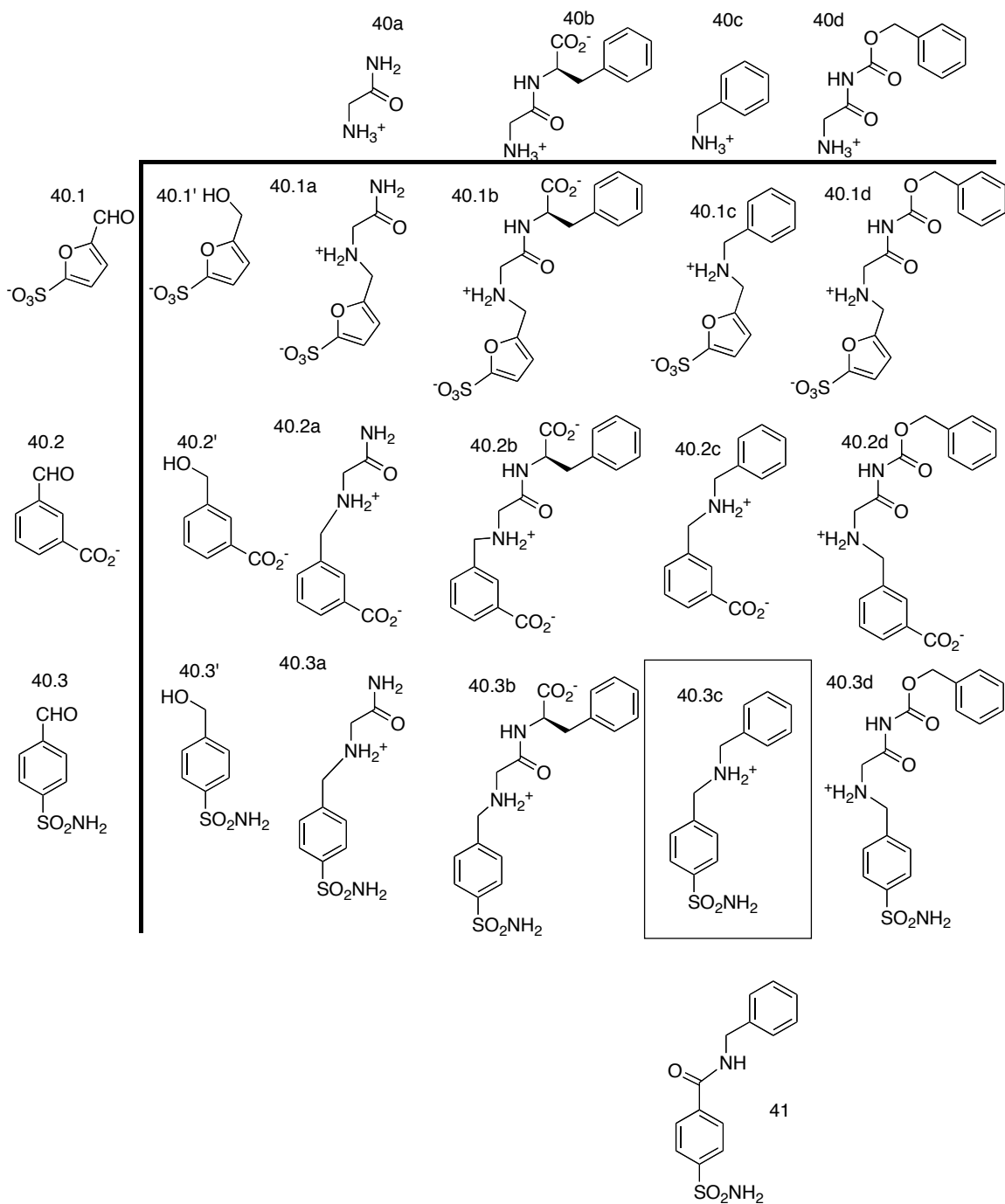
**Figure 13.** Lehn's imine library for selecting carbonic anhydrase inhibitors. **40.3c** was the amplified species. Note the similarity to **41**, a known carbonic anhydrase inhibitor.

Hydrazone exchange can also be used to construct libraries of enzyme inhibitors. Lehn utilized a hydrazone library consisting of hydrazides **42.1-42.4** and aldehydess **42A-I** templated on acetylholinesterase to discover an inhibitor. The dihydrazone **42.4$_2$I** was discovered to be a 2.3 nM inhibitor of acetylcholinesterase by a process of deconvolution wherein libraries were generated in which building blocks were systematically omitted.
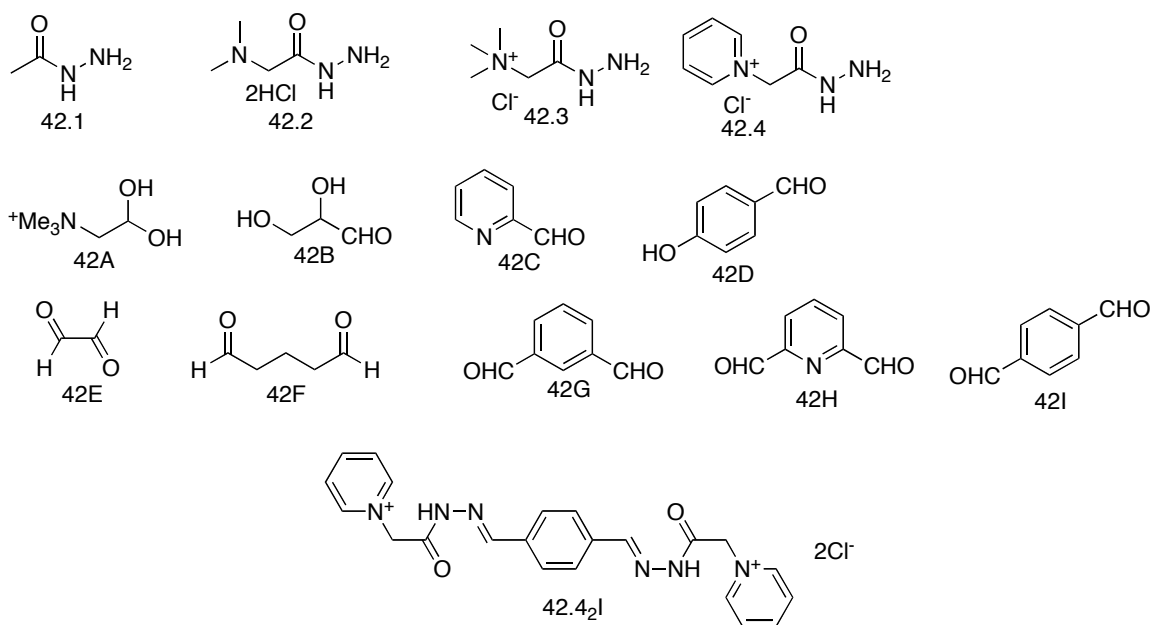


**Figure 14.** Building blocks for a hydrazone DCL of acetylcholinesterase inhibitors.

Imine exchange was used to generate a dynamic combinatorial library of glucosamine-derived inhibitors of hen egg-white lysozyme (HEWL).[28] (Figure 15) Amines **43.A** and **43.B** were equilibrated with aldehydes **43.1-43.6** in the presence of HEWL. Reduction of the library with sodium cyanoborohydride and analysis of products by RP-HPLC revealed that amine **43.A2** is amplified in the presence of the enzyme

template. This species was found to be a weak competitive inhibitor of HEWL with a $K_i$ of 0.6 mM.
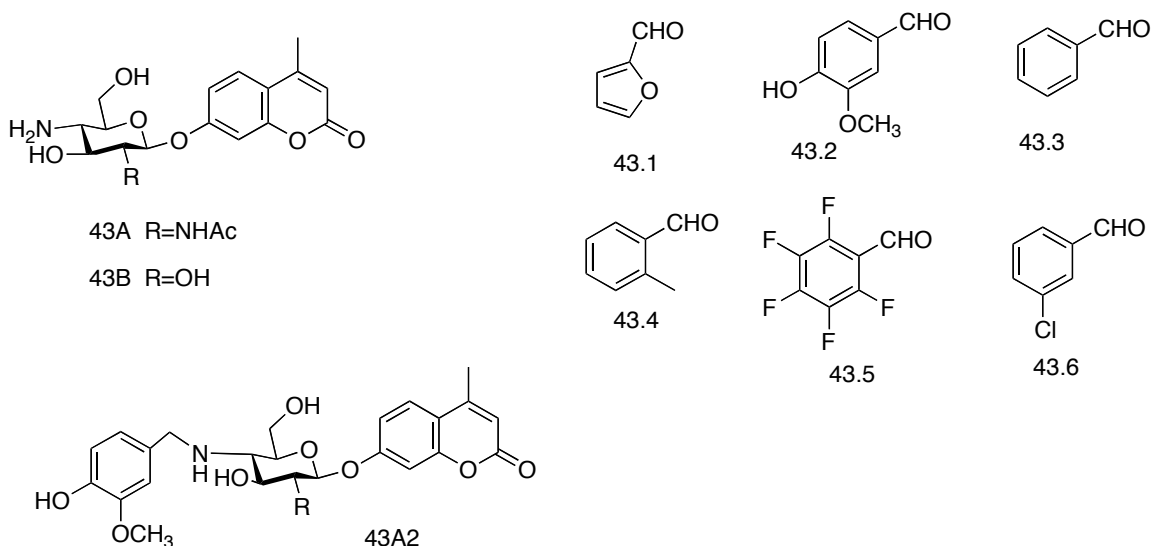


**Figure 15.** Imine library of inhibitors of Hen Egg White Lysozyme.

## 1.2.3 Examples of DCL in which receptors are "molded" by binding to guest molecules

In the conceptual obverse of "casting," a small molecule substrate (or TSA) is used to transmit structural information to a library of potential receptors (or catalysts). This is sometimes referred to as "molding".[26] The earliest reports of a receptor generated by DCL came from the research of Sanders. Sanders demonstrated the feasibility of using hydrazone exchange to construct libraries of pseudopeptide macrocycles.[29] Pseudopeptide hydrazones **44**, **45**, **46**, and **47** were synthesized and subjected to acid catalyzed oligomerization (Figure 16). By ESI-MS, a broad range of cyclic oligomers were observed, up to cyclic undecamers for the **44** + **45** library and cyclic pentamers for the **46** + **47** library.

18
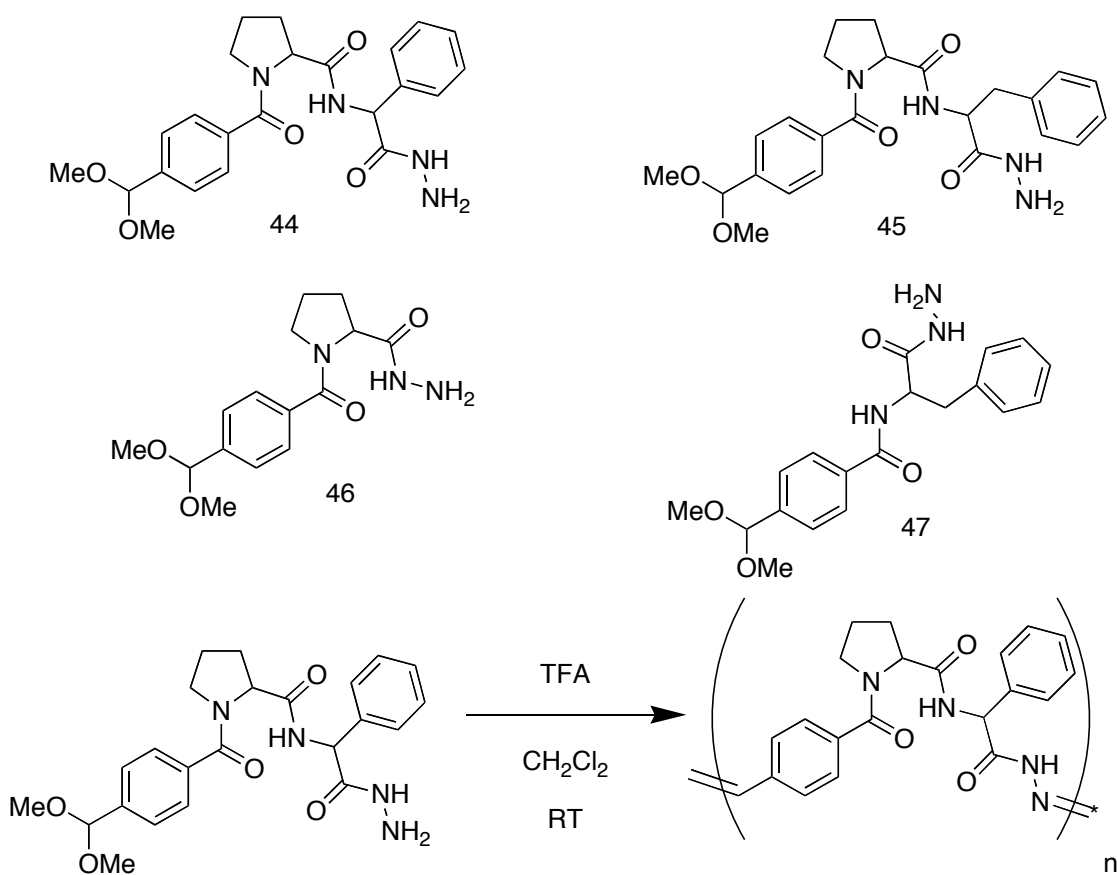
**Figure 16.** Sanders' et al. hydrazone pseudopeptide DCL.

Libraries of **45** were subsequently demonstrated to undergo template-directed equilibrium perturbation in the presence of lithium ions in 98:2 $CHCl_3$:MeOH.[30] In the untemplated library, cyclic trimer coexists with cyclic dimer, cyclic tetramer, and cyclic species up to the cyclic undecamer. In the presence of lithium iodide, the equilibrium is shifted drastically toward the production of cyclic trimer. HPLC analysis shows that all other species are consumed to produce predominately cyclic trimer. ^{1}H-NMR experiments indicate that the cyclic trimer coordinates lithium ion with an estimated binding constant of $4 \times 10^4$ $M^{-1}$.
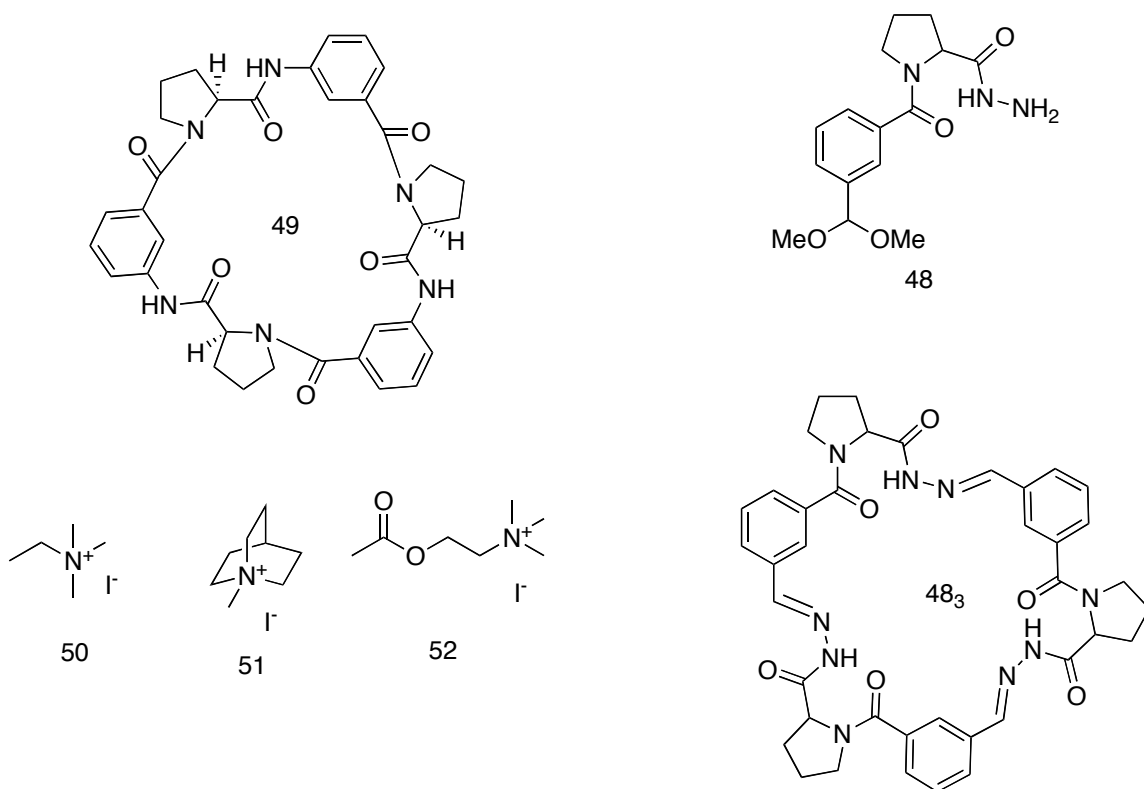
**Figure 17.** Templated formation of alkylammonium receptor **48₃.**

Sanders also demonstrated that organic templates, such as alkylammonium salts (**50**, **51**, **52**) could interact sufficiently with library members to produce templating phenomena. Hydrazone pseudopeptide monomer **48** was found to form a library of cyclic dimer, trimer, and tetramer.[31] (Figure 17) At equilibrium, the control library consisted predominately of cyclic dimer. In the presence of alkylammonium templates **50**, **51**, or **52**, the library converged to predominately cyclic trimer (**48₃**). **48₃** strongly resembles the cyclic pseudopeptide receptor **49**, which had been reported by Kubik et al.[32] to bind alkylammonium ions in chloroform with stability constants on the order of 10000 M$^{-1}$.

Interestingly, Sanders reported that in the presence of acetylcholine, after 44 days of equilibration, monomer **45** forms a hexameric species which turns out to be a [2]-

catenane.[33] The catenane constitutes 70% of the material in the templated library at equilibrium. MS/MS fragmentation of the amplified hexameric species exhibited direct fragmentation into a cyclic trimer species, indicating that the amplified species is a [2]-catenane composed of two units of cyclic trimer.
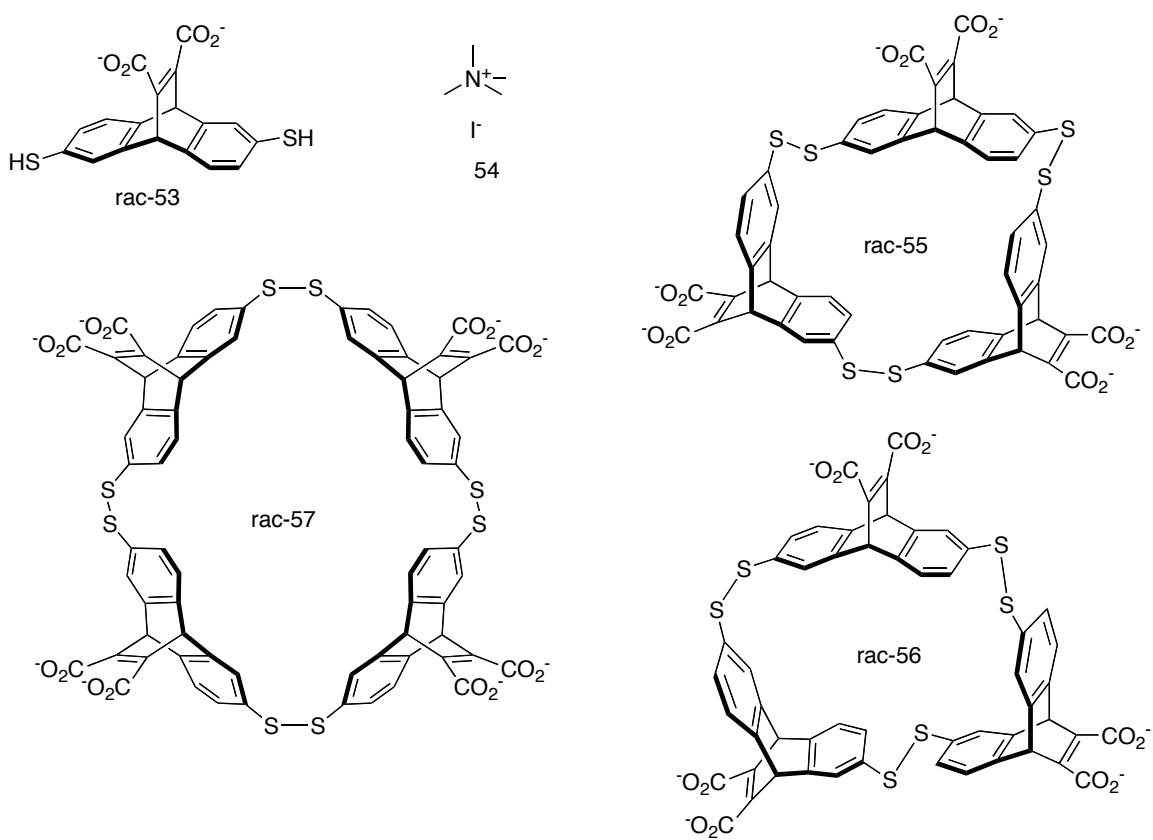


**Figure 18.** Generation of an alkylammonium receptor from a disulfide DCL

Sanders, et al. showed that disulfide exchange could be used to produce libraries of arene-walled macrocyclic capsules that bind cationic species in water.[34] (Figure 18) Racemic dithiol **53** forms two racemic cyclic trimers (rac-**55** and rac-**56**) and a meso cyclic tetramer rac-**57** at equilibrium. In the presence of tetramethylammonium iodide **54**, the library equilibrium is pulled predominately to the rac-**57**. The binding behavior of rac-**57** with **54** was studied by isothermal titration calorimetry. A binding constant of 4 x

$10^6$ $M^{-1}$ was observed. Alkylammonium binding is accompanied by pronounced peak sharpening in the proton NMR spectrum of rac-**57**.

Otto and Kubik[35] used a disulfide library to select a neutral receptor for iodide and sulfate anions in water. The cyclic hexapeptide **58**, which has itself been shown to bind anions in water, was thiol-functionalized and oxidized to produce a DCL dimer **60**. Dithiol linkers **59a-f** were introduced in order to produce a library of disulfide linked receptor candidates. Addition of potassium iodide or potassium sulfate amplified the receptors **62** and **63**. Receptor **62** bound iodide with $K_a$ of 2.9 x $10^4$ $M^{-1}$ and sulfate with $K_a$ of 5.4 x $10^6$ $M^{-1}$. Receptor **63** bound iodide with $K_a$ of 5.6 x $10^4$ $M^{-1}$ and sulfate with $K_a$ of 6.7 x $10^6$ $M^{-1}$.
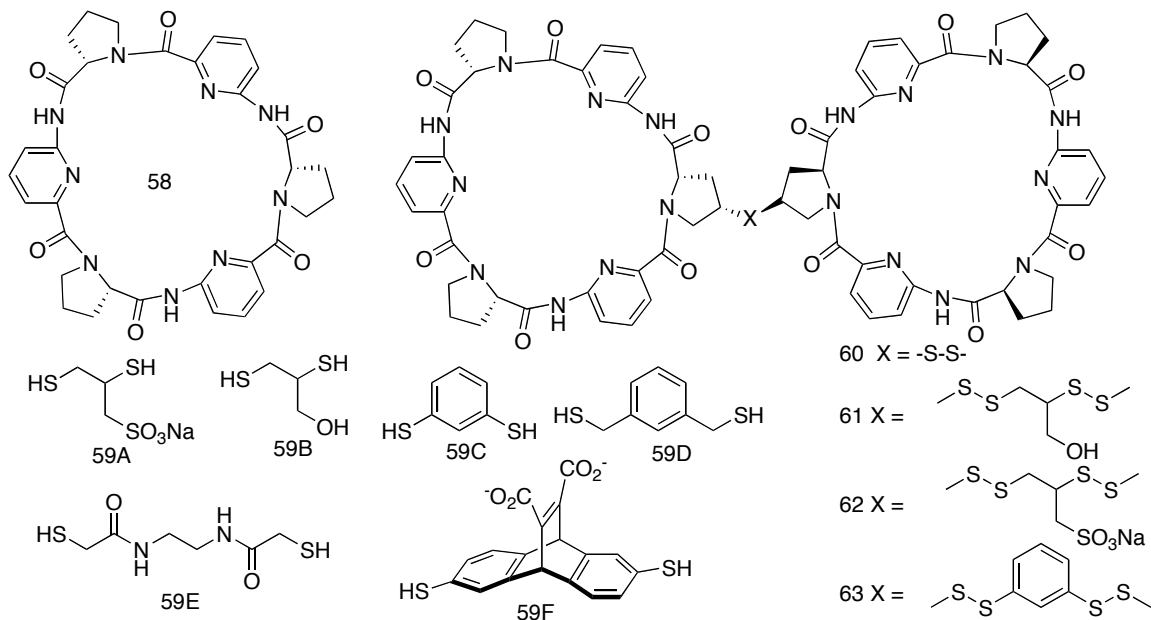


**Figure 19.** Disulfide DCL of anion receptors.

**1.2.4 DCLs in which coordination chemistry takes a central role**

Coordination chemistry has been utilized extensively in DCC; in fact the first reports of templated thermodynamic synthesis (pre-dating the term DCL) were metal-

templated syntheses of macrocyclic Schiff base ligands. For example, it has been known since 1964 that 2-aminobenzaldehyde **63** undergoes a thermodynamically controlled cyclization in the presence of nickel(II) ions to form a macrocyclic ligand-nickel complex **64**.[36] In the absence of metal template, a linear trimer **65** is formed.[37,38] Coordination chemistry provides a powerful platform for DCC for several reasons: metal coordination can provide a geometrically controllable bond (dictated by the nature of the metal ion and the ligand), the bond is often labile enough that complex formation is under thermodynamic control, and the driving force for formation of coordination complexes is often quite strong. Coordination chemistry continues to inspire a rich array of dynamic chemical systems, and can provide a powerful tool for DCL, both as a recognition element and for exchange chemistry.
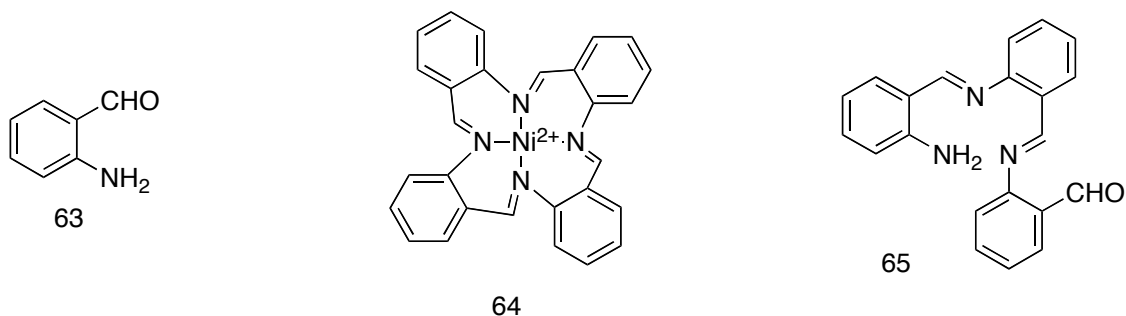


**Figure 20.** The earliest DCL: metal-templated synthesis.

Lehn used trispyridinedialdehyde **66** and a series of hydrazides **67a-e** and hydroxylamines **68a-e** to generate a diverse library of tridentate ligands under mildly acidic conditions.[39] (Figure 21) In addition, these ligands form exchange-labile bis-meridional octahedral complexes with cobaltous ion. This system represents a double-level orthogonal DCL, in which coordination chemistry (cobaltous ion binding) and dynamic covalent chemistry (hydrazone/oxime exchange) operate independently. The

two exchange processes could be independently switched off by either oxidation of the metal center (shutting down ligand exchange) or increasing the solution pH (shutting down hydrazone/oxime exchange).
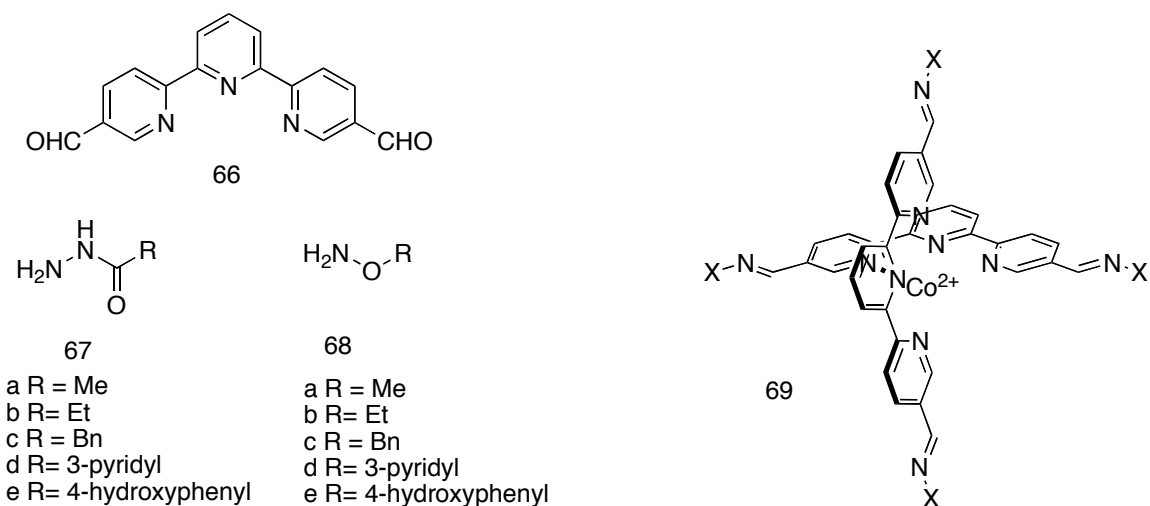


**Figure 21.** Lehn's demonstration of double-level DCL, combining coordination chemistry and dynamic covalent chemistry.

In another example of coordination chemistry in DCL, Morrow used libraries of imine ligands[40] (Figure 22) and hydrazone ligands[41] (Figure 23) to explore the extraction of divalent metal ions. Equilibrating mixtures of pyridinealdehydes **70**, **71**, and **72** and aminophenols **73A-D**, **75**, and **76** as well as 2-aminobenzyl alcohol **74** were tested for their ability to extract zinc and cadmium ions into chloroform. A bis-Schiff base zinc complex consisting of imine **70-73B** and **70-73D** was found to extract zinc into chloroform with the best cooperativity. Hydrazone ligands **77A-C**, **78**, **79A-D**, **80A-L**, **81A-E** were investigated for their ability to form chloroform soluble complexes with zinc and cadmium, and to explore the possibility of double-level orthogonal DCL. It was found that hydrazone exchange did not occur under the experimental conditions within a

reasonable time scale. Instead, ligand exchange was used as the dynamic feature of the experiment. The ligand combination **79A + 79B** showed the highest selectivity (12 : 1) for zinc extraction over cadmium.



73A R = R' = H
73B R = CH₃, R' = H
73C R = H, R' =CH₃
73D R= H, R' = t-Bu
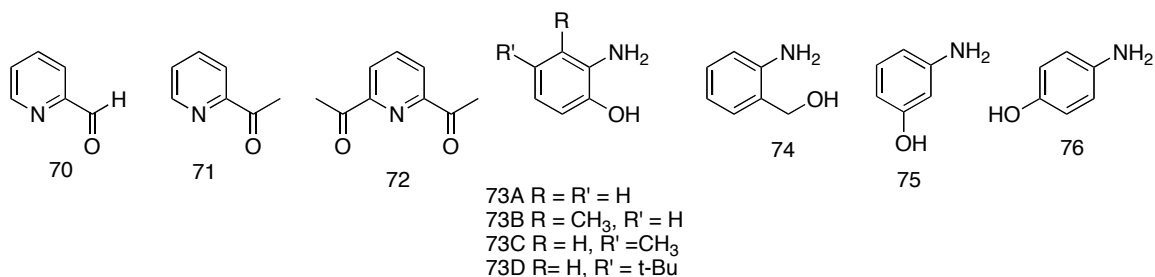
**Figure 22.** Building blocks for Morrow's imine DCL for metal ion extraction into chloroform.



77

A  X = Y = H
B  X = CH₃, Y = H
C  X= H, Y = CH₃

79

A  X= H, A = CH₃
B  X = CH₃, A = CH₃
C  X= H, A = Cl
D  X = CH₃, A= Cl

80

A  X= H, Z= Cl
B  X= CH₃, Z = Cl
C  X = H, Z = CH₃
D  X = CH₃, Z = CH₃
E  X = H, Z = tBu
F  X = CH₃, Z = tBu
G  X= H, Z = OH
H  X= CH₃, Z = OH
I  X = H, Z = OCH₃
J  X = CH₃, Z = OCH₃
K  X =H, Z= Ph
L  X= CH₃, Z= Ph

81

A  X = H, Q = H
B  X= CH₃, Q= H
C  X= H, Q = Ph
D  X = CH₃, Q= Ph
E  X= CH₃, Q = n-Pr
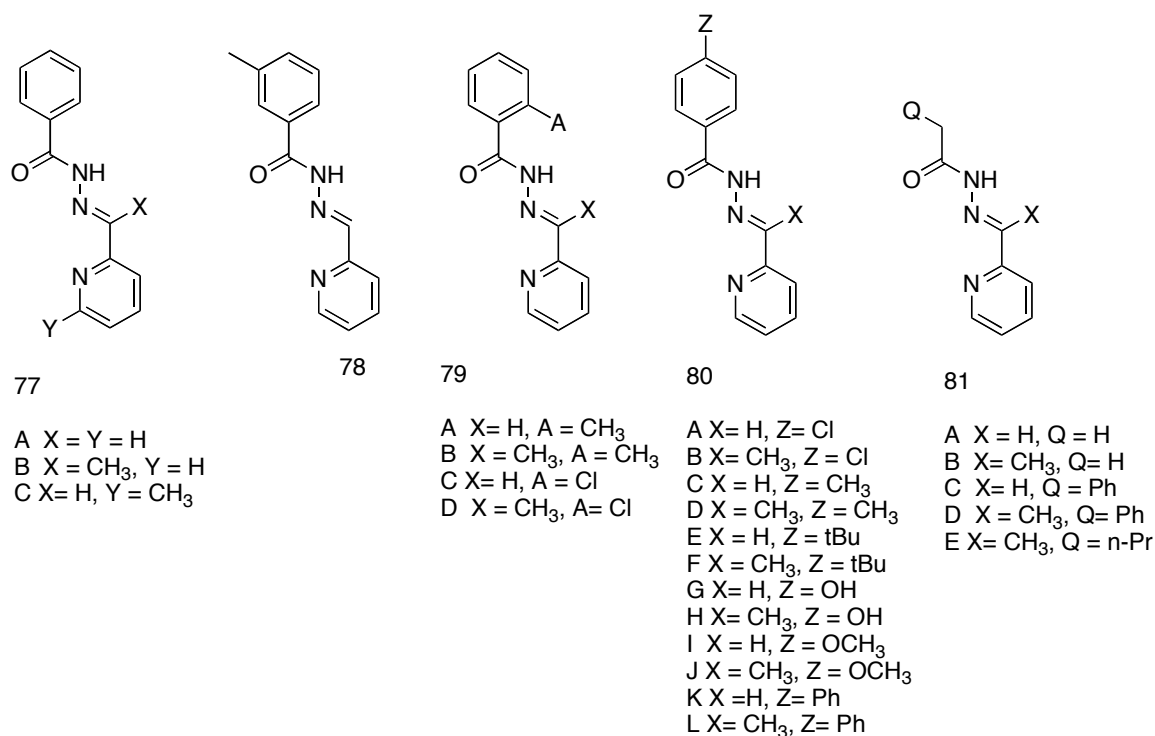
**Figure 23.** Morrow's hydrazone library for metal ion extraction.

Severin[42] used ruthenium and iridium η⁶-*p*-cymene complex metallacycles **82** and **83** in a DCL templated with lithium ions. (Figure 24) It was found that at low lithium ion

concentration, the all-ruthenium metallacycle **82** was amplified, whereas in the presence of 40 equivalents of lithium, the weakly binding mixed metallacycle **84** was amplified. Lithium complexes of the metallacycles were directly detected by ^{7}Li NMR. It was found that in conditions of large excess of template, correlation between binding affinity and amplification begins to break down.
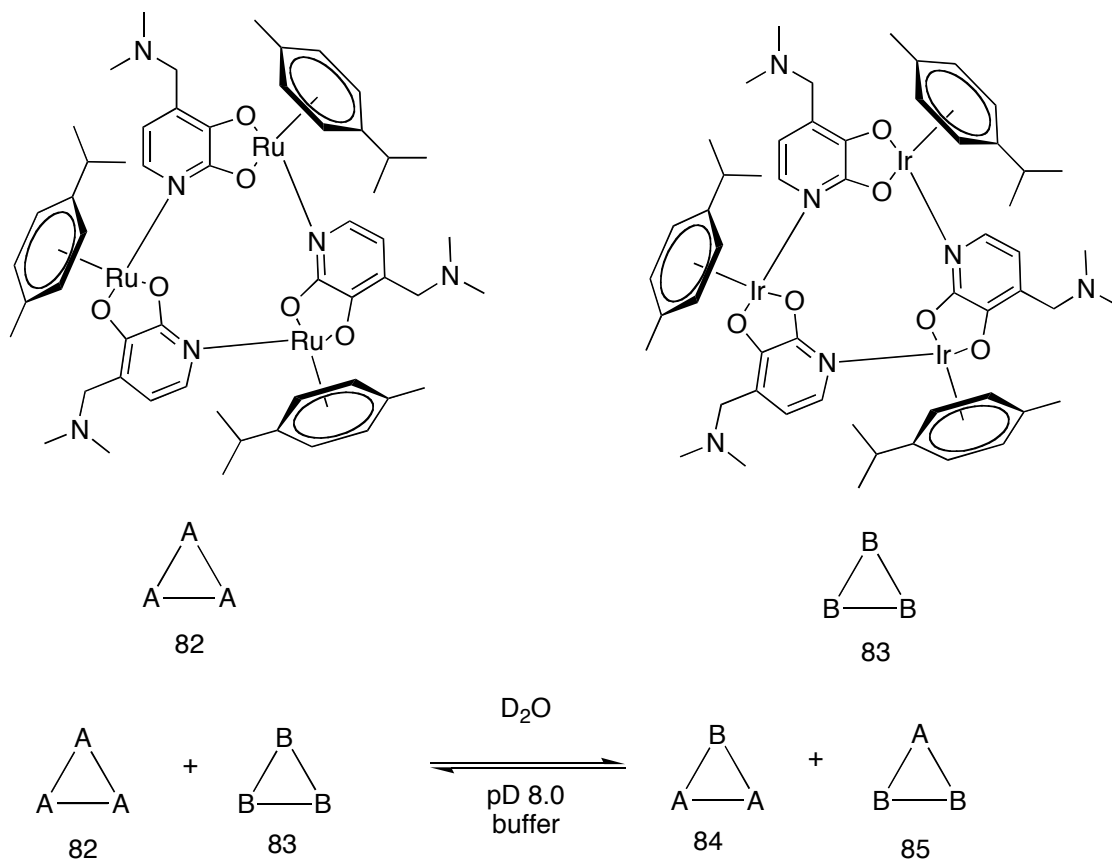


**Figure 24.** Severin's organometallic DCL, demonstrating the importance of template concentration.

Fujita found that palladium cage compounds can be produced under DCL conditions.[43] (Figure 25) From a library produced from an assortment of six building blocks, palladium "clip" **85**, and pyridine-derived linkers **86 – 90**, the anionic guest

sodium trichloroacetate **91** induces the formation of the receptor **92**, which consists of 2 molecules of **86** and one molecule of **87** held together by 4 units of **85. 92** was characterized by proton NMR and CSI-MS (Cold-spray ionization mass spectrometry). Receptor **92** was found to only form in the presence of guest **91**.
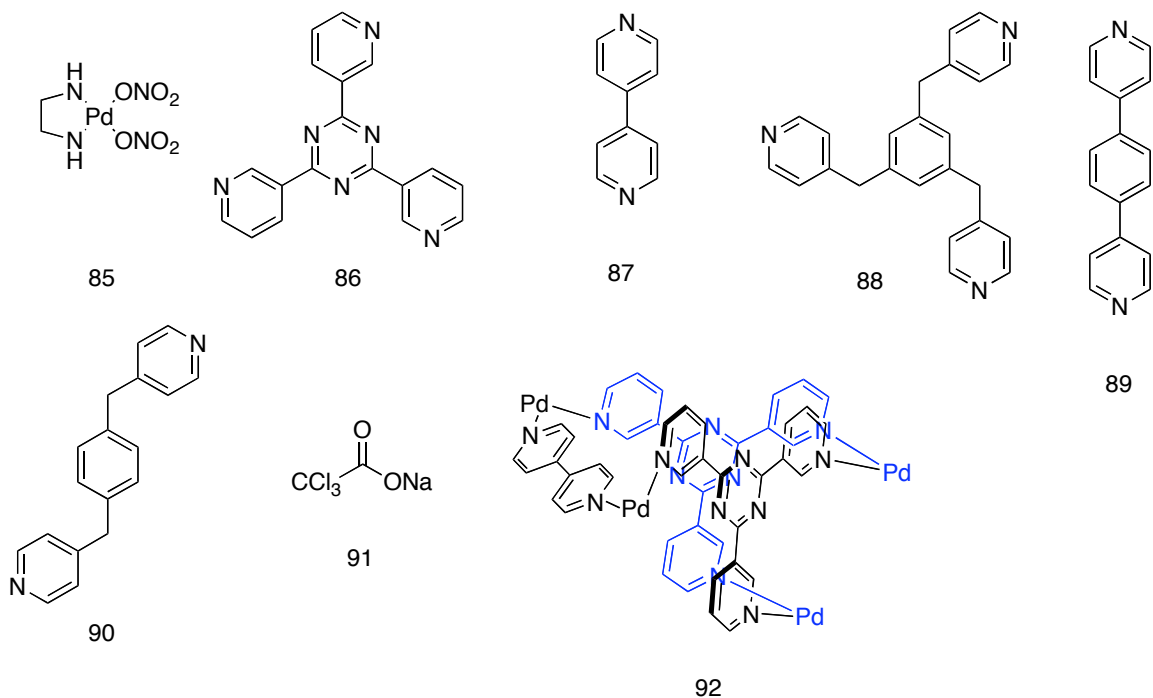


**Figure 25.** Fujita's DCL of metallocages, which produces anion receptor **92** only in the presence of guest **91**.

Nitschke has reported extensively the simultaneous use of imine exchange and coordination chemistry to generate DCLs of metal complexes.[44] Nitschke's DCLs utilize metal-templating to control their composition. They are demonstrations of the concept of coordination-driven self-selection, self-assembly, and self-sorting. The outcome of each complex reaction is thermodynamically controlled. For example, the use of substituent effects and chelate effects to drive successive transformations of copper (I) complexes in

one pot were demonstrated.[45] (Figure 26) By the successive addition of a designed sequence of amines, the transformation **93** to **94** to **95** to **96** was effected with greater than 93% yield at each step.
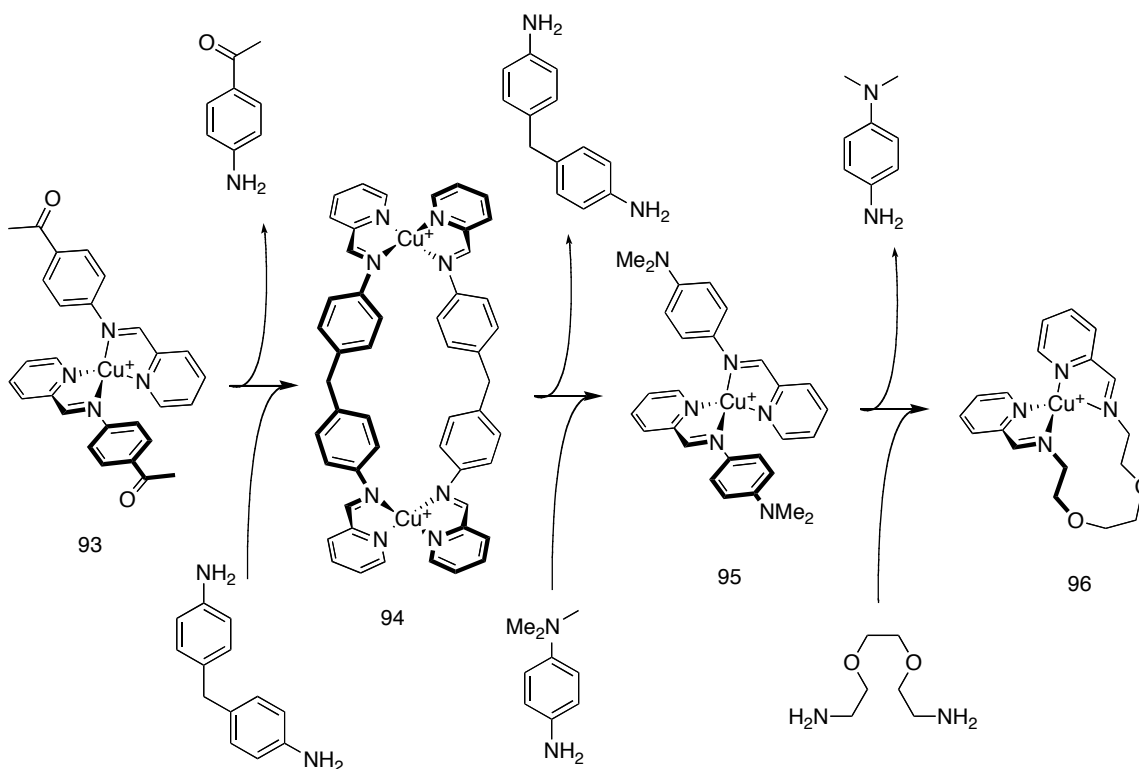


**Figure 26.** Nitschke's electronic substituent-effect and chelate-effect-driven successive thermodynamic syntheses of copper (I) imine complexes.

In a beautiful example of self-assembly driven by coordination chemistry, aldehydes **97** and **98** and amines **99** and **100** self-assemble in the presence of 1.5 equivalents of cuprous terafluoroborate and 1 equivalent of ferrous sulfate to exclusively form complexes **101** and **102**.[46] (Figure 27) In the absence of metal ions, a complex mixture is formed. Formation of **101** is driven by the chelate effect; the ligand derived from **97** and **99** is potentially hexadentate and is capable of satisfying the coordination preference of octahedral iron (II). Aldehydic building block **98** is excluded from this

complex owing to its sterically demanding 6-methyl substituent, which would clash with the rest of the ligand in the crowded octahedral environment. Formation of **102** is driven by the favorability of bis-bidentate binding for the tetrahedral copper (I) complex. Aldehyde **98** is incorporated because the tetrahedral geometry is less sterically congested, and because the methyl substituent increases the donor character of the pyridine ligand.
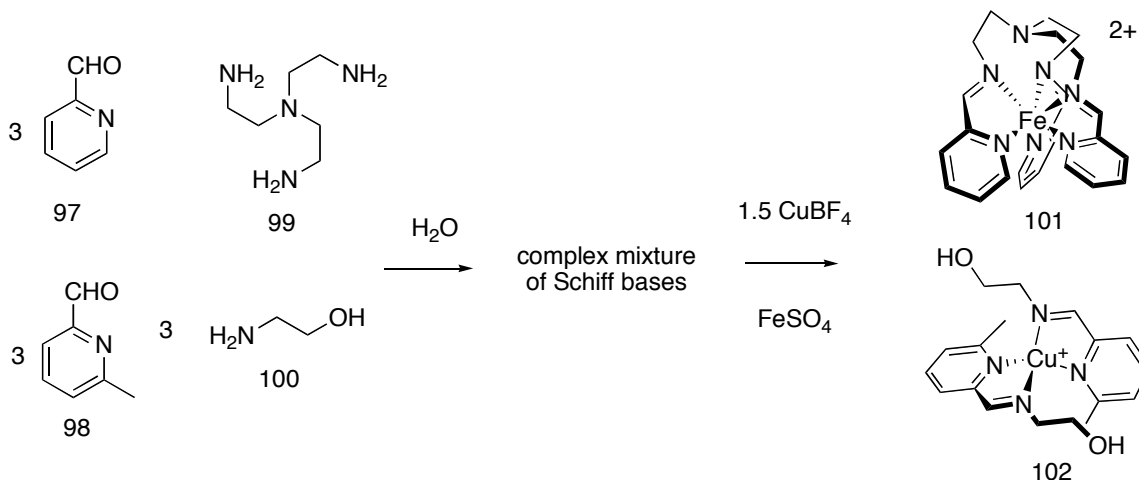


**Figure 27.** Self-sorting of Schiff base ligands in the presence of ferrous and cuprous ions.

Lüning has extensively demonstrated the synthesis of macrocyclic Schiff base ligands under metal-templated conditions.[47,48] (Figure 28) For example, dialdehyde **103**, and diamines **104** and **105** form a complex mixture in the absence of template ions, but form macrocycle **106** (**104**+**103**, 57%) in the presence of magnesium ions and macrocycle **107** (**105** + **103**, 71%) in the presence of calcium ions. Reduction by sodium borohydride yields the macrocyclic ligand products. The ring size of the major macrocyclic product appears to be controlled by the size of the template ion.
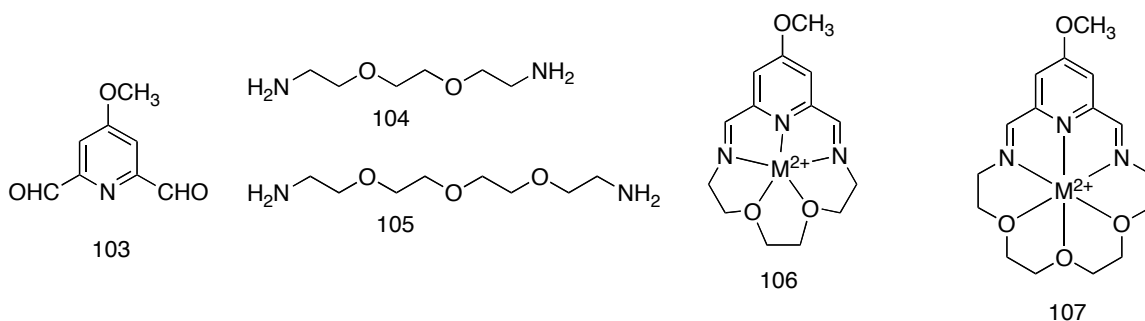
**Figure 28.** Lüning's DCL of crown-ether-like macrocycles

The diastereoselective amplification of a chiral macrocycle from a DCL was achieved by templating with cadmium ions.[49] Mixture of rac-**108** and **109** produces a complex mixture of 2+2, 3+3, and 4+4 cyclic oligomers as several different diastereomers. Preferential stabilization of a single diastereomer by cadmium ion leads to the amplification of a single species. In the presence of cadmium ions, racemic macrocycle **110** is produced as one diastereomer. Reduction with sodium borohydride gives the cyclic polyamine derivative of **110**.
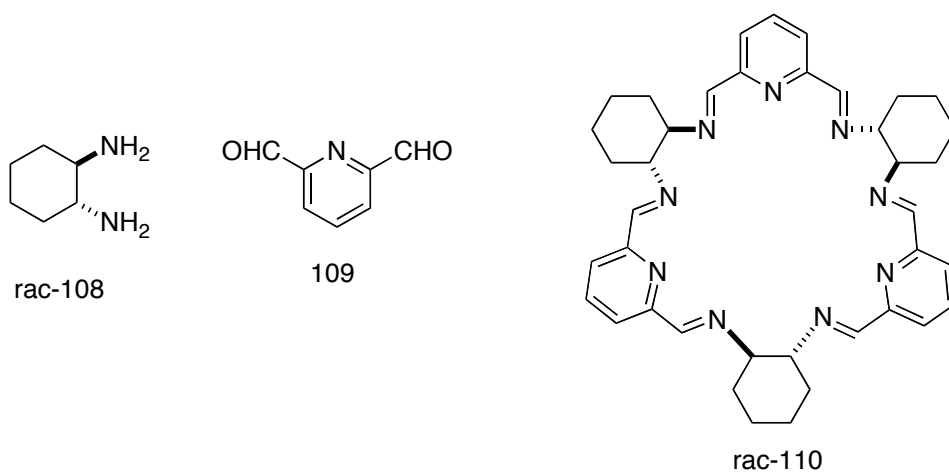


**Figure 29.** Diastereoselective amplification of "3 + 3" product **110** by cadmium ions.

**1.2.5 DCLs in which a species amplified by a TSA catalyzes a reaction**

The first report of a catalyst amplified via DCC emerged in 2003.[50] A DCL was constructed from dithiol building blocks **111**, **112**, and **113**. The resulting library of disulfide-linked hydrophobic macrocycles was exposed to cationic template **116**, chosen as a TSA for the Diels-Alder reaction of cyclopentadiene and acridizinium bromide **115**. Compound **116** is the product of the Diels-Alder reaction, and the authors reasoned that it might serve as an adequate analog for the transition state of the Diels-Alder reaction. The amplification of two macrocyclic trimers **117** and **118** was observed. Upon isolation, **117** was determined to catalyze the Diels-Alder reaction with a $k_{cat}$ of $1.9 \times 10^{-3} \, s^{-1}$. It is likely that acceleration of the Diels-Alder reaction by **117** is due to the increased effective concentration due to substrate binding in the hydrophobic interior of **117**.

Similarly, a disulfide library was used to "discover" the catalysis of acetal hydrolysis by **117**.[51] A mixture of dithiol building blocks **112**, **113**, and **114** was allowed to equilibrate in the presence of TSA **121**. **121** was designed to simulate the transition state for the hydrolysis of acetal **119**. Macrocycle **117** was amplified, and was subsequently found to accelerate the hydrolysis of **119** by a factor of 2. Catalysis of acetal hydrolysis by **117** is most likely due to stabilization of developing positive charge by the anionic host **117**.
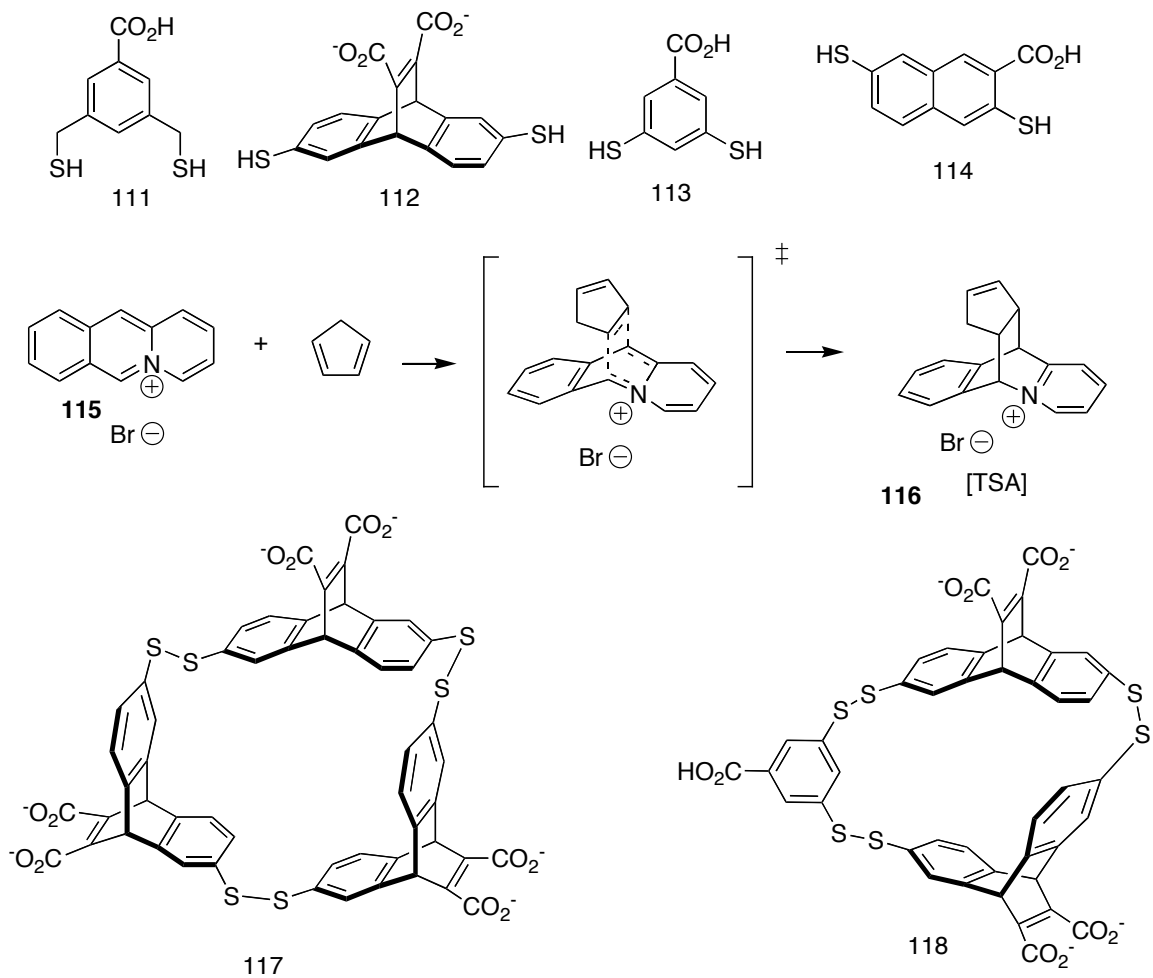
**Figure 30.** Building blocks for Sander's disulfide library that generates catalyst **117** for a Diels-Alder cyclization. **116**, the product of the reaction, was also used as TSA.
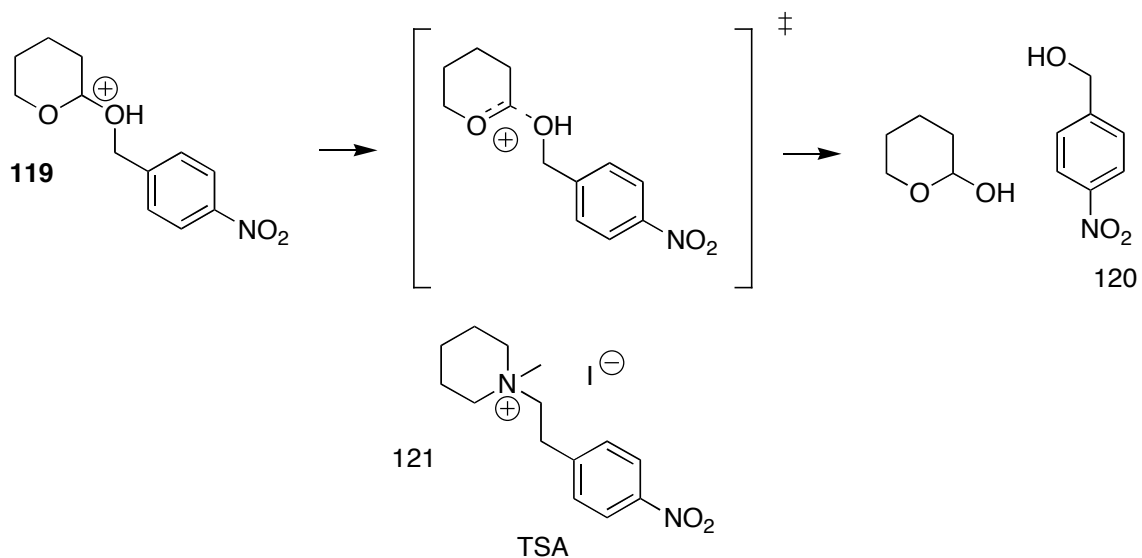
**Figure 31.** Acetal hydrolysis catalyzed by amplified macrocycle **117**. **121** was used as TSA.

In a related work, Scrimin, et al. used a DCL to probe reactivity in a noncatalytic setting.[52] A dynamic library consisting of a tethered TSA and a variety of exchangeable reactive groups was produced. Competition experiments were carried out in which the extent of hydrazone formation from phosphonate-aldehyde **121** and a functionalized hydrazide library **124 A-I** was measured. Hydrazides **124A** and **124I** were found to possess the most favorable equilibrium for hydrazone formation with aldehyde **121**. It was found that the amplified species contained reactive groups that promoted the esterolysis of substrate compounds.

33
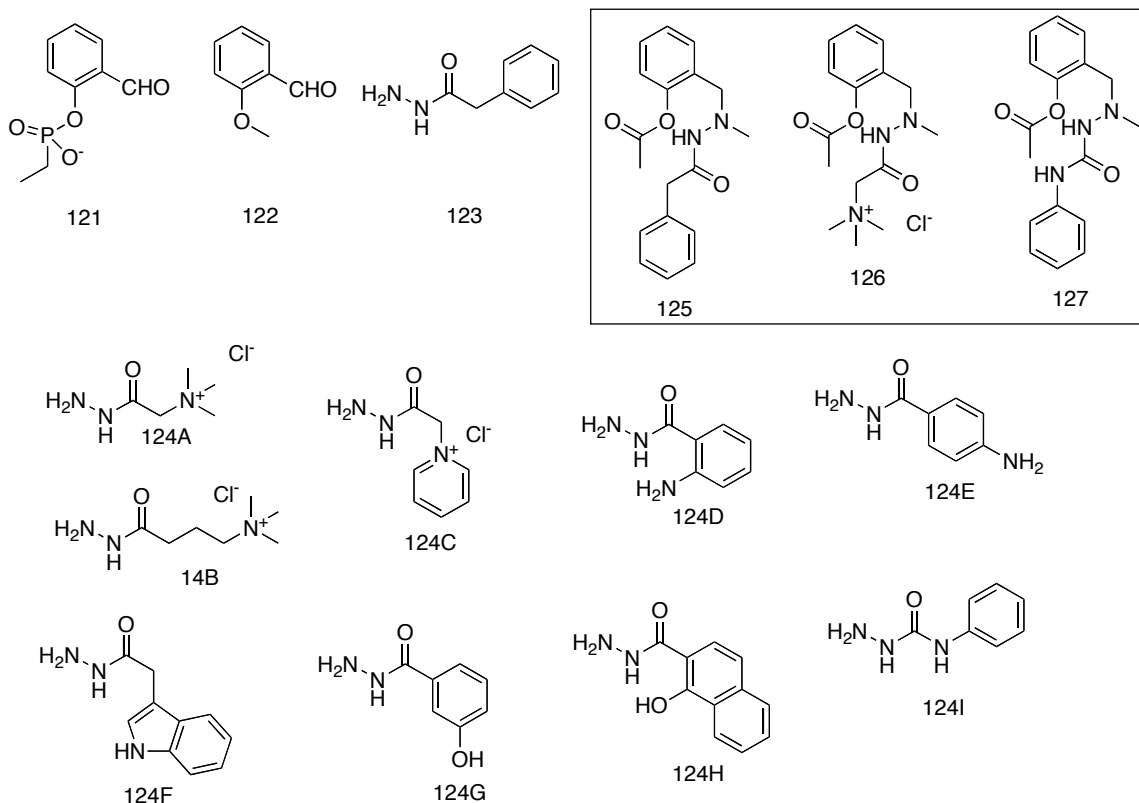
**Figure 32.** DCL designed to probe neighboring group effects in esterolysis reactions. In the box are the ester substrates that were tested.

Esters **125**, **126**, and **127** were prepared and assayed for neighboring-group promoted hydrolysis. It was found that **126** was hydrolyzed 4.8 times faster than the control substrate **125**, and **127** was hydrolyzed 1.6 times faster than **125**. This kinetic behavior correlates qualitatively with the DCL amplification behavior. The rate acceleration by **126** can be rationalized by the ability of the cationic alkylammonium group to stabilize the developing negative charge in the tetrahedral transition state of esterolysis as well as stabilize the tetrahedral oxyanion intermediate. To a lesser extent, the urea moiety in **127** can stabilize the transition state and intermediate of esterolysis by hydrogen bonding. These interactions also explain the enhanced formation of the

corresponding hydrazone adduct in the DCL, since the phosphonate TSA simulates the geometry and electronics of the transition state of esterolysis.

**1.3 Conclusion**

As the domain of small-molecule catalysts becomes more thoroughly exhausted and the demands for more selective and sophisticated catalysts increase, an evolutionary approach will become more attractive. Catalytic antibodies and molecular imprinted polymers provide a vivid proof of principle for the production of catalysts by a TSA templating approach. However, both of these methods suffer from fundamental methodological disadvantages.

The catalytic antibody approach is extremely expensive and requires specialized facilities and expertise that do not exist in most laboratories. Catalytic antibodies are not amenable to modification, and cannot be operated under conditions hostile to their proteinaceous nature. Molecular imprinted polymers, though promising, have a disadvantage. Their synthesis is kinetically controlled, leading to a large number of different types of active sites with varying structure. This not only compromises their catalytic activity, but it makes them difficult to study. Several features of a DCL approach to catalysis provide an ideal complement to catalytic antibodies and MIPs. DCL is inexpensive, operationally straightforward, and amenable to modification and study. Finally, DCL can produce homogenous catalysts of known structure and characteristics.

We note that a DCL approach to catalyst discovery is a fledgling field with very few entries. Despite challenges relating to the design, formation and analysis of DCLs, the application of DCC to catalysis appears to be very promising. Although catalyst-DCL

is still in the proof-of-concept stage, practical limits to explicit synthesis and screening of large and extremely complex libraries make an evolutionary approach attractive. We set out, therefore, to expand the role of DCC in catalyst-discovery, and explore the possibility of using metal-ligand and ligand-ligand interactions to template the formation of catalysts. Foremost among the issues we wished to address were whether it would be possible to access catalytically relevant species via DCL, and whether the amplification behavior in the DCL experiment could be correlated with the catalytic behavior of the library members. We noted that many of the concepts developed for the dynamic combinatorial chemistry of coordination complexes had not yet been explored in the context of catalyst evolution. Here we saw an opportunity to develop the dynamic combinatorial evolution of catalyst libraries. In the following chapters, we will describe the results of these endeavors.

## 2. DYNAMIC COMBINATORIAL CHEMISTRY OF HISTIDINE-DERIVED PSEUDOPEPTIDE OLIGOMERS

### 2.1 Histidine

The amino acid histidine is an important residue in enzyme catalysis. Although it makes up only 1.9% of residues in modern proteins,[53] it is present in a large number of catalytic sites. It is often found to participate in biological catalysis as either a ligand, a nucleophile, or a general acid/general base residue. The soft donor properties of the N3 (pyridine-like) lone-pair make imidazole an excellent ligand for many transition metals. Imidazole N3 is more nucleophilic than a primary or secondary amine, due to the sterically unhindered donor atom incorporated into a planar ring. N1 is easily deprotonated, while N3 is easily protonated, giving imidazole both hydrogen-bond donor and acceptor properties at neutral pH.[54]

Toward the generation of DCLs that produce catalytic species, it would be highly desirable to add to the selection of available building blocks, so that these artificial systems might reflect the function-group diversity of the proteinogenic amino acids. Our interest in a histidine-based building block **128** is due to the importance of histidine in enzyme active sites as an acid/base residue[54] and as a ligand for transition metals in non-heme metalloenzymes.[55-57]

There are a number of examples of dynamic combinatorial chemistry that exploit relatively strong transition metal-ligand interactions in order to achieve templating.[39-41,58-63] The goal of this stage of the project was to use histidine-based building blocks to produce metalloenzyme active-site mimics through templating on transition-metal-TSA

complexes (Figure 33). Acid-catalyzed hydrazone-exchange has been demonstrated to be a versatile reaction for DCL, and the suitability of bifunctional hydrazide/aldehyde building blocks synthesized from amino acids is well-established.[29,31,33,39,41,63-65] Our work incorporates the histidine residue into a DCL building block, providing entry to dynamic libraries of oligo-histidine macrocycles of possible use as imidazole-based catalysts. To our knowledge, this was the first DCL to incorporate histidine or any other imidazole-bearing building block.
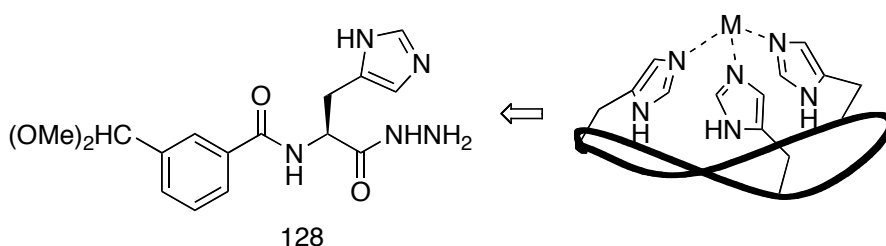


**Figure 33**. Dynamic combinatorial library of histidine-derived macrocycles.

## 2.2 Results and Discussion

### 2.2.1 mHis monomer synthesis

This work was published in a full paper in the Journal of Organic Chemistry.[66] Histidine-derived pseudopeptide hydrazide building block *mHis* **128** was synthesized via a modified literature method starting from 3-(dimethoxymethyl)-benzoic acid **130** (Fig 34).[31] The acid was coupled to L-histidine methyl ester dihydrochloride using carbonyldiimidazole as a coupling reagent.[67] Other methods using carbodiimide coupling reagents failed to produce the desired product. The coupling was carried out by refluxing acid **130** with carbonyldiimidazole in ethyl acetate overnight. L-histidine methyl ester dihydrochloride was added along with two equivalents of triethylamine to free the amines. This mixture was stirred until starting material had disappeared as checked by

TLC. The coupled product **131** was obtained as a crude foam in 80% yield and characterized by $^1$H-NMR and ESI-MS.

The crude product amide-ester **131** was subjected to room-temperature hydrazinolysis in methanol to yield the *mHis* monomer **128**. The crude product was triturated thrice with methanol to give pure material in 84% yield (2.64 g), which was characterized by $^1$H-NMR, $^{13}$C-NMR, IR, and ESI-MS.
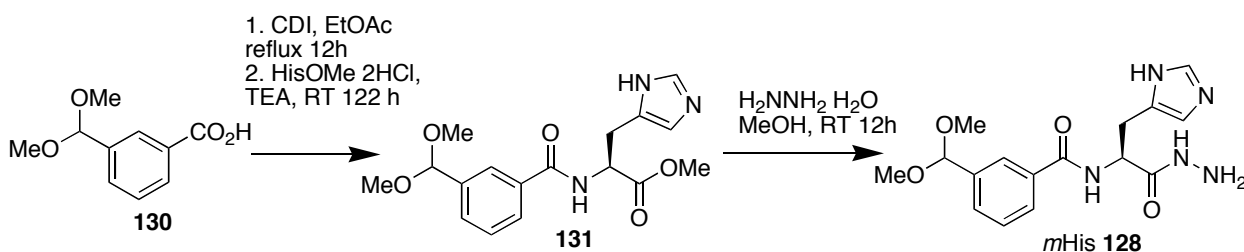


**Figure 34**. Synthesis of *mHis* (**128**)

## 2.2.2 Oligomerization of 128

Monomer **128** was placed in 3:1 acetonitrile/water and treated with excess TFA. (Figure 35) After 8 hours, the mixture was analyzed by RP HPLC using UV detection at 254 nm. (Figure 36). Three fractions of eluent were collected and analyzed by ESI-MS. (Figures 37, 38, 39) Fraction 1 (Figure 37) shows a peak with m/z value of 284.1 with a second (M + 1) peak at 284.6, an interval of one half mass, diagnostic of a double charge ion of mass 568.2. Based on this, the species in this fraction was assigned as cyclic dimer. Fraction 2 (Figure 39) shows a peak with m/z of 378.5 with a (M+1) peak at 378.8, an interval of 1/3 mass, indicative of a triply charged ion with mass 1135.5. There is also a peak with m/z 567.2 with a (M + 1) peak at 567.7, indicative of a doubly charged ion of mass 1134.4. Based on this, this fraction was assigned as the cyclic tetramer. Fraction 3

(Figure 38) shows a peak with m/z 284.1 with a (m+1) peak at 284.4, indicative of a triply charged ion with mass of 852.3. Fraction 3 also contains a peak with m/z 425.6 with (m+1) peak at 426.1, indicative of a double charge ion with mass of 851.2. This fraction was therefore assigned as the cyclic trimer. The initial mixture produced by the oligomerization of **128** was therefore found to be a mixture of cyclic oligomers, primarily dimer, trimer and tetramer, as indicated by HPLC (Figure 36) and ESI-MS (Fig 37, 38, 39).
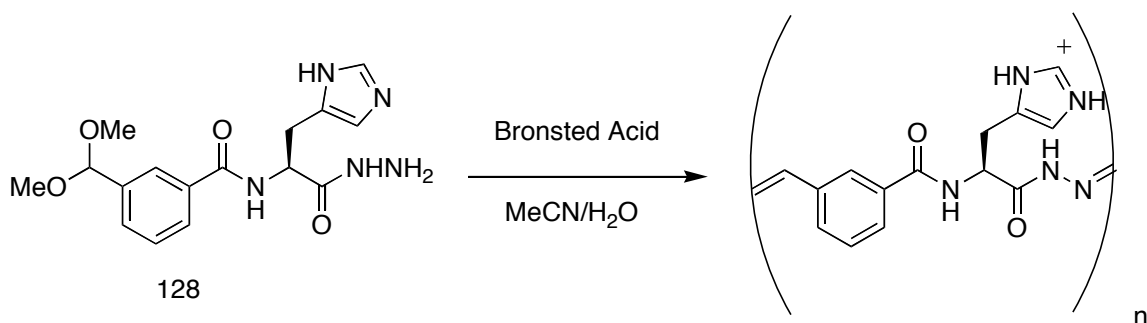


**Figure 35**. Oligomerization of *mHis* (**128**)
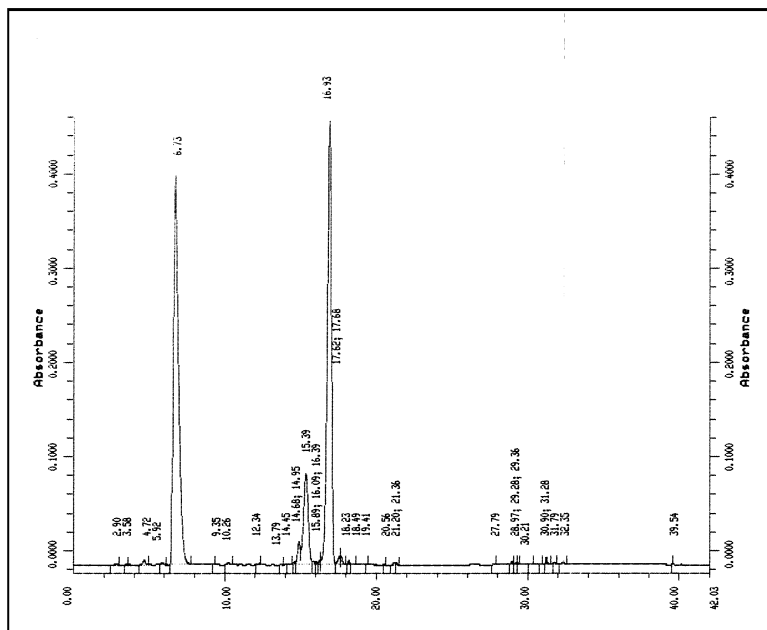


**Figure 36**. RP-HPLC chromatogram of initial mixture from oligomerization of **128**. The first peak is cyclic dimer, second peak is cyclic tetramer, and third peak is cyclic trimer.

**Figure 37**. ESI-MS of **128₂** cyclic dimer collected from RP-HPLC eluent.
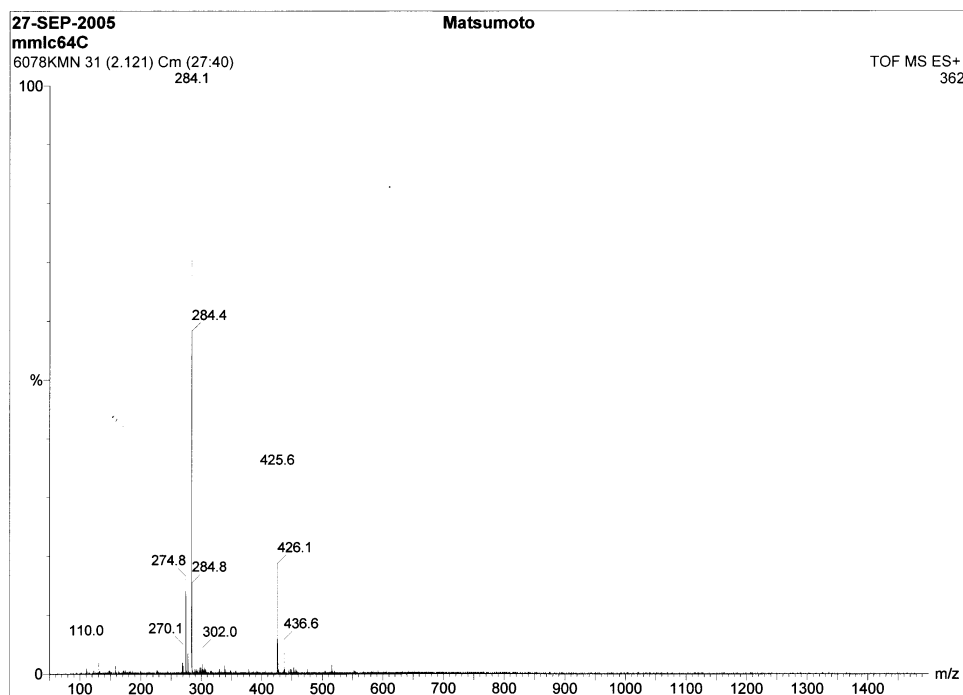


**Figure 38**. ESI-MS of **128₃** cyclic trimer collected from RP-HPLC eluent.
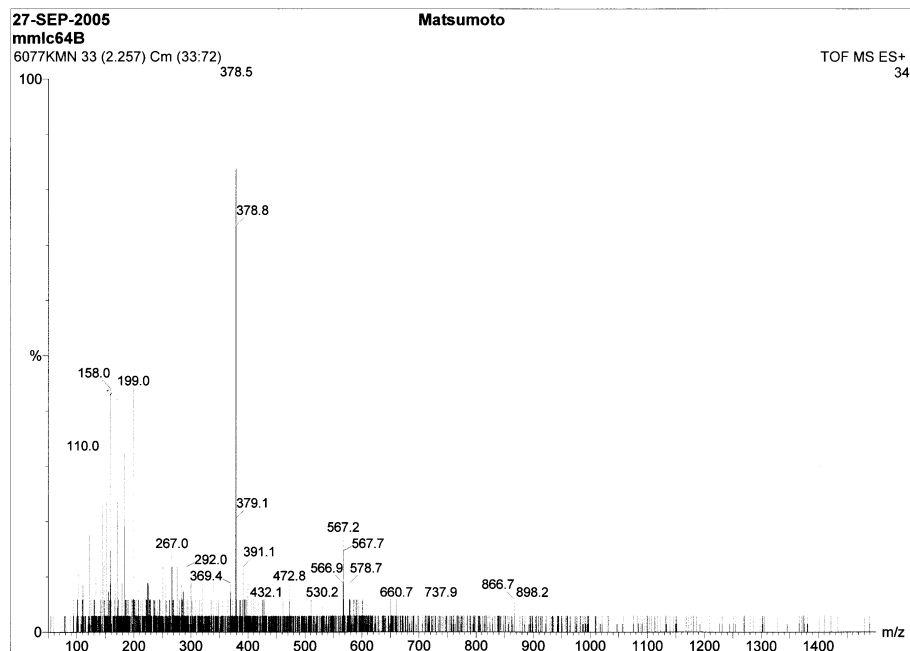
**Figure 39**. ESI-MS of **128**$_4$ cyclic tetramer collected from RP-HPLC eluent.

Note that the major ESI peaks are doubly and triply charged species due to multiple protonations. It is possible to distinguish the **128**$_2{}^{2+}$ peak form the **128**$_3{}^{3+}$ peak by the fine detail of the peaks, in which noninteger intervals of ½ or 1/3 are found corrsponding to doubly charged and triply charged $M+H^+_n$ species. After fourteen days, only the cyclic dimer remained (Figure 40). Longer reaction times always led to nearly complete conversion of the oliogomeric mixture to the cyclic dimer. When a large excess of acid was used, equilibrium was reached in 15 hours.
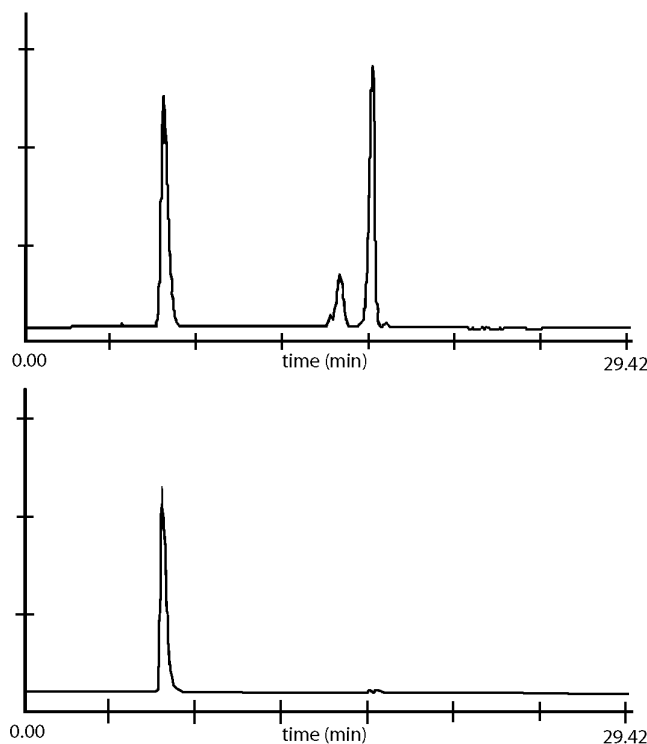
**Figure 40**. HPLC trace of reaction of **128** with 2 equiv of HCl at 8 hr (top), and 14 days (bottom). left, cyclic dimer; middle, cyclic tetramer; right, cyclic trimer. All peaks were identified by ESI-MS.

### 2.2.3 Analysis of 128 library by time-dependent ^{1}H-NMR

A time-dependent ^{1}H-NMR experiment in which *mHis* (**128**) was treated with excess d-TFA in $CD_3CN/D_2O$ confirmed that the initially formed aldehyde is consumed rapidly, leading to the formation of a mixture of oligomers, with dimer and trimer predominating (Fig. 41). The multiplet at 5.7 ppm (labeled B) is assigned to the cyclic dimer α-CH based on NMR characterization of the isolated cyclic dimer; it is observed steadily increasing in magnitude over time. The multiplet at 5.1 ppm (labeled A) is assigned to cyclic trimer α-CH. It is seen emerging initially before eventually

43

disappearing, and is the only discernible α-CH-type signal other than peak B. The presence of cyclic trimer at this stage is also apparent in the ESI-MS. These oligomeric species were slowly consumed over 15 hr to generate almost exclusively cyclic dimer.
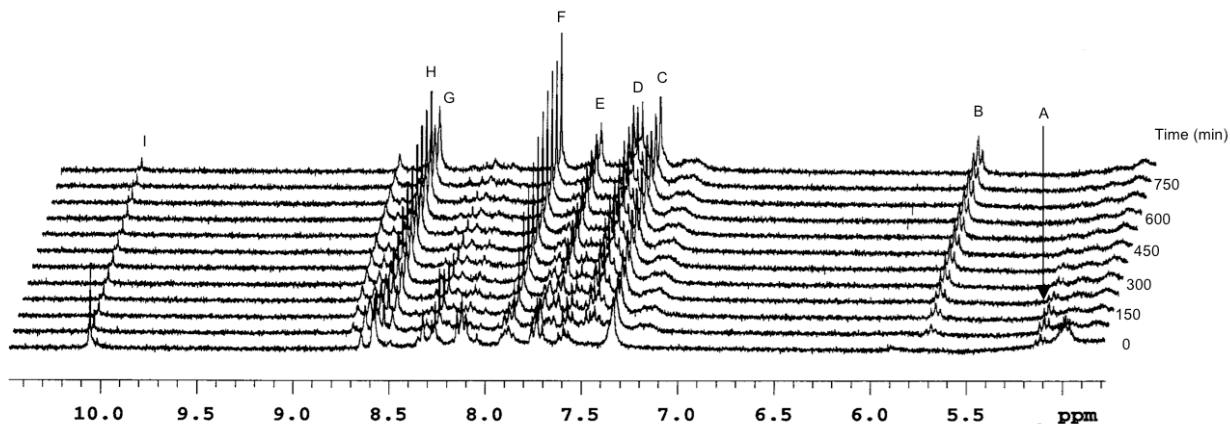


**Figure 41**. Time-dependent $^1$H-NMR spectra showing evolution of macrocycle library derived from **128** to the predominantly dimeric state. A, trimer a-CH; B, dimer a-CH; C, dimer imidazole C4/5; D, dimer aryl; E, dimer aryl; F, dimer imine CH; G, dimer aryl; H, dimer imidazole C2; I, linear oligomer aldehyde CH.

### 2.2.4 NMR studies on cyclic dimer $128_2$

Crude cyclic dimer hydrochloride salt was recovered from an equilibrium mixture by removal of solvent *in vacuo* and was analyzed by ESI-MS and NMR. Detailed NMR analysis was carried out in order to elucidate the structure of cyclic dimer $128_2$. The identity of $^1$H-NMR and $^{13}$C-NMR signals was established by use of 2D methods (gCOSY, HSQC, and HMBC). NOESY was used to identify proximal protons to ascertain conformation.

NOEs observed between the *ortho*-aryl C-H's and the hydrazone C-H and the α-amino acid C-H suggest that the structure of the dimer is as illustrated in Fig. 42. Molecular mechanics and gas-phase computational PM3 models[68] of the cyclic dimer dication (Fig. 43) are in agreement with this proposed structure with the two imidazolium units directed *exo*.
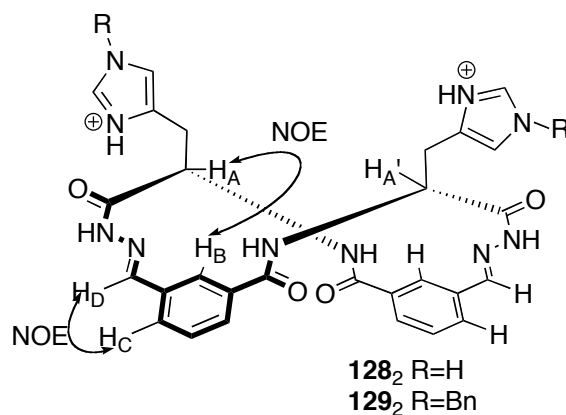


**Figure 42**. Proposed structure of cyclic dimers $128_2$ and $129_2$ based on NOESY data 2-D
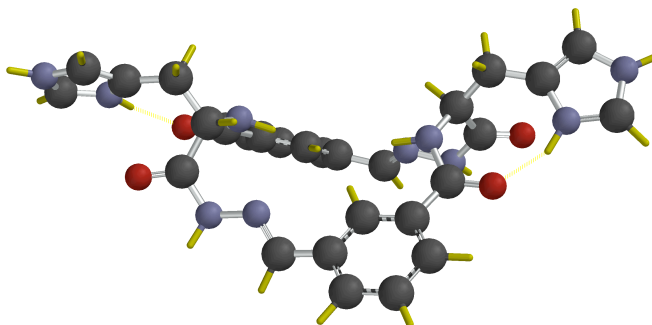


**Figure 43.** PM3 calculated structure of cyclic dimer $128_2$. Distance between $H_A$ and $H_B$ is approximately 4 Angstrom in the model, whereas the distance between $H_A$' and $H_B$ is approximately 4.5 Angstrom.
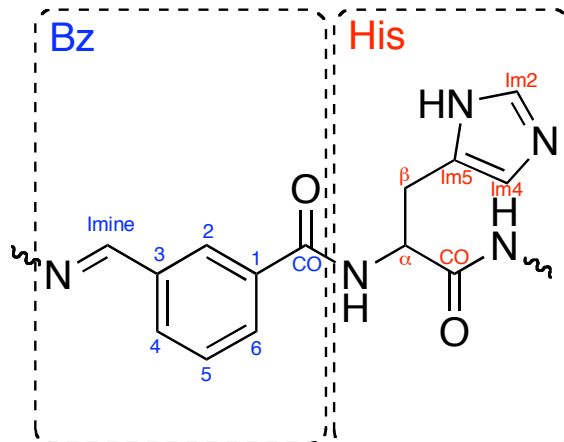
**Figure 44.** Legend for NMR assignment of **128₂**

**Table 1.** $^1$H-NMR and $^{13}$C-NMR signal assignments for **128₂.**

| Carbon | ppm | | Proton | ppm |
|--------|-------|---|-----------|------|
| His-BC | 26.0 | | His-Im2H | 8.76 |
| His-AC | 49.7 | | Bz-2H | 8.69 |
| His-Im4C | 117.3 | | Bz-ImineH | 7.81 |
| Bz-2C | 124.2 | | Bz-6H | 7.69 |
| Bz-6C | 127.1 | | His-Im4H | 7.44 |
| Bz-5C | 128.3 | | Bz-4H | 7.40 |
| His-Im5C | 130.6 | | Bz-5H | 7.38 |
| Bz-4C | 131.0 | | His-AH | 5.77 |
| Bz-3C | 132.5 | | His-BHa | 3.39 |
| His-Im2C | 133.1 | | His-BHb | 3.23 |
| Bz-1C | 134.7 | | | |
| Bz-ImineC | 143.3 | | | |
| Bz-C=O | 167.1 | | | |
| His-C=O | 171.0 | | | |

**Table 2**. $^1$H-NOESY crosspeak assignments for **128₂**.

| assignment: | ppm | ppm |
|-------------|-------|-------|
| **Bz4H-IH** | **7.395** | **7.808** |
| Bz5H-2H | 7.386 | 8.678 |
| Bz5H-6H | 7.362 | 7.684 |
| Bz6H-2H | 7.672 | 8.678 |
| **HisAH-Bz2H** | **5.780** | **8.678** |
| **HisAH-Im4H** | **5.779** | **7.419** |
| HisBHa-AH | 3.385 | 5.780 |
| HisBHa-Im4H | 3.379 | 7.419 |
| HisBHb-AH | 3.203 | 5.780 |
| HisBHb-Im4H | 3.213 | 7.419 |

## 2.2.5 Zinc complexes of $128_2$

When $128_2$ was treated with zinc triflate, the cyclic dimer also was observed by ESI-MS to form various complexes, with Zn (II) in methanolic solution, specifically, $[(128_2)_2Zn]^{2+}$, $[(128_2)_3(-H) Zn_2]^{3+}$, $[(128_2)_2(-2H)Zn_2]^{2+}$. (**Figure 45**) Simulations of the isotopic mass pattern are shown for reference (**Figure 46**).
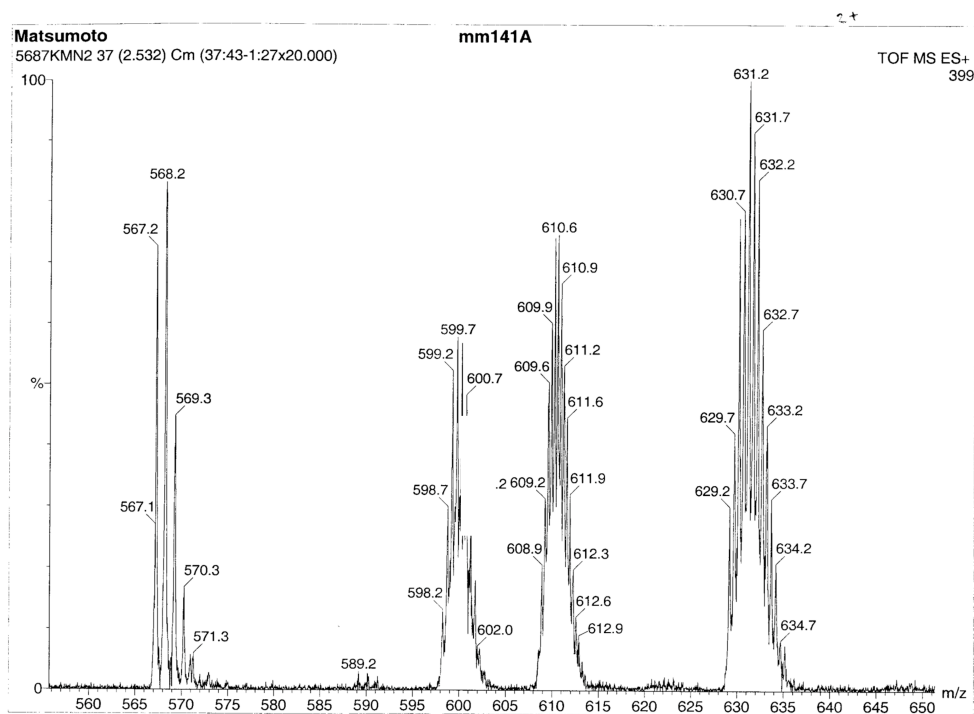


**Figure 45.** Positive ESI-MS for zinc $128_2$ complexes.
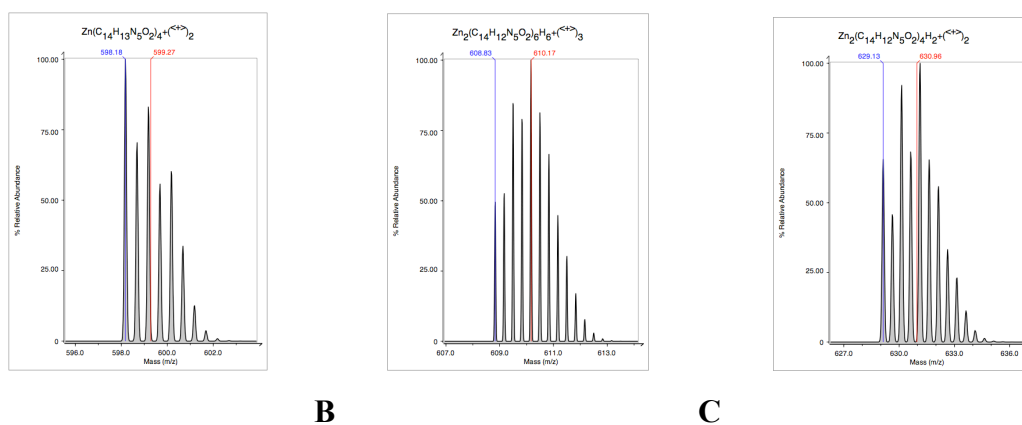
**Figure 46.** Simulated MS for zinc $128_2$ complexes. A, $[dimer_2Zn]^{2+}$. B, $[dimer_3(-H)Zn_2]^{3+}$. C, $[dimer_2(-2H)Zn_2]^{2+}$

## 2.2.6 Templating experiments on 128

In an attempt to perturb the equilibrium in the mHis library away from the all-dimer state, experiments were carried out in which template-candidates were added to the oligomer libraries or to the starting mixture of monomer and acid under various conditions.  Template candidates that we explored include metal ions (zinc triflate, cadmium chloride, mercuric chloride, copper (II) triflate, cobalt (II) chloride, iron (III) chloride) and anions (diphenylphosphate, phenylphosphonic acid).  These experiments were carried out in a variety of mixtures of acetonitrile and water, using 1.1 equivalents of TFA or 100 mM ammonium chloride buffer (pH 3) and analyzed by HPLC.  We observed no templating behavior, i.e., no change in the relative amount of species produced, in any of these experiments. We believe that in the case of the metal template-candidates, interactions between the imidazole and metal ions are suppressed by the fact that under the acidic conditions required for component exchange, the imidazoles are protonated. Under such conditions, no complexation of the metal ions would be expected.

It is also possible that the thermodynamically favored cyclic dimer forms metal ion complexes that are as (or are more) stable than the higher oligomers, so no detectible change in the equilibrium occurs in the presence of metal ion.  As noted previously we found that the cyclic dimer under neutral conditions formed various complexes with zinc that were detectible by ESI-MS.  In the case of anionic candidates, it is likely that there is no appreciable advantage to the trimeric or tetrameric cationic oligomer over the dimeric cationic oligomer for anion binding, especially considering that all species are strongly solvated in the largely aqueous experimental conditions.

### 2.3.1 τ-Benzyl monomer (129) synthesis

In order to explore the effect of substitution on the histidine imidazole, and to allow for library generation and templating studies in nonaqueous solvent systems, the *N*-benzyl-histidine derivative of the monomer **129** was synthesized according to Fig. 47.  τ-Benzyl-L-histidine **132** was converted to the methyl ester **133** by Fischer esterification in refluxing methanolic hydrogen chloride. Solvent and excess hydrogen chloride were removed under vacuum taking care not to allow contact with ambient moisture. The resulting hygroscopic crude ester dihydrochloride (97% yield) was freed with TEA and coupled to 3-(dimethoxymethyl)benzoic acid **130** using ethyldiisopropylaminoethylcarbodiimide hydrochloride (EDCI) and hydroxybenzotriazole (HOBT) in THF to give ester **134** as a crude brown brown oil. This material was chromatographed on flash silica eluted with ethyl acetate to give **134** in 61.5% yield.  The hydrazide monomer **129** was prepared by hydrazinolysis of the ester **134** stirring 3 days in methanol at room temperature.   The crude material was

chromatographed on flash silica using 9:1 dichloromethane/methanol to give 50% yield of **129**. The resulting monomer *m*Bn-His **129** was found to be soluble in polar organic solvents such as chloroform.
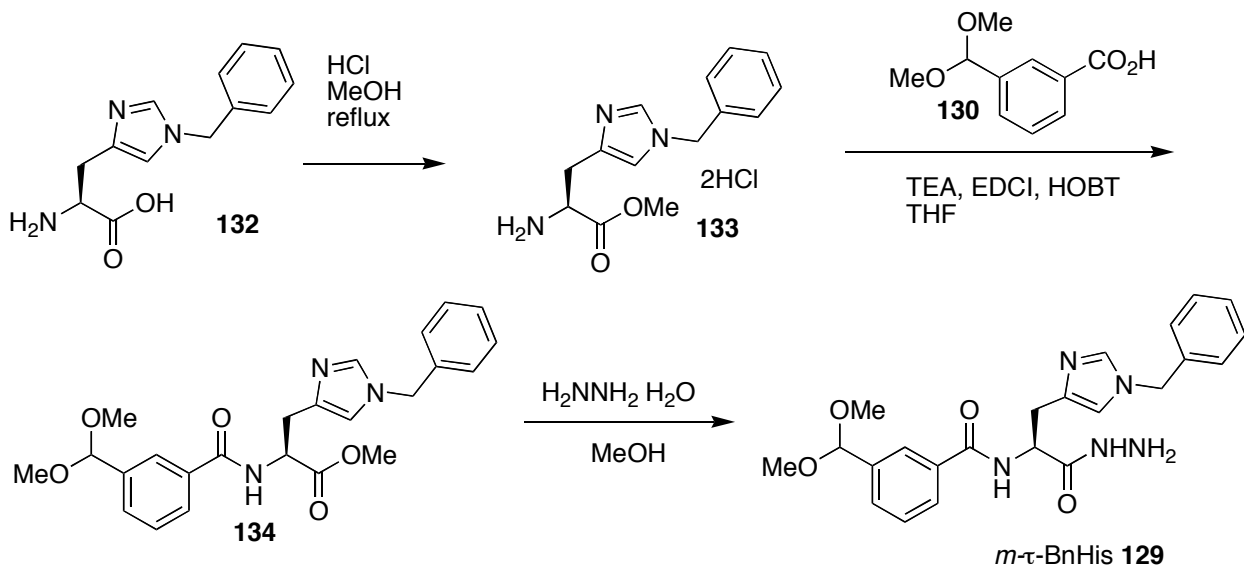


**Figure 47.** Synthesis of **129**

## 2.3.2 Oligomerization of 129

The benzyl-substituted monomer **129** was found to react to form cyclic oligomers in a similar fashion to the parent monomer. When treated at 5mM concentration with TFA in 75% acetonitrile in water, the monomer produced a library consisting of cyclic dimer, cyclic trimer, and cyclic tetramer, which were detected by LC/ESI-MS. Although monomer **129** was soluble in organic solvents such as chloroform and acetonitrile, these solvents were found to be unsuitable for library formation due to insolubility of the oligomeric salts formed under the acidic conditions of the DCL.

Monomer **129** was placed in 75% acetonitrile and water and treated with TFA. After 8 hours, the resulting mixture was analyzed by RP-HPLC (Figure 129). Three peaks are seen in the chromatogram. Two fractions corresponding with these peaks were collected and examined by ESI-MS. The fraction corresponding to the small peak that merges with the shoulder second large peak was collected but upon analysis, was found to contain no identifiable species.

The ESI-MS of the first fraction contains a peak with m/z of 374.2 with a (m+1) peak at 374.7, indicative of a double charge species of mass 748.4. Based on this, the fraction was assigned as the cyclic dimer. The ESI-MS of the second major fraction contains a peak with m/z of 374.2 with (m+1) peak at 374.5, indicative of a triple charge species of mass 1122.6. The ESI-MS also contains a peak with m/z of 560.8 with a (M+1) peak at 561.3, indicative of a double charge peak with mass 1121.6. This is indicative of the presence of the cyclic trimer.
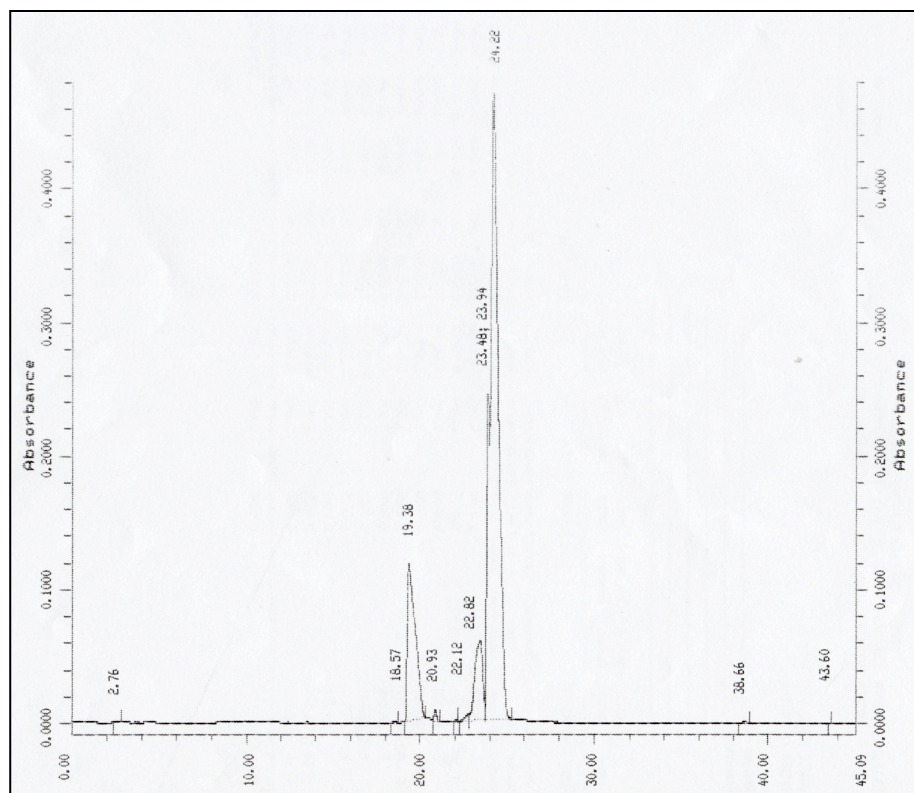
**Figure 48.** RP-HPLC chromatogram of initial mixture from oligomerization of **129**. First peak is cyclic dimer, second major peak is cyclic trimer. The shouldering peak could not be isolated.
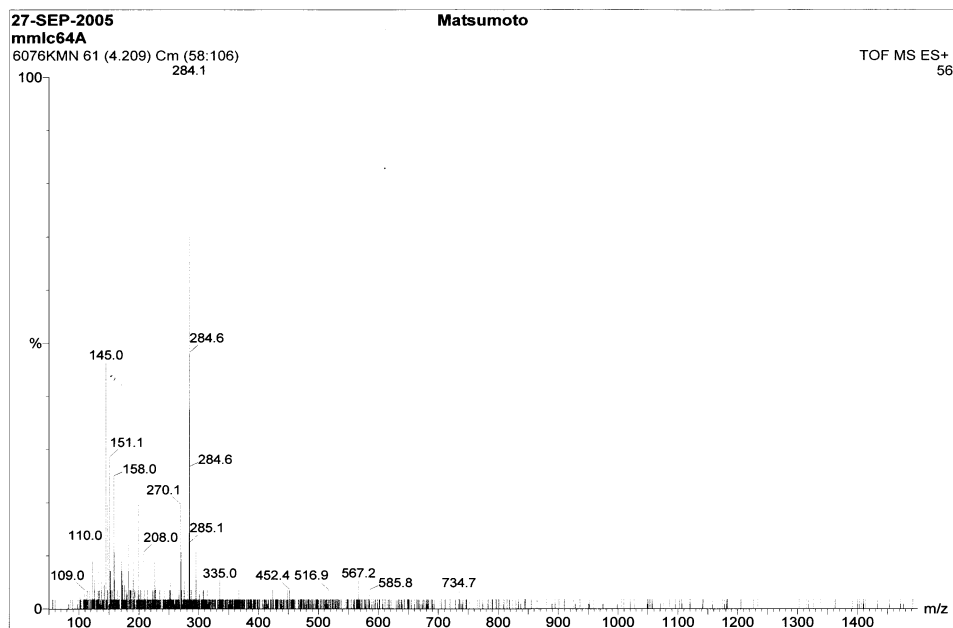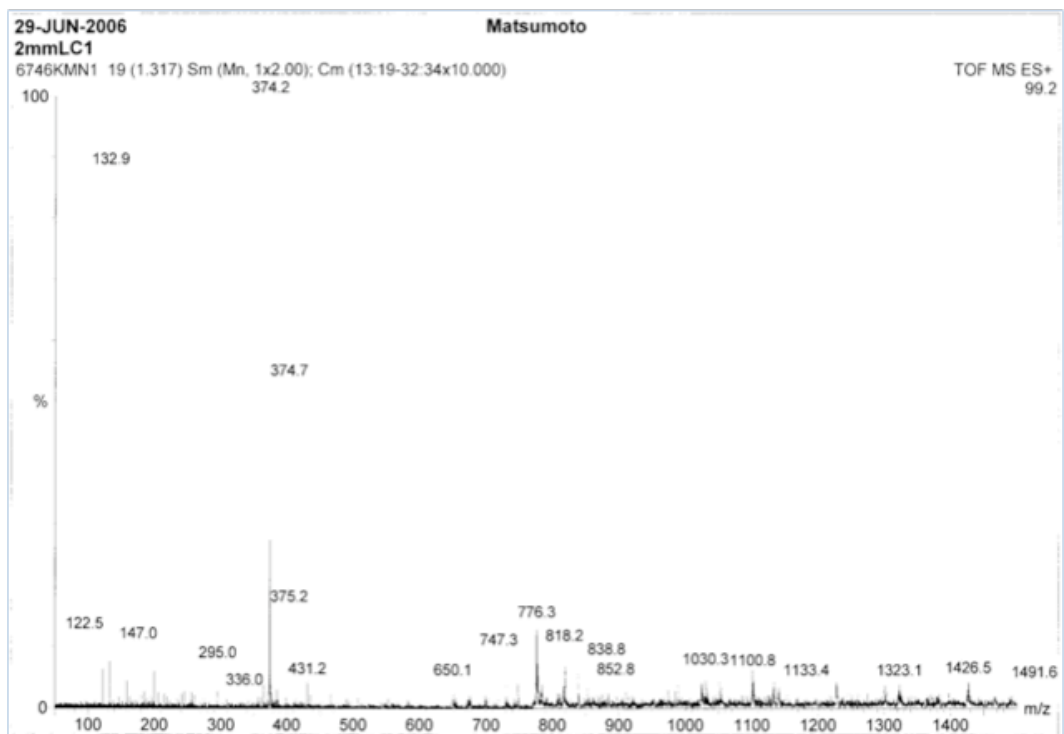
**Figure 49.** ESI-MS of cyclic dimer **129₂** collected from HPLC eluent
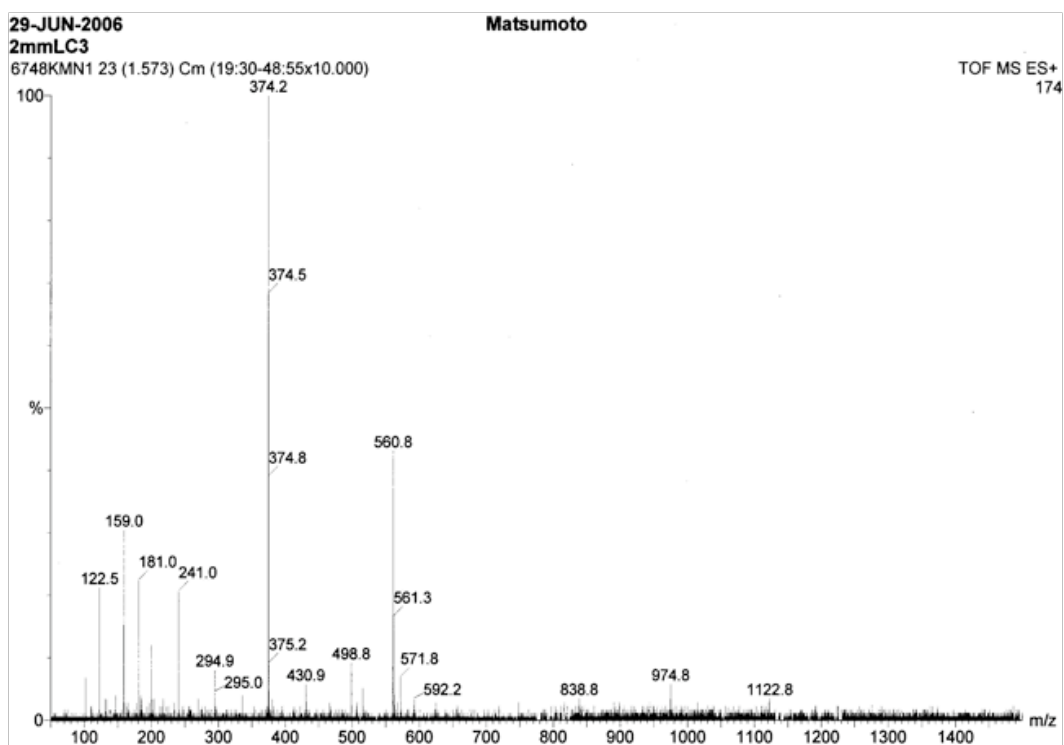


**Figure 50.** ESI-MS of cyclic trimer **129₃** collected from HPLC eluent

### 2.3.3 Time-dependent 1H-NMR study of oligo-129 library

The evolution of the mixture was also followed by proton NMR (Fig. 51). Over a 60 hour period, the oligomers were consumed to produce only the cyclic dimer.
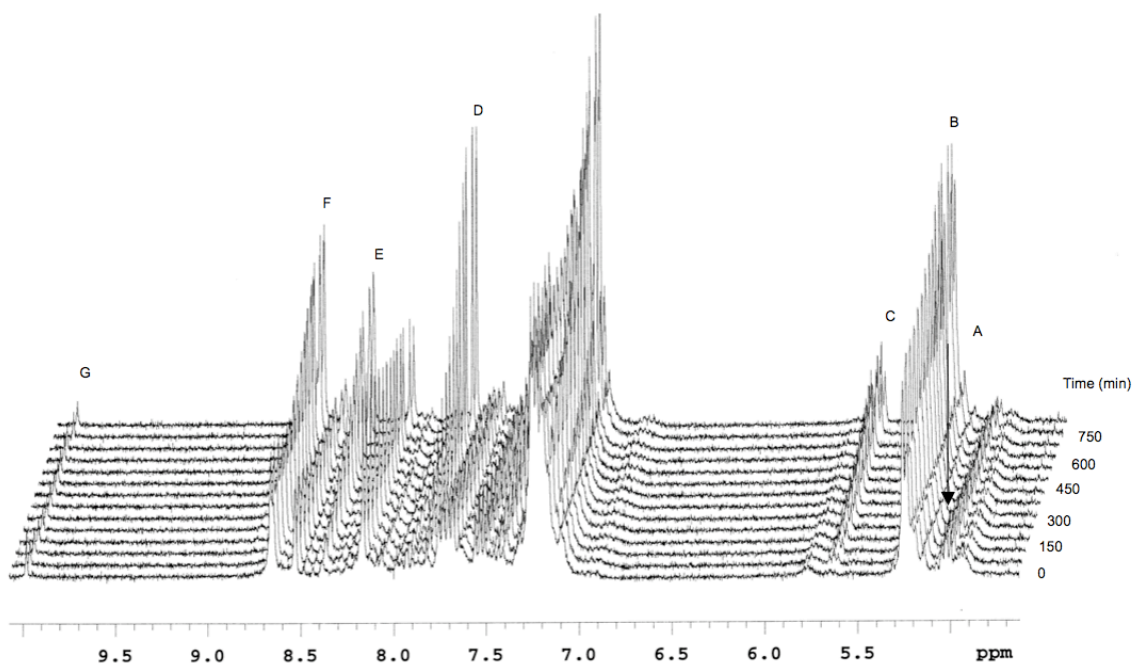


**Figure 51**. Time-dependent $^1$H-NMR of oligomer library derived from **129**. A, trimer histidine alpha proton; B, benzylic protons; C, dimer histidine alpha protons; dimer imine CH; E, dimer aromatic CH; F, dimer imidazole 5 position.

### 2.3.4 Probable structure of 129$_2$

The Bn-His dimer **129$_2$** could be produced and isolated on a preparative scale by treating a 3:1 acetonitrile/water solution with excess trifluoroacetic acid at rt for 10 days. Solvent evaporation left the dimer in moderately high purity as a ditrifluoroacetate salt. NOESY data for the Bn-His cyclic dimer **129$_2$** (Fig. 5) reveals an NOE enhancement between the histidine alpha proton (5.8 ppm) and the 2 position of the 3-iminyl-

benzamide moiety (8.7 ppm) indicating the proximity of the histidine alpha proton to the aromatic ring 2 position.  This suggests that the cyclic oligomer is arranged in such a way as to place the histidine side-chain away from the aromatic backbone and the alpha proton toward the aromatic backbone.  In addition, we observe an NOE interaction between the imine CH and the aromatic ring's 4 position, suggesting the aromatic imine conformation illustrated in Figure 5.  The structure of the cyclic dimer derived from 2 is therefore analogous to the structure of the non-benzylated mHis cyclic dimer.

### 2.3.5 Templating experiments with 129

Templating experiments were carried out on the $\tau$-benzyl-L-histidine-derived monomer **129**. Template-candidates were added to pre-equilibrated mixtures of cyclic dimer **129$_2$** treated with TFA in acetonitrile/water. Monomer **129** and template candidates were also combined in acetonitrile/water with 1.1 equivalents of TFA. Samples were monitored by HPLC. Zinc triflate, cadmium chloride, mercuric chloride, copper (II) triflate, cobalt (II) chloride, iron (III) chloride were tried as metal ion templates. Anionic species such as diphenylphosphate, phenylphosphonic acid, trimesic acid, camphoric acid, and citrate were also tried.  These experiments were carried out in a variety of mixtures of acetonitrile and water, using 1.1 equivalents of TFA or 100 mM ammonium chloride buffer (pH 3) and analyzed by HPLC.  We observed no templating behavior, i.e., no change in the relative amount of species produced, in any of these experiments. All mixtures yielded the cyclic dimer at equilibrium. ESI-MS analysis of the metal-templated libraries showed no metal complexes of any of the oligomers. The oligomers are protonated under these experimental conditions, and it is likely that no interaction with

metal takes place.   In the case of anionic templates, it is likely that the ion-ion interactions we were attempting to exploit are not sufficiently discriminating to select higher oligomers over dimer. Apparently, the inherent stability of the protonated cyclic dimer drives the DCL to an all-dimer composition.


### 2.4.1 pKa of mHis cyclic dimer $128_2$.

We wished to determine if the presence of two imidazole moieties on the macrocycle would lead to any perturbation in basicity.  To characterize the acid-base properties of the mHis cyclic dimer a solution of the dimer in dilute aqueous HCl was titrated with sodium hydroxide solution and the pH monitored by a potentiometric probe as a function of added base.  The titrant was standardized with potassium phthalate. The first two equivalents of base are consumed by hydrochloric acid in the solution. Over the addition of two more equivalents of sodium hydroxide, there was only one discrete endpoint visible.  We interpret this to mean that the $pK_a$ for first and second protonation are quite close together.  The average of the $pK_a$ of the first and second protonation of the cyclic dimer appears to be approximately 6.6. (Fig. 52), as compared to 7.45 for 4-methylimidazole and 7.05 for N-acetyl histidine[69].  This depression in the averaged $pK_a$ iof $128_2$ is most likely due to the increased acidity of the doubly protonated dimer, possibly due to electrostatic interactions between the two imidazole moieties.
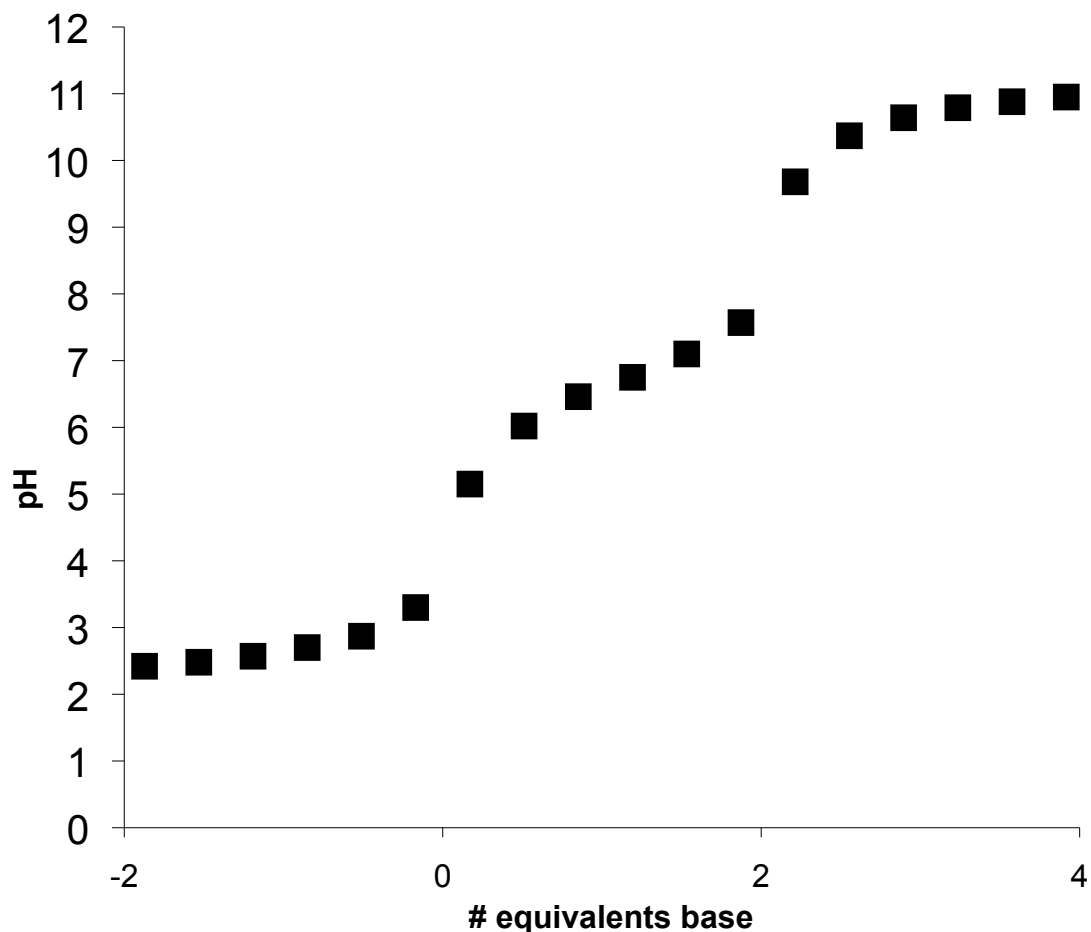
**Figure 52**. Titration curve for mHis dimer $128_2$.

## 2.4.2 Hydrolysis of *p*-nitrophenyl acetate catalyzed by mHis cyclic dimer.

Since the mHis cyclic dimer possesses two imidazole moieties, we wondered whether it would display hydrolytic activity toward *p*-nitrophenylacetate. Catalysis of *p*-nitrophenylacetate hydrolysis by mHis cyclic dimer $128_2$ was investigated by spectrophotometric assay of *p*-nitrophenol release at 320 nm. Reactions were carried out in 100 mM bis-tris buffer at pH 6.20, 6.60, and 7.00 at 25 °C. NPA concentration was 0.27 mM. Catalyst concentration was varied from 0.01 mM to 0.1 mM for $128_2$ and 0.1 mM to 1 mM for 4-methylimidazole . Second order rate constants were calculated by

plotting first order (in substrate) rate constant against catalyst concentration. The $k_2$ values for mHis cyclic dimer at pH 6.2, 6.6, and 7.0 were found to be 0.22, 0.83, and 0.95 $s^{-1}M^{-1}$, respectively. These values were found to be ten times the appropriate $k_2$ values for the electronically similar 4-methylimidazole (Fig 53; Table 3). The observed rate enhancement for the cyclic dimer catalyst relative to the simple imidazole could be explained by a greater effective concentration of a free imidazole unit in the dimer at pH 6.2-7.0 due to the greater acidity of protonated cyclic dimer. However, the fact that the pH profile of catalysis is similar for **128$_2$** and 4-methylimidazole argues against this. The enhanced catalysis observed for **128$_2$** may be due to participation of the second imidazole moiety. Though our results are not directly comparable to existing peptidic artificial esterases incorporating histidines[70,71] due to differences in experimental conditions, qualitatively the rate enhancements we observed are relatively small.
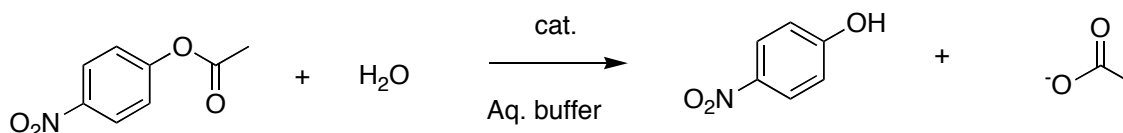


**Figure 53.** Catalytic hydrolysis of *p*-nitrophenylacetate.

**Table 3. Hydrolysis of *p*-nitrophenyl acetate catalyzed by dimer 128$_2$ and 4-methyl imidazole**

| pH | 128$_2$ cyclic dimer, $k_2/M^{-1}s^{-1}$ | 4-methylimidazole, $k_2/M^{-1}s^{-1}$ | background, $k_1/s^{-1}$ |
|---|---|---|---|
| 6.20 | 0.26 | 0.022 | 8.4E-06 |
| 6.60 | 0.83 | 0.083 | 1.7E-05 |
| 7.00 | 0.88 | 0.095 | 1.7E-05 |

**2.5 Conclusion**

We have synthesized two histidine derived pseudopeptide monomers which undergo thermodynamically controlled oligomerization under acidic conditions. Although the initial distribution of oligomers for both non-benzylated ($128_n$) and benzylated ($129_n$) systems included cyclic dimer, trimer, and tetramer, at eqilibrium both systems led exclusively to cyclic dimer. These results demonstrate that the monomer *mHis* can be incorporated into cyclic oligomers by dynamic combinatorial chemistry. The acid-base behavior of dimer $128_2$ was probed, and $128_2$ was found to hydrolyze NPA with a rate constant tenfold greater than 4-methylimidazole.

However, no conditions were found in which these libraries could be diverted from the all-dimer state by templating. Thermodynamic formation of the stable dimer salt is apparently controlled by an overwhelming driving force. Further, the highly acidic conditions required to render the hydrazone linkage kinetically labile also lead to the protonation of the histidine sidechains, rendering them insensitive to the presence of metals. Anionic templates were also unsuccessful, perhaps because the anions were highly solvated under the largely aqueous templating conditions. Although monomers of this type may prove useful in establishing DCLs with biomimetic functional diversity, the conditions required for hydrazone exchange preclude many biologically relevant interactions. Until these technical issues are overcome, this type of hyrazone pseudopeptide system is unsuitable for DCLs containing all but the most rudimentary catalytic function groups.

The problem of non-orthogonality of the exchange reaction and monomer-template interaction can in principle be addressed by modifying the chemistry of the monomer. For

example, the ligand/general base group could be modified to be less basic. Incorporation of nitro-groups (4-nitroimidazole) or other electron withdrawing motifs into the donor function group will decrease the basicity of the donor group, possibly preventing protonation under DCL conditions. However, this will also decrease the metal-binding ability of the ligand.Another strategy is to modify the hydrazide. Incorporation of electron-withdrawing groups on the hydrazide is known to increase the rate of the hydrazone exchange reaction under mildly acidic conditions. By these strategies, it should be possible to create conditions under which exchange and templating can occur simultaneously.

## 2.6 Experimental

**Materials and Methods**. All operations were carried out under nitrogen or argon by means of standard Schlenk and vacuum-line techniques.  Organic solvents were dried by standard procedures and distilled under $N_2$ before use.  $CH_2Cl_2$ was dried over $CaH_2$ and distilled under $N_2$ before use; THF was dried over Na using benzophenone as indicator and distilled under $N_2$ before use.  Methanol was dried over Mg and $I_2$ and distilled under argon. Ethyl acetate was dried over calcium hydride and distilled under argon. Glassware was oven-dried at 150 °C overnight.  IR spectra were recorded in KBr pellets with a Perkin-Elmer 283-B infrared spectrophotometer (resolution 4 cm$^{-1}$).  The $^1$H, and $^{13}$C NMR spectra were recorded on a Varian Mercury-300 spectrometer.  Mass spectra were acquired on a Finnigan TSQ 700 spectrometer in methanol or acetonitrile solution by ESI.  HPLC was carried out using Beckman System Gold with dual 110B solvent delivery pumps and 166 UV-vis detector with an ACE C-18 Ultrapure silica reverse phase column. HPLC-grade water and acetonitrile (Fisher) was filtered and

degassed before use. Reagents were purchased from Sigma-Aldrich. 3-(Dimethoxymethyl)benzoic acid (130)[31] and τ-benzyl-L-histidine **(132)** were prepared according to literature procedures.[72]

## 2.6.1 Synthesis of <u>3-(Dimethoxymethyl)benzoylhistidine methyl ester (131)</u>

Carbonyl diimidazole (1.82 g, 11.3 mmol) was dissolved in 45 mL of dry ethyl acetate.  3-Carboxybenzaldehyde dimethoxyacetal **(130)** (2.19 g, 11.2 mmol) was added to this solution, and the mixture was stirred under nitrogen for 3 hr.  The solution was refluxed overnight and the cooled.  L-histidine methyl ester dihydrochloride (4.06 g, 16.8 mmol) was added, followed by 6 mL (43 mmol) of triethylamine.  The mixture was stirred for 2 weeks at room temperature. The mixture was then diluted with 50 mL of chloroform and washed with saturated aqueous sodium bicarbonate (2 portions of 50 mL).  The resulting organic phase was evaporated *in vacuo* to produce 3.13 g of 3-(dimethoxymethyl)benzoylhistidine methyl ester as a light yellow foaming oil (80% crude yield).  This material was sufficiently pure to carry to the next step.

$^1$H-NMR: 300 MHz in CDCl$_3$; 7.97 (1H, s), 7.85 (1H, d, J=6.3 Hz), 7.62-7.64 (3H, m), 7.45 (1H, t, J=7.5 Hz), 6.87 (1H, s), 5.43 (1H, s), 5.00 (dt, J= 7.5, J= 5.1), 3.73 (3H, s), 3.33 (6H), 3.24 (2H, pseudo-t, J=9.3); Hi-res MS (ESI): 348.1533, Calc. mass (C$_{17}$H$_{22}$N$_3$O$_5$) 348.1559.
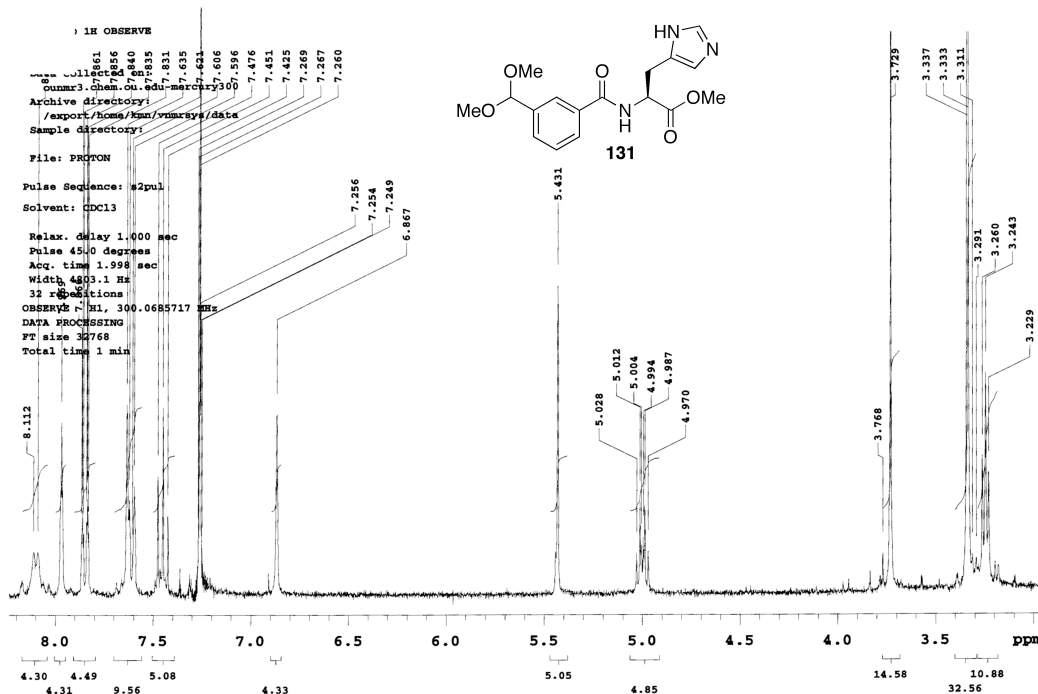
**Figure 54.** 300 MHz $^1$H-NMR spectrum of **131**

## 2.6.2 Synthesis of 3-(Dimethoxymethyl)benzoylhistidine hydrazide (128) (*m*His)

Crude 3-(dimethoxymethyl)benzoylhistidine methyl ester (**131**) (3.13 g, 9.00 mmol) was dissolved in 80 mL of methanol, filtered through filter paper, and treated with 2.5 mL hydrazine monohydrate. After 0.5 h stirring at room temperature, a white precipitate was observed. The mixture was stirred 72 h, evaporated *in vacuo*, and triturated three times with methanol. The insoluble solid product **128** was collected (2.64 g, 84% yield, 67% over two steps).

$^1$H-NMR: 300 MHz in 50% v/v CD$_3$CN/D$_2$O: 7.76 (1H, s), 7.73 (1H, d, J=9.3) 7.54-7.55 (2H, m), 7.45 (1H, t, J=7.5), 6.87 (1H, s), 5.38 (1H s), 4.70 (1H, dd, J=8.7, J= 6.0), 3.28 (6H), 3.03 (2H, m); $^{13}$C-NMR: 75.45 MHz in 50% v/v CD$_3$CN/D$_2$O: 172.5, 168.95, 139.8, 136.4, 134.7, 134.5, 131.1, 129.7, 128.6, 126.6, 117.5, 104.0, 54.0, 53.9, 30.1; IR: $\nu_{max}$/cm$^{-1}$ 3280, 3042, 2951, 2834, 1660, 1638, 1547; Hi-res MS (ESI): 348.1663, Calc. mass (C$_{16}$H$_{22}$N$_5$O$_4$) 348.1672.
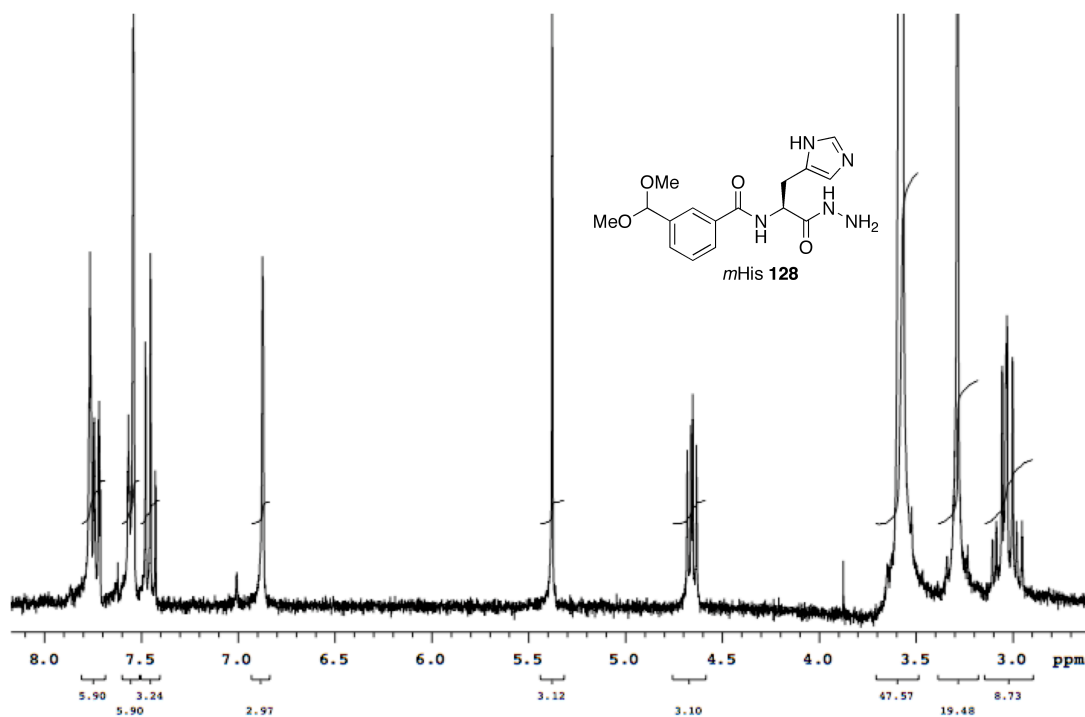


**Figure 54b.** 300 MHz $^1$H-NMR spectrum of **128**
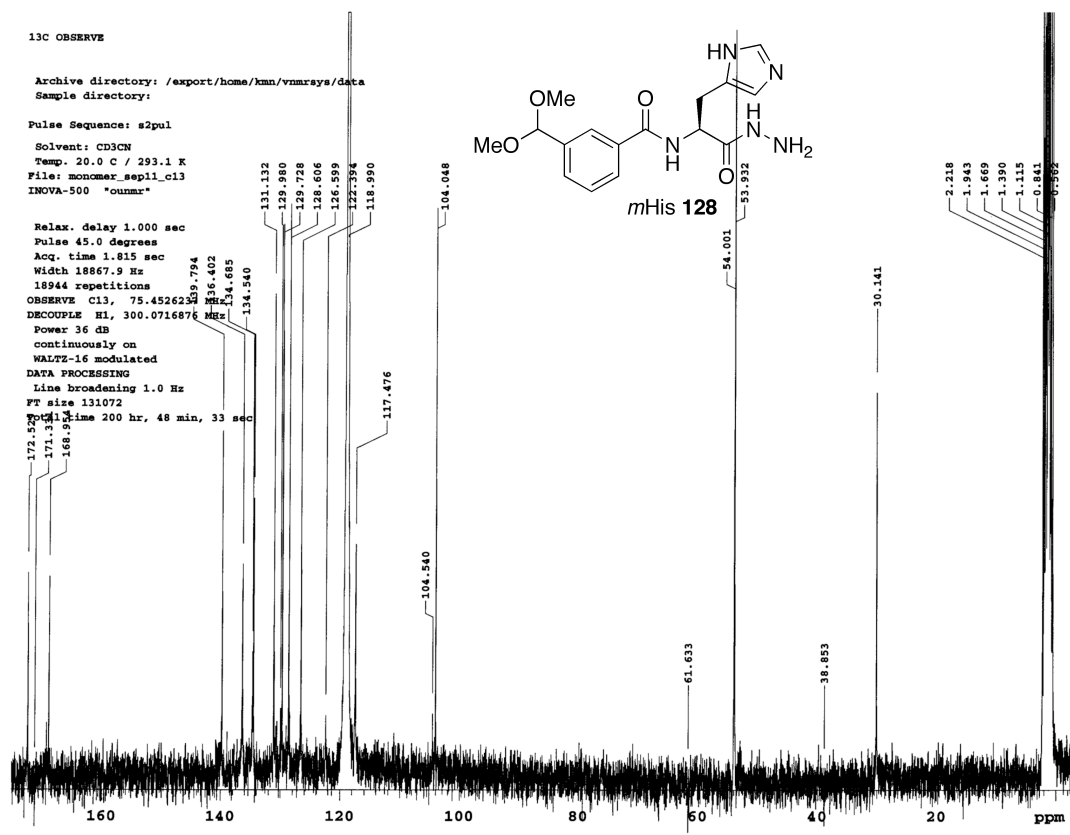
**Figure 54c.** $^{13}$C-NMR spectrum of **128**
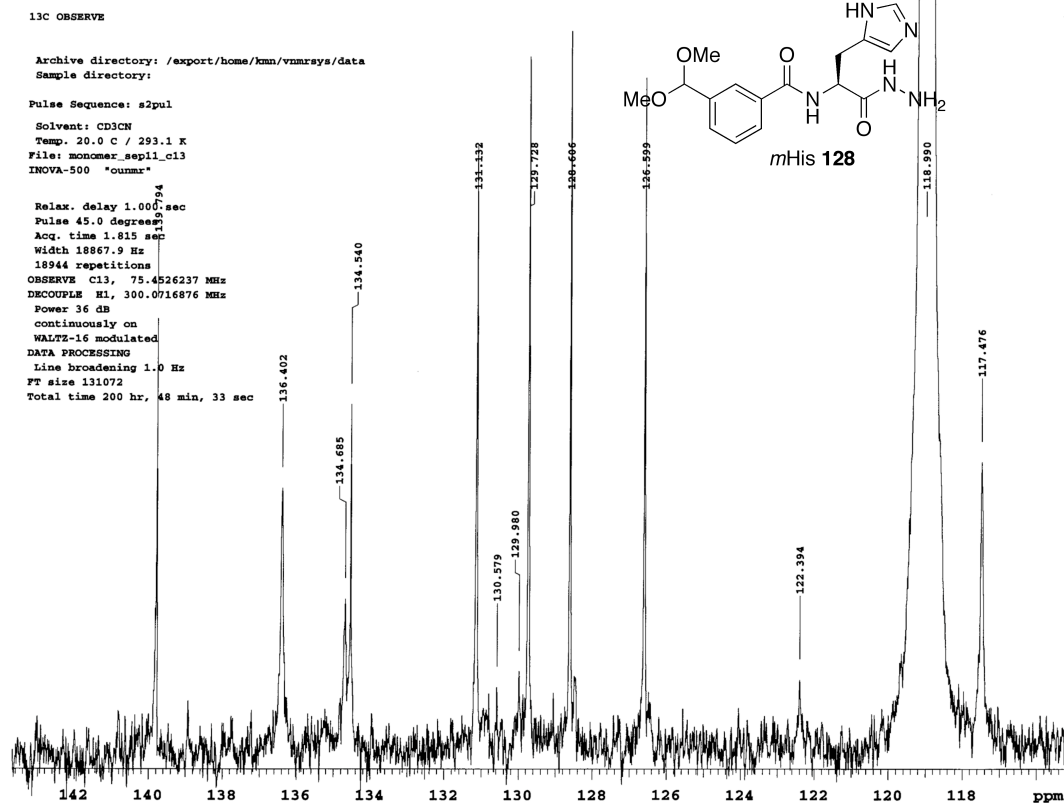
**Figure 54d.** $^{13}$C-NMR spectrum of **128** close-up

## 2.6.3 Synthesis of <u>τ -benzyl-L-histidine methyl ester dihydrochloride (133)</u>

τ-Benzyl-L-histidine **(132)** (6.5 g, 26.5 mmol) was placed in 100 mL of  3 M methanolic HCl and refluxed for 2 hours.  Solvent was removed under vacuum giving the crude τ-benzyl-L-histidine methyl ester dihydrochloride **(133), (**8.57 g, 97%). ESI-MS: 260.1397, M+H$^+$ (theoretical, 260.1399). 300MHz $^1$H-NMR in D$_2$O: 8.67 (1H, d, J=1.8 Hz), 7.26-7.36 (6H, m), 5.26 (2H, s), 4.30 (1H, t, J=6.9 Hz), 3.60, (3H, s), 3.26, (2H, d, J= 7.2 Hz).  $^{13}$C-NMR in D$_2$O: 169.54, 139.53; 136.09, 130.30, 129.47, 134.50, 128.37, 121.85, 54.68, 53.74, 52.57, 25.94.
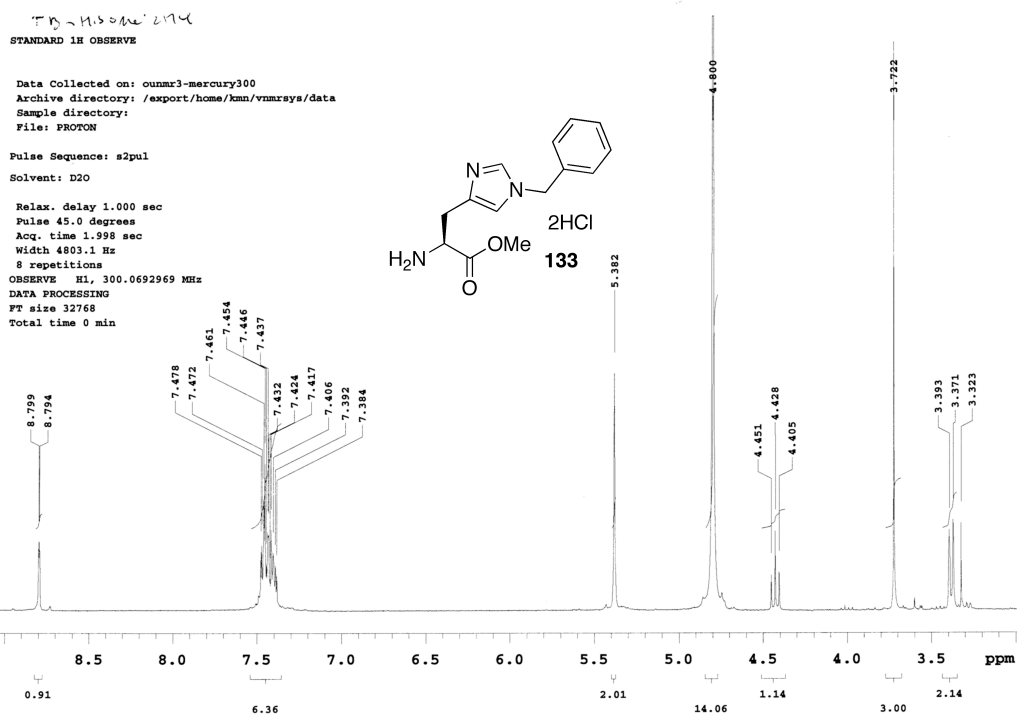
**Figure 54e.** $^1$H-NMR spectrum of **133**.
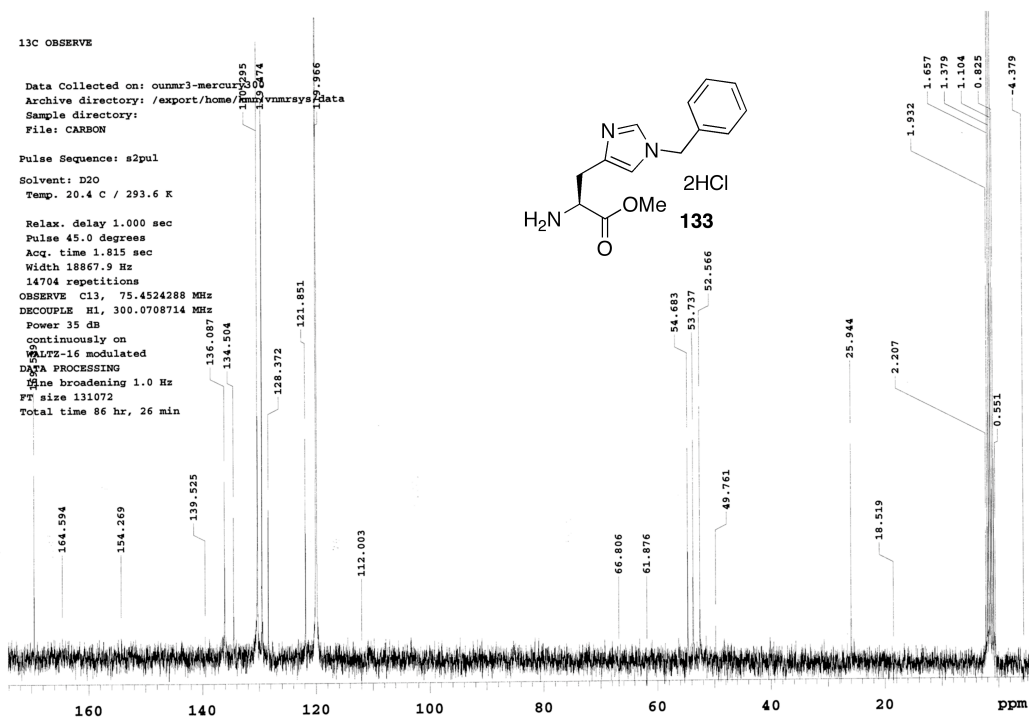
**Figure 55.** $^{13}$C-NMR spectrum of **133**.

## 2.6.4 Synthesis of 3-(dimethoxymethyl)benzoyl- τ -benzyl-L-histidine methyl ester (134)

τ-Benzyl-L-histidine methyl ester dihydrochloride (**133**) (0.85 g, 3.0 mmol), 3-(dimethoxymethyl)benzoic acid (**130**), (0.50 g, 3.0 mmol), and 1-hydroxybenzotriazole hydrate (0.40 g, 3.0 mmol) were placed in 100 mL dry THF and cooled in an ice bath. Triethylamine (1.18 mL, 9.9 mmol) was added, followed by ethyldiisipropyethylaminocarbodiimide hydrochloride (EDCI), (0.49 g 3.0 mmol). The reaction mixture was stirred for 4 days. Solvent was removed under vacuum. The crude residue was reconstituted in 200 mL chloroform and washed with three 10 mL portions of saturated sodium bicarbonate. The organic portion was dried with magnesium sulfate and

67

evaporated to brown crude oil. This was chromatographed on silica eluted with ethyl acetate to give 0.81 g of yellow oil (61.5 %). ESI-MS m/z 438.1937 (theory M+H$^+$ 438.2029). 300 MHz $^1$H-NMR in CDCl$_3$: 8.31 (1H, d J=7.5 Hz), 7.98 (1H, s), 7.83 (1H, d, J=8.1 Hz), 7.59 (1H, d, J=7.8 Hz), 7.48 (1H, s), 7.42 (1H, t, J=8.1 Hz), 7.24-7.33 (3H, m), 7.08-7.11 (2H, m), 6.68 (1H, s), 5.41 (1H, s), 5.04 (2H, s), 4.95 (1H, m), 3.64 (3H, s), 3.31 (6H, s), 3.14 (2H, m). $^{13}$C NMR: 172.20, 167.07, 138.79, 138.32, 137.36, 136.08, 134.26, 130.00, 129.25, 128.66, 128.59, 127.55, 127.45, 126.21, 117.31, 102.84, 53.18, 52.97, 52.94, 52.48, 51.12, 29.67.
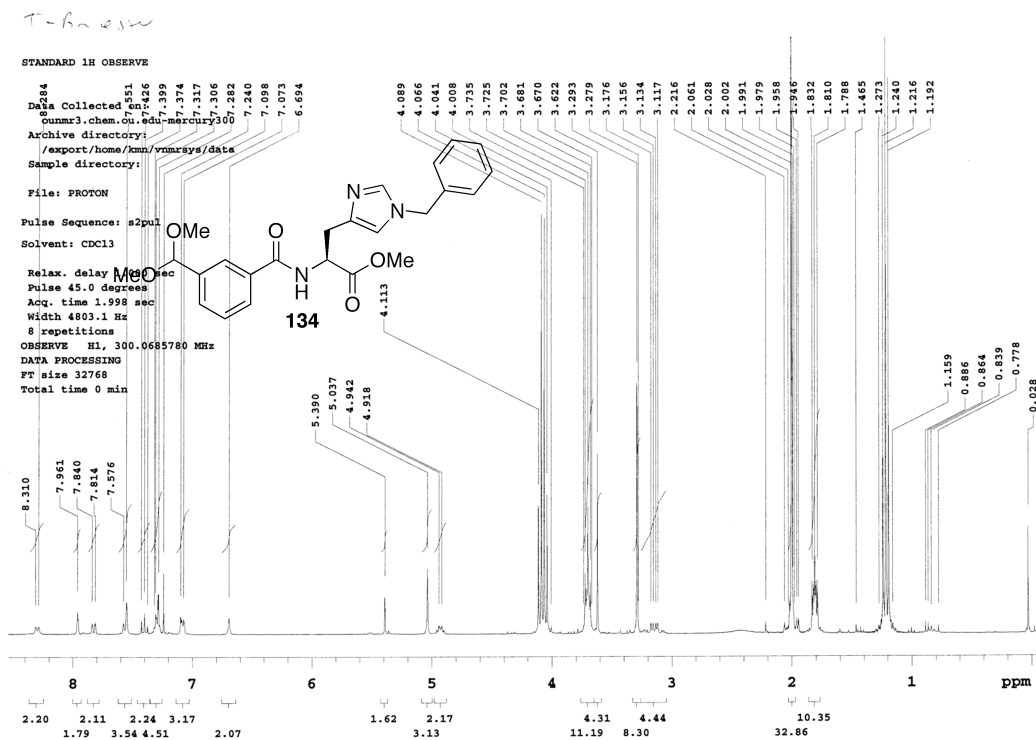


**Figure 56.** $^1$H-NMR spectrum of **134**.

68
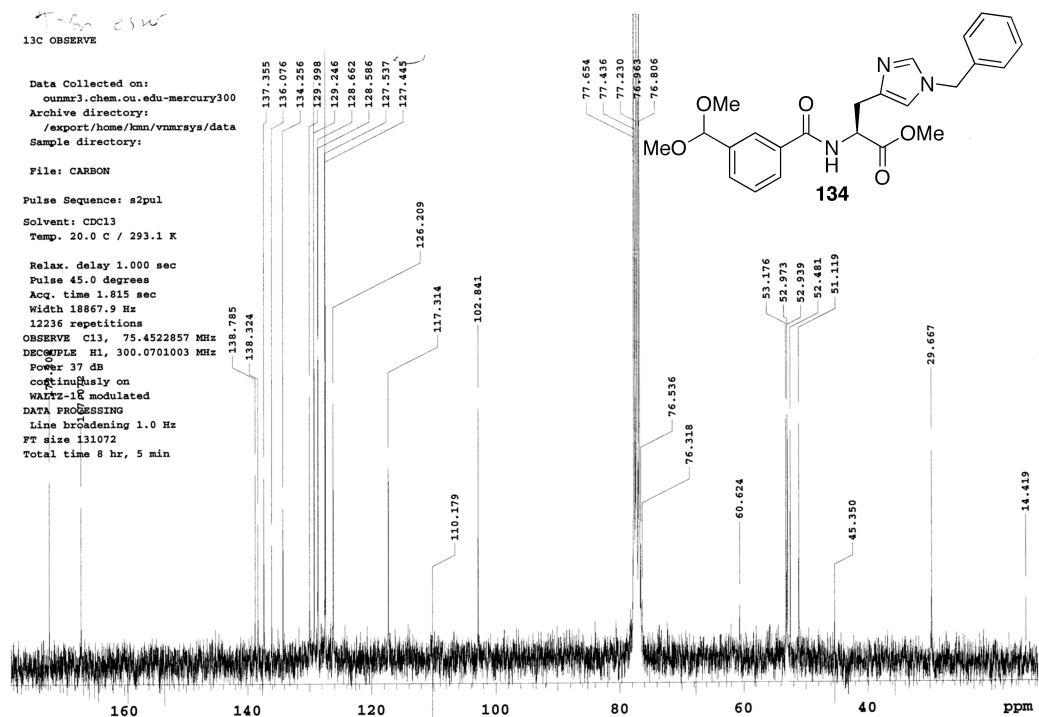
**Figure 57.** $^{13}$C-NMR spectrum of **134**.

## 2.6.5 Synthesis of 3-(dimethoxymethyl)benzoyl-τ-benzyl-L-histidine hydrazide (129)

3-(Dimethoxymethyl)benzoyl-τ-benzyl-L-histidine methyl ester **(134)** (0.81 g, 1.85 mmol) was dissolved in 20 mL of dry methanol and treated with 1 mL of hydrazine monohydrate. After stirring for 3 days at room temperature, solvent was removed under vacuum and the crude product was chromatographed on silica (9:1 dichloromethane/methanol) to give 0.405 g (50%) 3-(dimethoxymethyl)benzoyl-t-benzyl-L-histidine hydrazide. ESI-MS m/z 438.2112 (theory M+H$^+$ 438.2143). 300 MHz $^1$H-NMR in CDCl$_3$: 8.54, (1H, d, J=6.6 Hz), 7.96 (1H, s), 7.82 (1H, d, J=7.8 Hz), 7.57 (1H, d, J=7.5 Hz), 7.37-7.45 (2H, m), 7.24-7.30 (3H, m), 7.07-7.10 (2H, m), 6.74 (1H, s), 5.39

69

(1H, s), 5.00 (2H, s), 4.84 (1H, q, J=5.4 Hz), 3.29 (6H, s), 2.90-3.18 (2H, m). $^{13}$C NMR:

171.80, 167.22, 138.71, 138.37, 136.872, 135.89, 133.69, 130.09, 129.05, 128.67, 18.38,

127.45, 127.34, 125.84, 117.49, 102.51, 52.95, 52.76, 52.74, 51.12, 29.62.
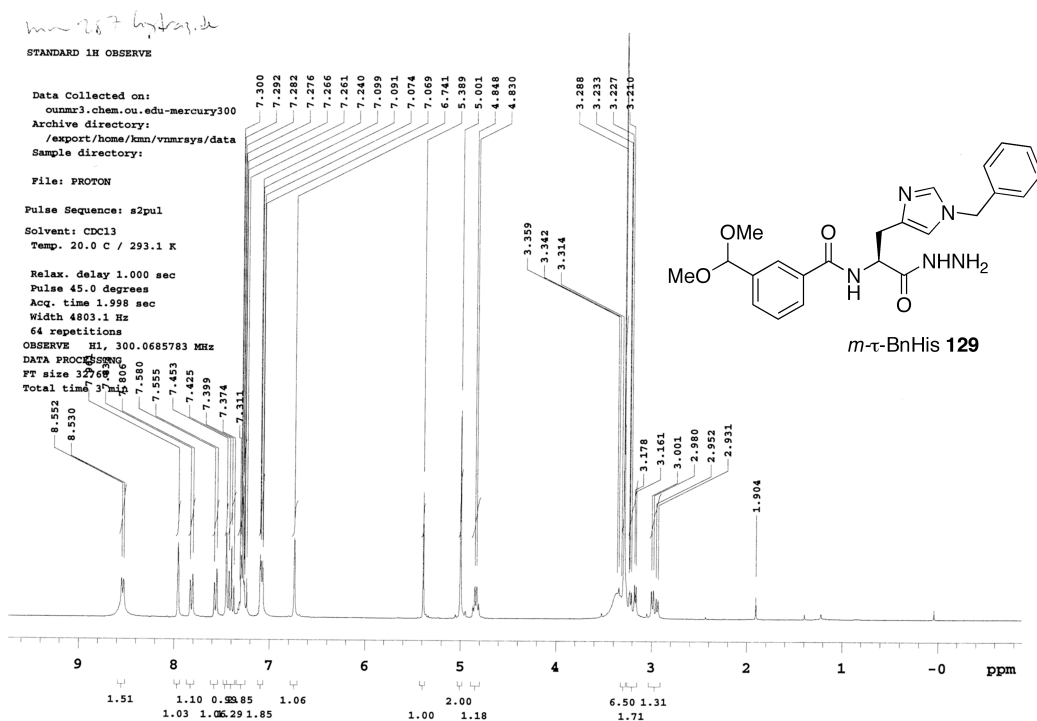


**Figure 58.** $^1$H-NMR spectrum of **129**.
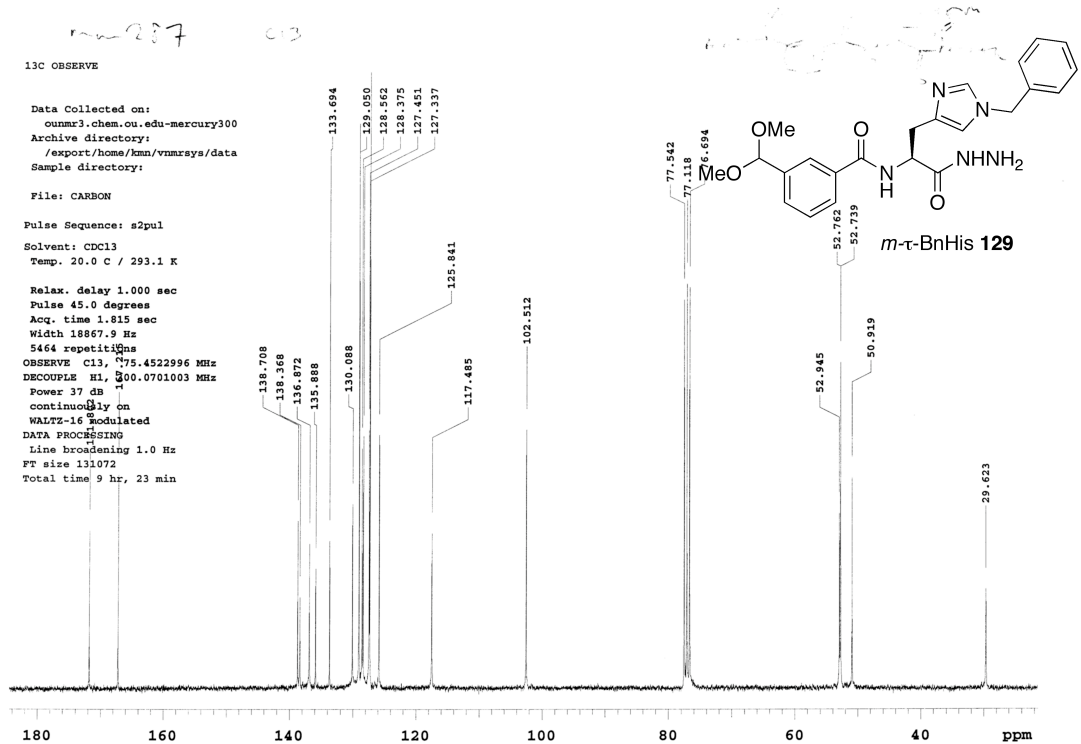
**Figure 59**. $^{13}$C-NMR spectrum of **129**.

## 2.6.6 Oligomerization of 128 (mHis monomer)

Analytical scale: monomer **128** (1.0 mg 2.88 mmol) was placed in 1 mL 75% acetonitrile v/v aqueous solution (2.88 mM). This was treated with 10 μl TFA (0.13 mmol, 46-fold excess) or 60 mL of 53.7 mM stock solution (0.2 mL in 50 mL) of TFA in water (1.1 eq. TFA with respect to **128**).

Cyclic dimer **128₂** (preparative scale): **128** (100 mg, 288 mmol) was placed in 100 mL of 75% acetonitrile v/v aqueous solution. Concentrated hydrochloric acid (0.5 mL) was added, and the solution was stirred for two weeks. The mixture was evaporated *in*

*vacuo* to produce a white amorphous solid (crude cyclic dimer hydrochloride salt). No further purification was required.

$^1$H-NMR 300 MHz in CD$_3$OD: $\delta_H$ 8.75 (1H, s), 8.69 (1H, s), 7.81 (1H, s), 7.69 (1H, pseudo-dt, J= 6.9, J=1.8), 7.35-7.43 (3H, m), 5.76 (1H pseudo-t, J=7.2 Hz), 3.40 (1H, dd, J= 15.6, J= 6.3Hz), 3.21 (1H, dd, J= 15.3, J= 7.5); $^{13}$C-NMR: 100.57 MHz in CD$_3$OD: 171.0, 167.1, 143.3, 134.7, 133.1, 132.5, 131.0, 130.6, 128.3, 127.1, 124.2, 117.3, 49.7, 26.0. ESI-MS: m/z=284.1, 284.6; Hi-res MS(ESI): 567.2278, Calc. Mass (C$_{28}$H$_{27}$N$_{10}$O$_4$) 567.2211.
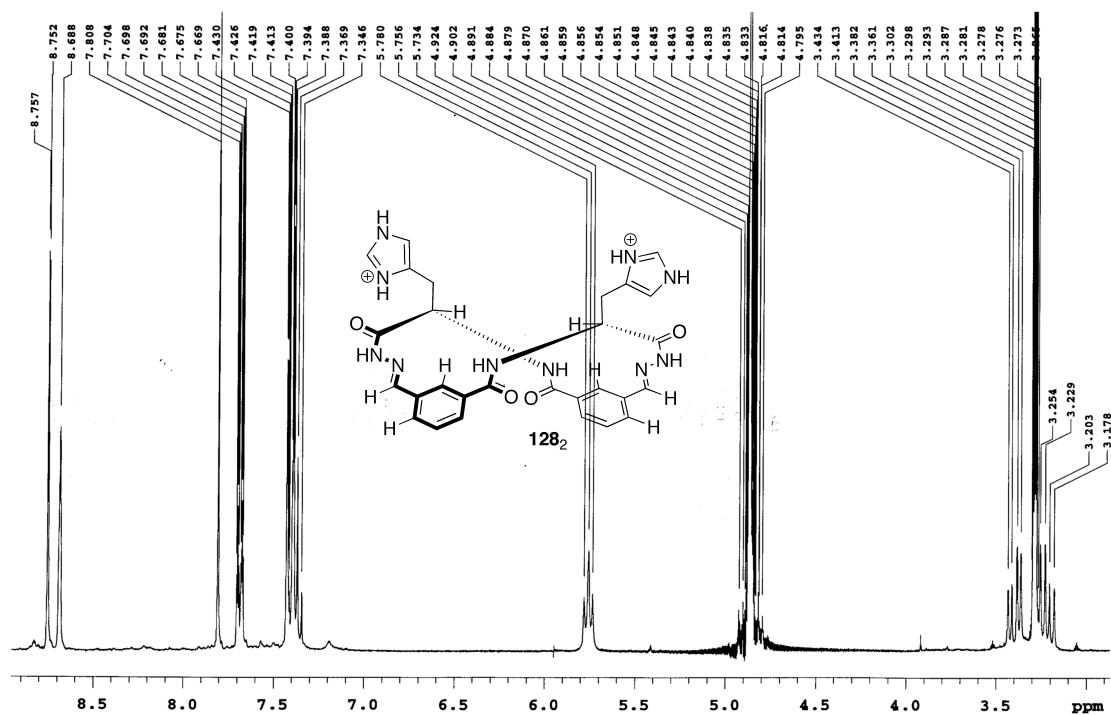


**Figure 60.** $^1$H-NMR spectrum of **128$_2$**.
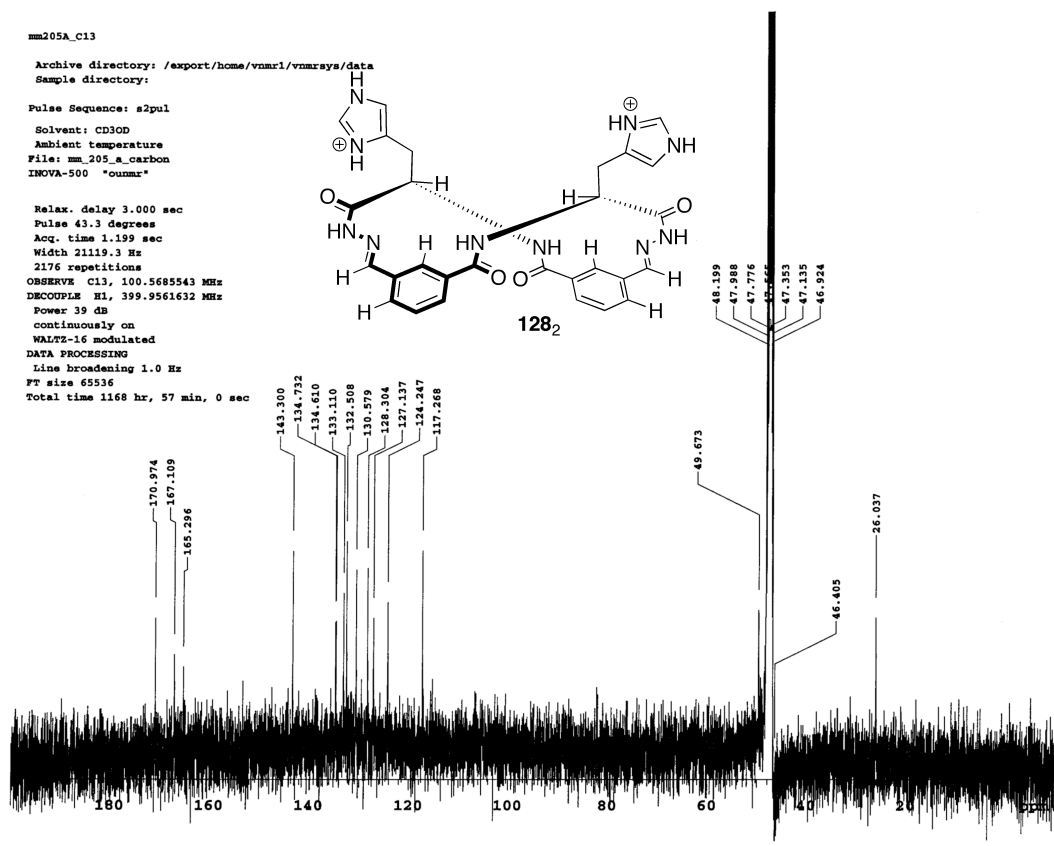
**Figure 61.** $^{13}$C-NMR spectrum of **128$_2$**.
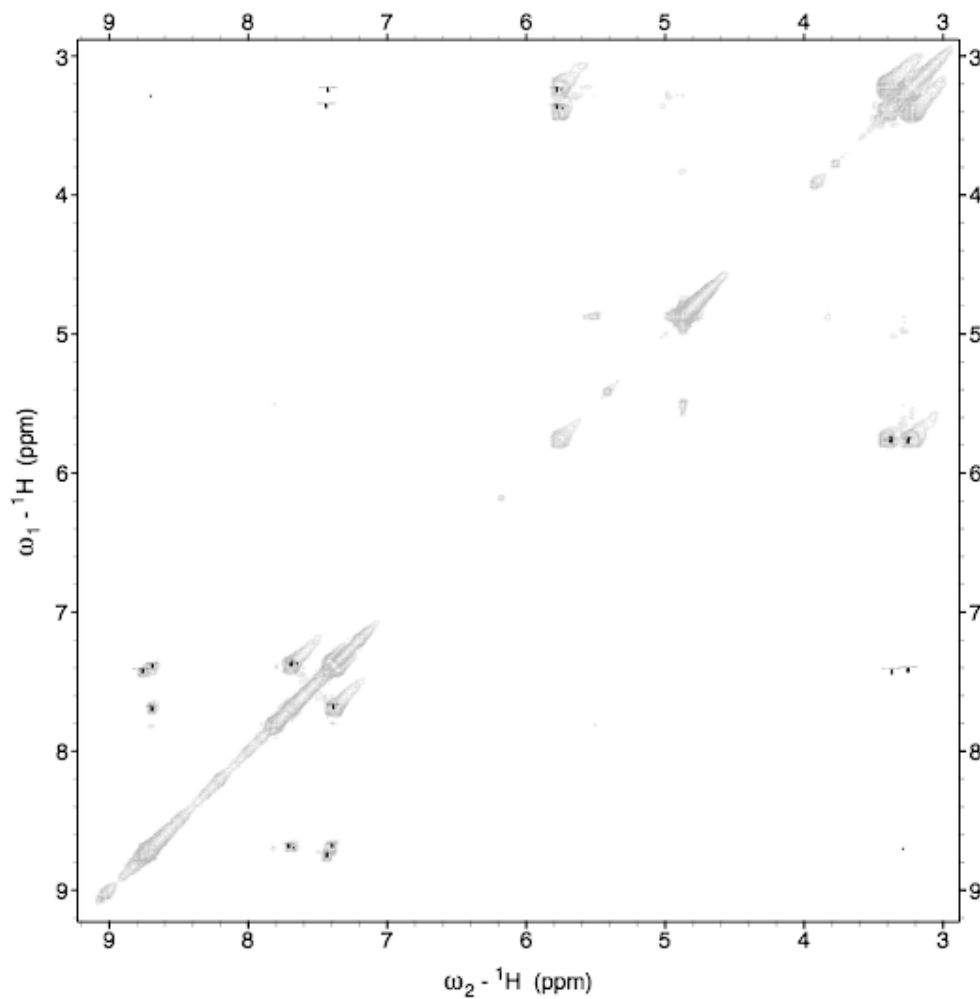
**Figure 62.** 300 MHz gCOSY of **128₂**.
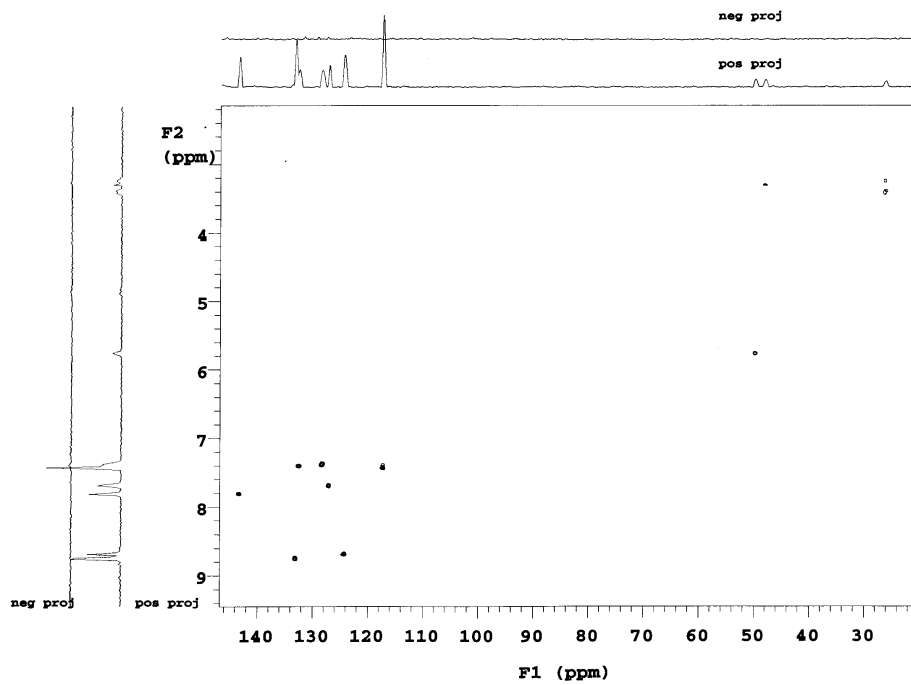
**Figure 63.** 400 MHz HSQC of **128**$_2$.
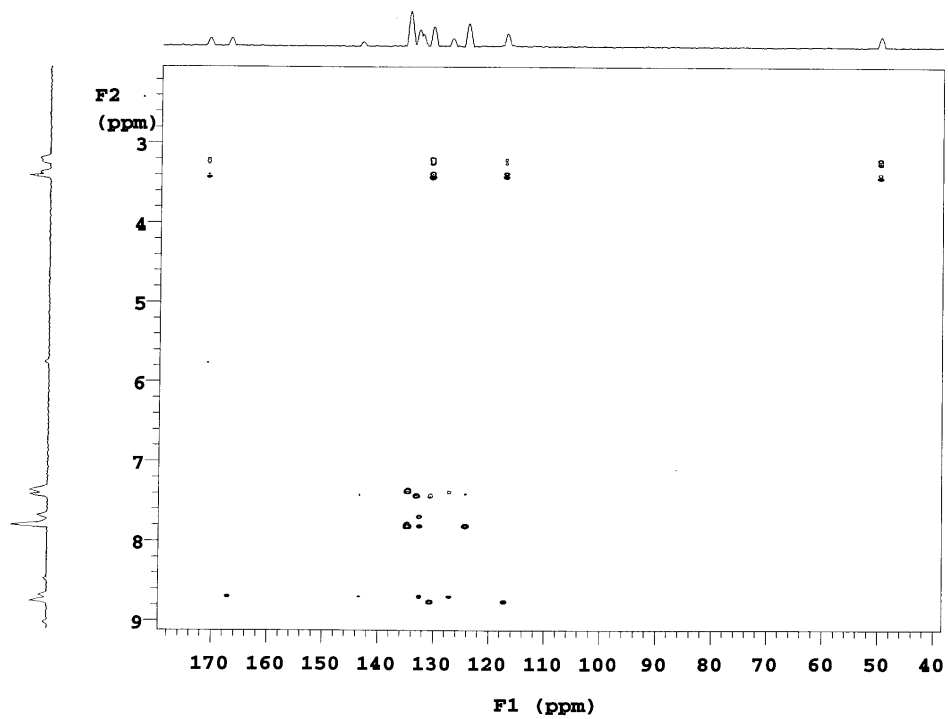


**Figure 64.** 400 MHz HMBC of **128**$_2$.
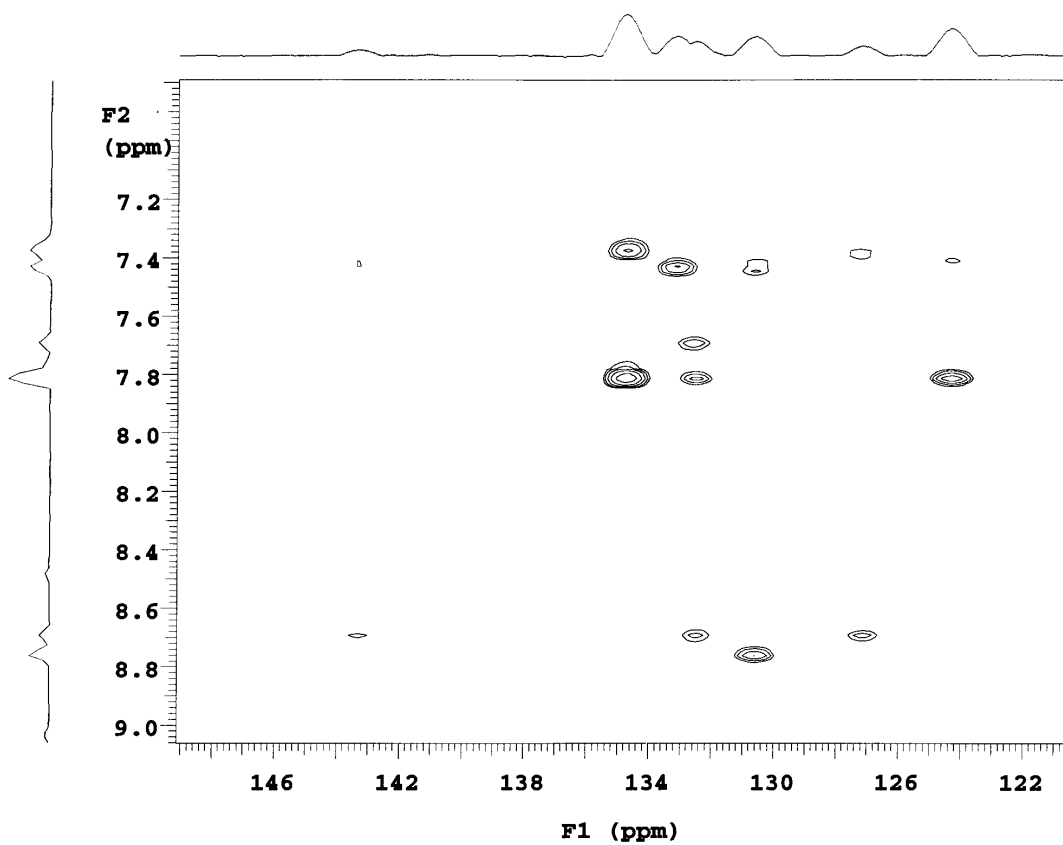
**Figure 65.** 400 MHz HMBC of **128₂**. Magnification of aromatic and imidazole signals.

**Figure 66.** 300 MHz NOESY (green/red) with superimposed *g*COSY (cyan)of **128₂**.

### 2.6.7 HPLC Method

HPLC analysis was carried out on a Beckman System Gold HPLC with an ACE C-18 column. Samples were diluted in water before injection. Samples were eluted with a gradient of 15% acetonitrile to 100% acetonitrile over 25 minutes. Effluent was collected and analyzed by ESI-MS. [ESI MS specifications]

Peak A, 6.73 min.; Peak B, 15.39 min.; Peak C, 16.93 min.

### 2.6.8 ESI MS of mHis oligomeric mixture

Peak A, dimer, m/z=284.1, 284.6 ($M_2H_2^{2+}$); Peak B, tetramer, m/z=378.5, 378.8, 379.1 ($M_4H_3^{3+}$); Peak C, trimer, m/z=284.1, 284.4, 284.8 ($M_3H_3^{3+}$); m/z=425.6, 426.1 ($M_3H_2^{2+}$).

### 2.6.9 Time-dependent NMR

Monomer **128** (1.0 mg, 2.88 mmol) was dissolved in a 3:1 mixture of $CD_3CN$ and $D_2O$. The solution was treated with 0.01 ml (46-fold excess) deuterio-trifluoroacetic acid. The sample was analyzed by $^1H$ NMR over 15 hours.

### 2.6.10 Catalysis of *p*-nitrophenylacetate hydrolysis by mHis cyclic dimer

All reactions were carried out in 100 mM Bis-tris buffer and analyzed spectrophotometrically at 320 nm at 25 °C in a 1 cm cuvette. Assays were carried out at pH 6.20, 6.60, and 7.00. *p*-Nitrophenylacetate concentration was 2.69 x $10^{-4}$ M. 4-methylimidazole and mHis cyclic dimer concentrations were varied. First order constants

$k_1$ were calculated from initial rates and substrate concentrations. First order constants $k_1$ were plotted against catalyst concentration to give apparent second order constant $k_2$.
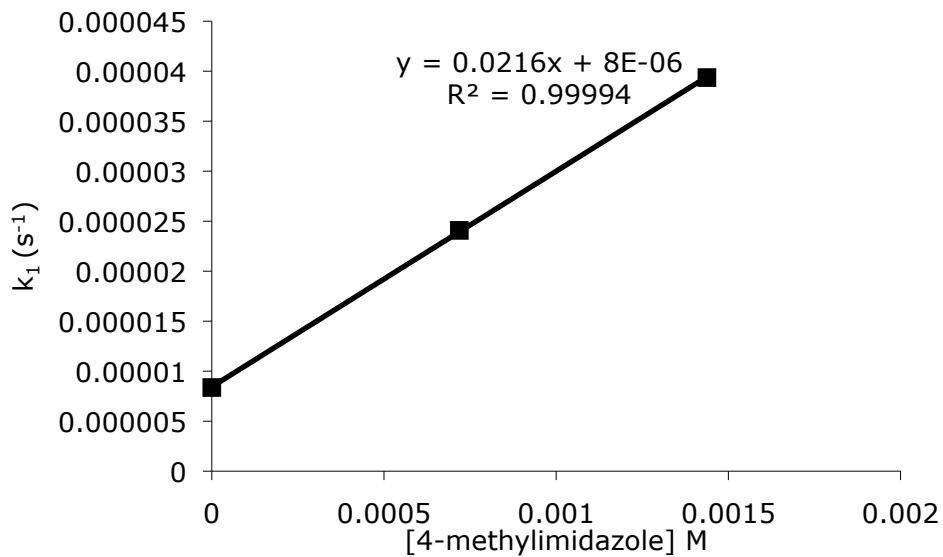


**Figure 67.** Catalyst-dependence of kinetics of NPA hydrolysis by 4-methylimidazole at pH 6.2.
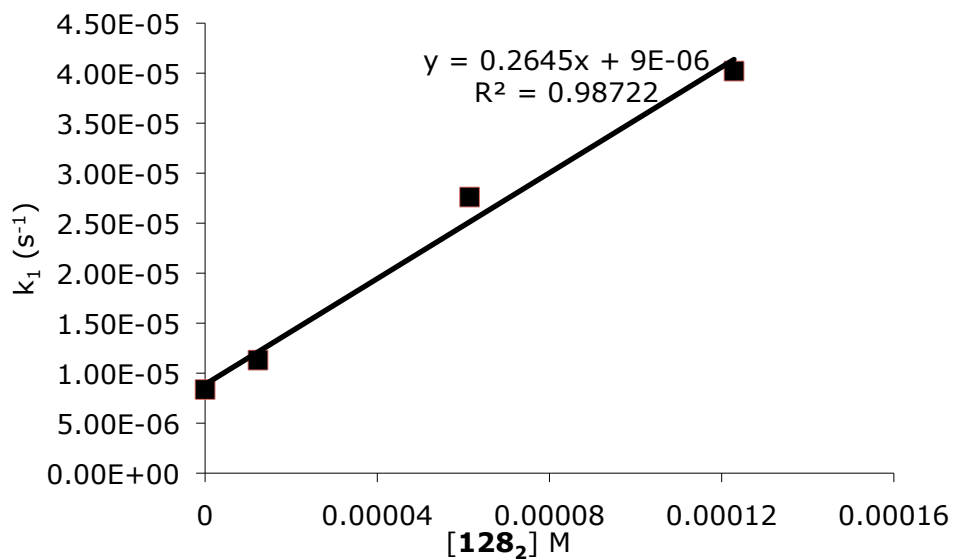


**Figure 68.** Catalyst-dependence of kinetics of NPA hydrolysis by **128₂** at pH 6.2.
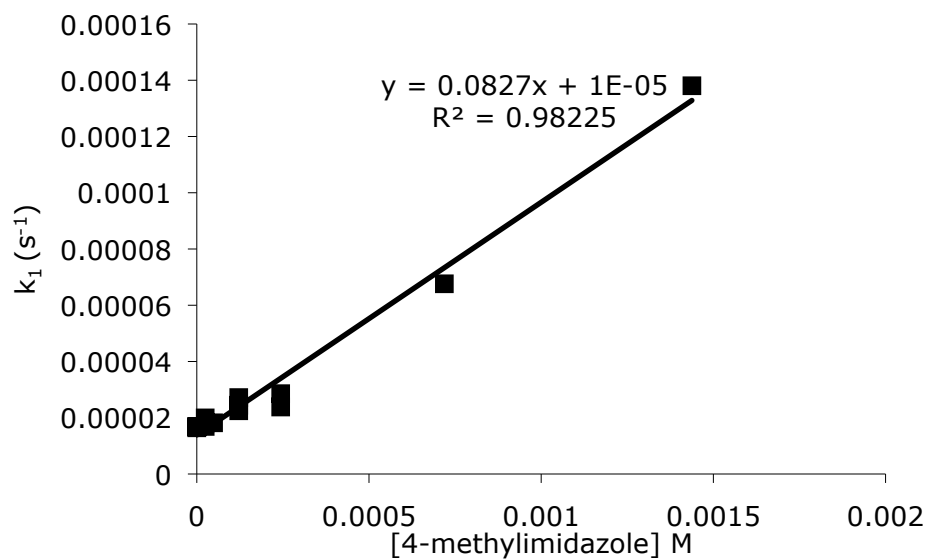
**Figure 69.** Catalyst-dependence of kinetics of NPA hydrolysis by 4-methylimidazole at pH 6.6.
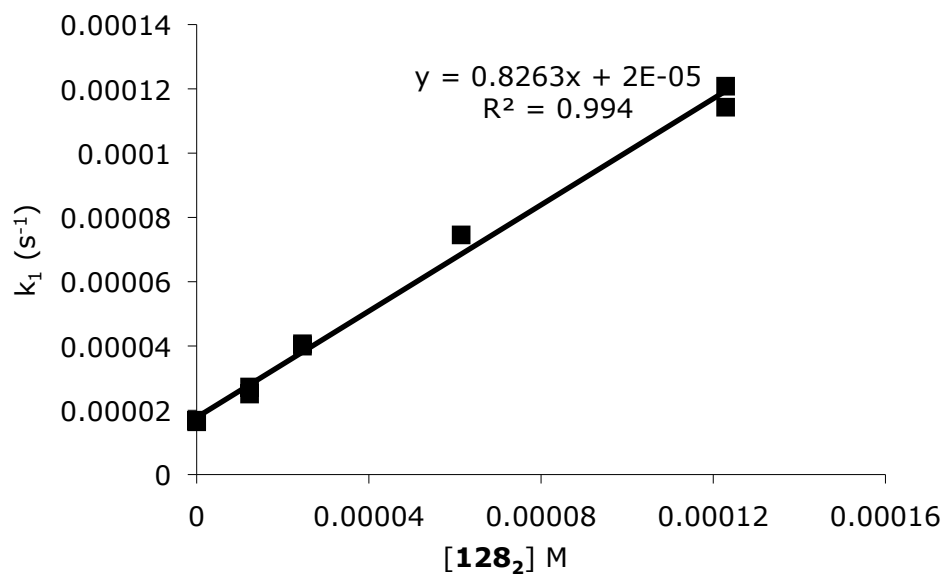


**Figure 70.** Catalyst-dependence of kinetics of NPA hydrolysis by $128_2$ at pH 6.6.
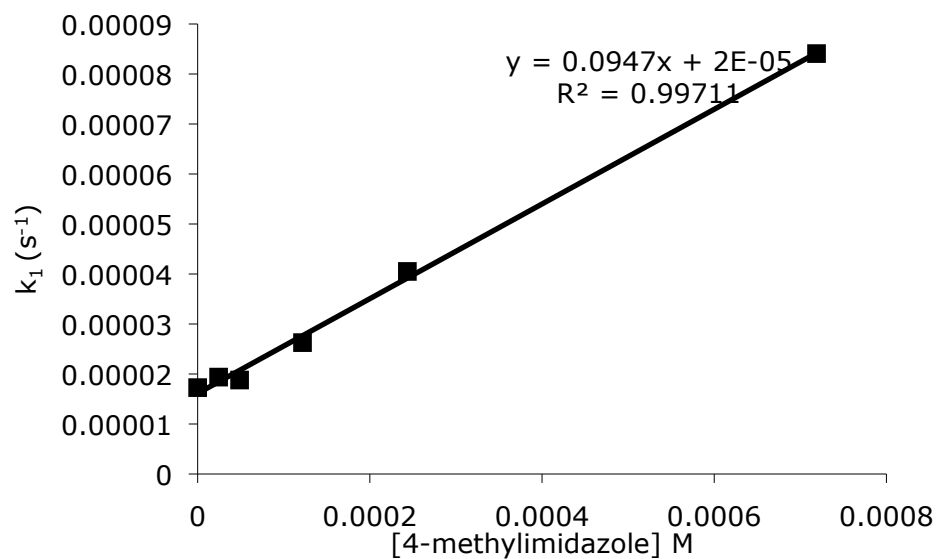
**Figure 71.** Catalyst-dependence of kinetics of NPA hydrolysis by 4-methylimidazole at

pH 7.0.
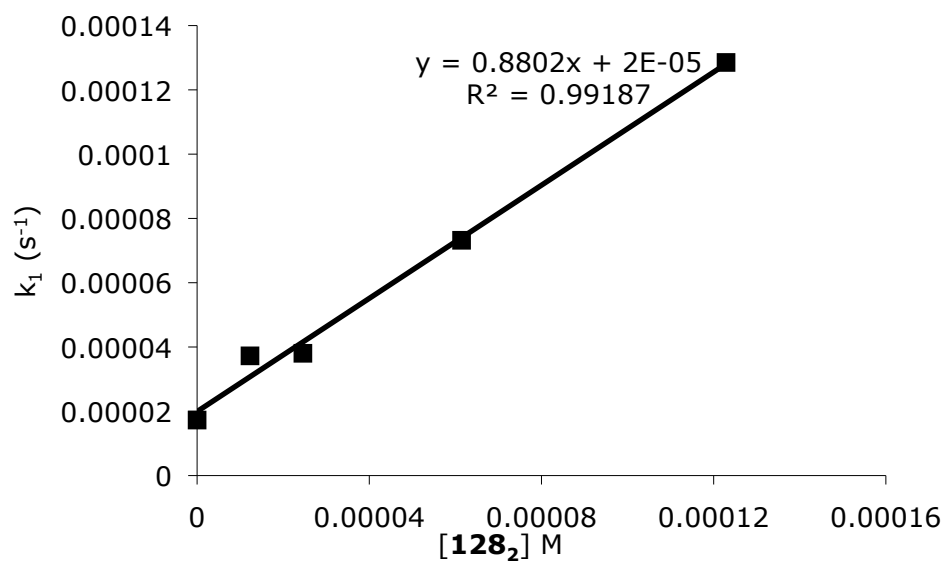


**Figure 72.** Catalyst-dependence of kinetics of NPA hydrolysis by **128₂** at pH 7.0.

**2.6.11 Formation of oligomer libraries from BnHis monomer**

3-(Dimethoxymethyl)benzoyl-τ-benzyl-L-histidine hydrazide **129** (2.5 mg, 5.7 mmol) was placed in 75% acetonitrile/25% water (v/v, 1 mL) and treated with 5 μl trifluoroacetic acid.

**2.6.12 Analysis of BnHis oligomer libraries by HPLC/ESI-MS**

A 50 μL aliquot of the unequilibrated τ-BnHis oligomer library at 24 hours was analyzed by HPLC using 25% acetonitrile 75% water (50 ppm TFA) as eluent. Fractions were collected and analyzed by ESI-MS.

**2.6.13 Analysis of BnHis oligomer libraries by NMR**

Monomer **129** (2.5 mg, 5.7 mmol) was dissolved in a 3:1 mixture of $CD_3CN$ and $D_2O$. The solution was treated with 0.01 mL (23-fold excess) deuterio-trifluoroacetic acid. The sample was analyzed by $^1H$ NMR over 15 hours. The dimer histidine alpha peak is seen to increase in size over 15 hours. After 60 hours, the reaction mixture was observed to have evolved to all cyclic dimer.

**2.6.14 Preparative synthesis of BnHis cyclic dimer 129₂**

3-(Dimethoxymethyl)benzoyl-τ-benzyl-L-histidine hydrazide **129** (100 mg, 0.23 mmol) was dissolved in 40 mL 75% acetonitrile/25% water v/v. This solution was treated with 0.5 μL trifluoroacetic acid. After 10 days, solvent was removed under high vacuum and the residue was dried under sodium hydroxide to give 89 mg (0.091 mmol, 79%) τ-BnHis cyclic dimer ditrifluoroacetic acid salt.

300 MHz $^{1}$H-NMR in d4 methanol: 8.93 (1H, d, J=1.5 Hz), 8.66 (1H, s), 7.84 (1H, s), 7.56 (1H, dt, J=8.1 Hz, 0.9 Hz), 7.44-7.41, (2H, m), 7.34, (1H, t, J=7.2 Hz), 7.28-7.15, (5H, m), 5.83, (1H, m), 5.35, (2H, m), 3.36-3.29, (1H, m), 3.22-3.14, (1H, m). $^{13}$C-NMR: 172.54, 168.75, 144.98, 136.38, 136.31, 136.04, 135.59, 134.02, 133.12, 130.34, 130.11, 129.91, 129.20, 128.50, 126.10, 121.77, 53.813, 50.81, 27.90. NOESY: Strong NOE crosspeaks are present between alpha proton (5.83) and aromatic 2 position (8.66), and also between imine CH (7.84) and aromatic 4 position (7.41), indicating a conformation in which the imidazole-bearing sidechains are oriented outward from the macrocyclic structure. ESI-MS: m/z 747.3380 M+H$^{+}$ (calculated 747.3156).
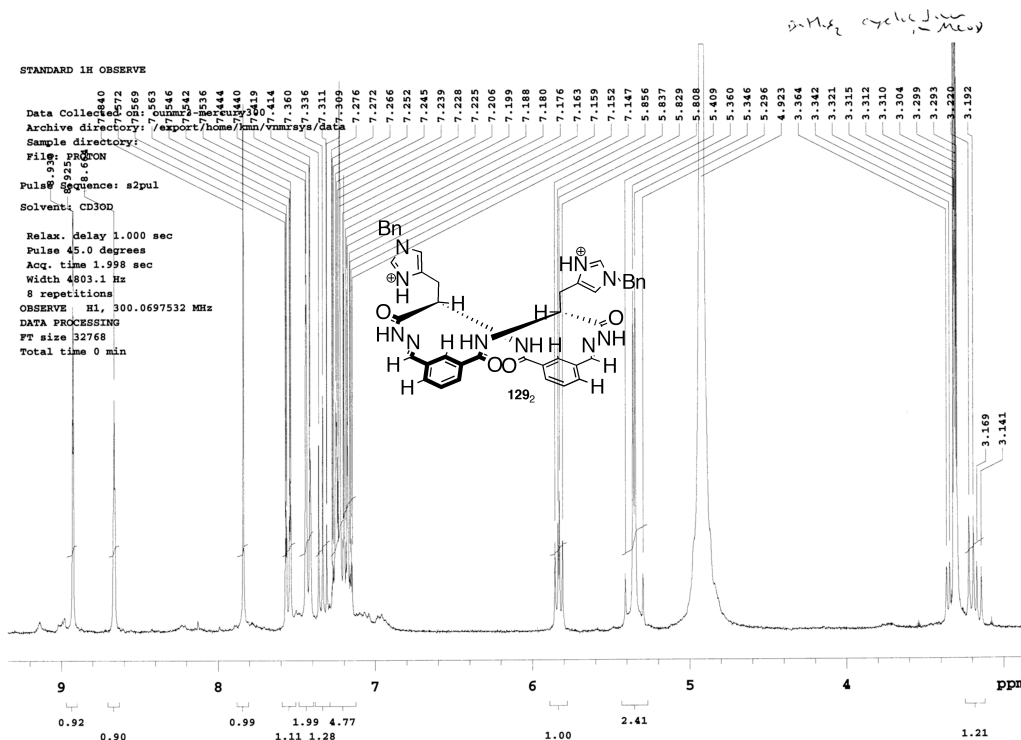


**Figure 73.** $^{1}$H-NMR spectrum of **129$_2$**.
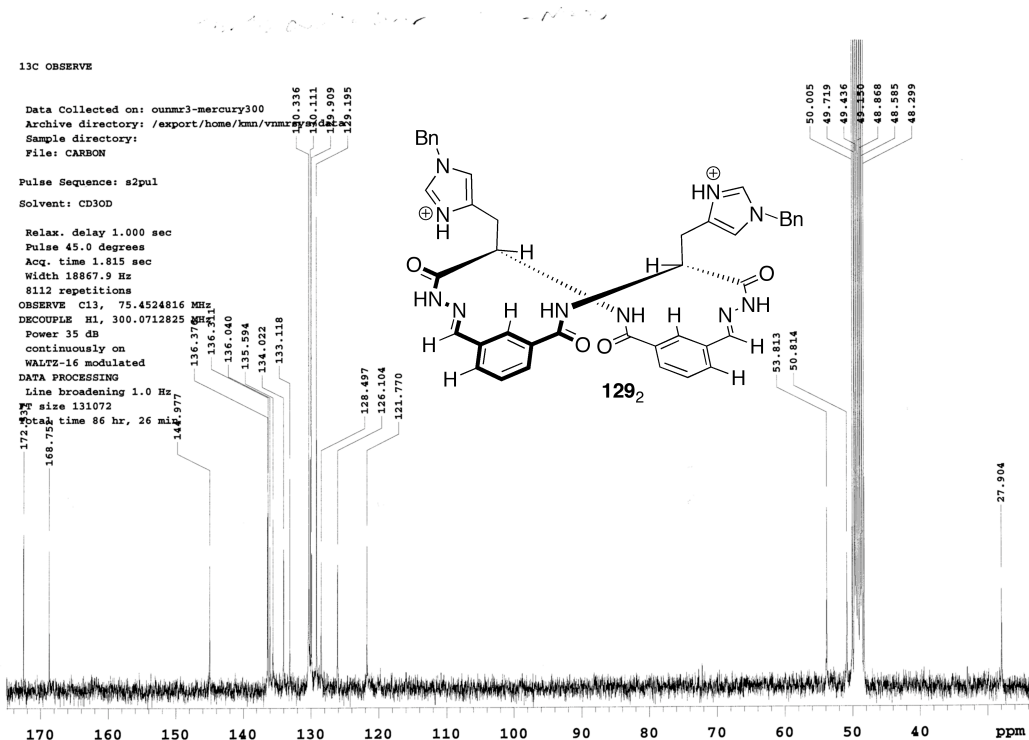
**Figure 74.** $^{13}$C-NMR spectrum of **129$_2$**.

## 2.6.15 Templating Experiments for 128 and 129

Solutions of monomer (**128** or **129**, 5 mM) were prepared in 75% acetonitrile 25% water and treated with a stock solution of TFA in acetonitrile to bring the amount of TFA to 1.5 equivalents in relation to monomer. Templating agents were added to these solutions using stock solutions. Templates were added in 0.33 equivalent, 1 equivalent, and 10 equivalent quantities. Templating agents used include zinc triflate, copper (II) triflate, cobalt (II) chloride, nickel (II) chloride, iron (II) chloride, cadmium (II) chloride, mercury (II) chloride. Organic templates which were used include diphenylphosphate,

trimesic acid, phosphoryl choline, *p*-toluenesulfonic acid, and phosphoric acid.  Samples

were analyzed over days by diluting in water (10:1) followed by HPLC analysis.

# 3 CATALYST EVOLUTION VIA TRANSITION STATE ANALOG-TEMPLATED DYNAMIC COMBINATORIAL LIBRARIES

## 3.1.1 Zinc metalloenzymes as inspiration

Zinc is one of the most biologically important metals. Not only does nature utilize zinc in various structural motifs (zinc finger), but it exploits the characteristic coordinative flexibility, intermediate Lewis acidity, and fast ligand exchange kinetics to carry out an array of catalytic reactions including the hydrolysis of esters, amides, and phosphate diesters, as well as transfer oxidations (alcohol dehydrogenase) and carbon-carbon bond forming reactions (type-II aldolase).[73]

Because the zinc (II) ion has a $d_{10}$ electronic configuration, it experiences no ligand field effects; it is for all intents and purposes a sphere with high coordinative flexibility. The geometry of zinc complexes therefore depends heavily on the nature of the ligand. This poses difficulties for zinc chemistry since this coordinative flexibility essentially means it is very difficult to control the geometry of the zinc complex without specially designed ligands. On the other hand, it provides an interesting opportunity for DCL, since the goal of ligand/metal complex DCL is the selection of ligand architecture from a ligand library. Because of the wealth of biological examples of zinc-mediated catalysis, we can safely assume a vast "catalytic space" of ligand-controlled reactivity for zinc-containing catalysts. However, this space remains largely unexplored because of the ligand-controlled nature of zinc reactivity. This is precisely why zinc complexes should be attractive as a target for dynamic chemistry: their reactivity is highly dependent on

ligand design, and there are many known (biological) examples of interesting zinc catalysis.

The literature of the biological catalysis of zinc is vast, and within it there is a huge amount of work on synthetic mimics of zinc enzymes.[74] Because of the difficulty of constructing the appropriate tripodal ligand-set for a true hydrolase mimic, we decided to forgo an accurate reproduction of a biological catalyst in favor of a much more synthetically accessible zinc Schiff-base complex. Some of the problems that this presents are the lack of rigidity of the coordination behavior of such ligands, and the resulting tendency toward meridional coordination of the metal.[74] We were prepared to accept this compromise, based on practical considerations.


### 3.1.2 Design concept and strategy: criteria for catalyst DCL

We learned from the first stage of our project some key factors vital to successful DCL design. Roughly in the order of importance, these factors are: 1) Orthogonality of the exchange reaction and the templating interaction, 2) TSA template fidelity, 3) catalytic relevance of the building blocks.

We chose to work with a zinc Schiff base complex-based system for a variety of reasons. First, the chemistry of the azomethine linkage is well understood, and is labile to imine exchange reactions under near-neutral conditions. Importantly, the exchange reaction occurs in the presence of zinc and does not interfere with zinc binding. This satisfies the criteria of orthogonality of exchange reaction and recognition event. Second, the ligand-exchange kinetics for zinc are very fast (the rate constant for water exchange on zinc ion is on the order of $10^7$ $s^{-1}$).[75] This helps to ensure that the mixture will

equilibrate in a reasonable amount of time. The reaction we chose, metal-catalyzed esterolysis, is one which has been fairly well studied, and for which a reasonable TSA could be synthesized. Finally, an imine-ligand library could be generated which would produce zinc complexes which could catalyze the hydrolysis reaction.
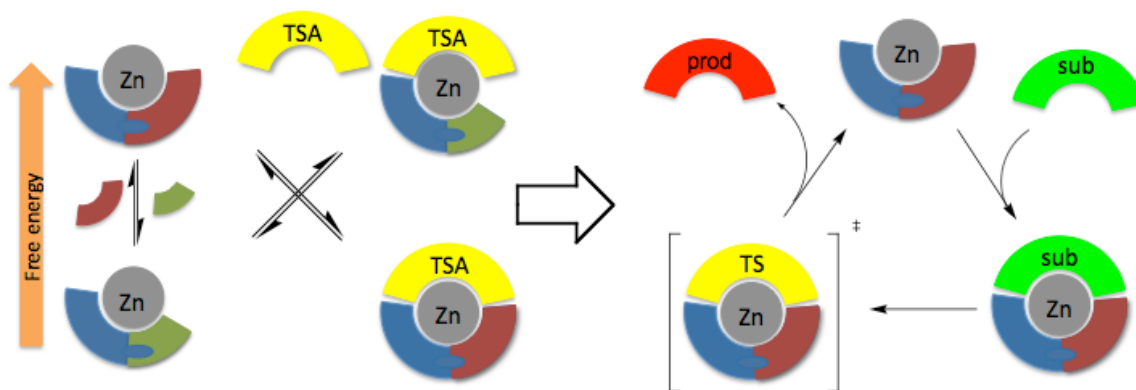


**Figure 75.** A schematic representation of catalyst evolution from a dynamic combinatorial library.

The essential features of our DCL are as follows: A library of zinc-Schiff base complexes is formed under equilibrium conditions. (Figure 76) The stoichiometry of the building blocks is such that there is competition for one or the other of the components (excess aldehyde and limiting amine, for example). Under these conditions, the Schiff base ligand that forms the most stable complex with zinc, solvent, and excess building blocks will predominate. This is called the control library. Upon addition of the pro-TSA, ternary complexes are formed consisting of ligand library members, zinc ion, and pro-TSA. Under these conditions, the Schiff base ligand that forms the most stable complex with zinc ion *and* pro-TSA will be favored. This is called the templated library. (Figure 75, left side) By comparing the composition of the control library and the template library, we will be able to observe template-driven amplification.
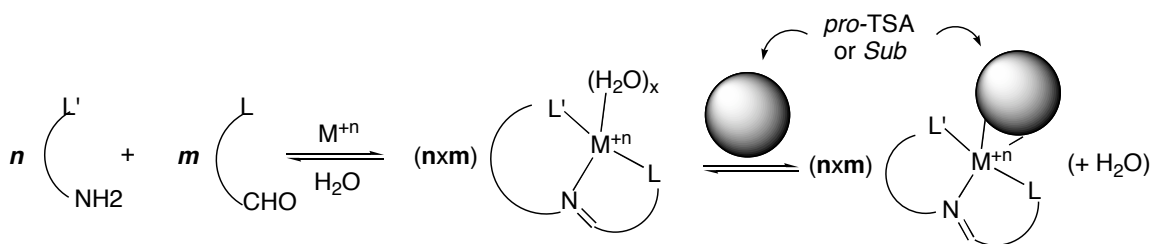
**Figure 76.** Metal and ligand templated Schiff-base libraries.

The catalytic relevance of the outcome of this TSA-template driven amplification can be tested by synthesizing the zinc-Schiff base complex and measuring the rate with which it hydrolyzes substrate. According to Jencks' model for catalysis by transition state stabilization[3], the amplified species ought to be a better catalyst than its non-amplified congeners. (Figure 77) Further, there ought to be a general correlation between amplification and catalysis.
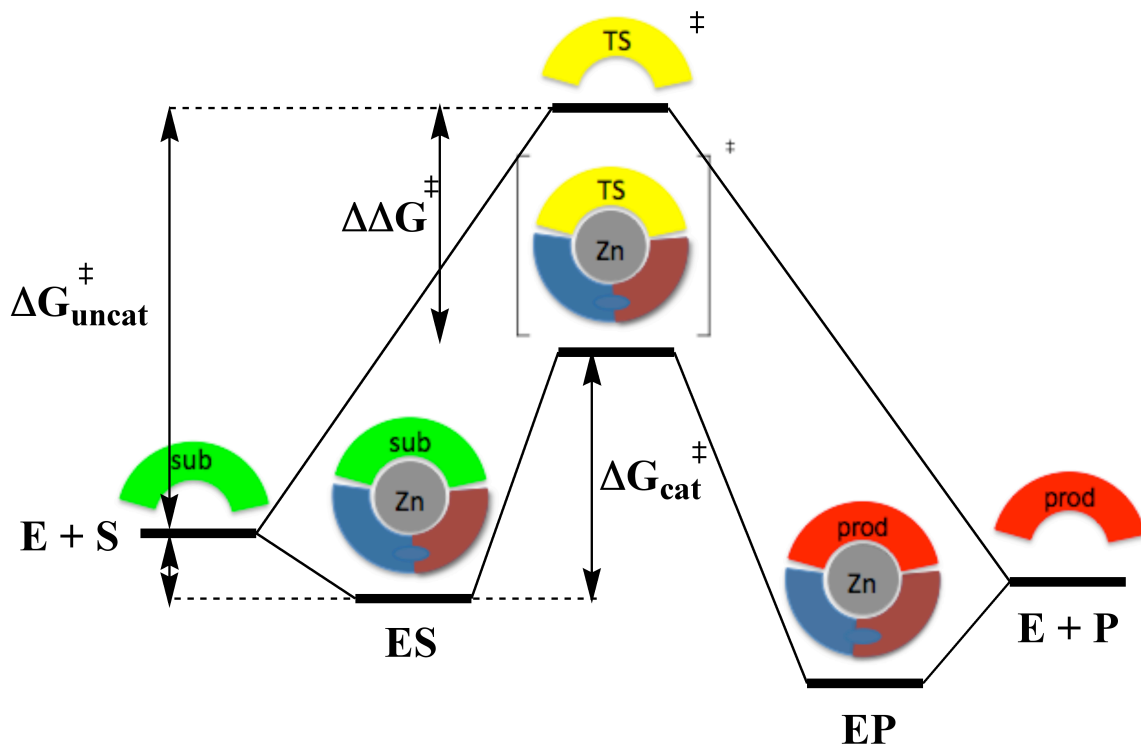


**Figure 77.** Schematic energy diagram for the catalyst selected by DCL.

The heart of the strategy is that in the DCL, the metal ion acts as a structural element, bringing together the ligand candidates and TSA. Through the formation of ternary complexes, we would use metal-ligand and ligand-ligand interactions to transmit information from the TSA to the ligand library (figure 75 left side). In the catalyst kinetics experiment, the same metal ion is a vital catalytic center (figure 75 right side). The very characteristics of the ligand that made it a good match with the TSA in the DCL experiment should make it a good *catalyst* in the kinetics experiment.

What we hoped to observe was 1) ligand amplification, 2) catalysis of esterolysis by the corresponding zinc-Schiff base complex, and 3) correlation between amplification and catalysis. In order to establish the etiology of the correlation, we also hoped to observe 4) the formation of a ternary (ligand-Zn-TSA) complex, and 5) thermodynamic data for the ternary complex. If the amplified species can be shown to be the better catalyst, and its formation can be shown to be mediated by the ternary complex with the pro-TSA, and the better catalyst is the better binder for the pro-TSA, then these observations taken together support the hypothesis that TSA-templating in a catalyst DCL will select the best catalyst.

## 3.2 Results

These results have been published in the European Journal of Inorganic Chemistry.[76]

### 3.2.1 Early attempt: using hydroxamate as TSA

We noted accounts of ternary hydroxamate zinc complexes in which the order of stabilities of the binary ligand zinc complex and the ternary ligand zinc hydroxamate complex were inverted.[77] This suggested to us a scenario in which a (relatively) poor ligand might become the (relatively) better ligand in the presence of a third ligand which would modify the properties of the metal. This is essentially the necessary condition for a metal complex DCL in which amplification is driven by preferential complex formation driven by ligand electronics. Hydroxamate was a candidate for such a ligand because it has been used as a transition state analog inhibitor of zinc metalloenzymes. A ternary complex (Figure 78) was prepared by titrating benzhydroxamate into the zinc triflate complex of a Schiff base derived from benzylhistamine and 1-methyl-2-imidazolecarboxaldehyde and observing the $^1$H-NMR chemical shifts of the ligand. (Figure 79) Up to one equivalent of benzhydroxamate, a small but detectible change in the chemical shift of the benzyl proton and the proton alpha to imidazole in benzylhistamine is observed. After one equivalent, there is a break in the curve, probably indicative of another species (free ligand) forming. This behavior is indicative of formation of the ternary complex with high association constant. ESI-MS also indicated the presence of the ternary complex.
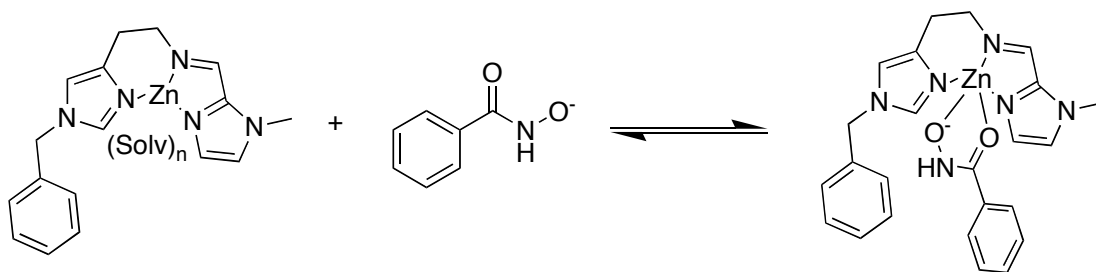


**Figure 78**. Hydroxamate-zinc-ligand ternary complex
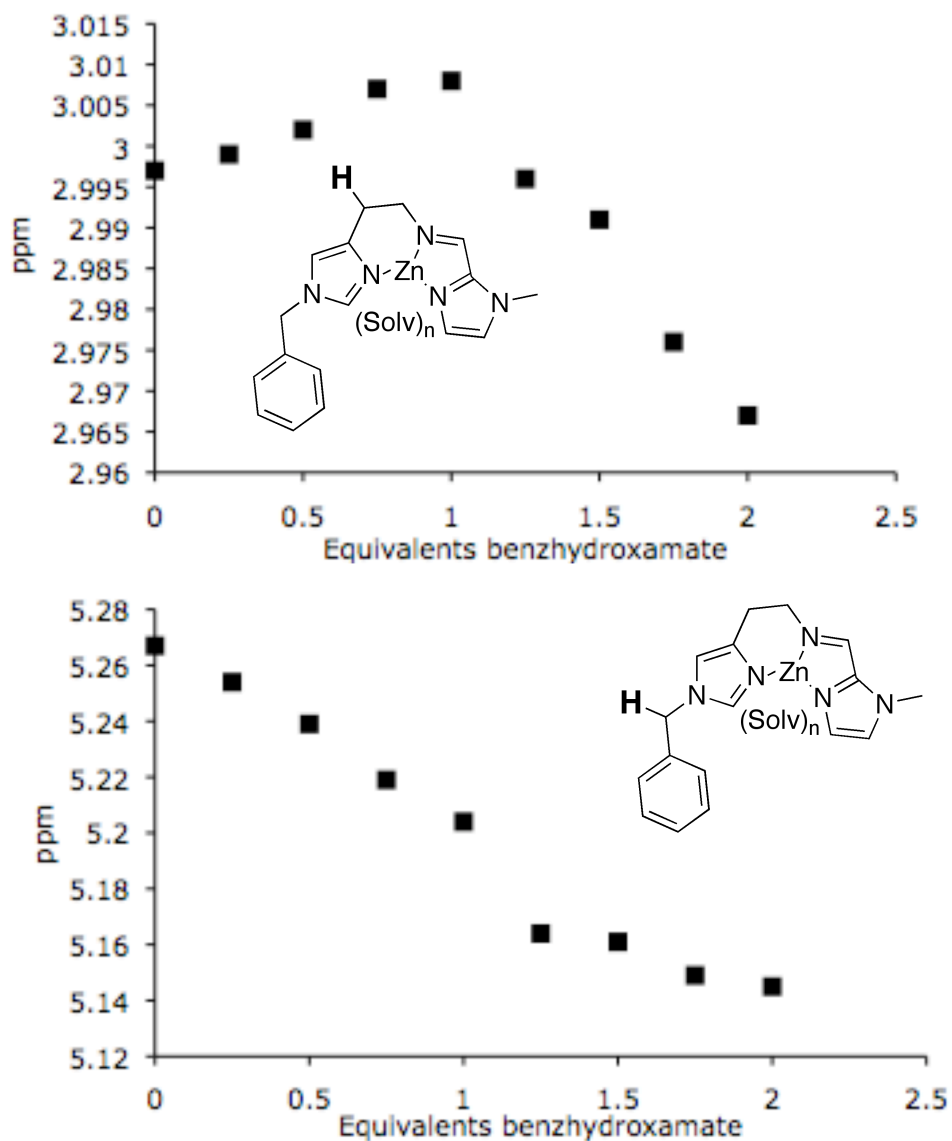
**Figure 79.** ^{1}H-NMR titration of zinc Schiff base complex with sodium benzhydroxamate showing strong complexation. Chemical shifts belong to the protons indicated in the inset structure.

Therefore we attempted to template Schiff-base zinc complex libraries with hydroxamates as TSA ligands. We established by ESI-MS and ^{1}H-NMR that the ternary complex of Schiff base ligand, zinc, and hydroxamate forms. A DCL consisting of 1-

methyl-2-imidazolecarboxaldehyde, 2-pyridinecarboxaldehyde, benzylhistamine, and zinc triflate in methanolic MOPS buffer (pH 7.0, 50% water) was produced. (Figure 80) A control library containing no benzhydroxamate and a templated library containing one equivalent benzhydroxamate were prepared. Both libraries were allowed to equilibrate for 48 hours and reduced with sodium borohydride. RP-HPLC analysis of the resulting reduced imine ligands showed that the difference between control and templated library were very small (less than 3% increase in the 2-pyridinecarboxaldehyde-derived ligand). The hydroxamate ligand does not appear to differentiate appreciably between the two possible zinc complexes. It may be that it is not a good TSA for a metal-mediated hydrolysis reaction. It quickly became clear that the appropriate choice of substrate and TSA would be critical in carrying out these studies.
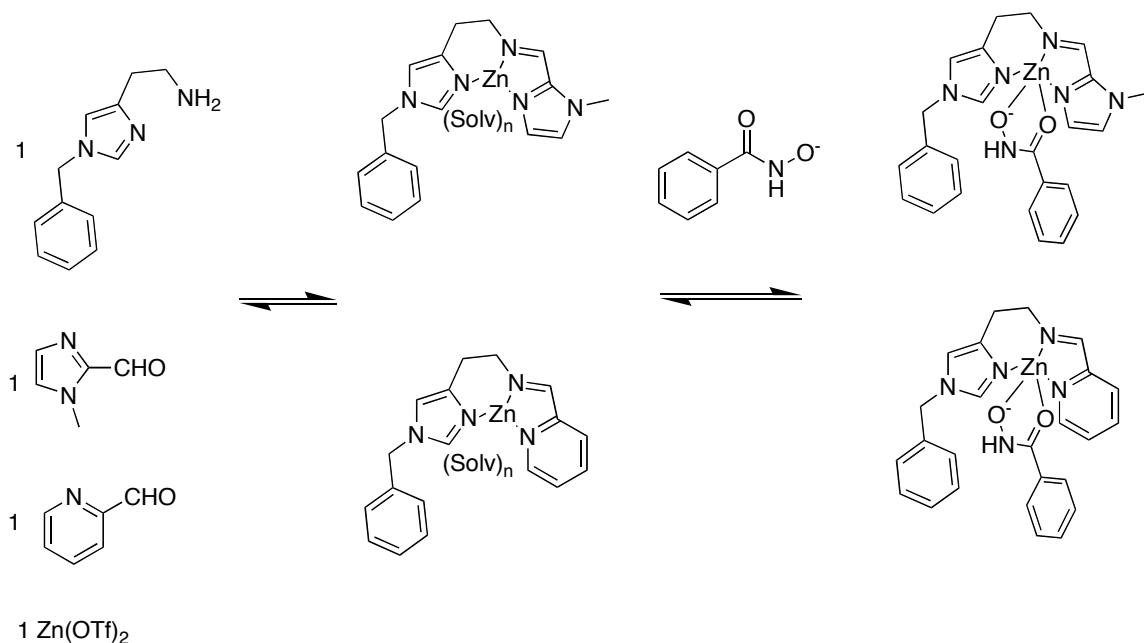


**Figure 80.** DCL of zinc complexes templated with benzhydroxamate led to less than 3% change in library composition.

93

### 3.2.2 Using pyridylphosphonate phenyl ester as TSA

The substrate *p*-nitrophenylpicolinate (**135**) has been utilized for the study of metal-mediated esterolysis owing to its metal-binding properties and convenient spectroscopic properties.[78] (Figure 81) The metal-catalyzed hydrolysis of this substrate is thought to proceed through the formation of a substrate-metal complex and subsequent nucleophilic attack by water or hydroxide on the Lewis-acid-activated ester carbonyl. We reasoned that the pyridylphosphonate ester **136** would be a good TSA for the metal-catalyzed hydrolysis of **135**, as well as a good ligand for zinc. This is a critical factor, since the formation of a ternary complex of the TSA and the metal complex catalyst will be essential for templating to occur. It should be noted that **136** actually resembles the tetrahedral intermediate formed by the addition of water to **135**. Arguably, it is a better mimic for the tetrahedral intermediate than for the transion state. However, according to the Hammond postulate, in an endergonic process (such as this addition step), the transition state ought to resemble the product more than the reactant; since the rate limiting step for the hydrolysis of **135** is thought to be the addition step, this TSA should be sufficient for emulating the transition state for the relevant step.
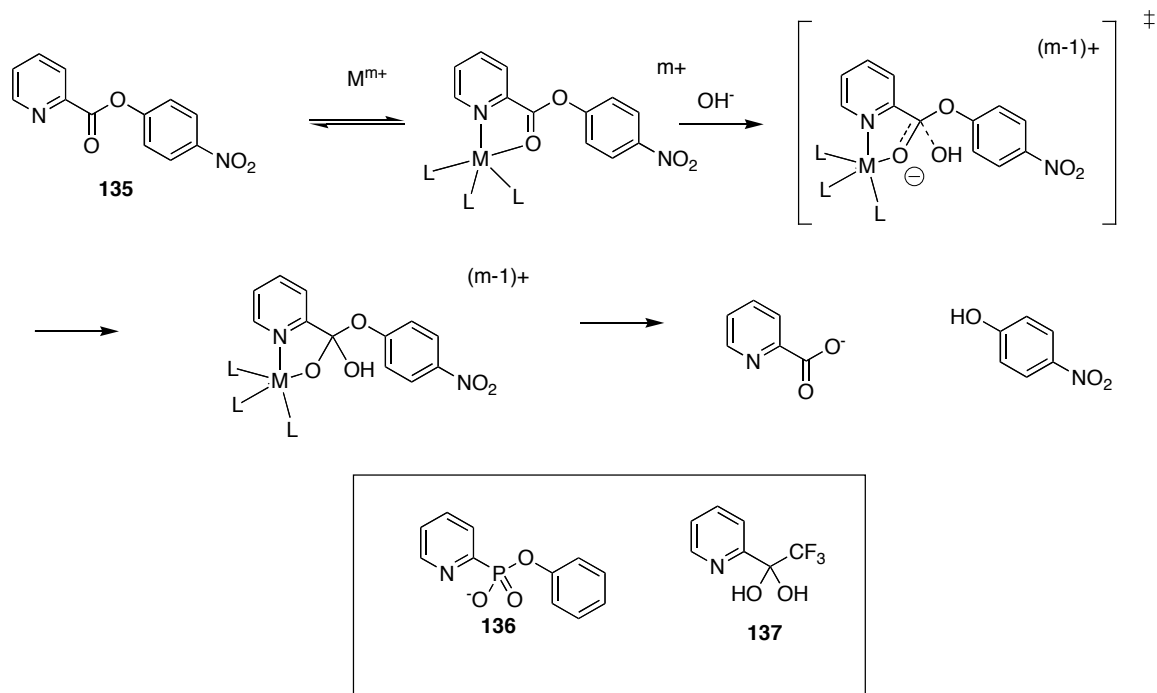
**Figure 81.** The targeted hydrolysis reaction via DCL and the TSA used for templating experiments

### 3.2.2.1 Synthesis

The substrate *p*-nitrophenylpicolinate **135** was prepared by a literature procedure, using DCC to couple picolinic acid to p-nitrophenol.[79] The product was crystallized from ethanol. The pro-TSA phenylpyridylphosphonic ester **136** was prepared by a literature procedure, using DCC to couple pyridylphosphonic acid to phenol.[80]

### 3.2.2.2 A DCL containing two zinc complexes (141-Zn and 142-Zn) templated with TSA 135

A control library was produced from 1-methyl-2-imidazolecarboxaldehyde **139**, 1-methyl-2-benzimidaolecarboxaledehyde **140** and pyridylethylamine **138** and zinc in a

1:1:1:1 ratio. The solvent was 50% acetonitrile in water. Under these conditions, rapid imine exchange is expected to occur and lead to a thermodynamic mixture of Schiff bases and Schiff base zinc complexes. However, owing to the stoichiometry of the mixture, not all the aldehyde present can be incorporated into a Schiff base ligand. After equilibrating 48 h, the mixture was treated with excess sodium borohydride to effect rapid reduction of the imines and aldehydes present. (Figure 82) Borohydride reduction has been demonstrated as a method for 'fixing' the Schiff base library for analysis.[47,81] This is expected to produce a secondary amine mixture whose composition reflects that of the imine library. After acidification and dilution, the mixture was analyzed by RP-HPLC. (Figure 83) The product mixture was found to be composed of **143**:**144** in a 1:0.9 ratio. The templated library was produced in a similar way except that 1 – 2 equivalents of pro-TSA was added to the mixture. In the templated library, **144** was found to be amplified 1.4-fold, whereas **143** was attenuated 0.9-fold. (Figure 84) We believe that the composition of the reduced ligand mixture reflects the composition of the thermodynamically controlled ligand library, and this in turn reflects the population of zinc ligand complexes and therefore the relative stability of the zinc-ligand-TSA complexes.
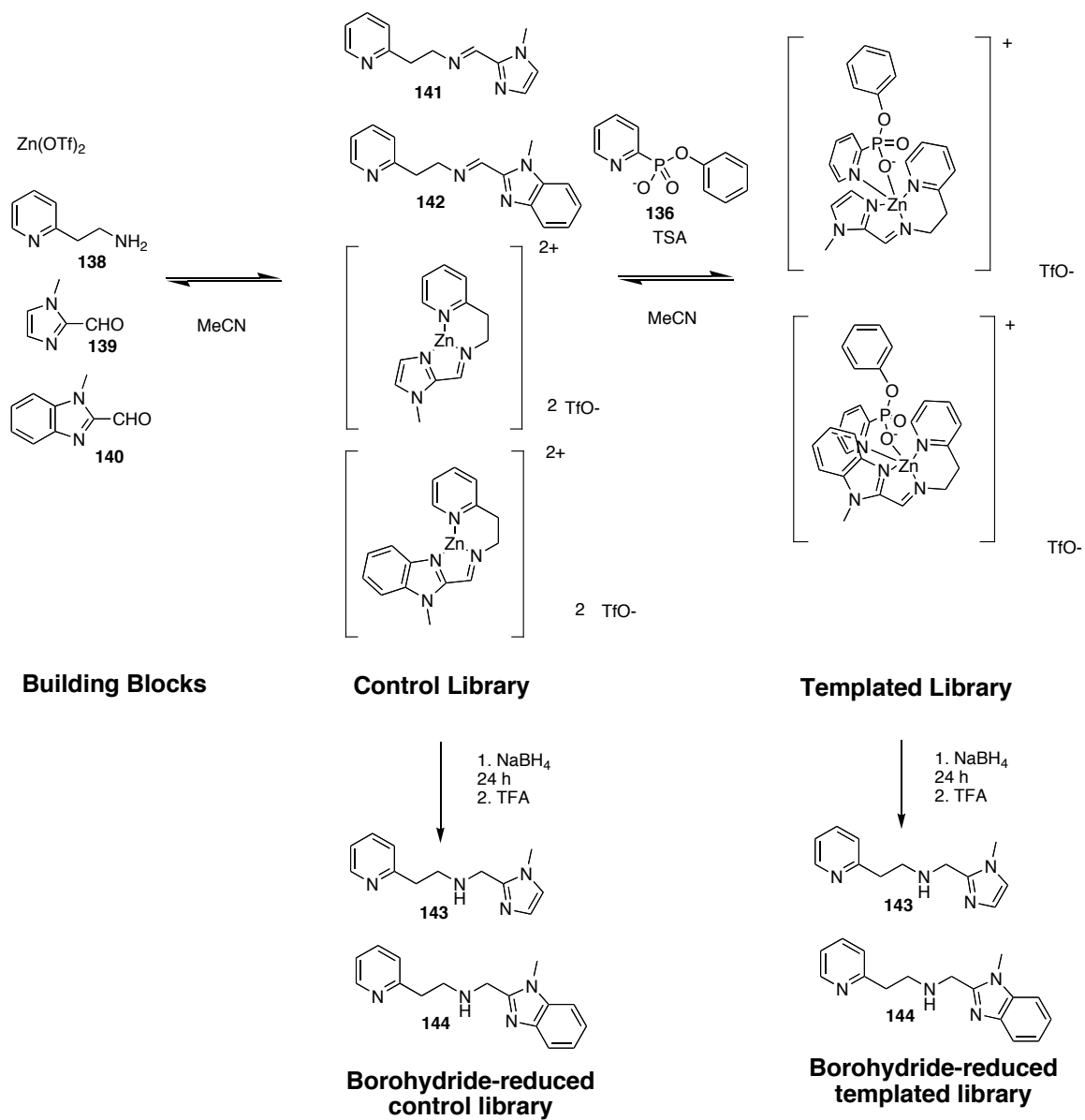
**Figure 82.** Library I.
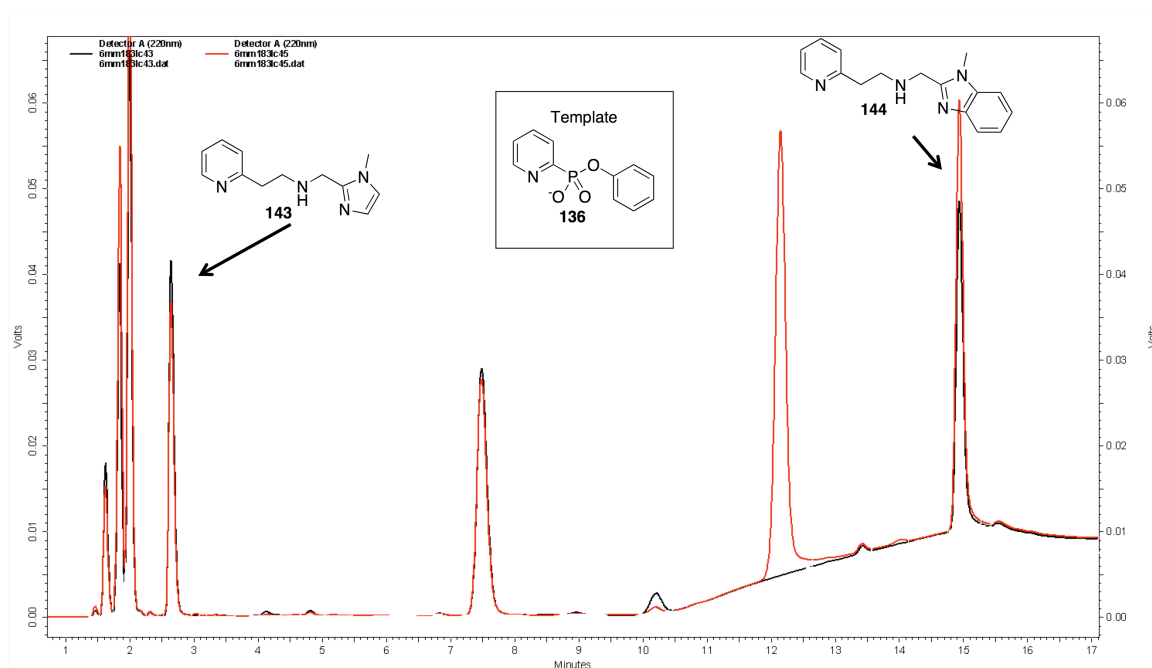
**Figure 83**. RP-HPLC chromatograms of control (black) and templated (red) library I.



equiv. phenyl-2-pyridylphosphonate (**136**)
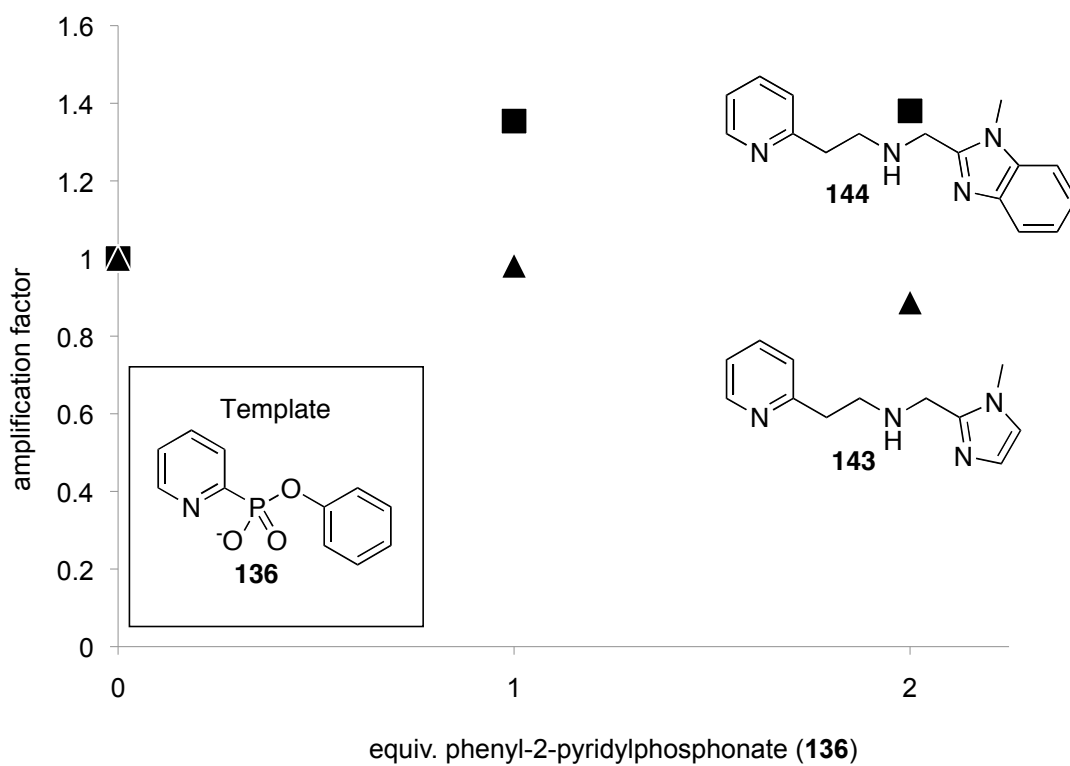
**Figure 84.** Library I. Amplification behavior of **143**(▲) and **144**(■) in the presence of

**136**. Amplification factor (AF) is $[L]_{TEMPLATE}/[L]_{CONTROL}$.

### 3.2.2.3 Kinetics

Single-turnover kinetics for the hydrolysis of substrate **135** by **141**-Zn(OTf)$_2$ and **142**-Zn(OTf)$_2$ was measured spectrophotometrically by observing the formation of *p*-nitrophenol at 400 nm. The reaction solution 30% methanol in water buffered at pH 7.5 using MOPS at 25° C. **141**-Zn(OTf)$_2$ and **142**-Zn(OTf)$_2$ were prepared in situ by mixing zinc triflate, aldehyde and amine in methanol and allowing the mixture to equilibrate at room temperature for 48 hours. Substrate **135** concentration was held at 0.082 mM, and catalyst was varied from 0.2 to 0.6 mM. Reaction rate was plotted against substrate concentration times catalyst concentration. The linearity of the curve indicates that the reaction is first order in catalyst in this region. (Figure 85) The second order rate constant for hydrolysis of **135** was 30 M$^{-1}$min$^{-1}$ for **141**-Zn(OTf)$_2$ and 90 M$^{-1}$min$^{-1}$ for **142**-Zn(OTf)$_2$.
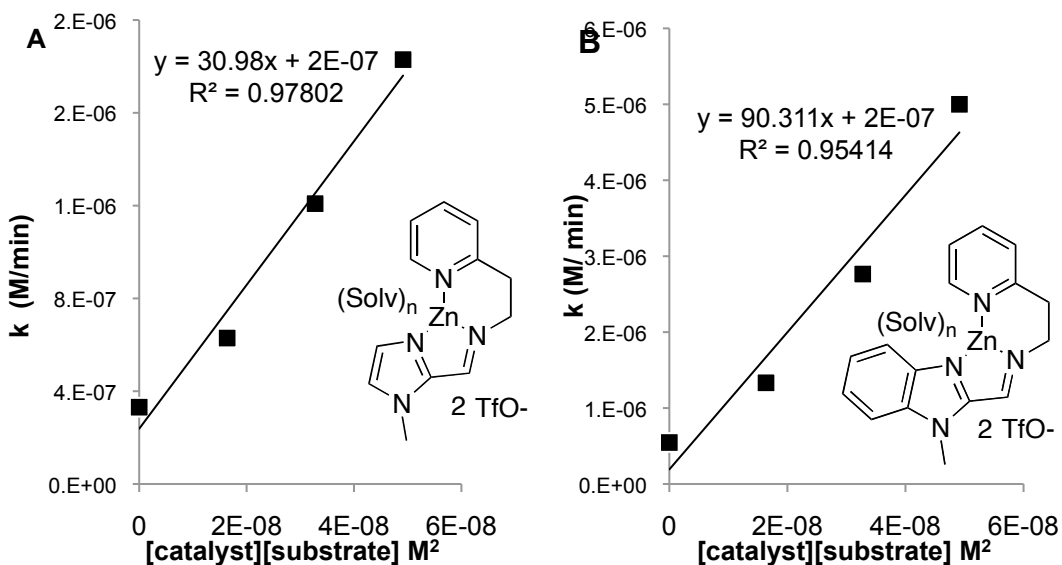


**Figure 85.** Single turnover kinetics for **141**-Zn (**A**) and **142**-Zn (**B**).

**3.2.2.4 Job plot**

     In order to establish the stoichiometry of the ternary complex, an NMR Job plot was constructed by producing 1:9, 3:1, 1:1, 1:3, and 9:1 mixtures of **142**-ZnL and TSA **136** while holding the total concentration of ZnL and TSA constant at 10 mM. Samples were observed by ^{31}P-NMR. (Figure 86) We observed that there is a local maximum corresponding to a 1:1 complex, but global maximum on the excess of **136**- side of the plot indicating that in the presence of a large excess of **136** a new species is formed with a high phosphonate to zinc ratio. One explanation for this behavior is that a 1:1 complex is formed at and near the 1:1 point, but as more **136** is added, the phosphonate begins to displace **142**. Since we are observing the ^{31}P signal of **136**, this displacement leads to a maximum chemical shift.
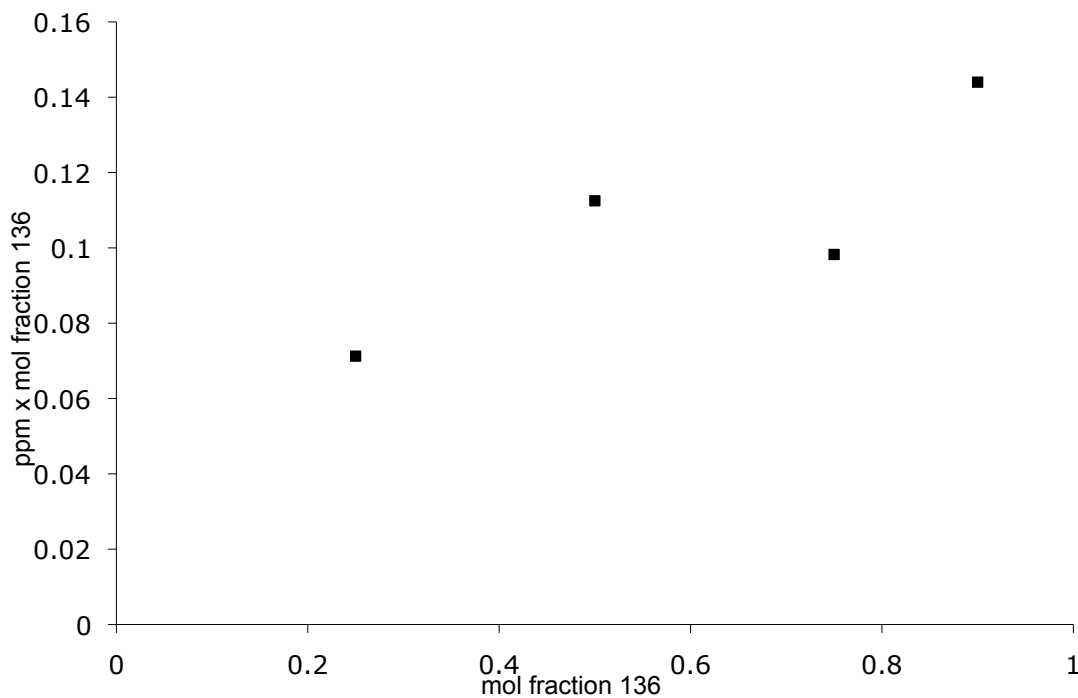


**Figure 86.** ^{31}P-NMR Job Plot for the **142**-Zn-**136** ternary complex.

### 3.2.2.5 Competitive Binding experiment

The affinity of pro-TSA for zinc complexes was too high to measure directly with any accuracy. Instead, we used a competition experiment in which the pre-formed ternary complex of ligand, zinc, and TSA (**141**-Zn-**136** and **142**-Zn-**136**) was titrated with a competing ligand **145** (ethyl picolinate) designed to resemble the substrate **135**. (Figure 87) The $^{31}$P NMR signal of the TSA **136** was observed as the substrate analog was titrated in. As a large excess of titrant was used, a Scatchard analysis[82] could be utilized to analyze the data. (Figure 88) The relative affinity of the TSA vs the substrate analog ought to correspond to the catalytic activity of the zinc-ligand complex. We found that the relative affinity of TSA (vs substrate analog) for complexes **141**-Zn and **142**-Zn was 10 and 19. The ratio of these relative affinities is 1:2, roughly corresponding to both the ratio of catalytic activities and to the amplification behavior.
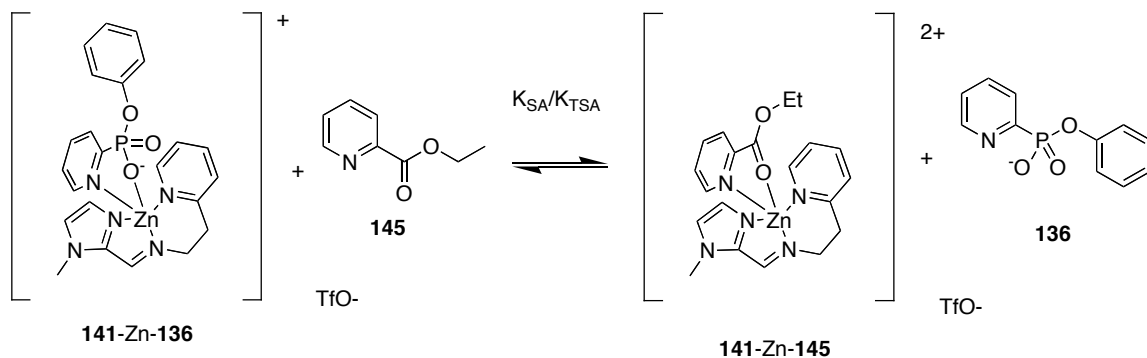


**Figure 87.** Competititive binding of **145** investigated through NMR titration
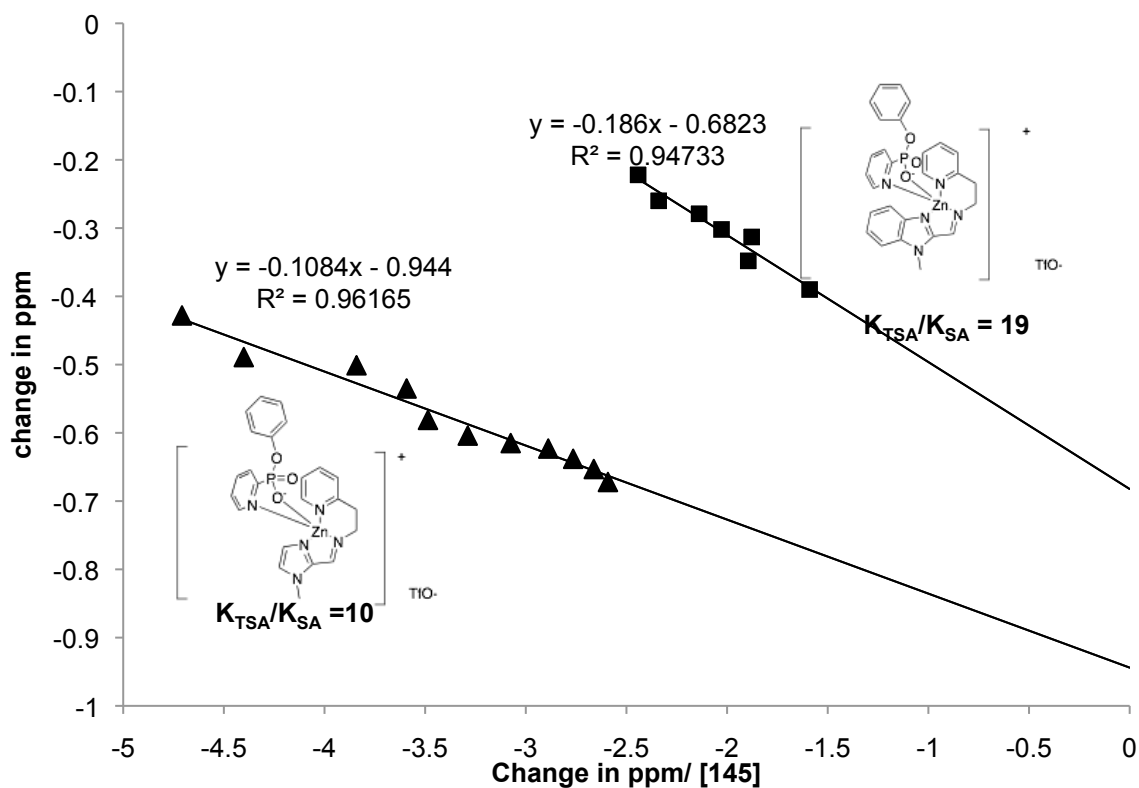
**Figure 88.** Scatchard plot of competitive binding experiment for **141**(▲) and **142**(■).

### 3.2.2.6 ESI MS evidence

We used ESI-MS to detect the formation of the L-Zn-TSA ternary complexes (**141**-Zn-**136** and **142**-Zn-**136**) under templating conditions. (Figure 89) We were able to detect the ternary complex of **141**-Zn-**136** and **142**-Zn-**136** in the templated DCL before reduction, demonstrating that these ternary complexes are formed in the DCL.
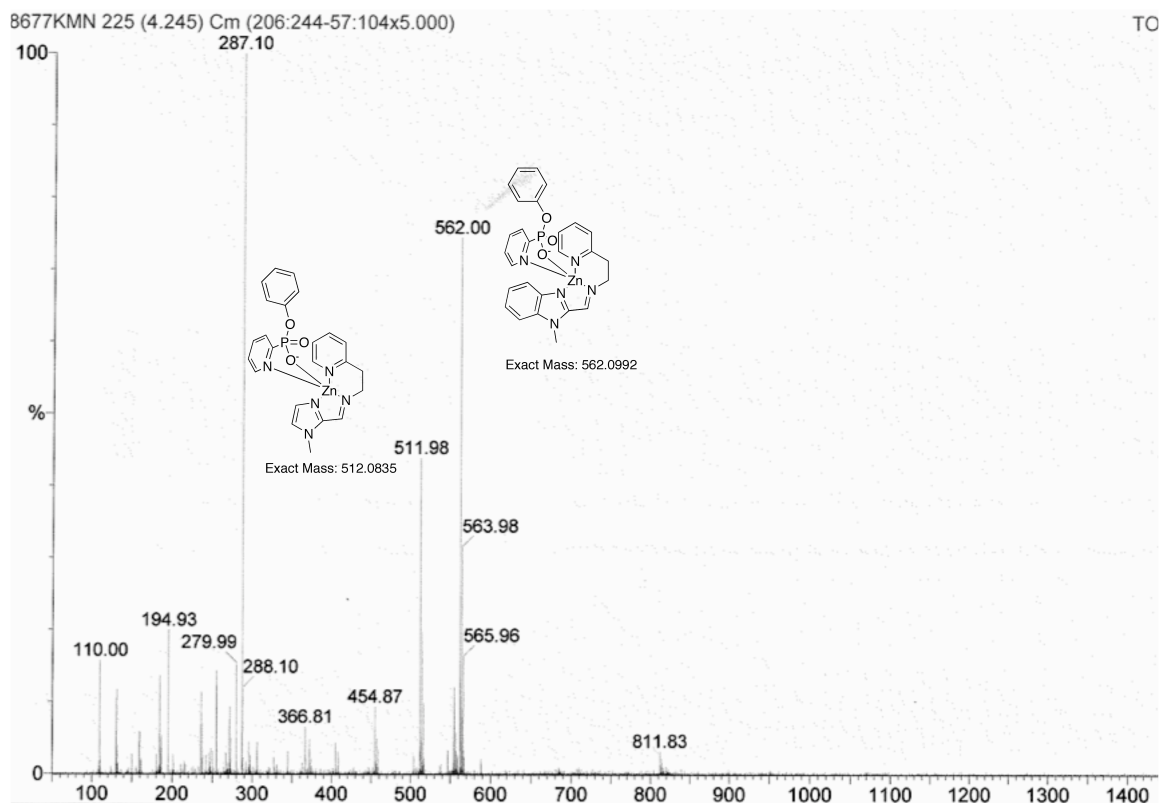
**Figure 89.** ESI-MS of templated library I shows evidence of the ternary complex **141**-Zn-**136** and **142**-Zn-**136**.

### 3.2.2.7 Inhibition by 136

Single turnover kinetic runs were carried out for **135** hydrolysis with fixed concentration of **141**-Zn and **142**-Zn as catalysts with varying concentrations (0 to 12 mM) of **136**. For both zinc complexes, the catalytic reaction was inhibited by the presence of **136**. (Figure 90)
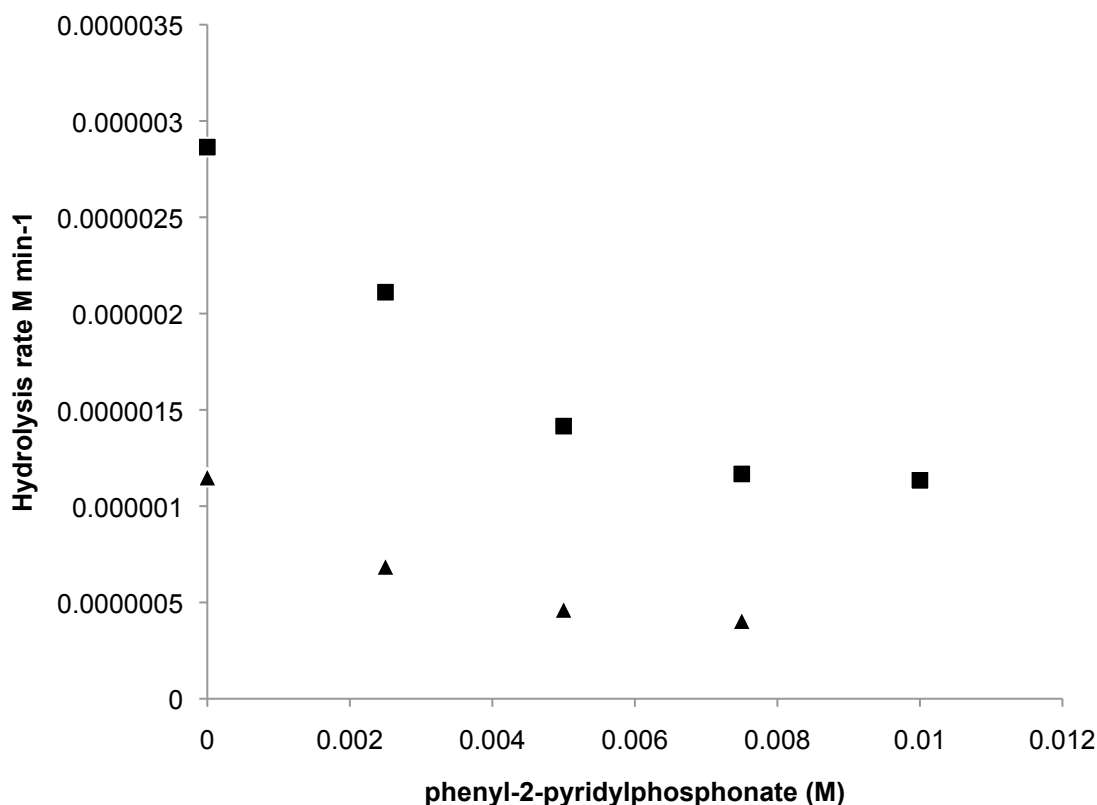
**Figure 90.** Inhibition of hydrolysis of **135** by TSA **136**: for **141**-Zn(▲) and **142**-Zn(■).

### 3.2.2.8 Discussion

DCLs consisting of zinc complexes of **141** and **142** were produced. (Figure 91) Upon templating with TSA **136**, ternary complexes **141**-Zn-**136** and **142**-Zn-**136** were formed (observed by ESI-MS), and ligand **142** was amplified 1.4-fold while **141** was attenuated 0.9-fold (observed by HPLC analysis after borohydride reduction to **143** and **144**). Assays of the catalysis of **135** hydrolysis by zinc complexes **141**-Zn and **142**-Zn gave second order rate constants of 30 $M^{-1}min^{-1}$ and 90 $M^{-1}min^{-1}$, respectively. The catalytic behavior of the library members thus correlates with the observed amplification. Hydrolysis of **135** by both zinc complexes was inhibited by TSA **136**. Titration of ternary

complexes **141**-Zn-**136** and **142**-Zn-**136** with a competing substrate analog **145** gave relative affinities for TSA **136** and substrate analog **145** ($K_{TSA}/K_{SA}$) for **141**-Zn and **142**-Zn (10 and 19, respectively) that are consistent with TSA-templated amplification. A NMR Job plot showed some 1:1 complex formation as well as formation of **136**$_n$Zn species in presence of excess **136**.



| | 139 | 140 |
|---|---|---|
| 138 | 141 | 142 |
| k | 30 M$^{-1}$min$^{-1}$ | 90 M$^{-1}$min$^{-1}$ |
| AF | 0.9 | 1.4 |
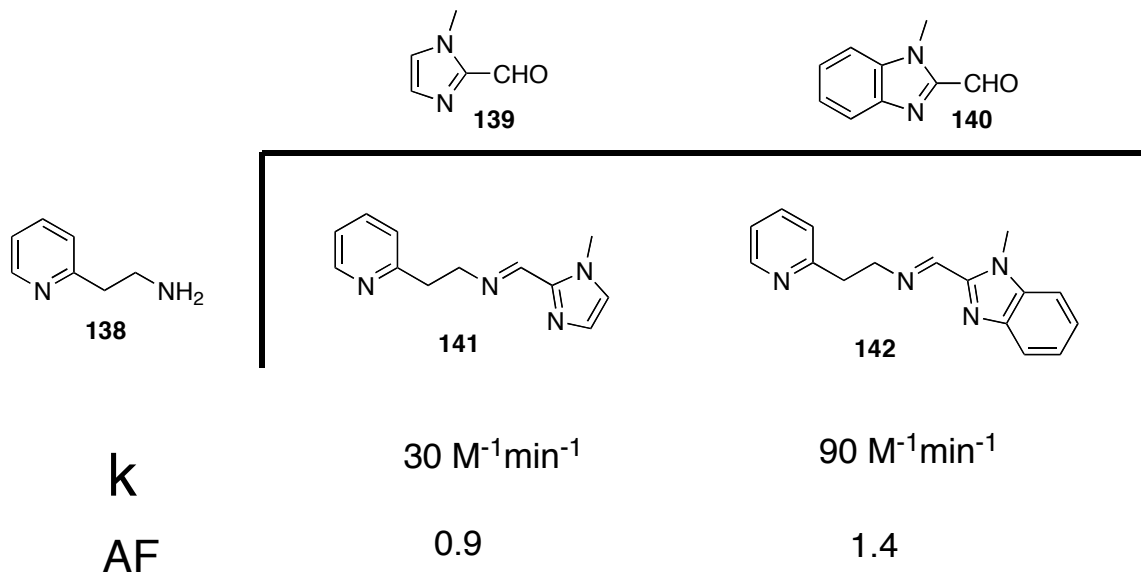
**Figure 91.** Summary of results for library I.

This data supports the hypothesis that a ternary-complex-mediated templating is occuring which amplifies the best binder for the TSA. It also suggests that the interaction leading to the templating is a catalystically relevant one. The amplified species is shown to be a better catalyst than the attenuated species for the hydrolysis of the relevant substrate. We postulate that the binding behavior with TSA **136** and the difference in catalytic activity toward **135** have a common cause, which is the difference in electronic characteristics furnished by building blocks **139** and **140**. The superior donating ability of imidazole decreases the Lewis-acidity of the zinc center in comparison to the

benzimidazole ligand. By the same reasoning, the imidazole ligand **141** forms a less stable ternary complex with Zn-**136**, because the anionic chelating TSA **136** is very electron-donating; the less donating benzimidazole ligand **142** is a better match. As an approximate measure of the electronic character of N-methylimidazole and N-methylbenzimidazole, the pKa of protonated N-methylimidazole versus protonated N-methylbenzimidazole is informative: they are 7.2 and 5.6, respectively. [83]

## 3.2.2.9 A DCL containing two zinc complexes (147-Zn and 142-Zn) templated with TSA 136

In library II, two amine building blocks and one aldehyde building block were used to produce zinc complexes of two possible Schiff base ligands in order to test variation on the amine side of the reaction. (Figure 92) A control library and TSA-**136**-templated libraries were produced from aldehyde **140** and amines **138** and **146** with zinc triflate. After 24 hours of equilibration, the libraries were reduced with sodium borohydride and analyzed by RP-HPLC. When the templated library was compared to the control library, it was found that the reduced form of imine **142** was amplified 2.6-fold, whereas the reduced form of imine **147** was attenuated 0.9-fold. (Figure 93)

| k | 52 M⁻¹min⁻¹ | 90 M⁻¹min⁻¹ |
| AF | 0.9 | 2.6 |

$$k \quad 52 \text{ M}^{-1}\text{min}^{-1} \quad 90 \text{ M}^{-1}\text{min}^{-1}$$
$$AF \quad 0.9 \quad 2.6$$
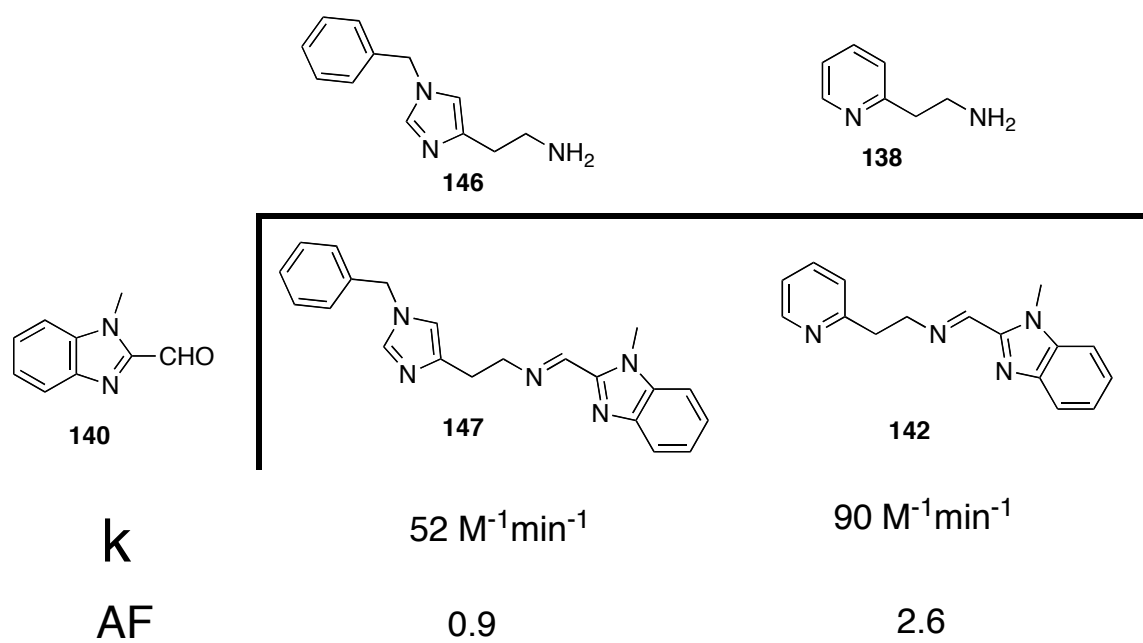
**Figure 92.** Summary of results for library II.
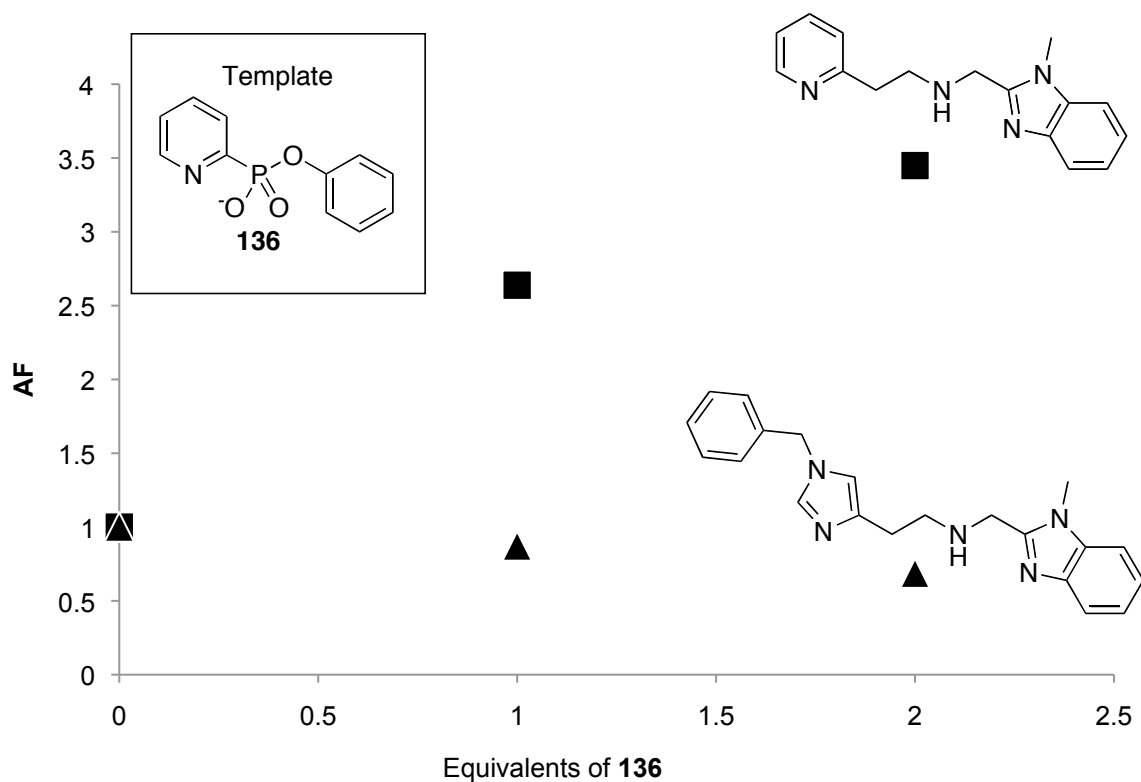


**Figure 93.** Library II. Amplification behavior in the presence of **136**, for reduced derivative of **147**(▲) and **144**(■).

### 3.2.2.10 Kinetics

Single-turnover kinetics for the hydrolysis of substrate **135** by **147**-Zn(OTf)$_2$ was measured spectrophotometrically by observing the formation of *p*-nitrophenol at 400 nm. The reaction medium was 30% methanol in water buffered at pH 7.5 using MOPS at 25$^o$ C. **147**-Zn(OTf)$_2$ was prepared in situ by mixing zinc triflate, aldehyde and amine in methanol and allowing the mixture to equilibrate at room temperature for 48 hours. Substrate **135** concentration was held at 0.082 mM, and catalyst concentration was varied from 0.2 to 0.6 mM. The linearity of the plot of rate against catalyst concentration times substrate concentration indicates that this reaction is first order in catalyst. (Figure 94) The second order rate constant for hydrolysis of **135** was 52 M$^{-1}$min$^{-1}$ for **147**-Zn(OTf)$_2$.
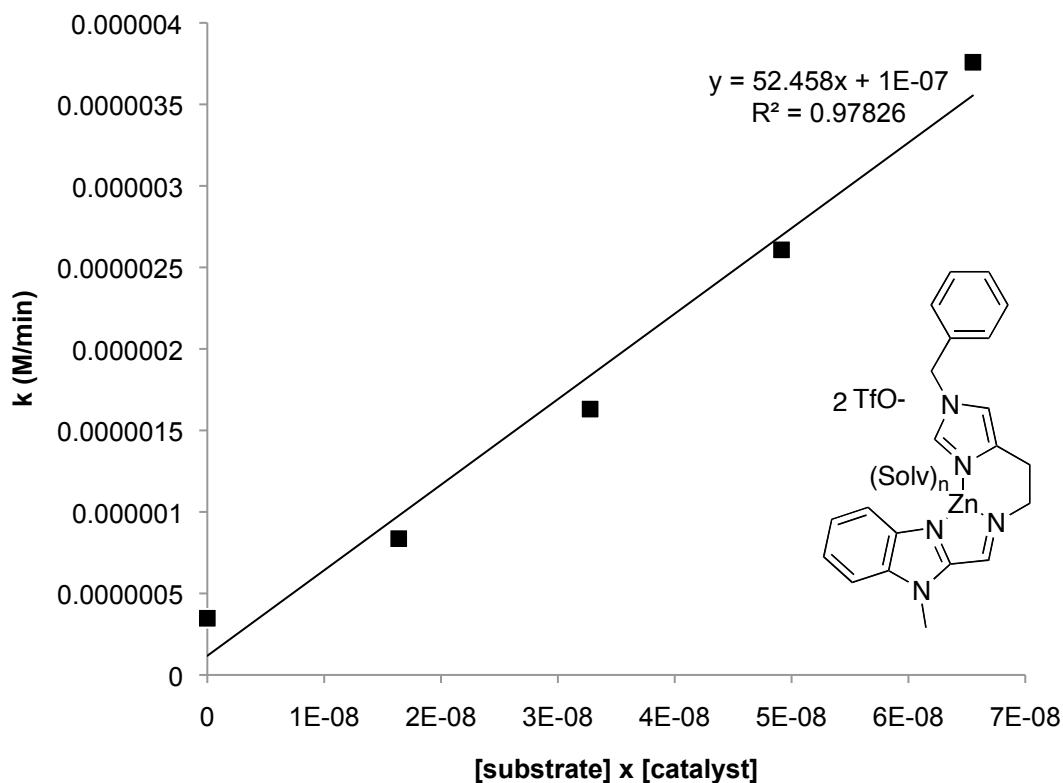


**Figure 94.** Single turnover kinetics of hydrolysis of **135** by **147**-Zn.

### 3.2.2.11 Discussion

The template-mediated amplification of **142** at the expense of **147** correlates with the relative reactivities of **142**-Zn and **147**-Zn toward substrate **135**. The rationale for this is that the benzylimdazole moiety of **147** is a more powerful electron-donor to zinc than the pyridine in **142**. This decreases the Lewis acidity of **147**-Zn, therefore decreasing the reactivity of this complex toward substrate **135** and also decreasing the affinity of this complex toward TSA **136**.

### 3.2.3 Using a trifluoromethylketone as TSA

Trifluoromethylketones (TFMK) and their hydrates are known to inhibit a variety of serine proteases and deacylases, i. e., hydrolytic enzymes in which an acyl transfer to a nucleophilic function-group takes place.[84] The ketone hydrate easily loses water, and can form a covalent hemiketal adduct with the catalytically relevant alcohol. This gave us an alternative approach to a TSA for the hydrolysis of nitrophenyl picolinate, one in which the pro-TSA was capable of interacting covalently with the ligand. This proves particularly important in cases where the catalyst library contains ligands that are capable of behaving as nucleophiles toward the substrate.

### 3.2.3.1 Synthesis

2-Pyridyltrifluoromethylketone hydrate **137** was prepared by literature methods.[85]

### 3.2.3.3 Trifluoromethylketone-templating amplifies a hydroxy-bearing ligand

In order to test whether TSA **137** could discriminate between complexes of a ligand bearing a nucleophilic group (**151)** and complexes of a ligand without such a group (**150**), a templating experiment was carried out in which aldehyde **139**, amine **148**, and amino alcohol **149** were combined with zinc triflate in 1:1:1:1 ratio in acetonitrile. (Figure 95) Together with a parallel control experiment, a templated experiment was carried out with the addition of varying amounts of trifluoromethylketone **137.** After equilibrating for 48 hours, the libraries were reduced with sodium borohydride, acidified with trifluoroacetic acid, and analyzed by RP-HPLC. (Figure 96) The expectation that complexes of the hydroxy-bearing ligand **151** would be amplified by TSA **137** at the expense of complexes of unsubstituted ligand **150** was confirmed. 2-fold amplification of the reduced species **153** was observed, along with 0.5-fold attenuation of **152**. (Figure 97)
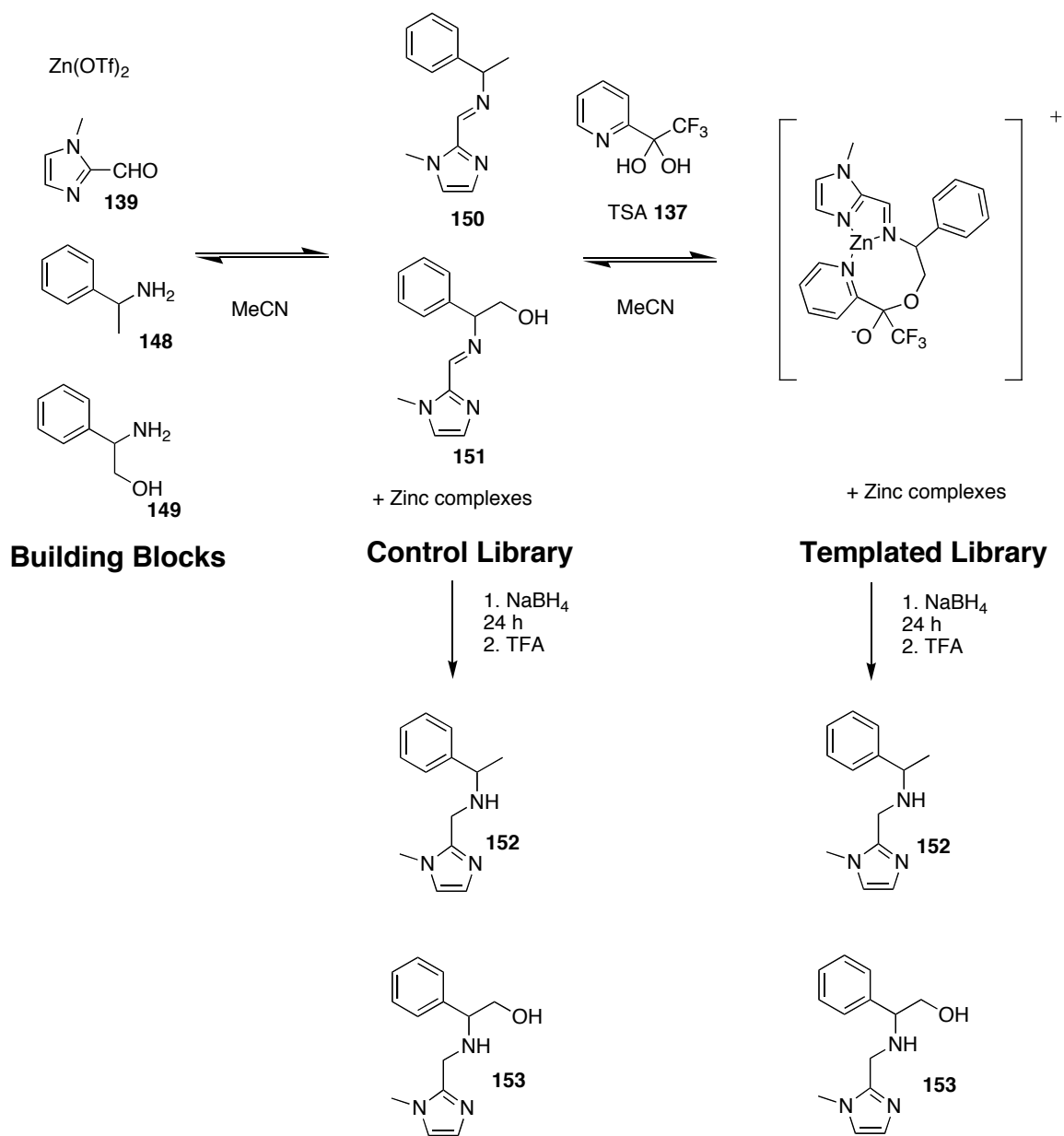
**Figure 95.** Library III, containing hydroxy-bearing building block **149** and its non-functionalized analog **148**.

**Figure 96.** RP-HPLC chromatograms of control (black) and templated with **137** (red) library III.
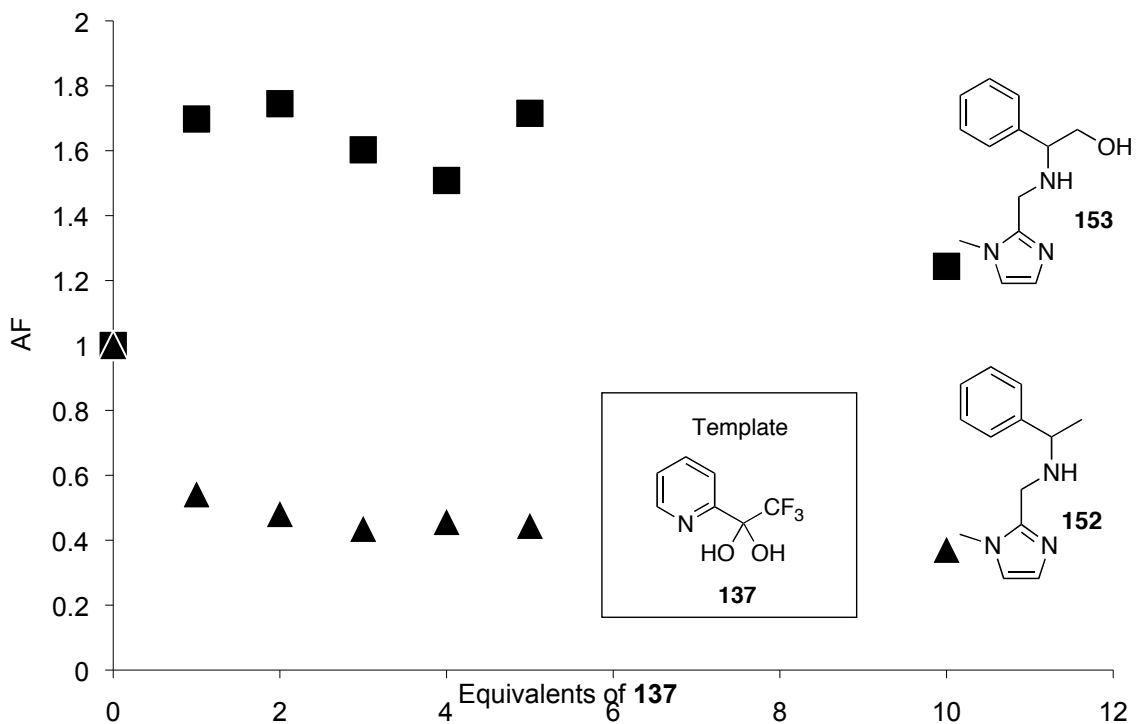


**Figure 97.** Library III Amplification behavior of **152**(▲) and **153** (■) in the presence of

**137**.

### 3.2.3.4 Kinetics

Zinc complexes **150**-Zn (OTf)$_2$ and **151**-Zn (OTf)$_2$ were prepared by mixing the amine, aldehyde and zinc triflate in methanol and allowing to equilibrate 48 hours. These species were tested for single-turnover hydrolysis of substrate **135**. Hydrolysis was measured spectrophotometrically by observing the formation of *p*-nitrophenol at 400 nm. The reaction solution 30% methanol in water buffered at pH 7.5 using MOPS at 25$^\circ$ C. Substrate **135** concentration was held at 0.082 mM, and catalyst was varied from 0.2 to 0.6 mM. (Fig 98) The dependence of rate on catalyst concentration was found to be linear, indicating that the reaction is first order in catalyst. The second order rate constant for hydrolysis of **135** was 160 M$^{-1}$min$^{-1}$ for **150**-Zn(OTf)$_2$ and 430 M$^{-1}$min$^{-1}$ for **151**-Zn(OTf)$_2$. This represents the nucleophilic participation of hydroxy group from ligand **151**, which is absent in **150**.
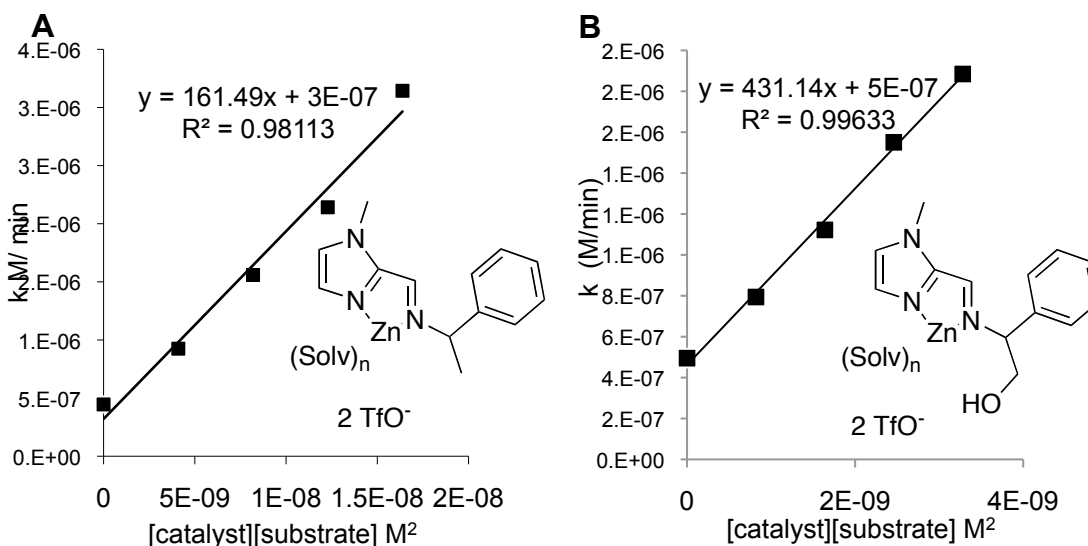


**Figure 98.** Single-turnover kinetics for hydrolysis of **135** by **150**-Zn (A) and **151**-Zn (B).

**3.2.3.5 ESI-MS**
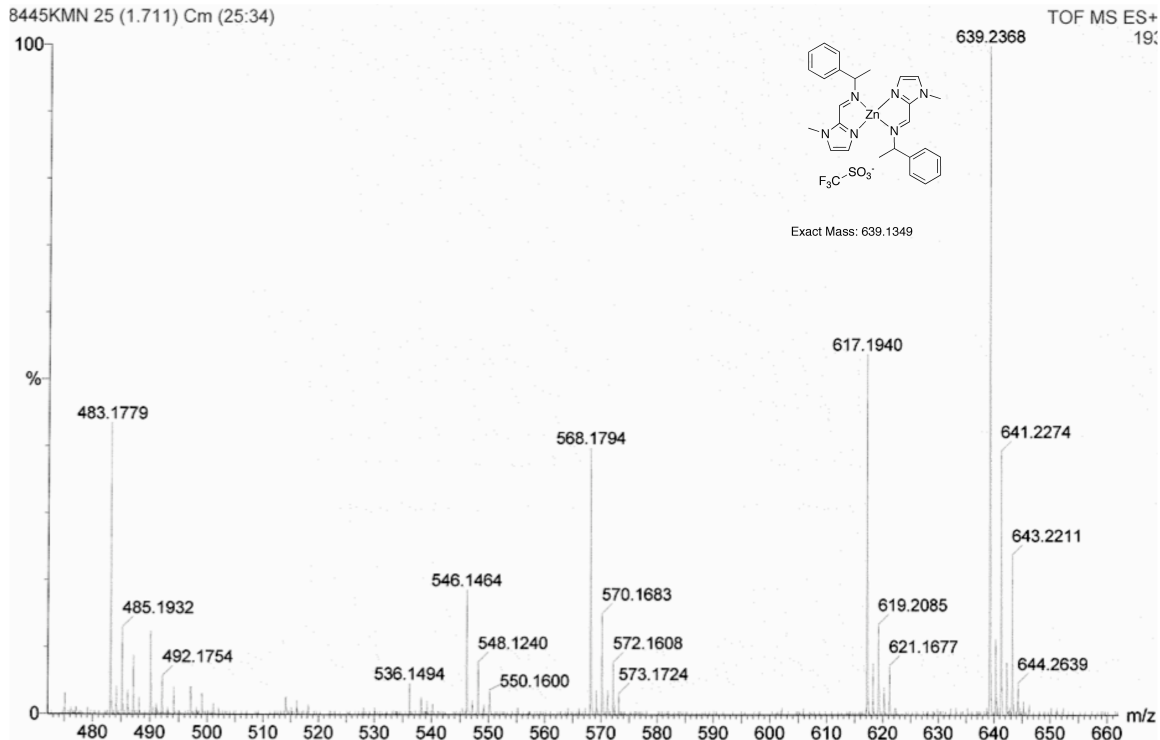


**Figure 99.** ESI-MS of a mixture of Zn(OTf)$_2$, **139**, **148**, and TSA **137**. No ternary complex or adduct is detected.

When **150**-Zn is combined with **137** in acetonitrile, and observed by ESI-MS, **150**-Zn does not appear to form ternary complexes with TSA **137**. (Figure 99) Instead, the complex **150$_2$**Zn (OTf) is the major species. However, when **151**-Zn is mixed with **137**, the hemiketal adduct of **137** with **151**-Zn was detected by ESI-MS. (Figure 100) We believe this is the key species that is responsible for the templating behavior. Also observed was **151**-Zn-(**137**-H$_2$O)MeOH. Importantly, an ESI of the DCL mixture itself (from the templated library) reveals two species incorporating TSA **137**, the ligand-zinc-TSA hemiketal adduct **151**-Zn-(**137**-H$_2$O) and TSA adduct **151$_2$**-Zn$_2$-(**137**-H$_2$O), which incorporates two zinc ions and two ligands (Figure 101)
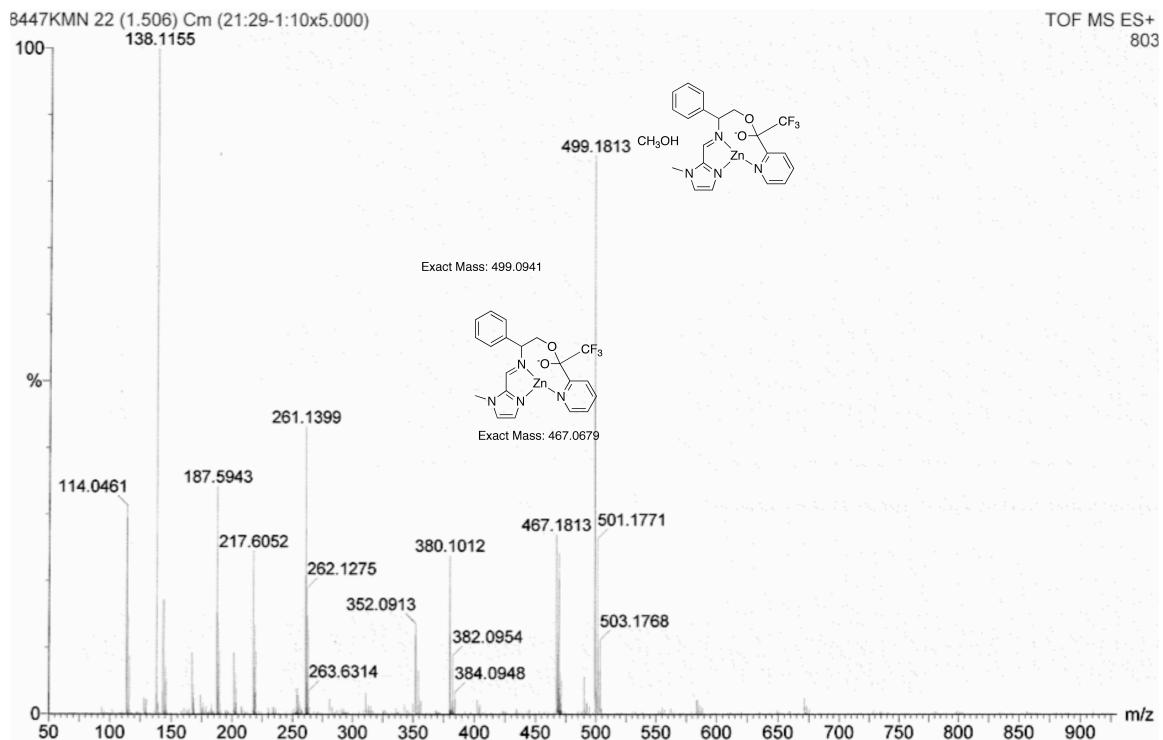
**Figure 100.** ESI-MS of a mixture of Zn(OTf)$_2$, **139**, **149**, and TSA **137.**
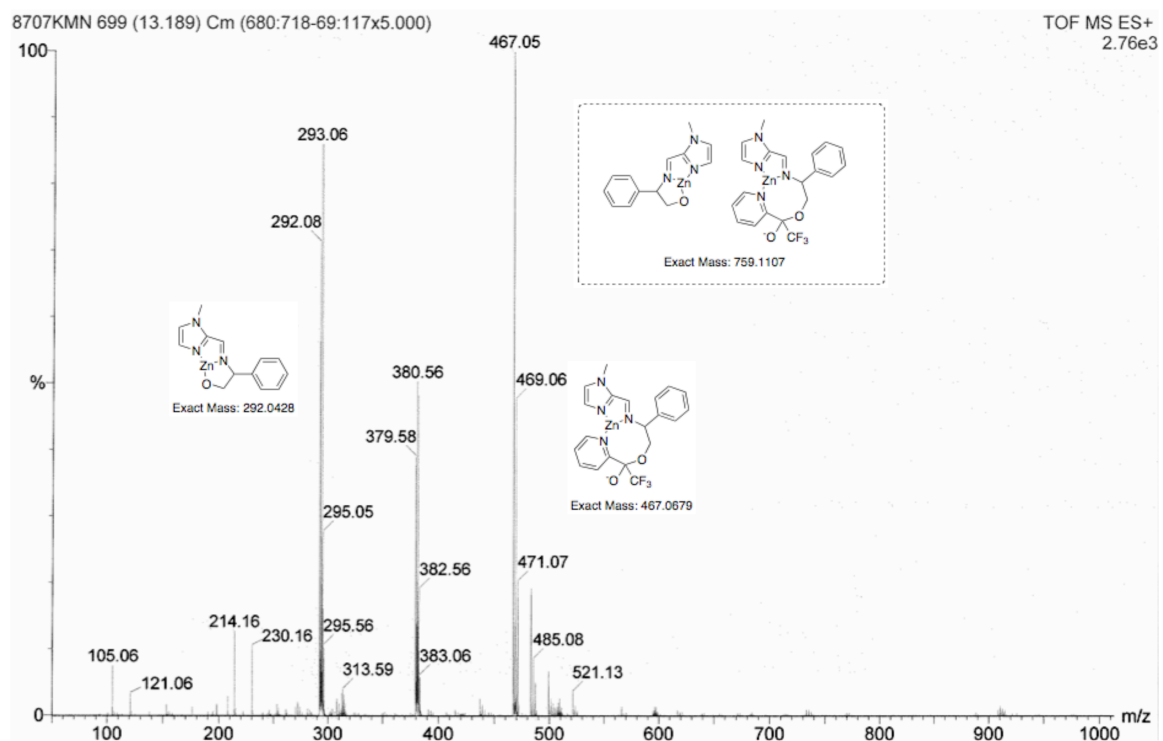


**Figure 101.** ESI-MS of templated library III shows the hemiketal adduct **151**-Zn-(**137**-H$_2$O).

### 3.2.3.6 $^{19}$F NMR Job Plot

In order to establish the stoichiometry of the ternary complex adduct, an NMR Job plot was constructed by producing 1:9, 3:1, 1:1, 1:3, and 9:1 mixtures of **151-**ZnL and TSA **137** while holding the total concentration of ZnL and TSA constant at 10 mM. (Figure 102) Samples were observed by $^{19}$F-NMR. The apparent stoichiometry of the ternary complex adduct is 2:1 **151**-Zn:**137**. This was corroborated by the presence of the Zn$_2$ **151$_2$** (**137**-H$_2$O) peak in the ESI-MS.
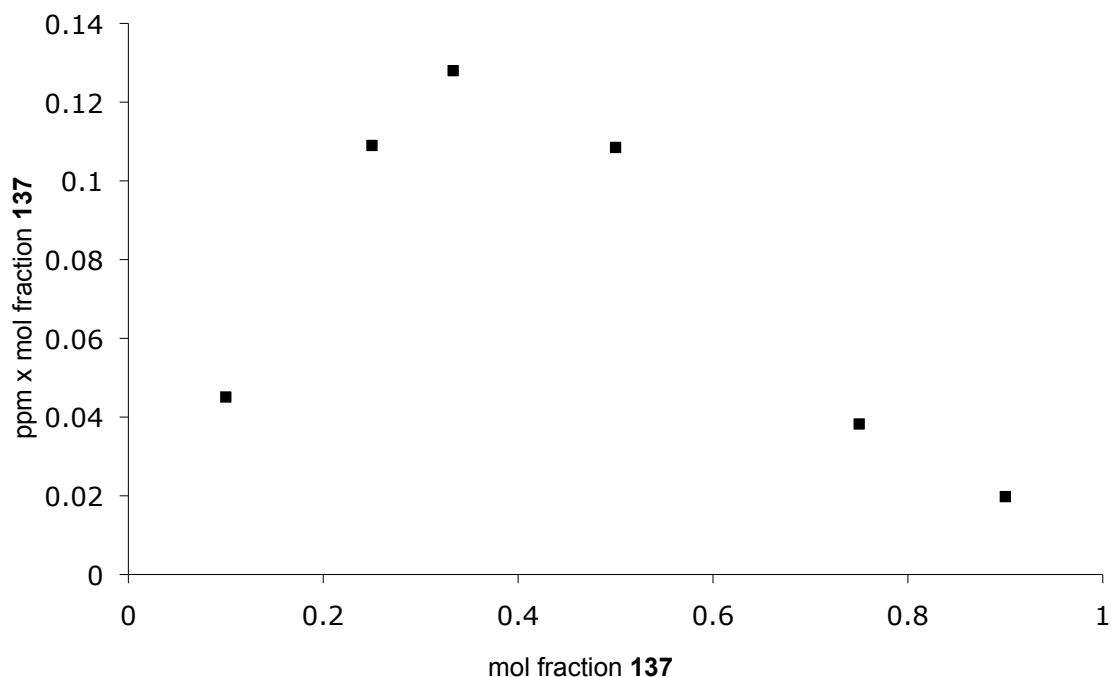


**Figure 102.** $^{19}$F-NMR Job Plot for **151-**Zn and **137** shows a 2:1 complex.

### 3.2.3.7 Templating with 136

Interestingly, when phosphonate TSA **136** was used as the template, the opposite templating trend was observed. In library III, in the presence of 1 equivalent of **136**, **152** is amplified 1.3-fold and **153** is attenuated 0.6-fold. (Figure 103)
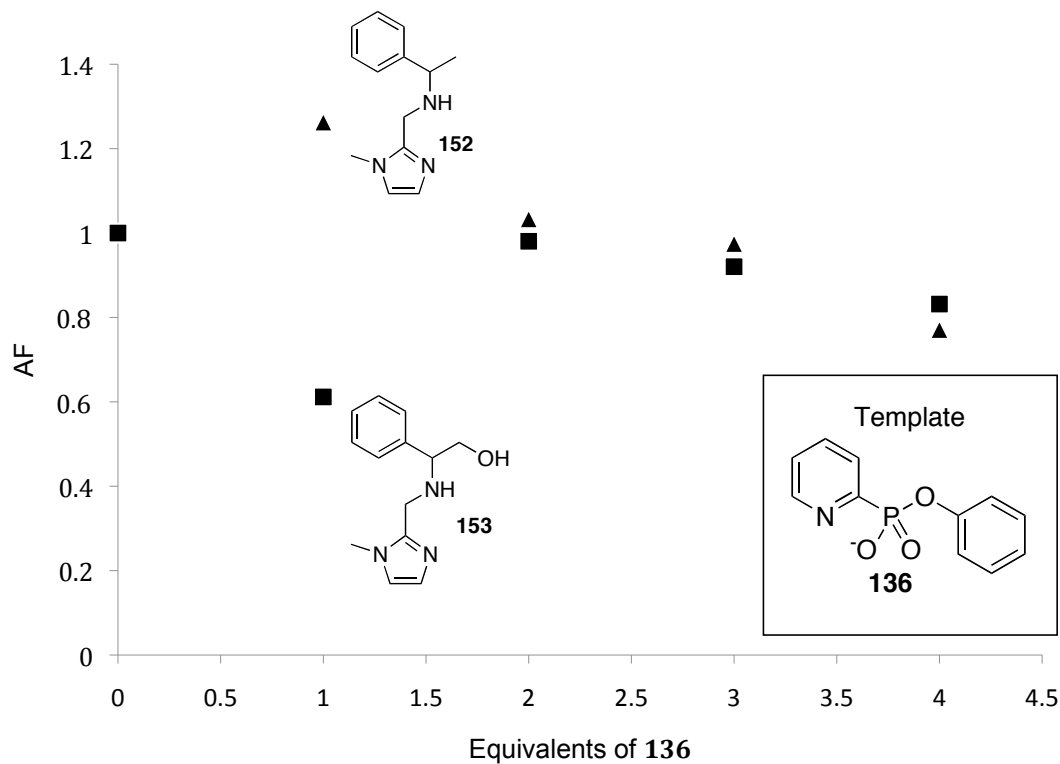


**Figure 103.** Library IIIb templated with phosphonate TSA **136** shows amplification which is opposite that which is observed in the presence of TSA **137**: Amplification of **152**(▲) and attenuation of **153** (■).

## 3.2.3.8 Discussion
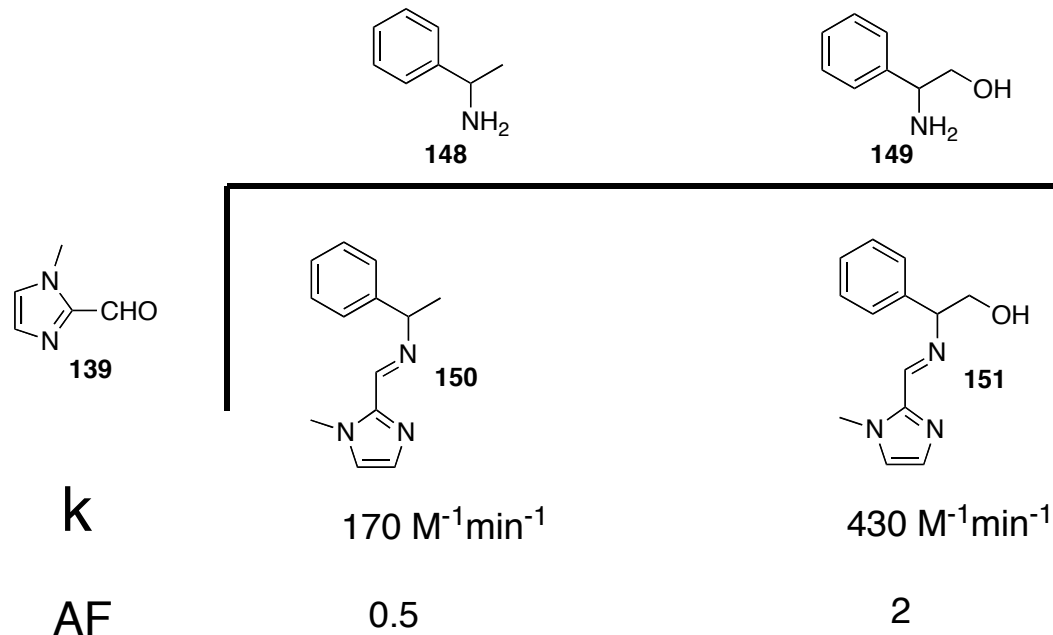


**Figure 104.** Summary of results for library III.

Templating with trifluoromethylketone **137** leads to amplification of a hydroxy-bearing ligand **151** at the expense of an unsubstituted analog **150**. This is reflected in the catalytic behavior of **150** and **151** in the hydrolysis of **135**. (Figure 104) The ternary hemiketal adduct Zn **151** (**137**-H$_2$O) was detected in the DCL mixture by ESI-MS, as well as a dizinc complex Zn$_2$**151**$_2$(**137**-H$_2$O). The ^{19}F-NMR Job plot indicates a 2:1 complex matching this stoichiometry. Ligand **150** is unable to form a hemiketal adduct with TSA **137**, and is therefore 'less fit' than **151** in the presence of **137**. The same can be said regarding its hydrolysis of **135**; the hydroxy group of **151** most likely assists in the hydrolysis of **135** by acting as a neighboring-group nucleophile.[79,86-88]

Interestingly, phosphonate TSA **136** yields the opposite amplification result, probably due to the fact that it does not possess the ability to exchange its phosphonate

oxygens for the hydroxy group of the ligand. Instead, the hydroxy group may interfere with the binding of the phosphonate, and lead to the amplification of **150**. This illustrates the importance of the mechanism of the catalysis in determining the structure of the appropriate catalytically relevant TSA.

### 3.2.4 A DCL containing two competing amino alcohol building blocks (149 and 154) templated on TSA 137

In order to examine whether TSA **137** could be used to elicit finer discrimination than between complexes of hydroxy-bearing and non-hydroxy-bearing ligands (**150** and **151**), library IV was prepared, (Figure 105) containing building blocks **149** and **154**, which differ by the donor characteristics of the amine as well as the geometric disposition of the hydroxy group.
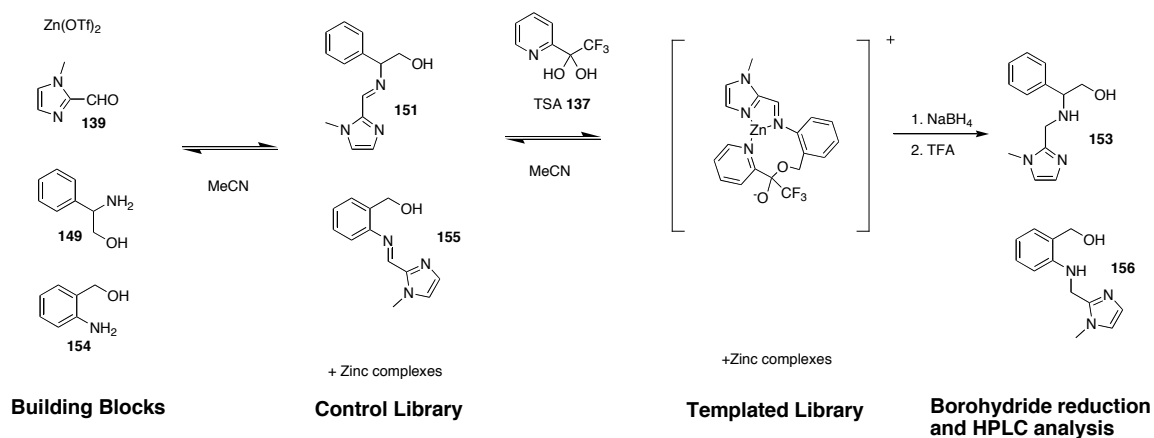


**Figure 105.** Library IV

### 3.2.4.1 Templating result

When a 1:1:1:1 mixture of Zn(OTf)$_2$, **139, 149,** and **154** was made in acetonitrile and allowed to equilibrate 48 hours, a control library of complexes of two competing

hydroxy-bearing ligands **151** and **155** was established. Varying amounts of TSA **137** were added to an otherwise identical mixture (templated library). Both libraries were reduced with sodium borohydride (overnight, rt), treated with TFA and analyzed by RP-HPLC. (Figure 106) Ligand **156** was found to be amplified 2.5-fold, and **153** attenuated 0.5-fold by the presence of TSA **137**. (Figure 107)
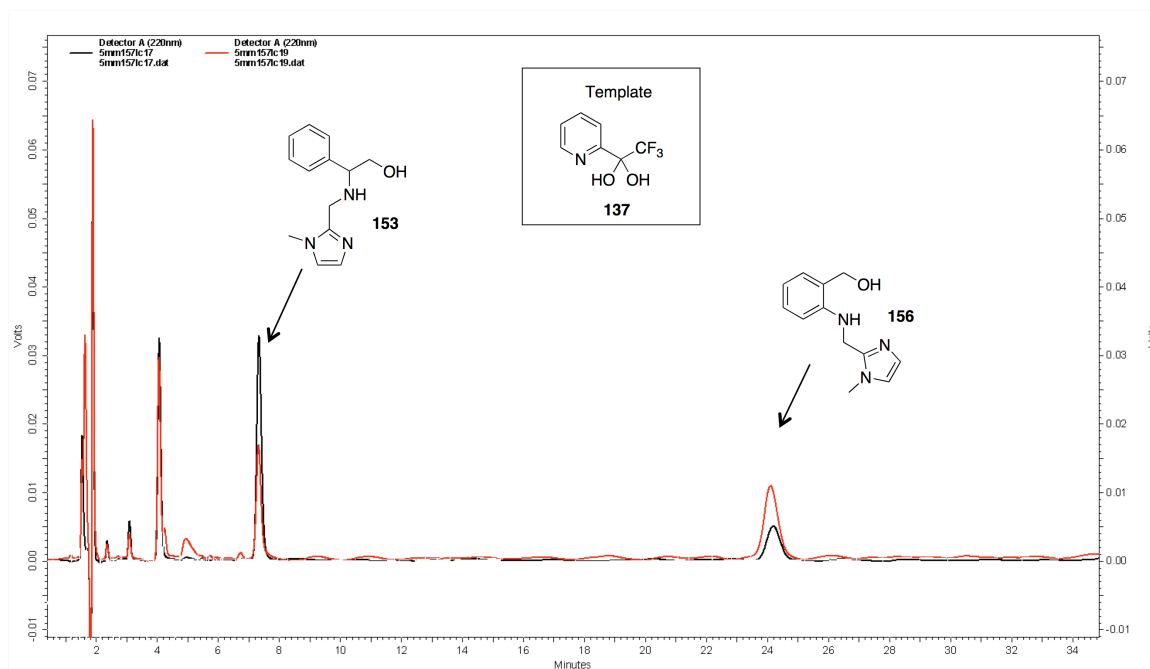


**Figure 106.** RP-HPLC chromatograms of  control (black) and templated with **137** (red) library IV.
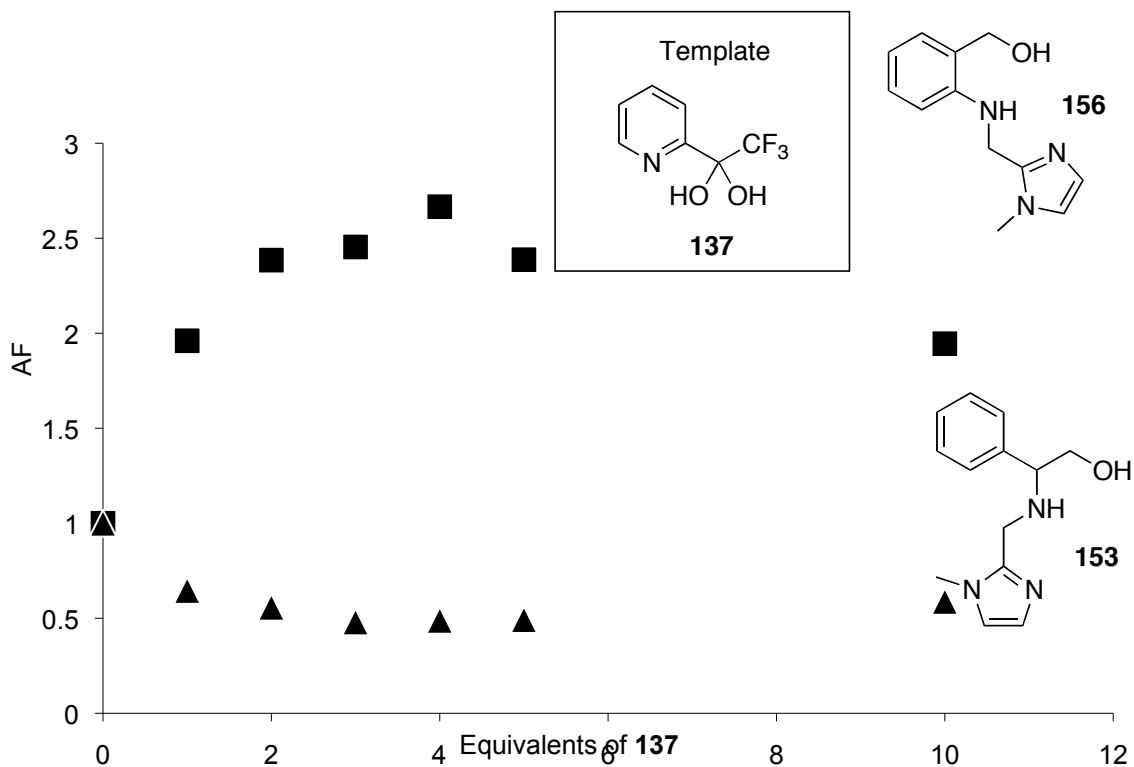
**Figure 107.** Library IV. Amplification behavior of **153**(▲) and **156** (■) in the presence of **137**.
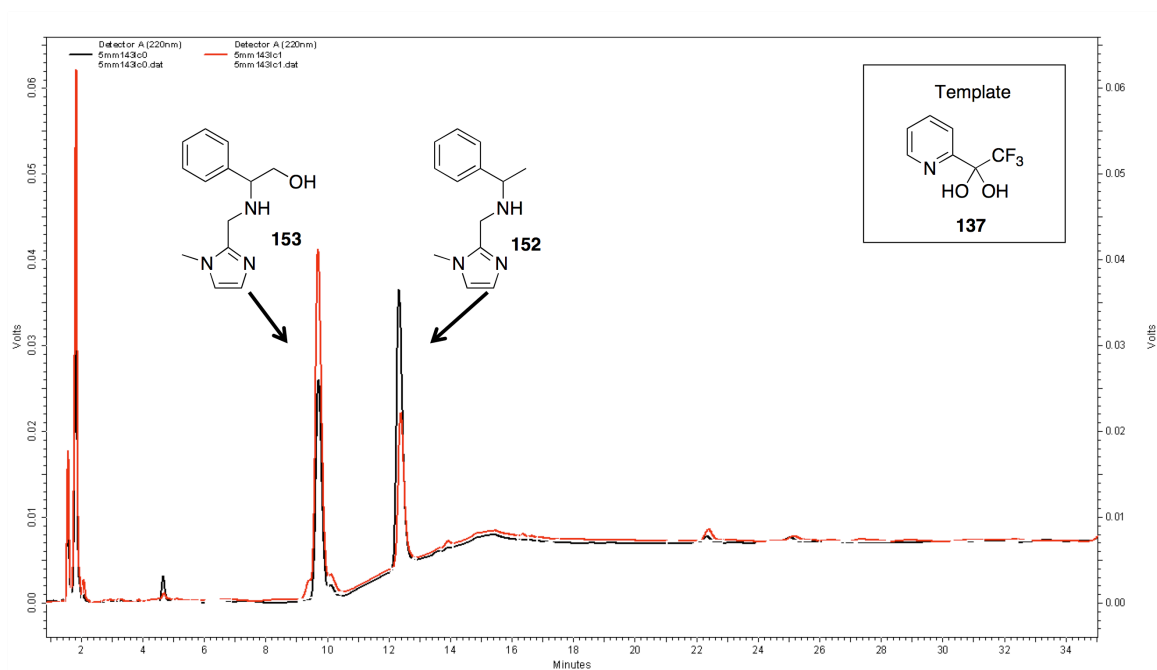
### 3.2.4.2 Single turnover kinetics

The zinc complex **155**-Zn (OTf)$_2$ was prepared by mixing the amine, aldehyde and zinc triflate in methanol and allowing to equilibrate 48 hours. This species was tested for single-turnover hydrolysis of substrate **135**. Hydrolysis was measured spectrophotometrically by observing the formation of *p*-nitrophenol at 400 nm. The reaction solution 30% methanol in water buffered at pH 7.5 using MOPS at 25$^{\circ}$ C. Substrate **135** concentration was held at 0.082 mM, and catalyst was varied from 0.2 to 0.6 mM. The rate dependence on catalyst concentration was first order. (Figure 108) The second order rate constant for hydrolysis of **135** was 1930 M$^{-1}$min$^{-1}$ for **155**-Zn(OTf)$_2$.

Recall that the second order rate constant for hydrolysis of **135** was 430 M$^{-1}$min$^{-1}$ for **151**-Zn(OTf)$_2$ (see section 3.2.3.4).
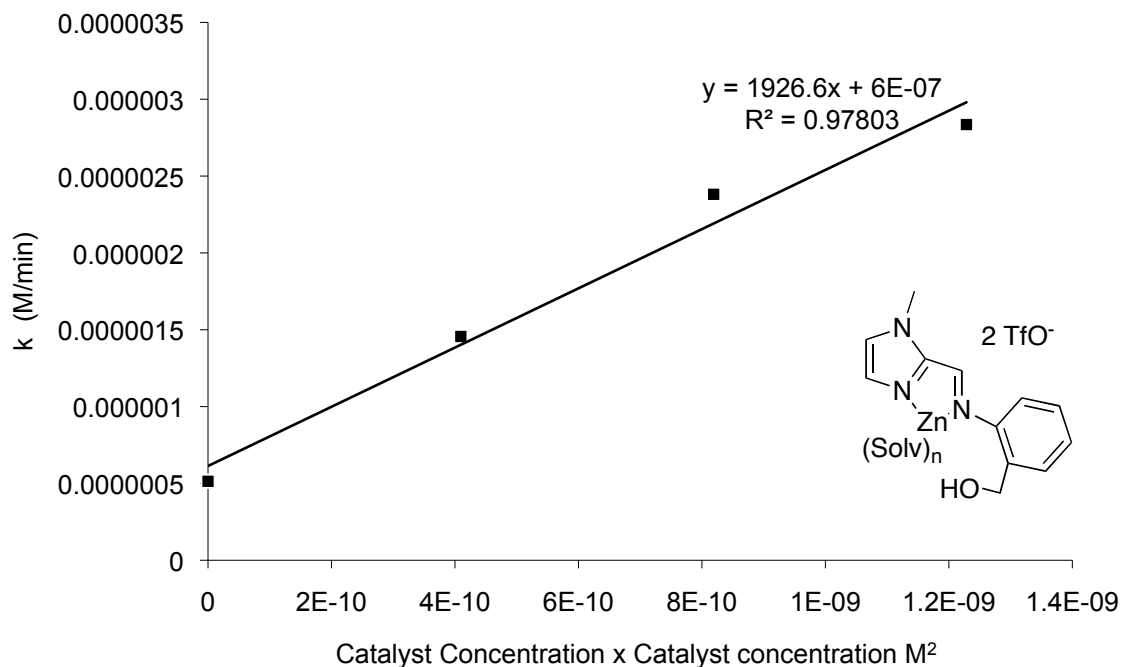


**Figure 108.** Single-turnover kinetics for hydrolysis of **135** by **155**-Zn.

### 3.2.4.3 Multiple turnover kinetics

The catalytic activity of complexes **151**-Zn(OTf)$_2$ and **155**-Zn(OTf)$_2$ were studied for the hydrolysis of **135** under multiple turnover conditions (excess substrate), varying the catalyst concentration. The concentration of **135** was 0.82 mM, and the catalyst concentration was varied from 0.02 mM to 0.08 mM. Reactions were observed for 16 minutes, with the region from 4 to 8 minutes used for the analysis (this was calculated to correspond to 2-4 turnovers, or 4%-10% conversion, depending on the catalyst concentration). The assay was carried out at 25° C in the presence of 75% aqueous 100 mM MOPS buffer held at pH 7.5, and observed at 400 nm. Rate dependence on catalyst

concentration was first order. (Figure 109) The second order rate constant for hydrolysis of **135** was determined to be 118 $M^{-1}min^{-1}$ for **155**-Zn(OTf)$_2$ and 70 $M^{-1}min^{-1}$ for **151**-Zn(OTf)$_2$.
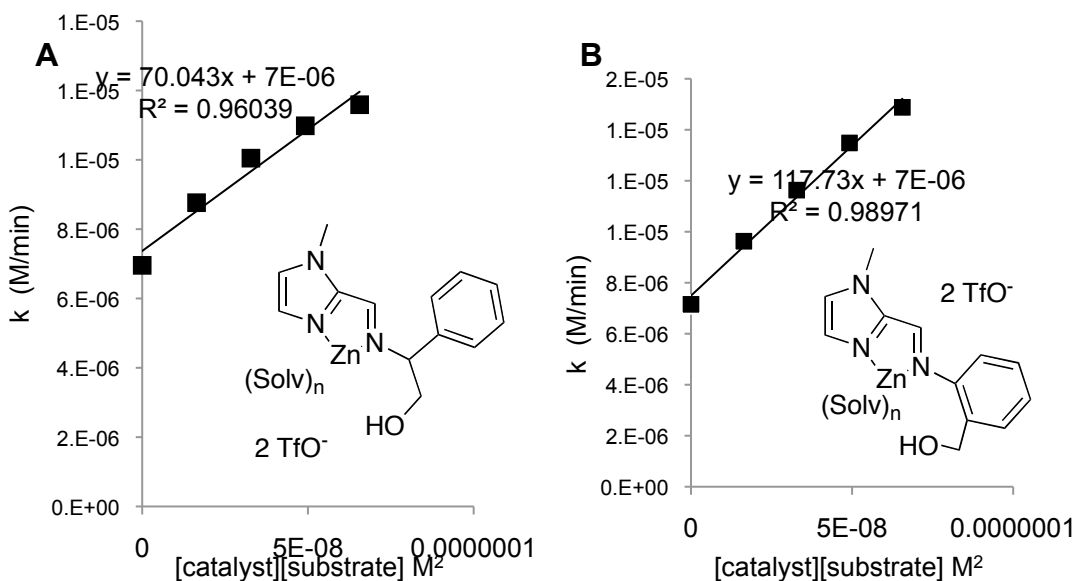


**Figure 109.** Multiple-turnover kinetics for **151**-Zn (A) and **155**-Zn (B).

### 3.2.4.4 Saturation kinetics

Since a bound substrate is involved in the hydrolysis of substrate **135** by these zinc complexes, we wondered whether catalysts **151**-Zn and **155**-Zn would exhibit saturation kinetics. The 4-nitrophenylpicolinate (**135**) hydrolysis assay was carried out under conditions of excess substrate (steady state conditions), varying the substrate concentration while holding Zn-Schiff base complex concentration constant. Kinetics runs for zinc amino alcohol imine ligand complexes were made in a 1 cm quartz cuvette containing 1 mL of solution consisting of 750 μL of 100 mM pH 7.5 MOPS buffer, 250 μL methanol, 40 μM Zn(**151**) or Zn(**154**), and **135** varying from 0.3 mM to 1.6 mM.

Spectrophotometric measurements were made at 400 nm at 25°C over a period of 8 minutes with 1 reading per 14 seconds. Both **151**-Zn and **155**-Zn complexes displayed saturation behavior. (Figures 110 and 112) Lineweaver-Burke plots were constructed by plotting reciprocal substrate concentration on the ordinate and reciprocal reaction rate on the abcissa (Figures 111 and 113). From the reciprocal of the y-intercept (the limit of reaction rate as substrate concentration approaches infinity) $V_{max}$ was determined to be $5.8 \times 10^{-6}$ $Mmin^{-1}$ and $2.0 \times 10^{-5}$ $Mmin^{-1}$ for Zn-**151** and Zn-**155**, respectively. From the reciprocal of the x-intercept, $K_M$ was determined to be $1.0 \times 10^{-2}$ M and $2.0 \times 10^{-3}$ M for Zn-**151** and Zn-**155**, respectively. The value of $k_{cat}$ ($V_{max}$/[catalyst]) was determined to be 0.15 $min^{-1}$ and 0.5 $min^{-1}$ for Zn-**151** and Zn-**155**, respectively.
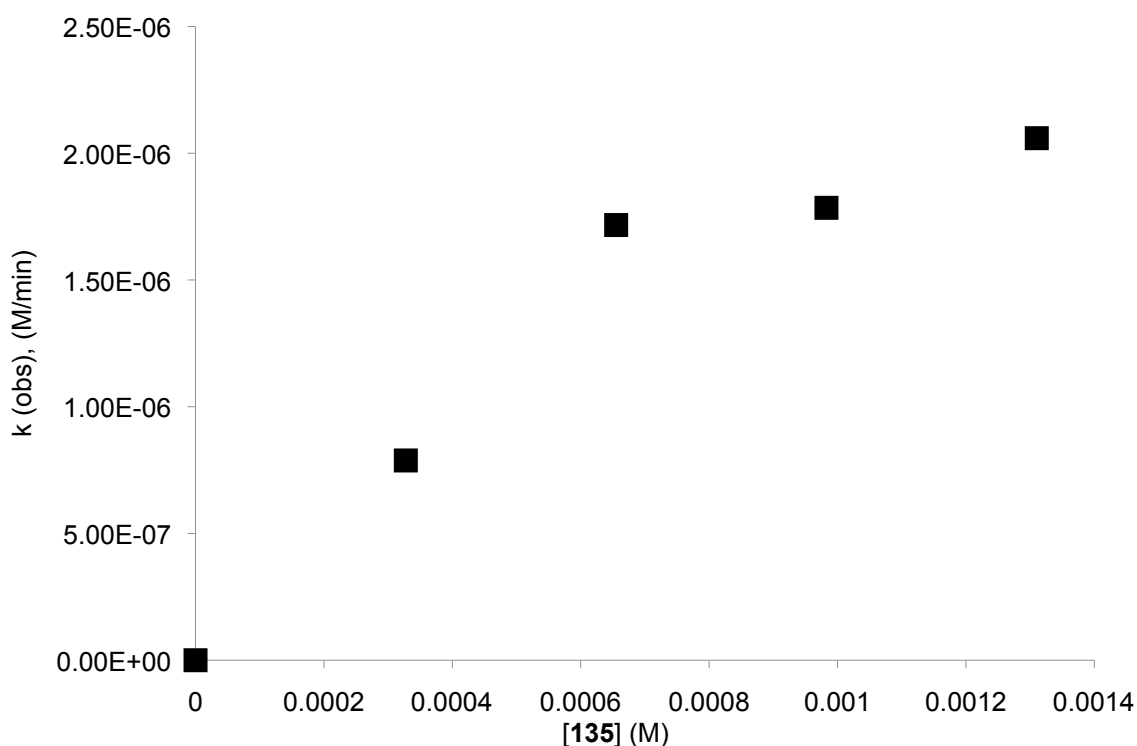


**Figure 110**. Saturation kinetics behavior for **151**-Zn.
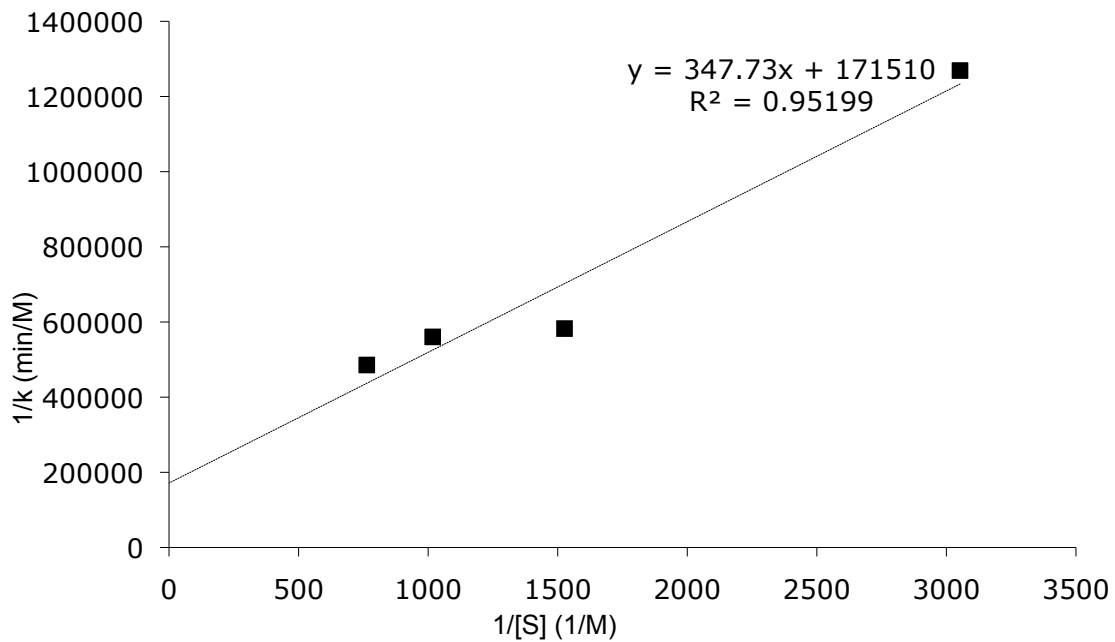
**Figure 111.** Lineweaver-Burke plot for hydrolysis of **135** by **151**-Zn.
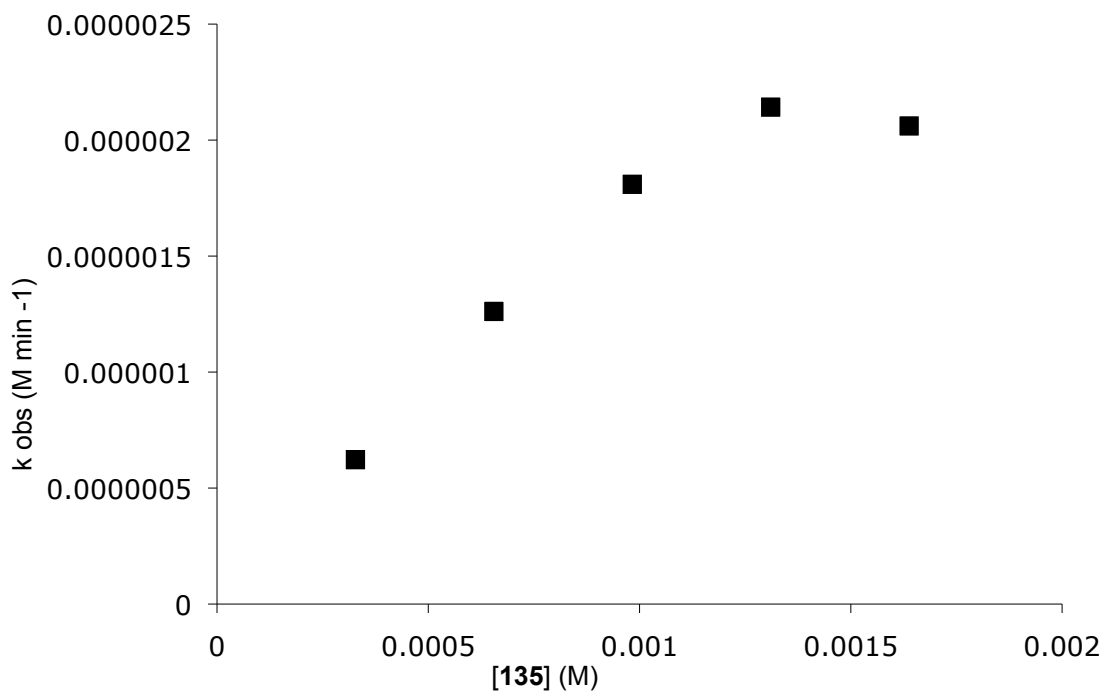


**Figure 112.** Saturation kinetics for hydrolysis of **135** by **155**-Zn.
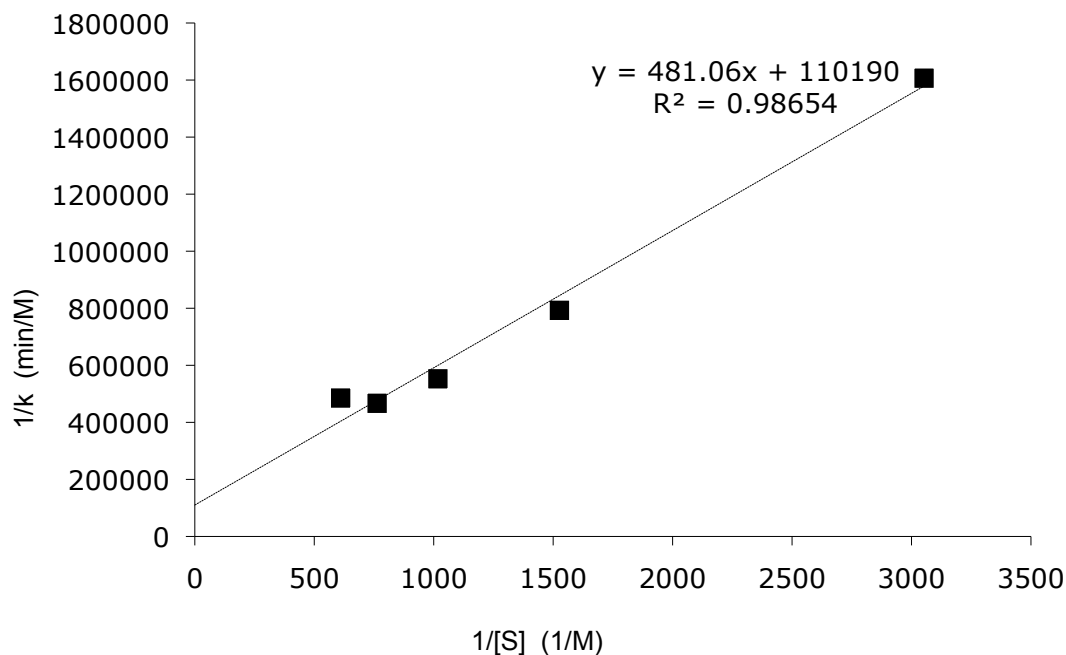
**Figure 113.** Lineweaver-Burke plot for hydrolysis of **135** by **155**-Zn.

### 3.2.4.5 Inhibition by TSA 137

The hydrolysis of **135** by Zn(**151**) and Zn(**155**) was followed under saturation conditions in the presence of TSA **137**. The experiments were carried out using 40 μM Zn(**151**) or Zn(**154**), **135** varying from 0.3 mM to 1.6 mM, and **137** varying from 0.05 mM to 0.4 mM. Both **151**-Zn and **155**-Zn are inhibited by TSA **137**. Lineweaver Burke treatments were made from the data. (Figures 114 and 115) In both cases, the presence of increasing concentrations of inhibitor appears to alter the slope of the Lineweaver-Burke plot, but not the y-intercept. This indicates that the inhibition can be overcome by the presence of a large quantity of substrate, i.e., in the limit of infinite substrate concentration, the inhibited and uninhibited Lineweaver-Burke plots converge at $1/V_{max}$. Therefore **137** acts as a competitive inhibitor of **151**-Zn and **155** Zn.
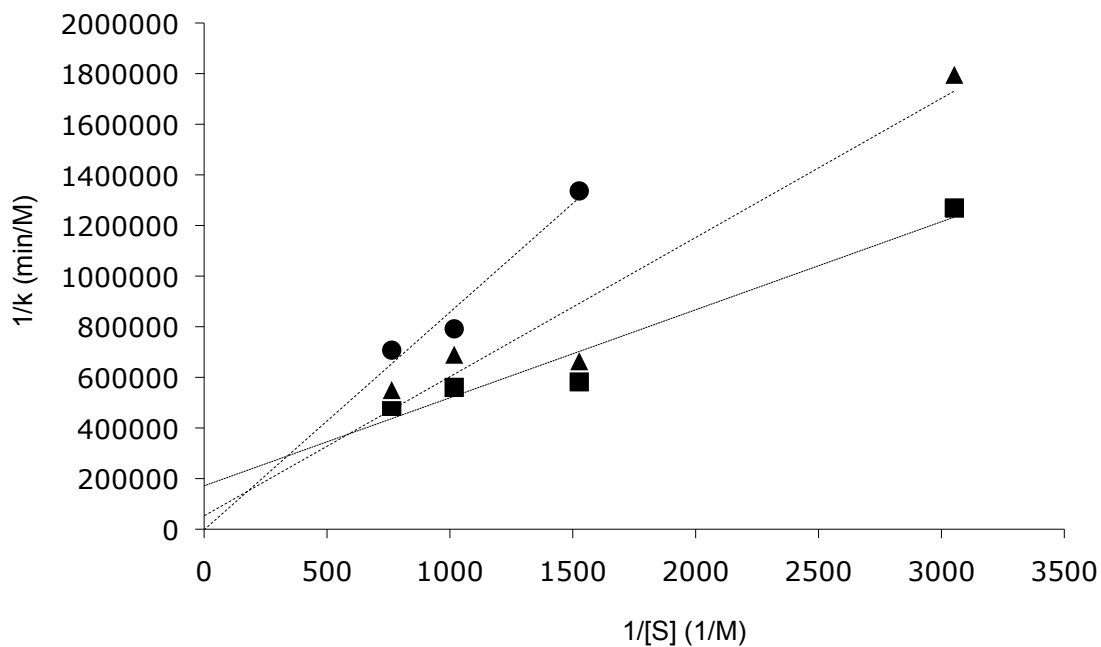
**Figure 114.** Lineweaver-Burke plot of hydrolysis of **135** by **151**-Zn in the presence of inhibitor **137**. No inhibitor (■), 0.1 mM inhibitor (▲), and 0.4 mM inhibitor (●).
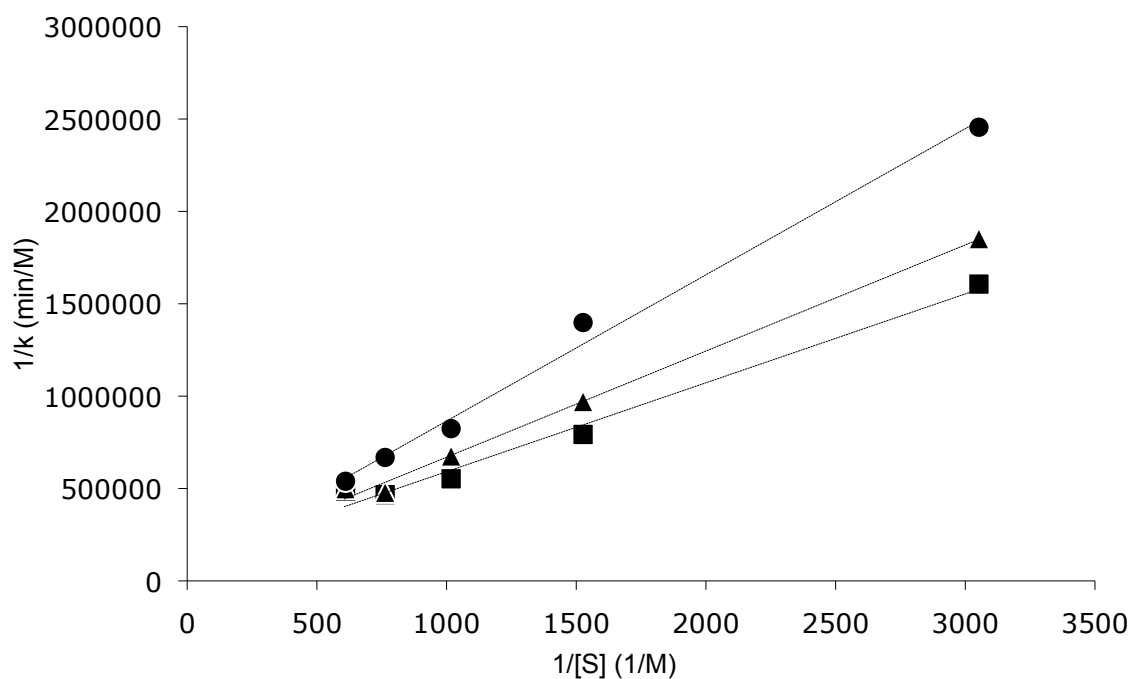


**Figure 115.** Lineweaver-Burke plot of hydrolysis of **135** by **155**-Zn in the presence of inhibitor **137**. No inhibitor (■), 0.04 mM inhibitor (▲), and 0.2 mM inhibitor (●).

### 3.2.4.6 ESI-MS

An ESI-MS of templated library IV (Figure 116) reveals five species containing TSA **137**. These are **155₂**-Zn₂-(**137**-H₂O)²⁺, (**155**)(**151**)-Zn₂-(**137**-H₂O)²⁺, **151₂**-Zn₂-(**137**-H₂O)²⁺, **155**-Zn-(**137**-H₂O)⁺, and **151**-Zn-(**137**-H₂O)⁺. These species represent hemiketal adducts of ligands and **137**. The complexes appear to have some tendency toward dimerization, although whether this is strictly an ionization-related phenomenon is not clear.
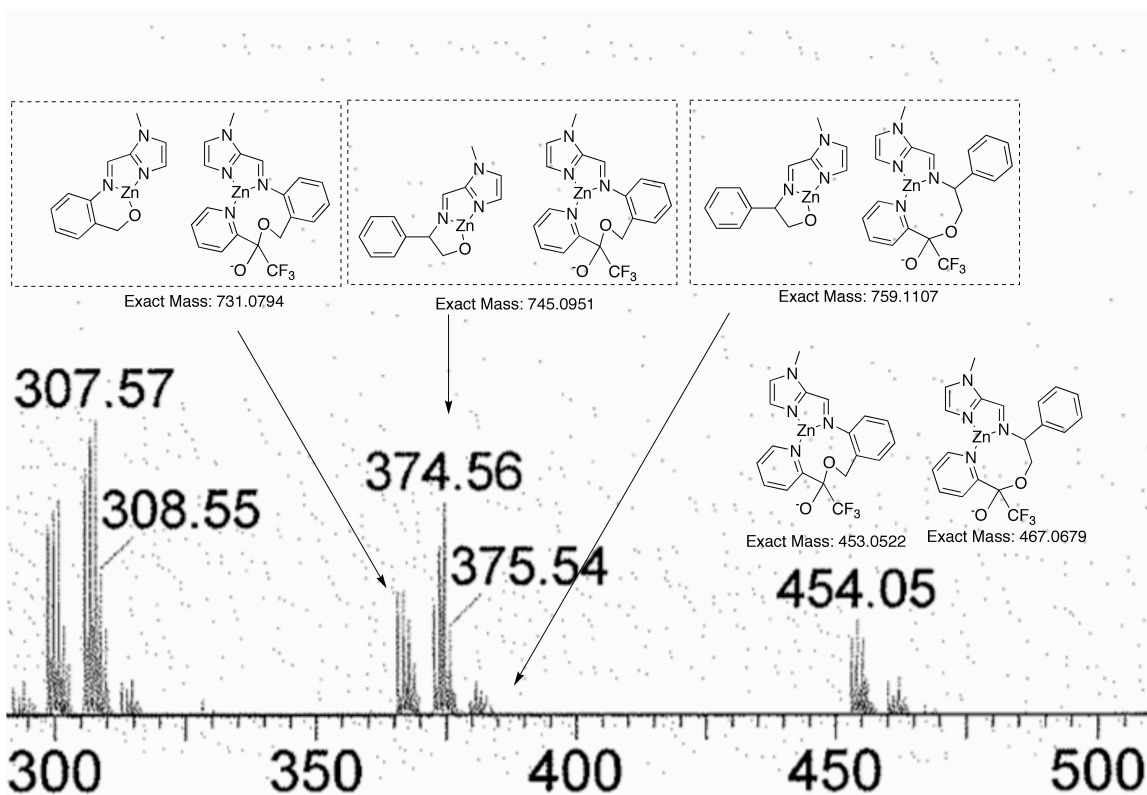


**Figure 116.** ESI-MS of library IV.

**3.2.4.7 Job Plot**

A $^{19}$F-NMR Job plot was constructed for **155**-Zn and TSA **137** by producing 1:9, 3:1, 1:1, 1:3, and 9:1 mixtures of **155**-ZnL and TSA **137** while holding the total concentration of ZnL and TSA constant at 10 mM. (Figure 117) A maximum at 0.5 mol fraction **137** indicates that the stoichiometry of the complex is 1:1.
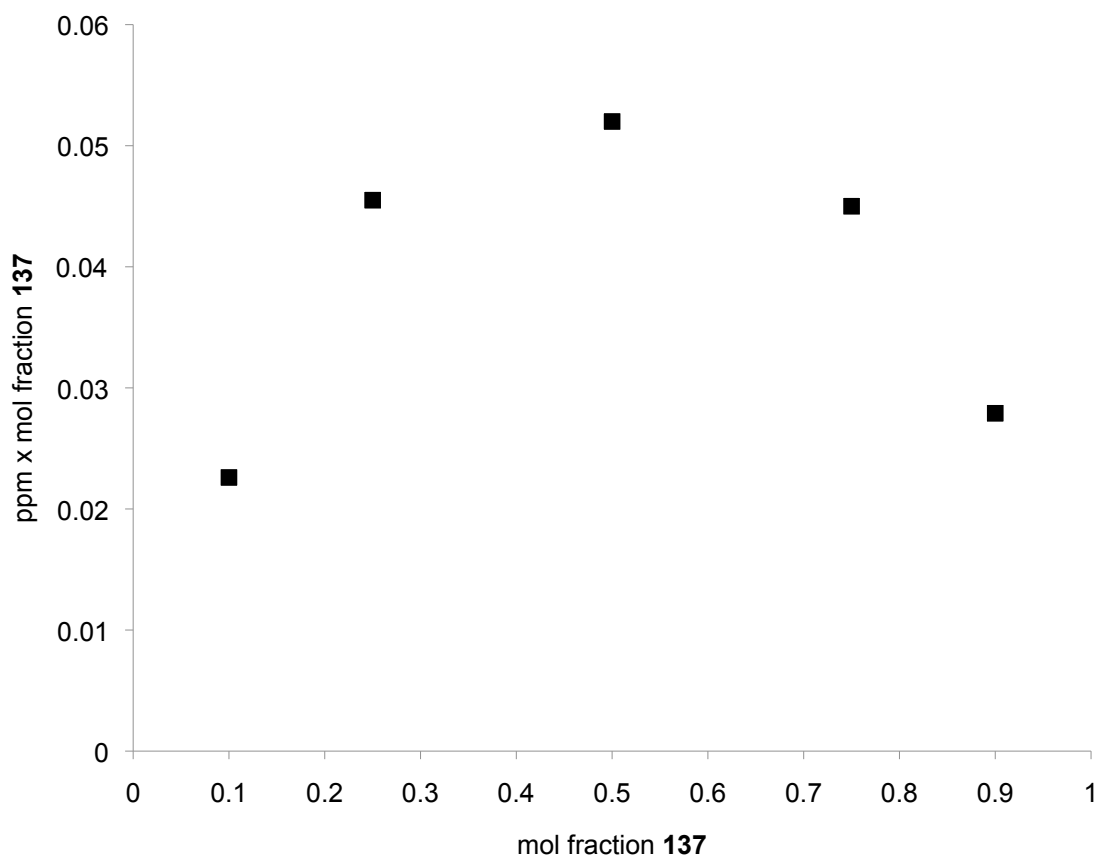


**Figure 117.** $^{19}$F-NMR Job plot for **155**-Zn and **137.**

**3.2.4.8 Templating with 136**

A 1:1:1:1 mixture of Zn(OTf)$_2$, **139, 149,** and **154** was made in acetonitrile (library IV). Phosphonate ester TSA **136** was added. The library was allowed to equilibrate 48 hours, and reduced with sodium borohydride. In the resulting library we observed the

amplification of **153** and attenuation of **156**, the opposite of the behavior seen for TSA

**137**. (Figure 118) Again, this is due to the fact that the phosphonate ester is not capable

of easily accepting the nucleophilic hydroxy group of these ligands, and is therefore not a

good TSA considering the likely mechanism of catalysis for the hydrolysis of **135**. The

amplification of **153** by the phosphonate ester underlines the importance of the choice of

TSA to match the mechanism of the catalytic reaction.
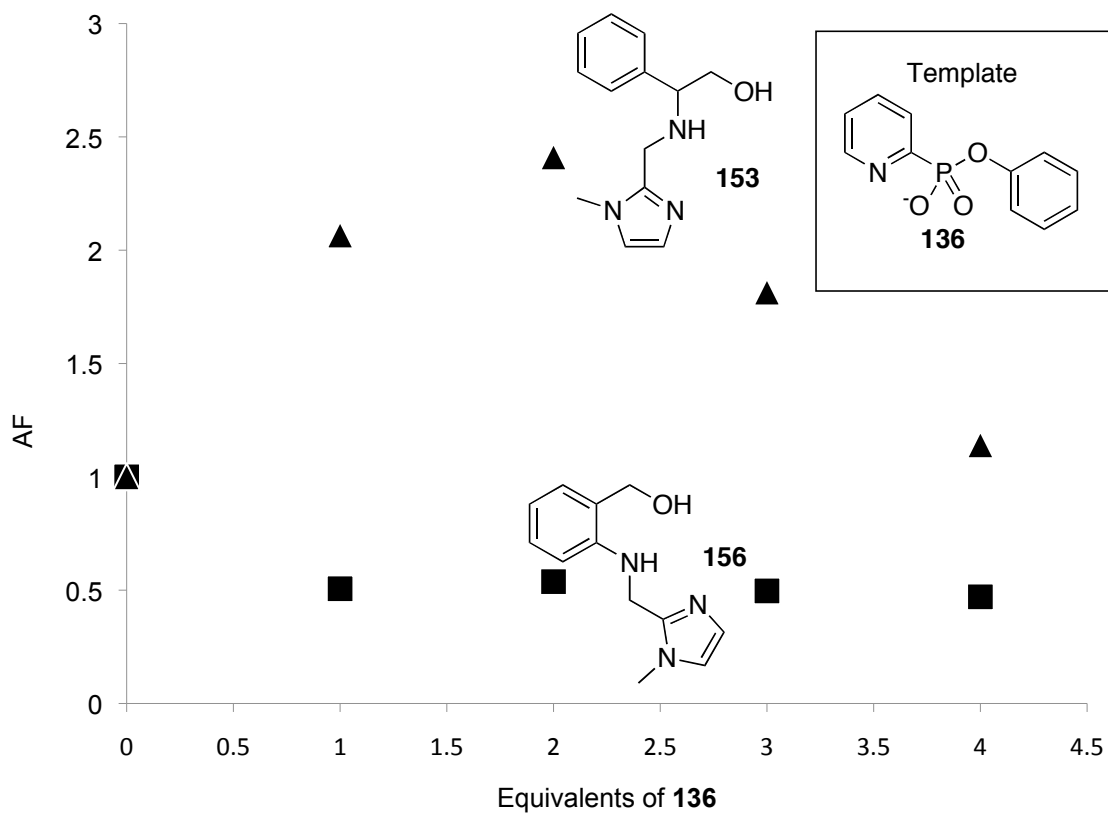


**Figure 118.** Library IVb templated with phosphonate TSA **136** showing amplification of

**153**(▲) and attenuation of **156** (■), in contrast to the **137**-templated library.

### 3.2.4.9 Discussion

TSA **137** can indeed discriminate between two different hydroxy-bearing ligands with differing catalytic activity for the hydrolysis of substrate **135**. A 2.5-fold amplification of **156** at the cost of **153** was observed in the presence of **137**. (Figure 120) ESI-MS of the library mixture reveals several zinc complexes in which **137** has formed a hemiketal adduct with ligand. A NMR Job plot revealed that the stoichiometry of the adduct of **155**-Zn and **137** is 1:1. Single-turnover rate constants for these to catalysts parallel the amplification behavior. Although considerably smaller, the multiple-turnover rate-constants also parallel amplification behavior. This is likely due to the fact that under multiple turnover conditions, the rate-determining step becomes the deacylation of the picolinate ester of the ligand by zinc-bound hydroxide, which is a slower step than addition of the ligand hydroxy to **135**.[79] (Figure 119) Fortuitously, TSA **137** is also a decent mimic for this deacylation step.
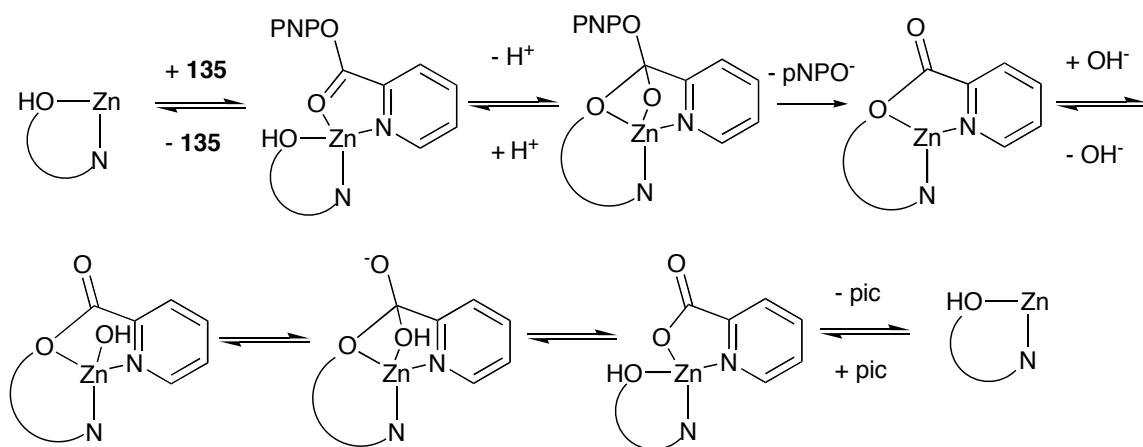


**Figure 119**. Probable mechanism of turnover for **135** hydrolysis by hydroxy-bearing zinc complexes.
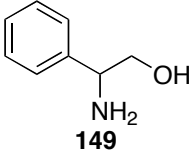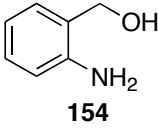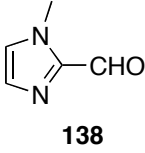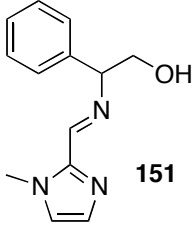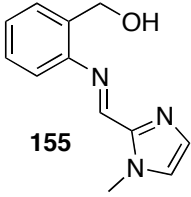
131

**Figure 120**. Summary of library IV results.

Rate experiments using varying excess substrate **135** with constant L-Zn showed saturation behavior, suggesting that the reaction proceeds through the formation of a substrate-catalyst complex. The values for $k_{cat}$ for **151**-Zn and **155**-Zn are 0.15 min$^{-1}$ and 0.5 min$^{-1}$, respectively, also paralleling the templating trend. Inhibition by TSA **137** was studied under these conditions, revealing somewhat competitive, probably mixed inhibition.

Templating with phosphonate ester TSA **136** yields the opposite result, leading to the amplification of the worst catalyst for **135** hydrolysis. This is likely due to the inadequacy of the phosphonate ester as a mimic of the transition state of the mechanistically relevant reaction. The use of a phosphonate ester TSA, owing to its non-

labile phosphonate oxygens, assumes no covalent involvement of the catalyst in the reaction.

The rationale for the selection of **155** over **151** is twofold. **155** is an aniline-derived Schiff base, considerably less electron-rich than the aliphatic amine-derived **151**. This should render **151**-Zn less Lewis-acidic than **155**-Zn. The two ligands also differ in the position of the hydroxy group. The larger chelate ring size made possible by **155** may better accommodate TSA **137**.

This data supports our hypothesis that catalytically relevant templating is taking place in this zinc-imine DCL. Further, it demonstrates that covalent participation of the catalyst can be accommodated by the correct choice of TSA.

### 3.2.5 A DCL containing amino alcohols substituted with methyl and phenyl groups templated on 137

Methyl- and phenyl- substituted building blocks **157** and **160** were used to probe the effect of steric bulk on the hydroxy-bearing arm of the ligand. (Figure 121) These compounds were prepared from 2-aminoacetophenone and 2-aminobenzophenone by a literature procedure.[89]
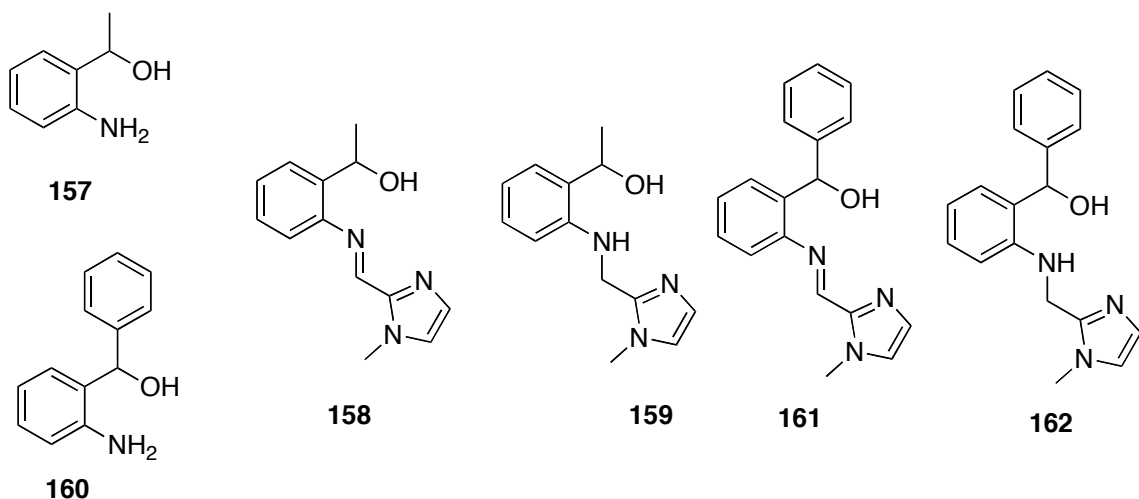
**Figure 121.** Methyl and phenyl-substitued building blocks, ligands, and reduced derivatives.

### 3.2.5.1 Templating results

In library V, zinc triflate and building blocks **154**, **157**, and **139** (1:1:1:1 in acetonitrile) were used to produce a library of zinc complexes of ligands **155** and **158**, differing only by a methyl group. (Figure 122) When **137** was used as a template, and the control and templated libraries were reduced and analyzed, the 2.7-fold amplification of **156** was observed, accompanied by the 0.5-fold attenuation of **159**. (Figure 123)

Similarly, in library VI, prepared by mixing 1:1:1:1 **139**, **154**, **160**, and $Zn(OTf)_2$ in acetonitrile, zinc complexes of ligands **155** and **160**, differing only by a phenyl group were produced. (Figure 124) When **137** was used as a template, and the control and templated libraries were reduced and analyzed, the 4-fold amplification of **156** was observed, accompanied by 0.1-fold attenuation of **162**. (Figure 125) This would seem to indicate that the additional steric bulk furnished by the methyl- and phenyl- substituted building blocks do nothing to enhance TSA-binding, but instead hinder the formation of

the adduct. This is reasonable considering that we are exchanging a primary alcohol with a secondary alcohol, which is well known to be less reactive as a nucleophile and less accessible to electrophiles.
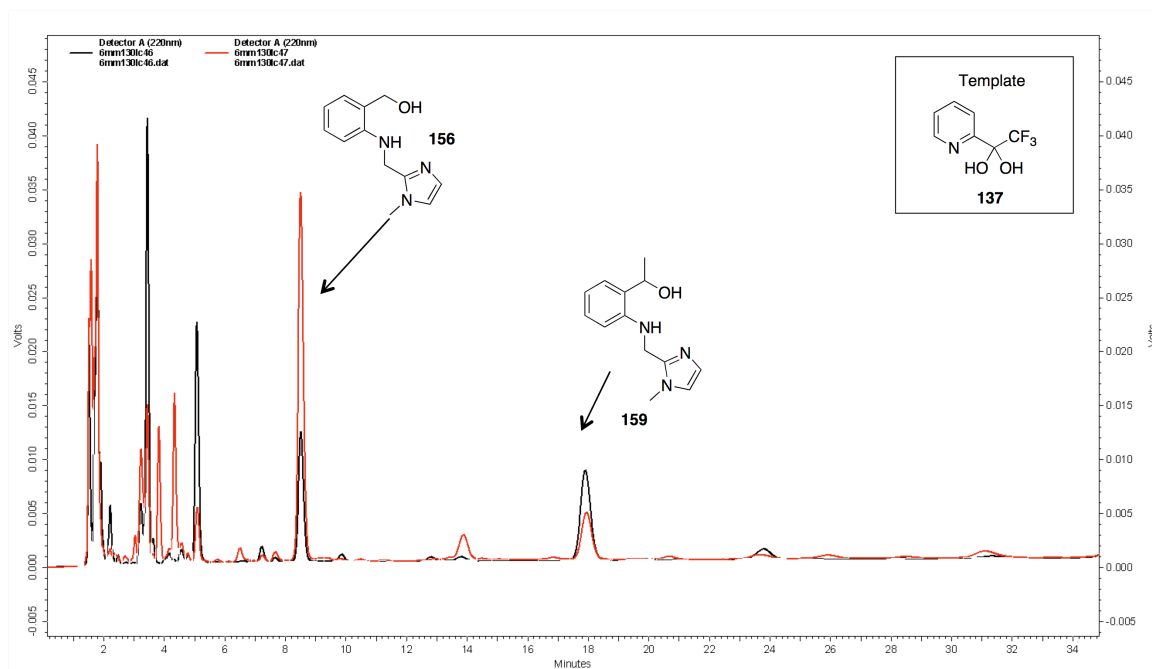


**Figure 122.** RP-HPLC chromatograms of control (black) and templated with **137** (red) library V.
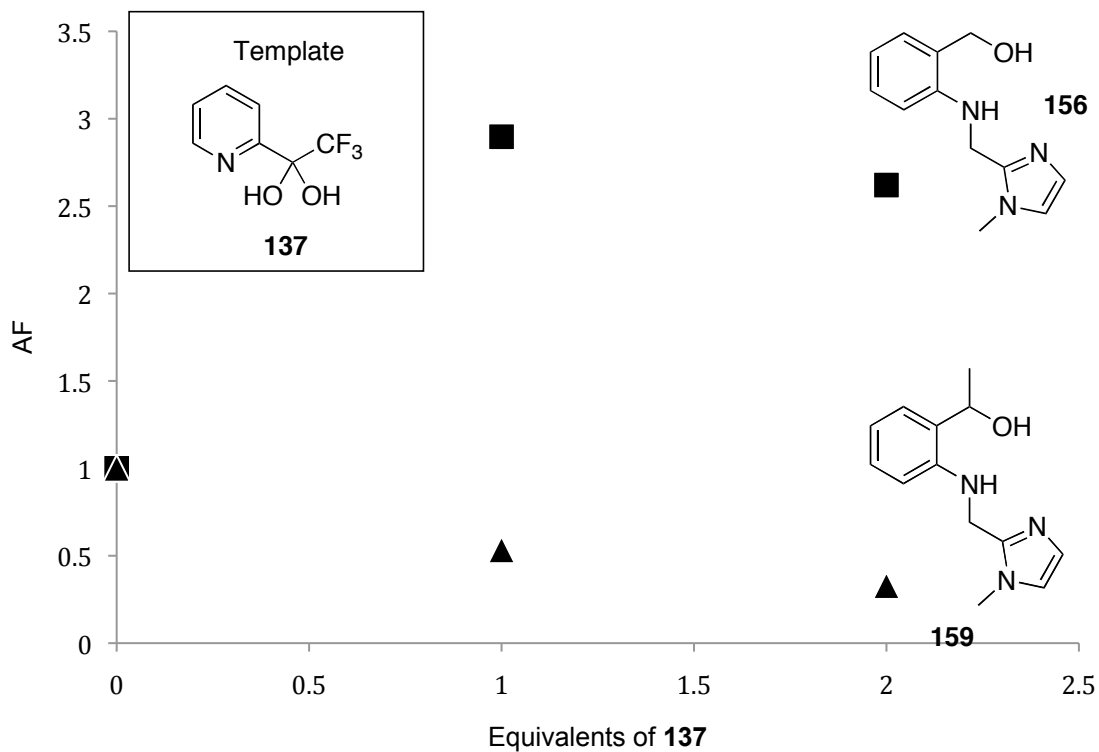
**Figure 123.** Library V. Amplification behavior of **159**(▲) and **156** (■) in the presence of **137**.
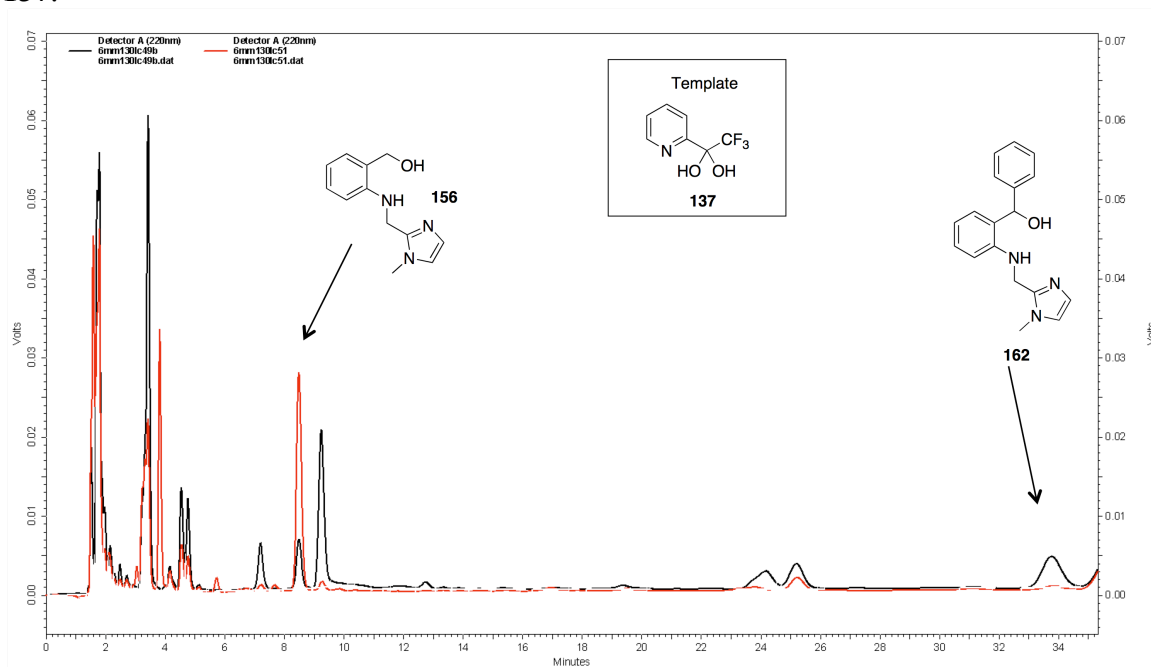


**Figure 124.** RP-HPLC chromatograms of control (black) and templated with **137** (red) library VI.

136
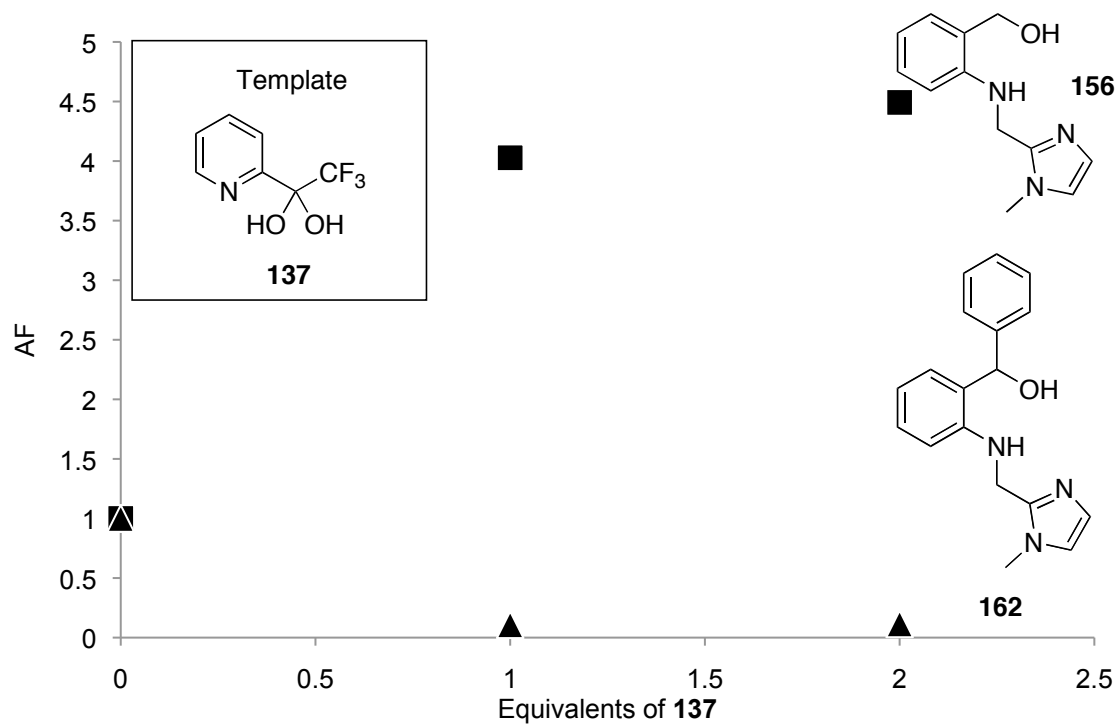
**Figure 125.** Library VI. Amplification behavior of **162**(▲) and **156** (■) in the presence of **137**.

### 3.2.5.2 Single-turnover kinetics

Single-turnover kinetics experiments for hydrolysis of **135** were carried out with **158**-Zn and **161**-Zn. The zinc complexes **158**-Zn (OTf)$_2$ and **161**-Zn (OTf)$_2$ was prepared by mixing the amine, aldehyde and zinc triflate in methanol and allowing to equilibrate 48 hours. These species were tested for single-turnover hydrolysis of substrate **135**. Hydrolysis was measured spectrophotometrically by observing the formation of *p*-nitrophenol at 400 nm. The reaction solution 30% methanol in water buffered at pH 7.5 using MOPS at 25° C. Substrate **135** concentration was held at 0.082 mM, and catalyst was varied from 0.2 to 0.6 mM. For both catalysts the rate dependence on catalyst concentration was first order. (Figure 126) The second order rate constant for hydrolysis of **135** was 1930 M$^{-1}$min$^{-1}$ for **155**-Zn(OTf)$_2$. The second order rate constants were

determined to be 202 $M^{-1}min^{-1}$ and 234 $M^{-1}min^{-1}$, respectively. Methyl- and phenyl fuctionalized catalysts **158**-Zn and **161**-Zn display considerably lessened reactivity in the single-turnover assay for **135** hydrolysis. This is best explained by the decreased nucleophilicity of a secondary alcohol in comparison to the primary alcohol of **155**-Zn. It is also likely that the added steric bulk of these ligands hinders the approach of the substrate, decreasing the concentration of the substrate-Zn-L complex.
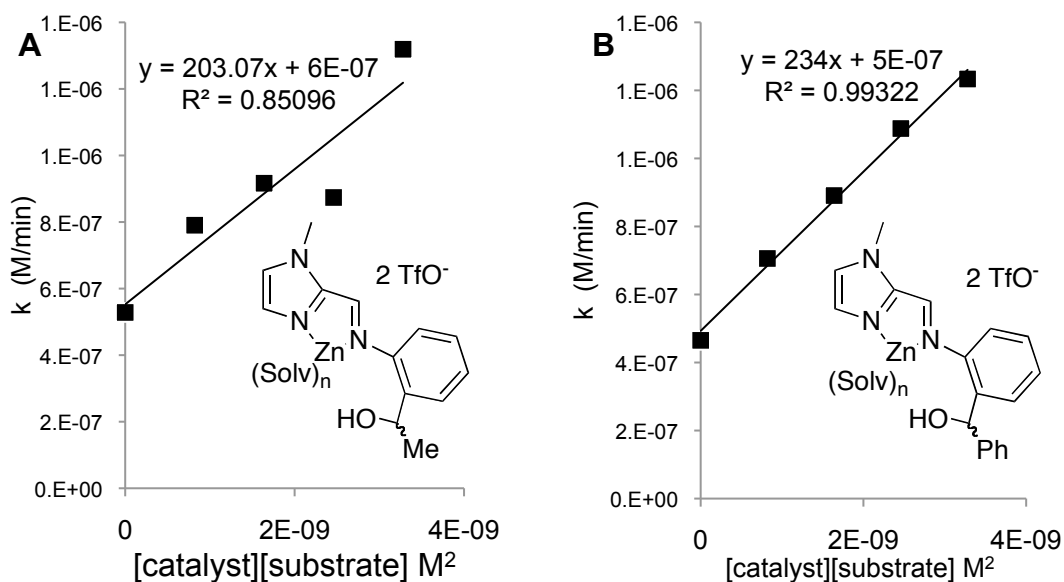


**Figure 126.** Single-turnover kinetics of hydrolysis of **135** by **158**-Zn (A) and **161**-Zn (B)

### 3.2.5.3 Multiple-turnover kinetics

Multiple-turnover kinetics experiments for hydrolysis of **135** were carried out with **158**-Zn and **161**-Zn. The hydrolysis of **135** was carried out under multiple turnover conditions (excess substrate), varying the catalyst concentration. The concentration of **135** was 0.82 mM, and the catalyst concentration was varied from 0.02 mM to 0.08 mM. Reactions were observed for 16 minutes, with the region from 4 to 8 minutes used for the analysis. The assay was carried out at $25^{o}$ C in the presence of 75% aqueous 100 mM

MOPS buffer held at pH 7.5, and observed at 400 nm. (Figure 127) The rate dependence on catalyst concentration was first order. The second order rate constants were determined to be 64 $M^{-1}min^{-1}$ and 45 $M^{-1}min^{-1}$, respectively. Complexes **158**-Zn and **161**-Zn are less active than **155**-Zn in the multiple-turnover assay.
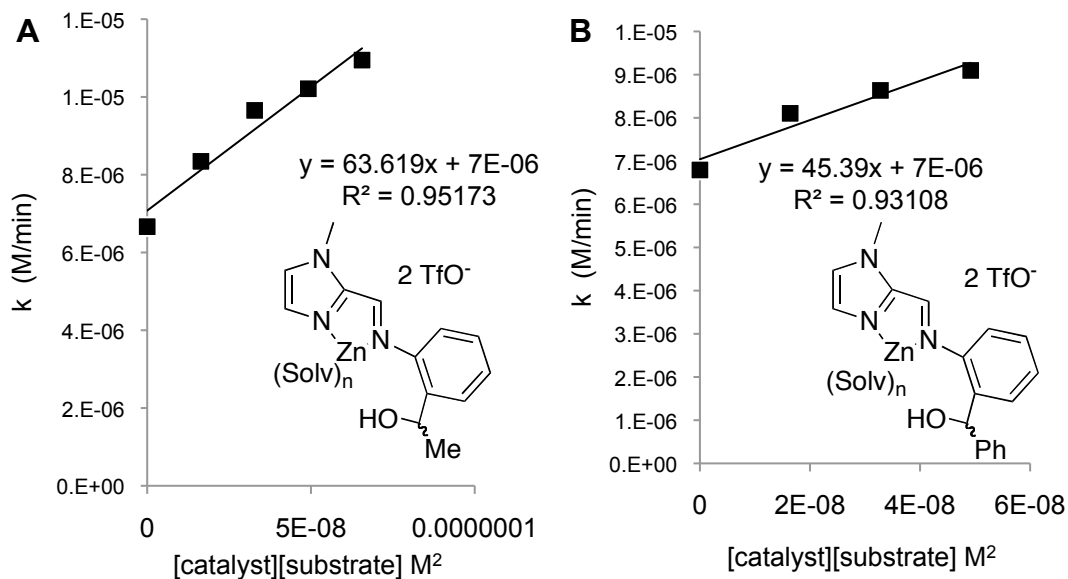


**Figure 127.** Multiple-turnover kinetics of hydrolysis of **135** by **158**-Zn (A) and **161**-Zn (B).

### 3.2.5.4 Job Plots

^{19}F-NMR Job plots of **158**-Zn + **137** and **161**-Zn + **137** were constructed. The Job plot for zinc complex of the methyl-bearing ligand **158** and **137** (figure 128) clearly shows a 1:1 stoichiometry, analogous to the non-methyl-functionalized ligand **155**. In contrast, the Job plot for the zinc complex of phenyl-bearing ligand **161** (figure 129) indicates a 2:1 complex with TSA **137**.
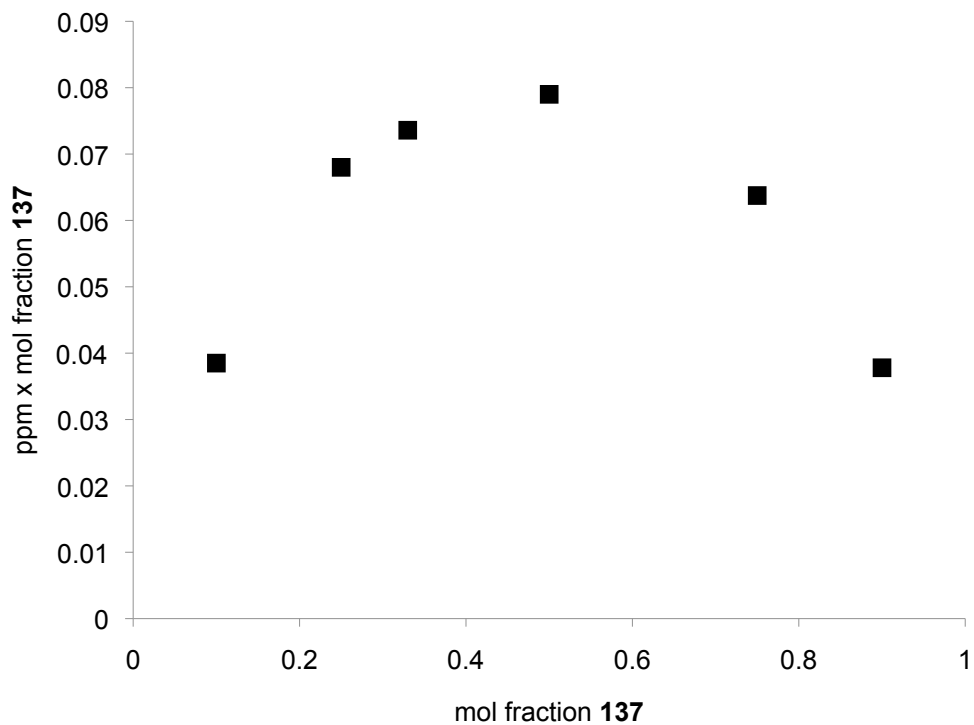
**Figure 128.** ^{19}F-NMR Job plot of **158**-Zn and **137**.
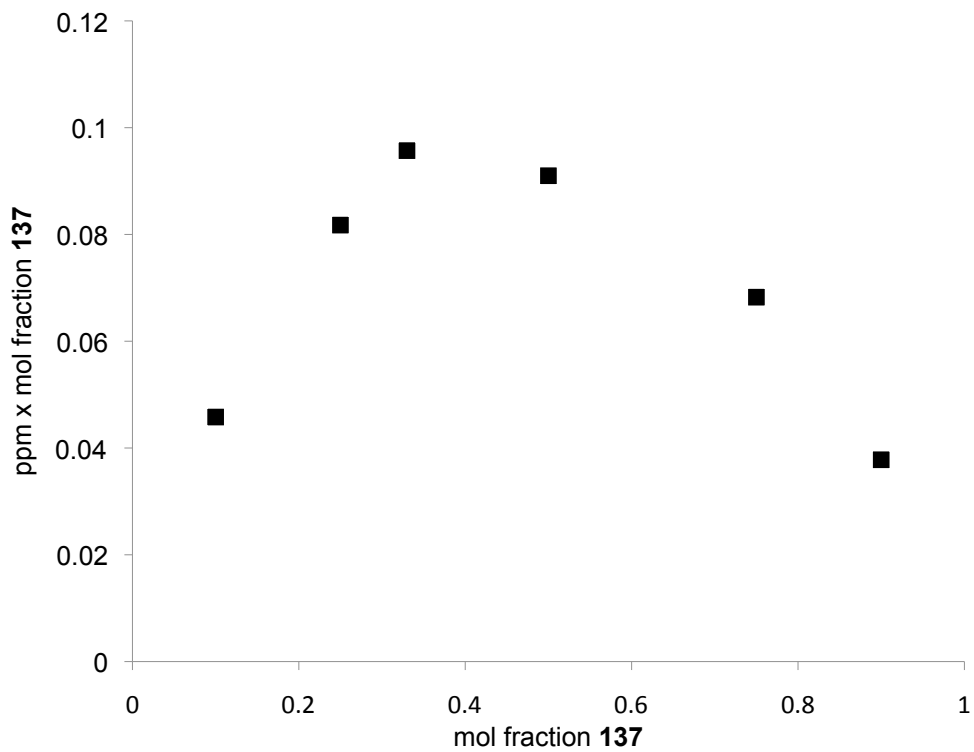


**Figure 129.** ^{19}F-NMR Job plot of **161**-Zn and **137**.

### 3.2.5.5 Discussion

Zinc complexes of the methyl- and phenyl-bearing derivatives (**158** and **161**) of 2-aminobenzyl alcohol-derived ligand **155** were compared with the zinc complex of **155** in templating behavior and hydrolytic behavior toward substrate **135**. (Figure 130) It was found that both methyl- and phenyl- functionalized complexes were inferior catalysts for the hydrolysis reaction compared to **155**, in both single-turnover and multiple-turnover conditions. This can be rationalized entirely by the fact that the additional steric repulsion furnished by the secondary alcohol in **158** and **161** render them less effective as nucleophiles in comparison to the primary alcohol of **155**.

This trend is reflected in a corresponding attenuation of the reduced ligand (**159** and **161**) in competition with **155** in libraries V and VI. It is likely that enhanced steric repulsion causes the adduct formation with template **137** to be less favorable.
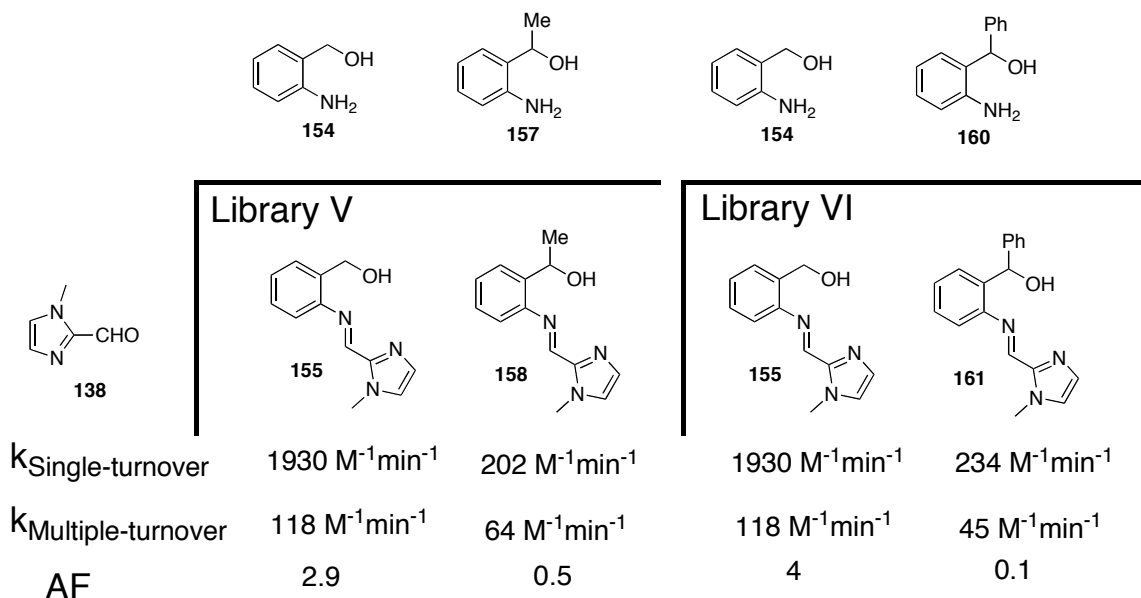


**Figure 130.** Summary of results for libraries V and VI.

### 3.2.6 A DCL containing four amino alcohol building blocks

We wondered whether the selection process illustrated above could be observed in a larger library. We constructed a library capable of yielding the complexes of four ligands **151**, **155**, **158**, and **161**. All building blocks were mixed in acetonitrile at a ratio of 1:1:1:1:1:1 (aldehyde **139**, amines **149**, **154**, **157**, **160**, and zinc triflate). The templated libraries contained 1 and 2 equivalents of trifluoromethylketone TSA **137**. Libraries were allowed to equilibrate 48 hours and then reduced with excess sodium borohydride, treated with TFA and analyzed by RP-HPLC. (Figure 131 and 132) The chromatograms clearly show the 2.8-fold amplification of **156** (reduced **155**), and the corresponding attenuation of **153**, **159**, and **162** (0.8-, 0.9-, and 0.3-fold, respectively). (Figure 133)
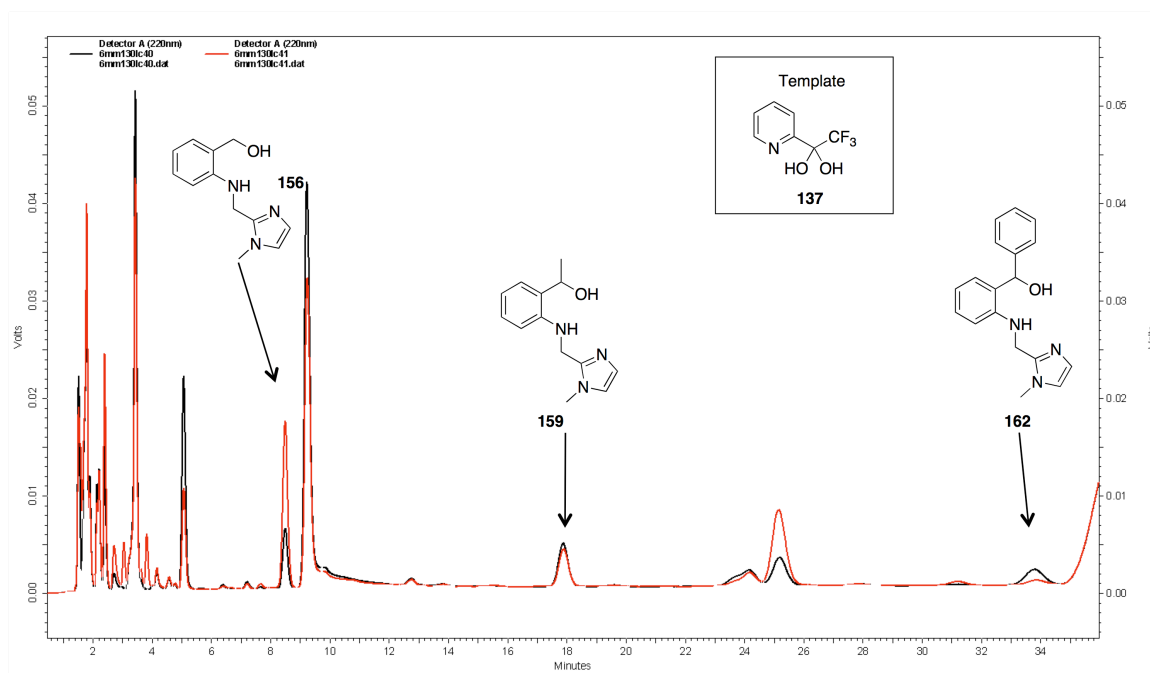


**Figure 131**. RP-HPLC chromatograms of control (black) and **137**-templated (red) library VII (late eluting species).
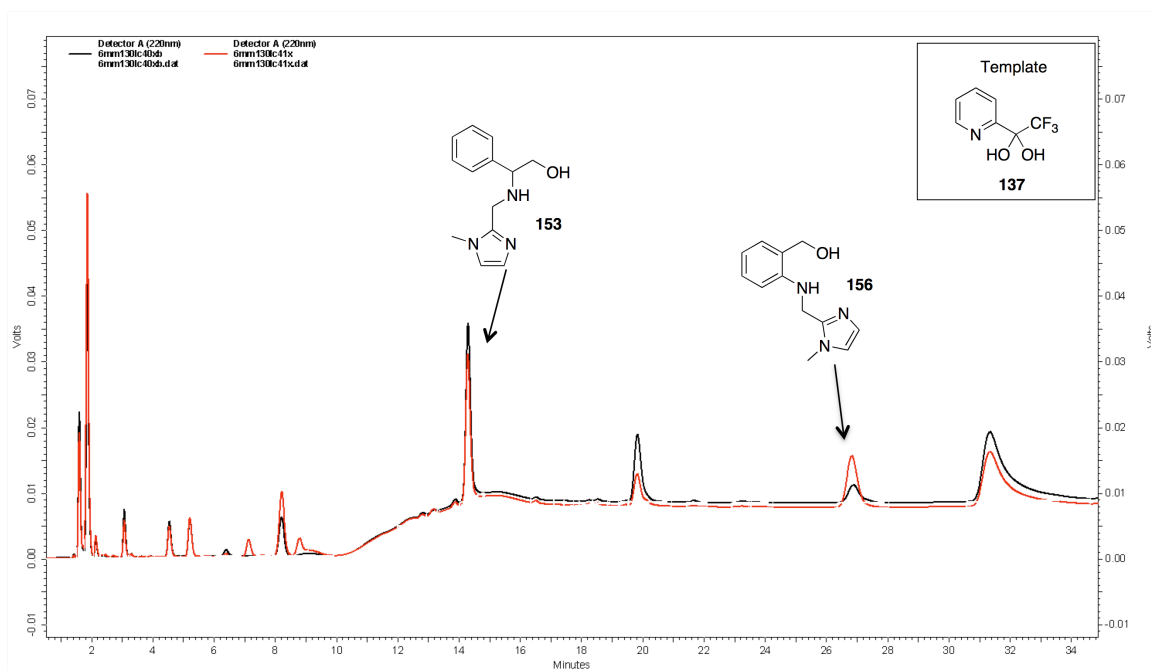
**Figure 132.** RP-HPLC chromatograms of control (black) and **137**-templated (red) library VII (early eluting species).
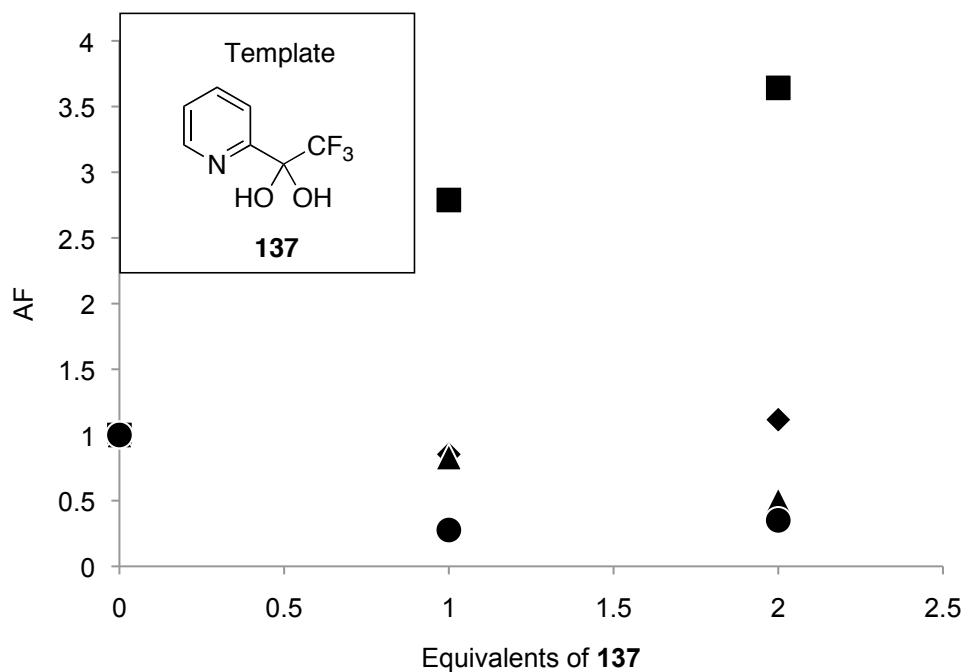


**Figure 133**. Library VII. Amplification behavior for **156** (■), **153** (▲), **159** (◆), and **162** (●).

### 3.2.6.2 Correlation of templating and kinetics

TSA **137**-templated amplification behavior of ligands in library VII reflects both single-turnover and multiple-turnover hydrolysis behavior. (Figure 134) When the single-turnover rate constant for each ligand-zinc complex is plotted against its amplification factor, a straight line is obtained (Figure 135). A plot of multiple-turnover rate constant for each ligand-zinc complex against its amplification factor also yields a straight line. (Figure 136) This is strong evidence for the correlation of amplification with catalytic activity in this library, indicating that we have made the right choices such that TSA-binding, catalysis, and amplification are well-matched in this system.



| | | | |
|---|---|---|---|
| $k_{Single-turnover}$ | 430 M$^{-1}$min$^{-1}$ | 1930 M$^{-1}$min$^{-1}$ | 202 M$^{-1}$min$^{-1}$ | 234 M$^{-1}$min$^{-1}$ |
| $k_{Multiple-turnover}$ | 70 M$^{-1}$min$^{-1}$ | 118 M$^{-1}$min$^{-1}$ | 64 M$^{-1}$min$^{-1}$ | 45 M$^{-1}$min$^{-1}$ |
| AF | 0.8 | 2.8 | 0.9 | 0.3 |
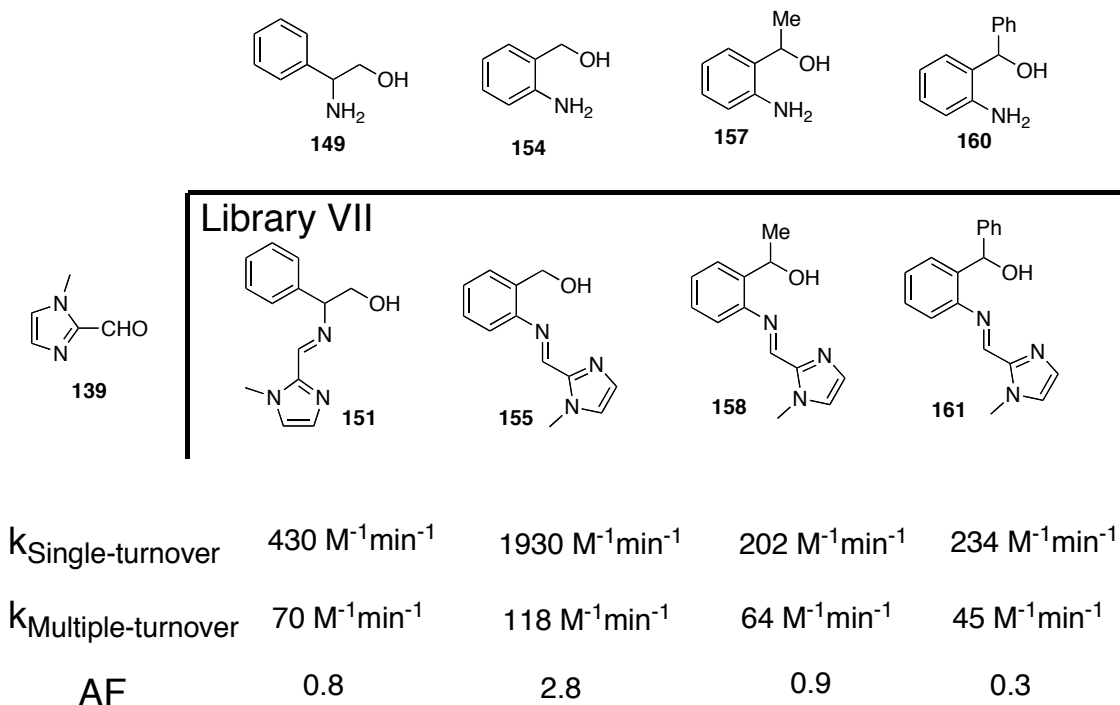
**Figure 134**. Summary of results for library VII.
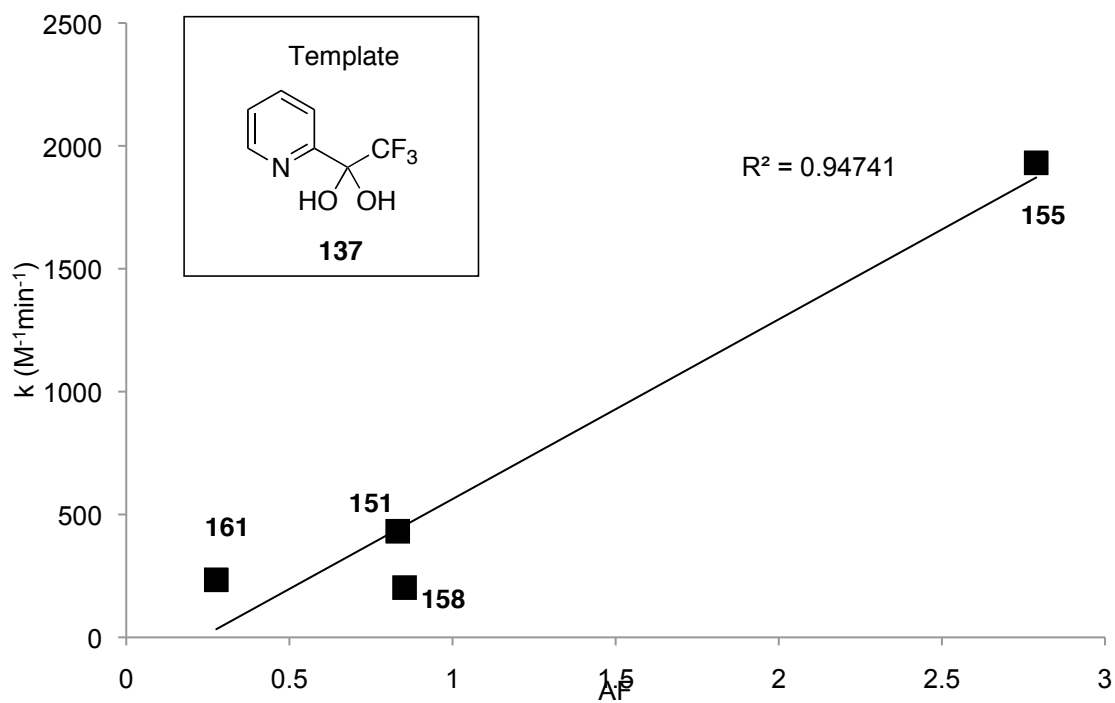
**Figure 135**. Correlation of single-turnover rate constant to AF in library VII.
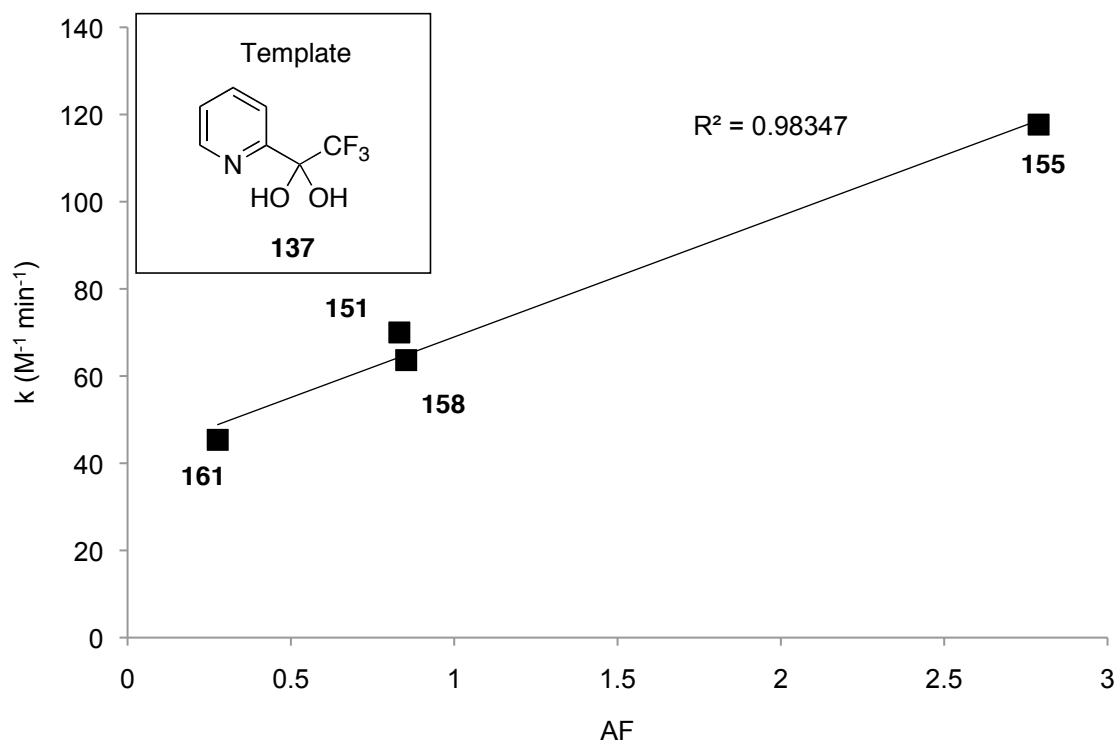


**Figure 136.** Correlation of multiple-turnover rate constant to AF in library VII.

145

**3.2.9 Discussion**

We have developed the first metal-complex DCL that amplifies catalysts via selection by a TSA-template. We have demonstrated ligand amplification in the presence of TSA, and correlated enhanced catalytic activity with amplification. We have strengthened the case for template-mediated amplification with evidence of ternary complex or TSA-adduct formation under library conditions, and ligand-zinc-TSA Job plots. In the case of phosphonate ester TSA **136**, we have provided evidence, via a competitive binding experiment, of the thermodynamic preference of TSA for one zinc complex over another.

Additionally, we have demonstrated the use of two different TSAs, **136** and **137**, a phosphonate ester and a trifluoromethylketone, in eliciting a response from the zinc-imined DCL. We found that each TSA is appropriate for a different ligand set, taking into account the likely mode of catalysis for the zinc-ligand catalyst. In the case of libraries containing no ligands with nucleophilic appendages, the phosphonate ester is a good TSA. When the library includes ligands bearing a hydroxy group that can participate covalently in the reaction, the trifluoromethylketone is more appropriate, since it can incorporate the ligand hydroxy-group into the transition-state analog via the formation of a hemiketal adduct.

Whereas previous DCLs have yielded catalytic species,[50,51] the relationship between catalyst structure (hydrophobic macrocycle) and reaction (cationic Diels-Alder and acetal hydrolysis) was extremely specialized, such that the results are difficult to generalize. Our work is potentially applicable to many reactions for which TSAs can be imagined and constructed, and is amenable to expansion by addition of many available or

easily synthesized ligand building blocks. We believe that this approach can potentially provide a new method for catalyst discovery. The technique is inexpensive, operationally simple, and amenable to study.

## 3.3 Conclusion and future work

In this work, we have exploited strong substrate-metal interactions to promote a reaction in which substrate binding plays a major role. This in turn facilitates the use of a TSA to form a ternary complex, through which ligand templating can take place. This was a strategic choice we made based solely on practical considerations. By building the recognition element into the specialized substrate/TSA pair (**135/136** or **135/137**) we made it possible to use easily available building blocks to construct a catalytically relevant DCL. Ultimately, the goal should be to move away from specialist substrates and their TSAs (**135**, **136** and **137**), to develop more useful reactions. This will mean shifting the burden of the recognition interaction away from the substrate onto the catalyst. This will require developing more sophisticated ligands containing recognition elements matched to the characteristics of the substrate. Many strong interactions are known from the natural world, and from synthetic receptors. It should not be difficult in principle to incorporate these motifs into a ligand library in such a way that the best match can be found between catalyst and transition state.

## 3.4 Experimental

**General Spectroscopic Methods.** $^1$H, and $^{19}$F, and $^{31}$P spectra were recorded on a Varian Mercury-300 spectrometer. Mass spectra were acquired on a Finnigan TSQ 700

spectrometer in methanol or acetonitrile solution by ESI. Spectrophotometry was carried out on a Beckman DU 640 spectrophotometer. HPLC analysis was carried out on a Shimadzu Class VP with ZORBAX Eclipse XDB-C18 column (4.6 x 140 mm) at 40 $^o$C.

### 3.4.1 Materials Preparation.

The following were prepared by literature methods:

<u>p</u>-nitrophenyl picolinate (**135**)[79]

300 MHz $^1$H-NMR in CDCl$_3$: δ 8.8 (1H, d, J = 4.5 Hz), 8.2-8.4 (3H, m), 7.96 (1H, t, J = 7.6 Hz), 7.60 (1H, m), 7.44 (2H, d, J= 9 Hz).

O-Phenyl-2-pyridylphosphonate (**136**)[80]

300 MHz $^1$H-NMR in CDCl$_3$: δ 8.83 (1H, d, J = 5.4 J), 8.59 (1H, t, J = 8.1 Hz), 8.24 (1H, t, J = 7.2 Hz) 8.10 (1H, t, J = 7.2 Hz), 7.33 (2H, t, J = 7.5Hz), 7.19 (1H t, J = 7.2 J), 7.00 (2H, d, J = 6.9 Hz).

2-pyridyltrifluoromethylketone hydrate (**137**)[85]

 300 MHz $^1$H-NMR in CDCl$_3$: δ 8.64 (1H, dm, J = 5.1 J), 8.04 (1H, td, J = 7.5 Hz, J = 1.8), 7.86 (1H, dm, J = 8.1 Hz), 7.58 (1H, ddd, J = 7.2 Hz, J = 4.8 Hz, J = 1.2 Hz).

1-methyl-2-formylbenzimidazole (**140**)[90]

300 MHz $^1$H-NMR in CDCl$_3$:  4.08 (3H, s), δ 7.36 – 7.45 (3H, m).  7.87-7.90 (1H, m), 10.06 (1H s).

_R,S_-1-(2-aminophenyl)ethanol (**157**) [89]

300 MHz $^1$H-NMR in CDCl$_3$: δ 7.08-6.99 (m, 2 H, ArH), 6.72-6.67 (m, 1 H, ArH), 6.60 (d, $J$ = 7.8 Hz, 1 H, ArH), 4.81 (q, $J$ = 6.7 Hz, 1 H, CH), 4.54-3.63 (br s, 2 H, NH2), 3.40-2.09 (br s, 1 H, OH), 1.51 (d, $J$ = 6.7 Hz, 3 H, CH$_3$).

_R,S_-(2-aminophenyl)(phenyl)methanol (**160**)[89]

300 MHz $^1$H-NMR in CDCl$_3$: δ 7.40-7.24 (m, 5 H, ArH), 7.10 (td, $J$ = 7.6, 1.5 Hz, 1 H, ArH), 6.98 (dd, $J$ = 7.6, 1.5 Hz, 1 H, ArH), 6.72 (td, $J$ = 7.5, 1.1 Hz, 1 H, ArH), 6.63 (dd, $J$ = 7.9, 1.0 Hz, 1 H, ArH), 5.78 (s, 1 H, CH), 3.87 (br s, 2 H, NH$_2$), 3.05 (br s, 1 H, OH).

### 3.4.2 Amplification/Analysis Method.

*General procedure*: A 100 mM stock solution of each building block was produced by dissolving 0.1 mmol of building block in 1 mL CH$_3$CN. A 100 mM stock solution of Zn(OTf)$_2$ was prepared in CH$_3$CN. A 100 mM stock solution of TSA **136** was prepared in 1 mL CH$_3$CN and the free base was produced by addition of 14 μL triethylamine. A 100 mM stock solution of TSA **137** was prepared in CH$_3$CN. Libraries were prepared by pipetting 50 μL aliquots of each building block and Zn(OTf)$_2$ into vials and diluting to 1 mL with CH$_3$CN. Control libraries contained no TSA, whereas templated libraries were treated with 50-250 μL TSA stock solution **136** or **137.** In cases where the overall solvent composition was to be 50% CH$_3$CN in water, the samples were diluted to 0.5 mL with CH$_3$CN and treated with 0.5 mL water.

After equilibrating 24-48 h at 20°C, the samples were treated with 25 mg NaBH$_4$ and stirred overnight with a needle in the vial lid to vent excess pressure. Samples were

then treated with 100 μL TFA to acidify, and diluted to 2 mL with water. A 100 μL aliquot of each sample was then taken and diluted to 1 mL in water to provide the HPLC sample.

*HPLC methods*: HPLC grade acetonitrile and water with 0.1% v/v TFA were used. Library I, II, III and IV: 3% acetonitrile 5 minutes, gradient to 10% acetonitrile over 5 minutes, 10% acetonitrile 20 minutes. Library V and VI: 15% acetonitrile, 30 minutes. Library VII: method 1: 5% acetonitrile, gradient to 10% acetonitrile over 5 minutes, 10% acetonitrile, 20 minutes. Library VII method 2: 15% acetonitrile, 30 minutes.

Library deconvolution was carried out by preparing libraries that were missing one of the building blocks. In cases where there were only three building blocks and two possible Schiff bases, peaks were identified by injecting samples containing building blocks and comparing to chromatograms of libraries containing only one of the possible reduced Schiff bases.


### 3.4.3 Job's plot analysis of binding stoichiometry.

A 100 mM stock solution of zinc-Schiff base complex was formed in 1 mL $CD_3CN$. A 100 mM stock solution of TSA **136** or **137** was prepared in 1 mL $CD_3CN$, with 14 μL TEA added in the case of **136**. NMR job plot samples were prepared by combining zinc complex and TSA stock solutions in the proportions 10 μL/ 90 μL, 25 μL/75 μL, 50 μL/50μL, 75 μL/25μL, and 90 μL/10 μL with 900 μL $CD_3CN$. Samples were analyzed by $^1$H-NMR and $^{31}$P-NMR, and $^1$F-NMR in the case of TSA **137**.

A Job plot for the ternary complex of **142**, zinc (II), and phenyl-2-pyridylphosphonate **136** was constructed by observing the $^{31}$P NMR chemical shift while simultaneously varying the concentration of zinc Schiff base complex and phenyl-2-

pyridylphosphonate. The Job plot shows a local minimum at 1:1 but also a large peak in the high phenyl-2-pyridylphosphonate to zinc ratio region, indicating the formation of complexes including multiple phosphonate ligands.

Job plots for the ternary complexes of amino alcohol Schiff bases **151, 155, 158**, and **161**, zinc ion and **137** were constructed by observing $^{19}$F NMR chemical shift while varying Schiff base complex and **137**. It was found that the stoichiometry was dependent on the Schiff base. Zinc complexes of **151** and **161** were found to form 2:1 complexes with TSA **137**, of the composition Zn$_2$**151**$_2$**137** and Zn$_2$**161**$_2$**137**, whereas zinc complexes of **155** and **158** formed the 1:1 complexes with TSA **137**.

### 3.4.4 ESI-MS of ternary complexes.

ESI-MS of library mixtures for Library I under templating conditions showed the formation of ternary complexes composed of zinc, Schiff base **142**, and phenyl-2-pyridylphosphonate **136**, as well as ternary complexes composed of zinc, Schiff base **141**, and phenyl-2-pyridylphosphonate **136**.

ESI-MS of the library III mixture shows evidence of the TSA-zinc-Schiff base adduct. Species of interest include a zinc complex of the adduct of **151** and **137**, Zn **151** **137**(-H$_2$O) (m/z=567.07) and a dizinc complex of the composition Zn$_2$(**151**)$_2$(**137**)(-H$_2$O)$^{2+}$ (m/z=379.56).

ESI-MS analysis of the templated library mixture from Library IV (Schiff bases **151** and **155**) shows a variety of zinc complexes that incorporate the transition state analog **137**. These include monozinc-Schiff base-TSA complexes Zn(**155**)(**137**) (-H$_2$O) (m/z=453.05), Zn(**151**)(**137**)(-H$_2$O) (m/z=567.07), and dizinc complexes of the

composition $Zn_2(155)_2(137)(-H_2O)^{2+}$ (m/z=365.54), $Zn_2(151)(155)(137)(-H_2O)^{2+}$ (m/z=373.56), $Zn_2(151)_2(137)(-H_2O)^{2+}$ (m/z=379.56). Also present are peaks corresponding to dizinc complexes without TSA, including $Zn_2155_2^{2+}$ (m/z=278.06), $Zn_2(155)(151)^{2+}$ (m/z=285.04), and $Zn_2151_2^{2+}$ (m/z=292.05).

### 3.4.5 Scatchard Analysis of 141/142 binding by NMR titration.

A 100 mM solution of Zn (**141**) or Zn (**142**) in $CD_3CN$ was prepared. A 100 mM solution of **136** in $CD_3CN$ was prepared, and 14 μL of triethylamine was added. A 10 mM solution of Zn(**141**)(**136**) or Zn(**142**)(**136**) was prepared from these stock solutions in $CD_3CN$. Trimethyl phosphate was added as a $^{31}P$ standard. A 1 M solution of ethylpicolinate in $CD_3CN$ was prepared. Ethylpicolinate **145** was titrated into the 10 mM solution of Zn(**141**)(**136**) or Zn(**141**)(**136**) in 25 μL aliquots while observing the $^{31}P$ chemical shift of TSA **136**. A Scatchard treatment of the data gives $K_{TSA}/K_{SA}$ values of 10 for Zn(**141**) and 19 for Zn(**142**).

### 3.4.6 Single-turnover Kinetics for the Hydrolysis of 135 catalyzed by Zn-imine complexes.

Generally, a 4 mM solution of each Zn(ligand) complex was prepared in methanol (25 mL) by combining zinc triflate, aldehyde and amine and allowing the solution to equilibrate 48 h. Analysis by $^1H$ NMR and borohydride reduction/HPLC showed full conversion to the Schiff base. A 0.82 mM solution of **135** was prepared in 25 mL $CH_3CN$.

Kinetics runs for Zn(**141**) and Zn(**142**) were made in a 1 cm quartz cuvette containing 1 mL of solution consisting of 700 μL of 100 mM pH 7.5 MOPS buffer, 100 μL

of **135** solution, and Zn(ligand) in methanol varying from 0 to 200 μL with the remaining volume compensated by methanol. The rate of 4-nitrophenylpicolinate hydrolysis by the Schiff-base zinc complexes was measured by spectrophotometric assay at 400 nm. The assay was carried out at 25° C in the presence of 75% aqueous 100 mM MOPS buffer held at pH 7.5, with catalyst in excess of substrate (single-turnover conditions) over a period of 8 minutes with one reading per 14 seconds. Plotting catalyst concentration x substrate concentration versus initial hydrolysis rate gives the second order rate constant.

Inhibition of **135** hydrolysis by **136** was studied under the same conditions as above while holding catalyst concentration at 0.4 mM and substrate at 82 mM. The concentration of **136** was varied from 0 to 10 mM. **136** appears to inhibit hydroysis by Zn (**141**) and Zn(**142**) with a concentration dependence that levels off rapidly.

**3.4.7 Multiple-turnover kinetics for the Hydrolysis of 135 catalyzed by Zn-imine complexes.**

The hydrolysis of **135** was carried out under multiple turnover conditions (excess substrate), varying the catalyst concentration. The concentration of **135** was 0.82 mM, and the catalyst concentration was varied from 0.02 mM to 0.08 mM. Reactions were observed for 16 minutes, with the region from 4 to 8 minutes used for the analysis. The assay was carried out at 25° C in the presence of 75% aqueous 100 mM MOPS buffer held at pH 7.5, and observed at 400 nm. The second order rate constants for the hydrolysis of 4-nitrophenyl picolinate under multiple-turnover conditions were determined to be 70 $M^{-1}min^{-1}$, 117 $M^{-1}min^{-1}$, 63 $M^{-1}min^{-1}$, 45 $M^{-1}min^{-1}$, for Zn-**151**, Zn-**155**, and Zn-**158**, and Zn-**161** respectively.

**3.4.8 Saturation kinetics for hydrolysis of 135 by Zn(151) and Zn(155).**

When the 4-nitrophenylpicolinate hydrolysis assay was carried out under conditions of excess substrate (steady state conditions), varying the substrate concentration while holding Zn-Schiff base complex concentration constant, saturation behavior was observed. Kinetics runs for zinc amino alcohol imine ligand complexes were made in a 1 cm quartz cuvette containing 1 mL of solution consisting of 750 μL of 100 mM pH 7.5 MOPS buffer, 250 μL methanol, 40 mM Zn(**151**) or Zn(**155**), and **135** varying from 0.3 mM to 1.6 mM. Spectrophotometric measurements were made at 400 nm at 25 $^{\circ}$C over a period of 8 minutes with 1 reading per 14 seconds. $V_{max}$ was $5.8 \times 10^{-6}$ $Mmin^{-1}$ and $2.0 \times 10^{-5}$ $Mmin^{-1}$ for Zn-**151** and Zn-**155**, respectively. $K_M$ was $2.0 \times 10^{-3}$ M and $1.0 \times 10^{-2}$ M for Zn-**155** and Zn-**151**, respectively. $k_{cat}$ was 0.5 $min^{-1}$ and 0.15 $min^{-1}$ for Zn-**155** and Zn-**151**, respectively.

## 4. ENANTIOSELECTIVE ESTEROLYSIS VIA CATALYSTS FROM A DCL

### 4.1.1 Kinetic resolution with metal complexes

In modern organic synthesis, there is a great demand for chiral enantiopure compounds. One of the strategies for producing enantiopure compounds is kinetic resolution. In a kinetic resolution, a chiral catalyst is used to react preferentially with one enantiomer over the other of a racemic substrate. (Figure 137) A subsequent separation yields enantioenriched product and substrate. Although kinetic resolution via ester hydrolysis by biological catalysts is a well-developed technique, the use of metal complexes for such kinetic resolutions is rather primitive.[91,92] Acylative and deacylative kinetic resolution catalyzed by chiral small molecules is hampered by the expense of the quite specialized catalyst. The discovery of new, efficient metal complex catalysts for esterolytic kinetic resolution would be a potentially useful chemical advance. To such an end, we wished to explore the use of DCL toward the development of catalysts for esterolytic kinetic resolution. The approach toward such a catalyst through DCL is in itself of great intellectual interest.

$$S_S + S_R \quad + \quad \text{Reagent} \quad \xrightarrow{\text{Chiral catalyst}} \quad S_S + P_R$$
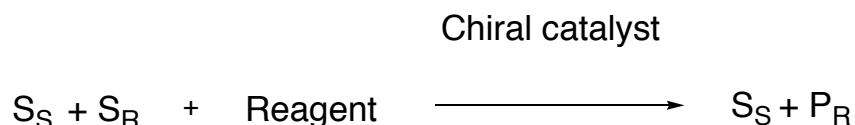
**Figure 137.** Schematic representation of an idealized kinetic resolution in which only the R-enantiomer of the racemic substrate reacts.

Kinetic resolutions based on Lewis-acid-catalyzed transesterification or hydrolysis of amino acid esters have been developed, but they are currently at the stage of proof of principle.[93-96] (Figure 138) Generally, chiral complexes of first-row transition metals are used to catalyze the methanolysis or hydrolysis of various N-protected racemic amino esters. Although the principle has been amply demonstrated, enantiodifferentiation is generally poor (with ER less than 5).
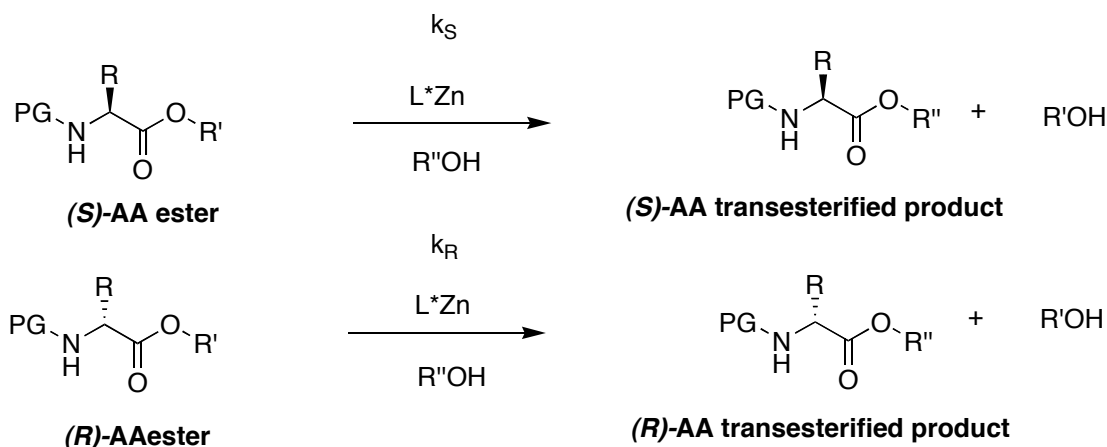


**Figure 138.** General scheme for kinetic resolution based on Lewis-acid catalyzed transesterification of amino acid esters. (PG = protecting group, acetyl, benzoyl, Cbz-, Boc-, or H for unprotected amino acid ester; R' = phenyl or 4-nitrophenyl, R''OH = methanol or water)

## 4.1.2 Kinetic resolution and DCL

Kinetic resolution, or the differential reaction of one substrate enantiomer over the other in the presence of an enantio-substrate-selective catalyst, is an ideal platform for studying catalyst DCL. The essence of the problem is to preferentially stabilize one diastereomeric transition state over the other. These diastereomeric transition state-catalyst adducts can in theory be explored by using their catalyst-pro-TSA complex

equivalents. (Figure 139) The only difference between the amplified species and the attenuated species, i.e. the good complex and the bad, will be the relative stereochemical arrangement of atoms and groups. This greatly simplifies the energetic situation regarding the interactions between the TSA and the catalyst.
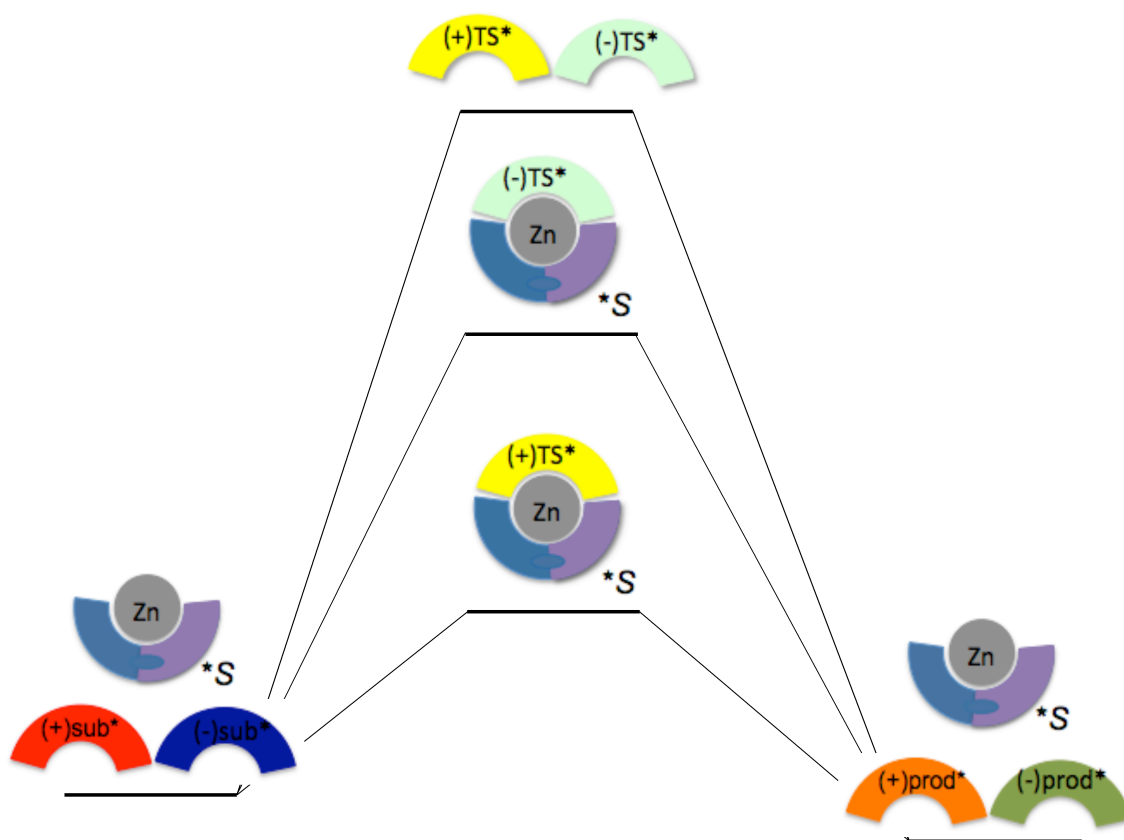


**Figure 139.** Simplified energy diagram showing the isoenergetic enantiomeric substrates (left), enantiomeric chiral products and isoenergetic chiral transition state of the uncatalyzed reaction (top), as well as the diastereomeric transition states of the reaction catalyzed by a chiral catalyst (middle and bottom). These transition states are rendered unequal in energy by the diastereomeric interaction of the chiral catalyst with the two enantiomers of substrate.

We chose to screen catalysts for enantioselective esterolysis before carrying out DCL experiments. Knowing the catalytic profile of the library members beforehand will allow us to design the library so that it is relevant to catalysis. In this sense, the project objectives were arranged in exactly the opposite fashion from a "real" DCL-based selection, or one operated in the discovery mode. That is, the catalytic behavior of library members is explored first, and templating experiments are carried out in order to determine the interaction of TSA/template with the library members. In practice, this allows us to concentrate our efforts on a few catalytically relevant species, and facilitates our goal of testing our hypothesis in a timely and efficient manner. Note that although the approach may seem backwards, it has no effect on testing the hypothesis.

In order to carry out the diastereomeric DCL experiment, there are two possible strategies that can be used. In the direct strategy, racemic building blocks are subjected to an enantiopure chiral TSA, and the resulting library is compared to the untemplated library. (Figure 140) The untemplated library, being composed of all racemic material, will be completely racemic in all components. The templated library, on the other hand, having been subjected to the chiral enantiopure TSA, will be enantioenriched in some components. Those components are species of interest as enantioselective catalysts. Specifically, one enantiomer of the catalyst will be amplified while the other is attenuated, due to the differing stabilities of the diastereomeric ternary complexes. This approach has the advantage of yielding a large amount of data at once, but requires that the capability of screening all members of the library for optical rotation. This is in principle possible using existing technology. Gagné et al. used laser polarimetry-detected RP-HPLC to screen the members of a DCL for optical rotation.[97] The inline laser

polarimetric detector allows assignment of an optical rotation sign and value to each eluting peak in the HPLC, providing an enantioenrichment profile for the separation. Such an approach, termed *deracemization* by Gagné, is ideal for an enantioselective catalyst DCL study.
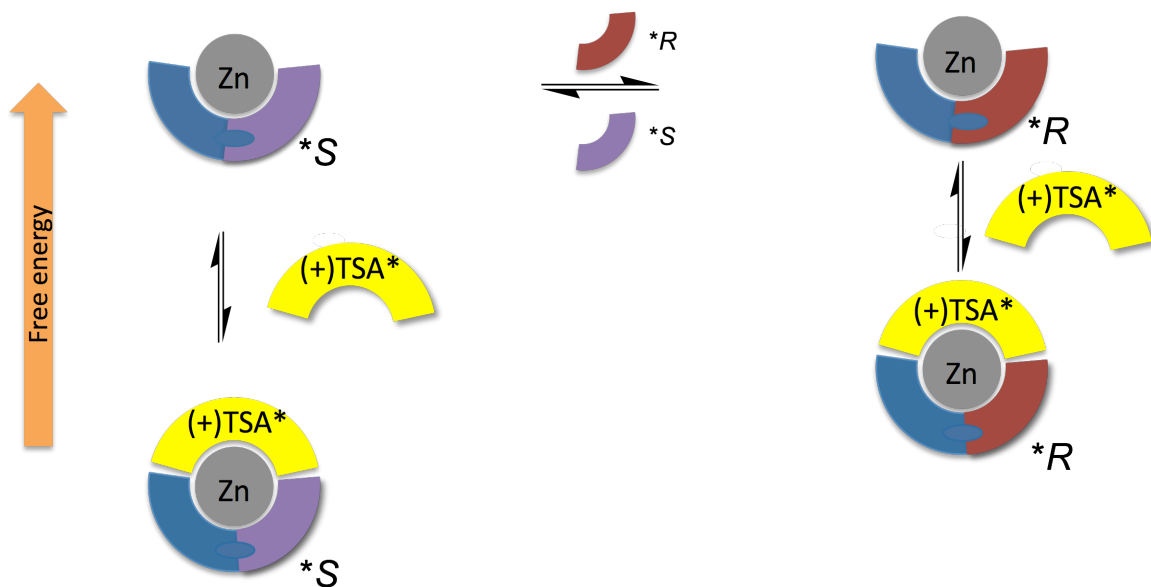


**Figure 140.** Deracemization of a dynamic combinatorial library by differential binding of a chiral enantiopure TSA leading to diasteromeric ternary complexes. The S-ligand and R-ligand form two diasteromeric ternary complexes (left and right). Due to energy differences of the ternary complexes, the overall equilibrium will be shifted toward the formation of (+)TSA-Zn-S-ligand complex, leading to the amplication of the S-ligand, i.e., deracemization of the DCL.

There is another possible approach that is indirect. Instead of using racemic building blocks, we can use enantiopure building blocks in an enantiopure library. (Figure 141) Two parallel enantiomeric DCL experiments are set up, and subjected to the enantiopure TSA of opposite chirality. The resulting diasteromeric interactions will yield

two different amplification results. It would be necessary to use an achiral dummy building block to ensure that an amplification event can be observed. The interaction of the chiral TSA with the dummy building block will be identical for the enantiomers of the TSA, but the interaction of the chiral TSA with chiral building block will be diastereomeric. The difference in energies of the two diastereomeric ternary complexes should be observable as a difference in outcome of the (+) and (-) TSA-templated libraries. Differential amplification by enantiomeric TSA pairs should theoretically correlate with relative stability of the diasteromeric ternary complex. This approach, though more complicated than deracemization, does not require a chiral stationary phase to detect the templating event.
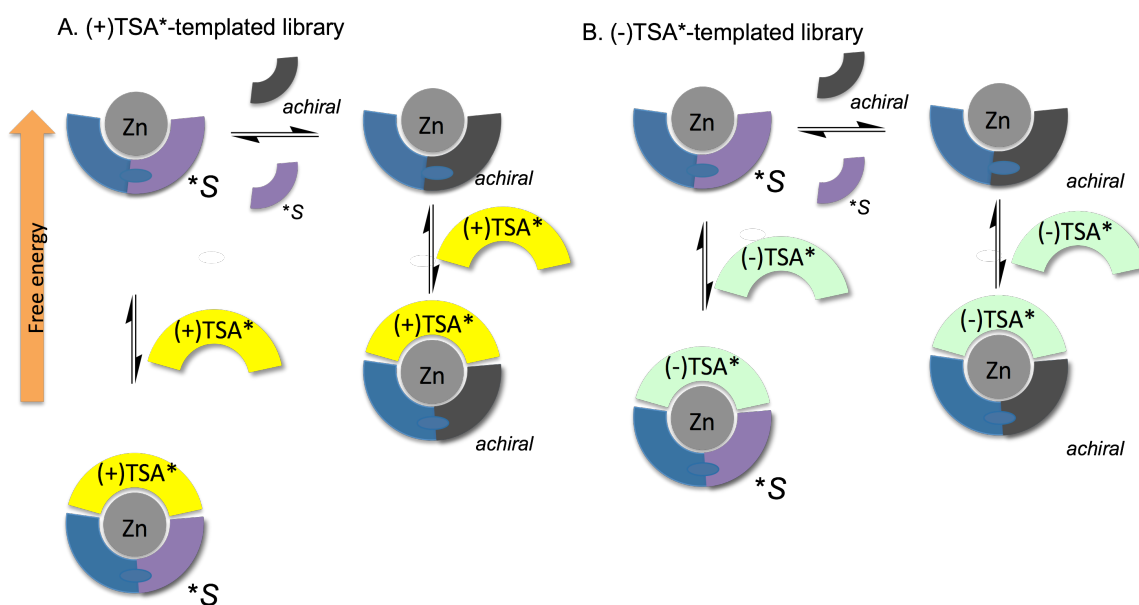


**Figure 141.** Indirect approach using two parallel enantiopure libraries (A and B) templated with chiral TSA of opposite handedness. The differing stabilities of the two possible diastereomers of the ternary complex in A and B will lead to two different amplification outcomes. Comparison of the two libraries will reveal the relative stabilities of the diastereomeric ternary complexes.

We hypothesize that the enantiomer of catalyst that is amplified by the chiral TSA will indicate the diastereomerically matched catalyst substrate pair, i. e., the faster catalytic reaction will result from the amplified catalyst and the substrate with the same chirality as the TSA that amplified it. More importantly, it should be the case that the extent of deracemization (in the direct experiment) or differential amplification (in the indirect experiment) will be directly proportional to the enantio-substrate-selectivity of the catalyst.

## 4.2 Results

A candidate system that we first explored for this project was the methanolysis of *p*-nitrophenyl esters of N-protected phenylalanine by amino alcohol-derived Schiff-base zinc complexes. (Figure 142) Chiral non-natural amino acids are valuable synthetic compounds, and although many enantioselective syntheses exist for these interesting building blocks, a general method for kinetic resolution of alpha amino esters would be practically useful. To this end the substrates *(S)*-**163** and *(R)*-**163** and matching TSAs *(S)*-**164** and *(R)*-**164** could be used to explore the dynamic combinatorial chemistry of zinc-ligand complexes for enantioselective esterolysis. (Figure 143) The release of *p*-nitrophenol by the methanolysis of this substrate can be conveniently tracked spectrophotometrically. A suitable phenylalanine-derived TSA **164** can be synthesized from literature methods.

161
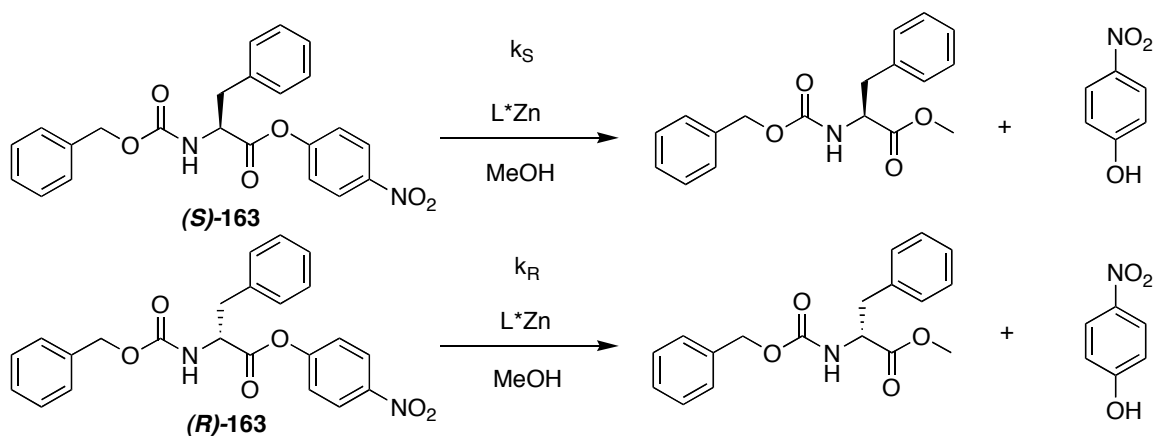
**Figure 142.** Differential methanolysis of enantiomers of **163** by a chiral zinc catalyst. Each rate constant is measured separately, and ER= $k_S/k_R$.
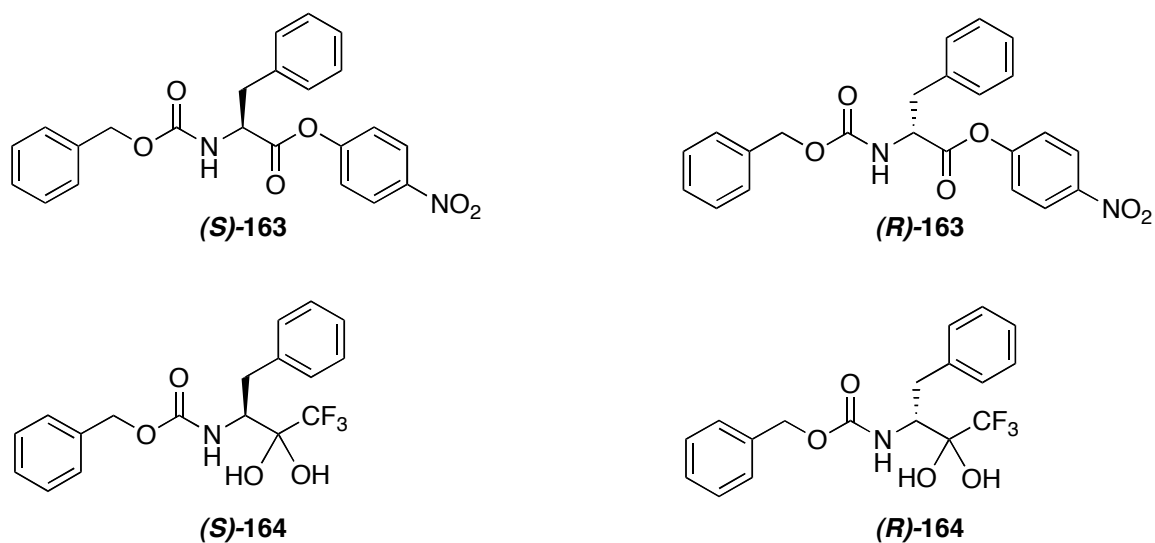


**Figure 143.** Substrates **163** and TSAs **164** for a model DCL for kinetic resolution.

### 4.2.1.1 Synthesis

Each enantiomer of Cbz-Phenylalanine p-nitrophenyl ester (**(S)-163** and **(R)-163**) was synthesized by literature methods.[98] TSAs **(S)-164** and **(R)-164** trifluoromethylketones were also synthesized by literature methods.[99]

**4.2.1.2 Kinetics**

As a screening for enantiodifferentiated methanolysis of nitrophenyl esters of Cbz-phenylalanine, we assayed the catalytic activity of a series of chiral-amino alcohol-derived Schiff base zinc complexes (Figure 144) for the methanolysis of the enantiomers (*(S)*-**163** and *(R)*-**163**) by spectrophotometrically observing the release of *p*-nitrophenol at 324 nm. This is a well-established method for initially screening for stereodifferentiation.[94-96] Zinc Schiff base complexes were prepared by combining chiral amino alcohol, aldehyde and zinc triflate in methanol and allowing the mixture to equilibrate for 48 hours. The zinc complexes were not isolated. In some cases, the zinc complexes were characterized by ESI-MS and $^1$H-NMR to check for formation of zinc Schiff base complexes. The exact composition of the complexes is not known. Each chiral, nonracemic zinc complex was tested for the rate enhancement of the hydrolysis of S and R enantiomers of Cbz-Phenylalanine *p*-nitrophenyl ester separately (Figure 142). This is an operationally convenient screening method, but suffers from the fact that it cannot detect nonlinear effects or inhibition; the results of the kinetics of esterolysis of enantiomeric substrates should be taken as a necessary, but not sufficient condition for viable kinetic resolution.
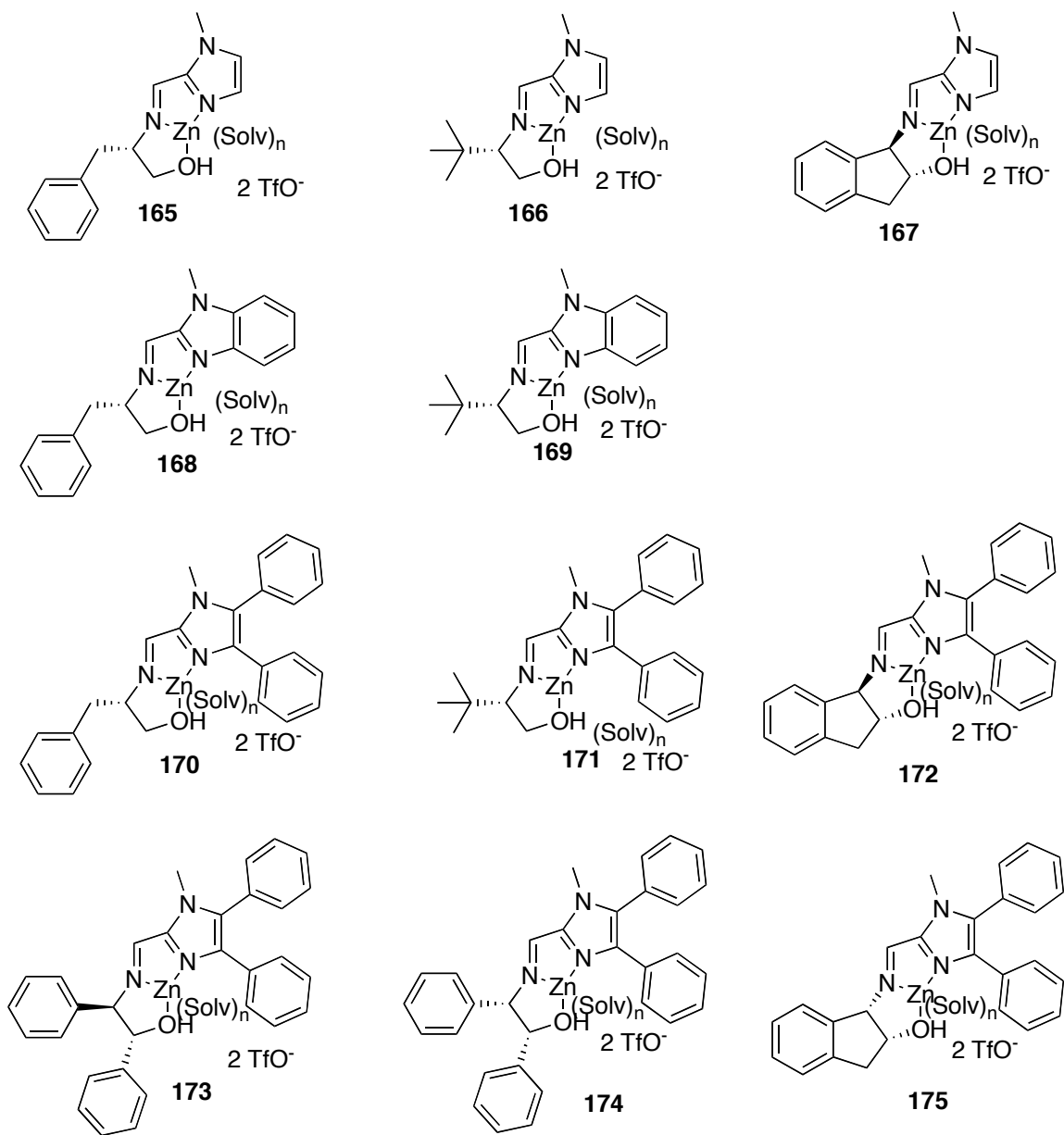
**Figure 144.** Chiral zinc Schiff base complexes used to catalyze methanolysis of *p*-nitrophenyl esters of Cbz-phenylalanine.

The substrate (**163**) concentration was 1.617 mM in 1 mL of 10% acetonitrile/methanol. The catalyst concentration was varied from 0.02 to 0.08 mM. The reaction was tracked by observing the production of *p*-nitrophenol spectrophotometrically

at 324 nm. The first 8 minutes of the reaction progress was used to calculate an initial rate. Rates were plotted against catalyst concentration times substrate concentration to give the second order rate constant. The plots were found to be linear except in the case of catalyst **175**.

**Table 4**

| catalyst | $k_S$ ($M^{-1}min^{-1}$) | $k_R$ ($M^{-1}min^{-1}$) | $k_S/k_R$ |
|----------|------------------|------------------|-----------|
| **165** | 26 | 23 | 1.1 |
| **166** | 30 | 24 | 1.3 |
| **167** | 18 | 18 | 1.0 |
| **168** | 60 | 57 | 1.1 |
| **169** | 52 | 43 | 1.2 |
| **170** | 30 | 33 | 0.9 |
| **171** | 27 | 23 | 1.2 |
| **172** | 20 | 14 | 1.4 |
| **173** | 92 | 80 | 1.2 |
| **174** | 11 | 12 | 0.9 |

The linear rate dependence on catalyst concentration indicates that the reaction is first order in catalyst (see data in section **4.4.3**, Figures 159-168). Unfortunately, enantiodifferentiation was very small in all cases. We believe that, given the nature of the assay, the ERs we report here are well within experimental error. An interesting pair is **173** and **174**, which differ only by the relative stereochemistry of phenyl groups. Complex **173** is eight to nine times faster than **174** for either enantiomer of substrate. Interestingly, for **175**, the catalytic reaction appears to be second order in catalyst. (Figure 145) A plot of rate against $[\textbf{175}]^2$ is a linear plot. (Figure 146) This may be indicative of a catalytically active dimeric species which is in equilibrium with **175**.
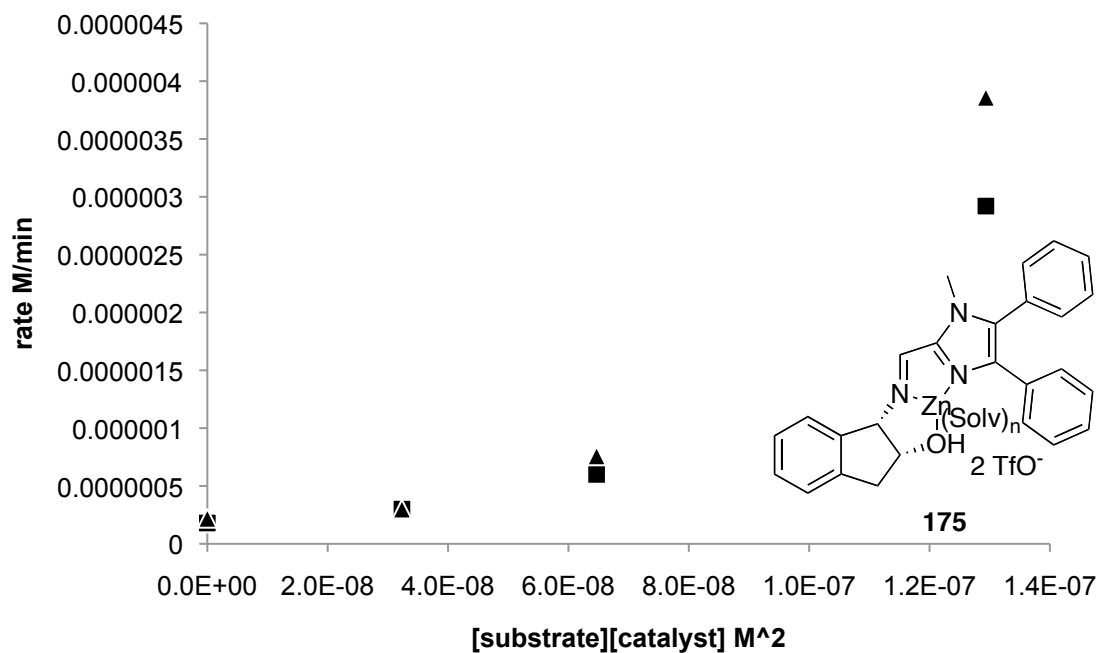
**Figure 145.** Kinetics of methanolysis by **175**. ■, *(S)*-**163**; ▲, *(R)*-**163**. Curve has a second order dependence on catalyst.
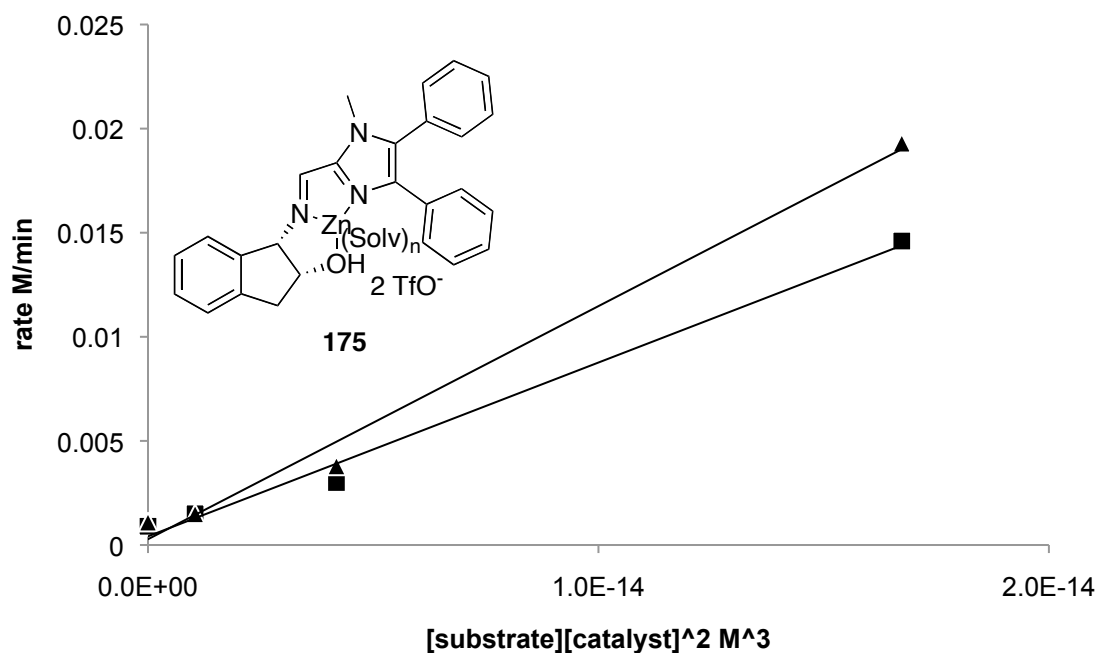


**Figure 146.** Kinetics of methanolysis by **175** plotted against square of catalyst concentration. ■, *(S)*-**163**; ▲, *(R)*-**163**.

### 4.2.1.3 Ternary complex
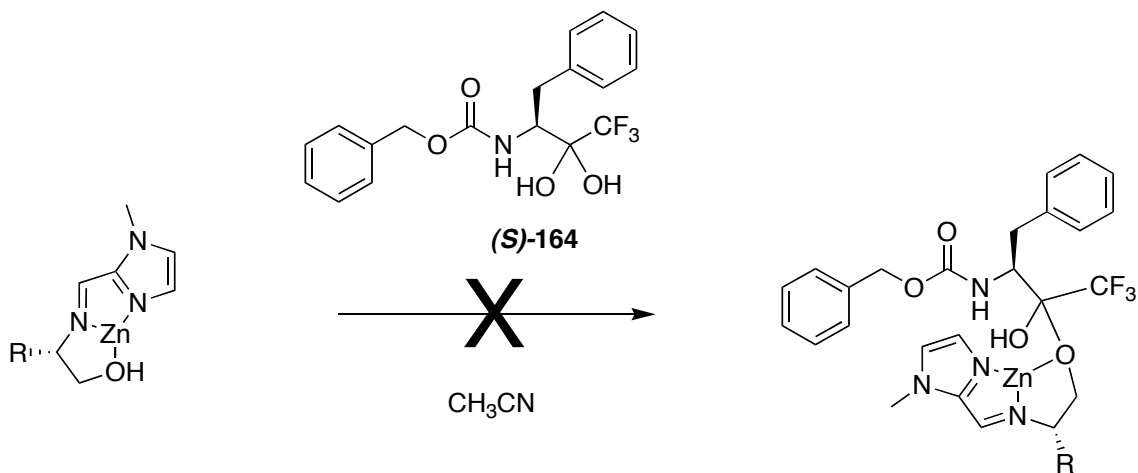


**Figure 147.** Attempts to form the ternary complex of TSA *(S)*-**164** with various zinc complexes failed.

Zinc complexes **166**, **167**, and **175** were tested for their ability to form a covalent adduct with TSA *(S)*-**164**. (Figure 147) Building blocks for each zinc-Schiff base complex, zinc triflate, and *(S)*-**164** were placed in 1 mL acetonitrile (5 mM each component) and allowed to equilibrate overnight. The mixtures were analyzed by ESI-MS. Although Schiff base zinc complexes were detected in each case, no ternary complexes or adducts containing *(S)*-**164** were detected. No ternary complexes were observed to form when TSAs (**164**) were combined with various hydroxy-functionalized zinc complexes. This is probably due to the lack of a coordinating function group on the TSA. This is at least consistent with the lack of enantiodifferentiation that we observed. This indicates the importance of a strong coordinating interaction between the TSA and the catalyst complex for ternary complex formation and templating to take place.

**4.2.1.4 Discussion**

The chiral amino-alcohol-derived Schiff base ligands we used to attempt to develop a kinetic resolution of p-nitrophenyl esters of Cbz-phenylalanine (**163**) were ineffective in enantiodifferentiating the chiral substrate. In addition, it was found that the TSA *(S)*-**164** did not form a detectible adduct with the Schiff-base zinc complex. The reason for these two findings is most likely that neither the substrate nor the transition state of this reaction displays a substantial affinity for the catalyst, making this substrate/catalyst building block combination a poor choice for DCL. This illustrates the importance of strong binding interactions for an effective substrate-catalyst combination. It should be pointed out, however, that this in no way should be taken as evidence that a DCL approach to methanolysis of this particular substrate is not viable; rather, the substrate and the catalyst building blocks are poorly matched. In order to access significant catalysis with this substrate, more sophisticated recognition elements will need to be included in the library building blocks.

**4.2.2 Chiral picolinate esters as substrates**

A system which is more closely related to our previous work and is more promising is the methanolysis of chiral picolinic esters by zinc Schiff-base complexes. (Figure 148) In this case, the picolinate ester is a good ligand, and the reaction is likely to proceed on the metal with a discretely oriented transition state. The transition state analog is the *sec*-phenethyl alcohol-derived chiral phosphonate ester **177**.
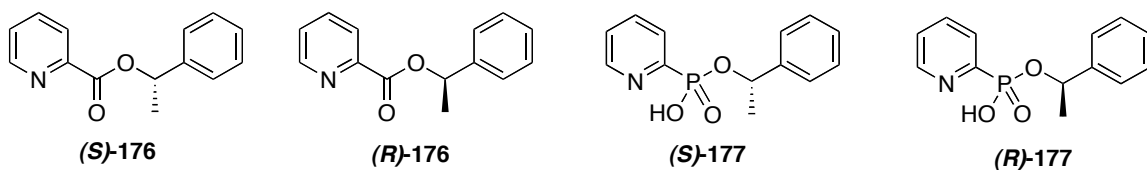
**Figure 148.** Pyridine-functionalized substrates and TSAs.

### 4.2.2.1 Synthesis

The picolinic esters *(S)*-176 and *(R)*-176 of *S*- and *R*- *sec*-phenethyl alcohol were synthesized by dicyclohecylcarbodiimide (DCC) coupling of the *sec*-phenethyl alcohol and picolinic acid in pyridine. Picolinic acid and *sec*-phenethyl alcohol were placed in pyridine and stirred in an ice bath. DCC was added, and the reaction was stirred and allowed to reach room temperature. The reaction was stirred for 24 hours before removing precipitated dicyclohexylurea by filtration. Solvent was removed from the collected filtrate under vacuum. The residue was chromatographed on flash silica (25% ethyl acetate/75% hexanes) and characterized by ^{1}H-NMR and ^{13}C-NMR.

The TSAs *(S)*-177 and *(R)*-177 *sec*-phenethyl alcohol phosphonate esters were prepared by DCC coupling of 2-pyridylphosphonic acid and the *sec*-phenethyl alcohol in pyridine. 2-pyridinephosphonic acid and *sec*-phenethyl alcohol were placed in pyridine and stirred in an ice bath. DCC was added, and the reaction was stirred and allowed to reach room temperature. The reaction was stirred for 48 hours before removing precipitated dicyclohexylurea by filtration. Solvent was removed from the collected filtrate under vacuum. The residue was crystallized from ethanol/diethyl ether and characterized by ^{1}H-NMR and ^{13}C-NMR.
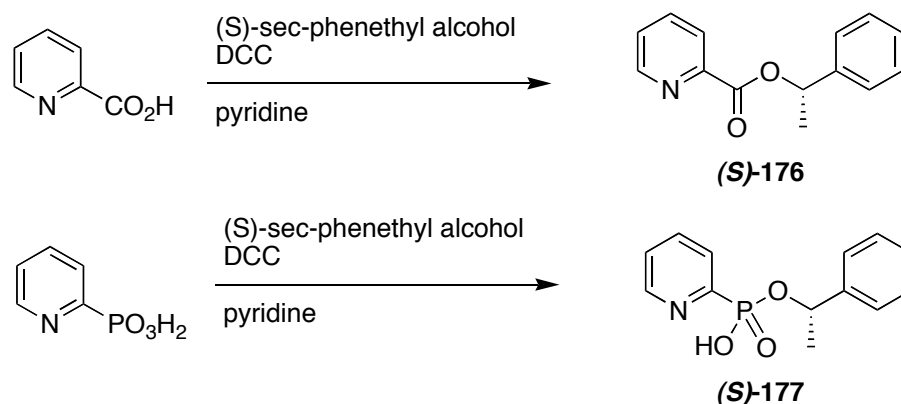
**Figure 149.** Synthesis of substrate *(S)*-**176** and TSA *(S)*-**177**.

### 4.2.2.2 Kinetics

Synthesis of diaminocyclohexane-derived N-tosyl Schiff base ligands **178**-**184** (Figure 150) was carried out by Dr. Ramu Kannapan, a postdoctoral fellow in the Nicholas Group. Subsequent kinetics experiments by ^{1}H-NMR were carried out by Dr. Kannapan and myself. Again, separate kinetics experiments were carried out on the enantiomeric substrates to determine the stereodifferentiation by the catalysts. In the case of the picolinate ester substrates, ^{1}H-NMR was used to observe the disappearance of the methyl doublet signal (1.87 ppm) of **176** and the emergence of the methyl doublet (1.61 ppm) of *sec*-phenethyl alcohol. Solutions (10 mM, 1 mL) of enantiopure **176** were prepared in 50% $CD_2Cl_2/CD_3OD$. Either 10 mol% or 1 mol% zinc complex was added to the NMR tube before beginning the time-dependent acquisition (32 transients, 1 spectrum per two minutes). Plots of *sec*-phenethyl alcohol concentration v. time were made. (Figures 149, 150, 151) The first few points were used to calculate initial rates. (Table 5)

170
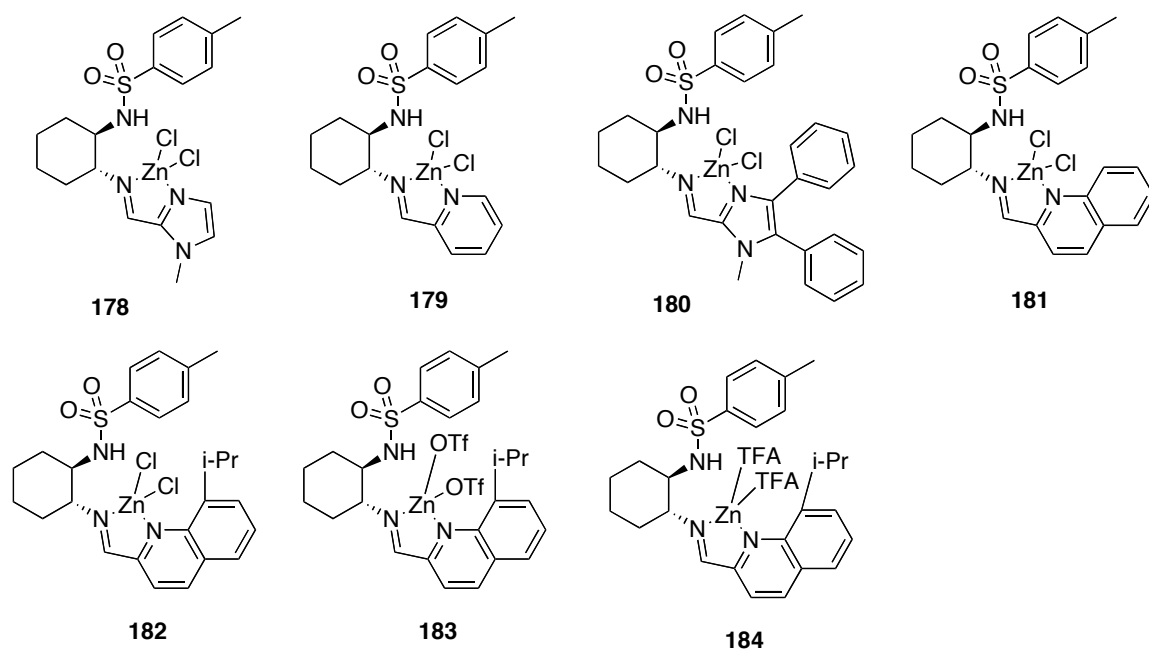
**Figure 150.** Diaminocyclohexane-derived complexes for kinetic resolution
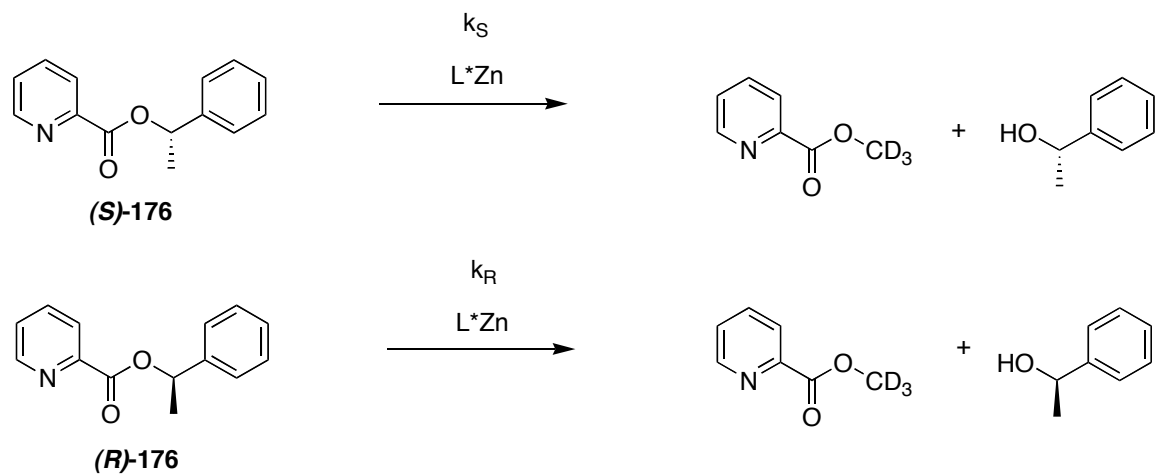


**Figure 151.** Differential methanolysis of enantiomers of **176** by a chiral zinc catalyst. Each rate constant is measured separately, and ER= $k_S/k_R$.

A summary of rate constants for the complex catalysts **178 – 184** is summarized in table 5. It was found that isopropylquinolinecarboxaldehyde-derived Schiff base **184** displayed a remarkably high 26:1 ratio between hydrolysis rates for the S and R enantiomers of the picolinic esters **176**. (Table 5)

**Table 5.** Methanolysis **176** by chiral zinc complexes

| catalyst | $k_S$ (mM$^{-1}$s$^{-1}$) | $k_R$ (mM$^{-1}$s$^{-1}$) | $k_S/k_R$ |
|---|---|---|---|
| **178** | 0.00066 | 0.00021 | 3.1 |
| **179** | 0.00012 | 0.00007 | 1.7 |
| **180** | 0.00014 | 0.00018 | 0.8 |
| **181** | 0.01 | 0.013 | 0.8 |
| **182** | 0.00079 | 0.00064 | 1.2 |
| **183** | 0.0002 | 0.000192 | 1.0 |
| **184** | 0.0066 | 0.00025 | 26.4 |

Complex **181**, on the other hand, containing a quinoline-derived imine, gave the highest rate of methanolysis, but no selectivity. Complex **184**, with its isopropyl-substituted quinoline, was much slower and much more selective. We believe this is due to the increased steric bulk near the metal center, leading to more pronounced differences in diastereomer energies.
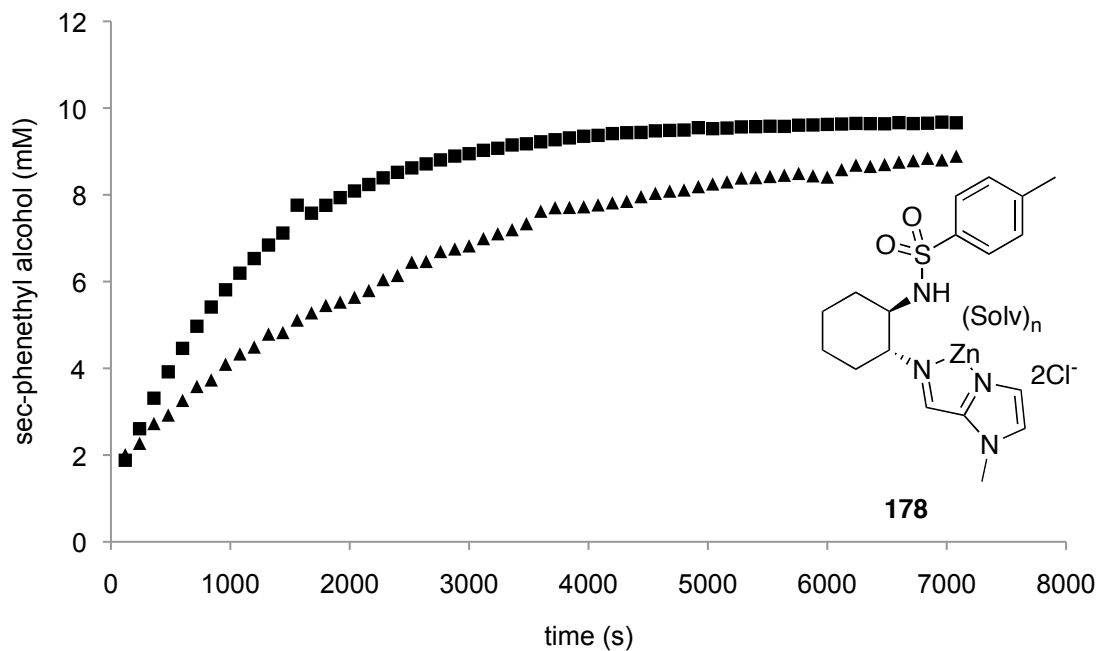
**Figure 152.** $^1$H-NMR-detected methanolysis by **178**. ■, *(S)-176*; ▲, *(R)-176*.
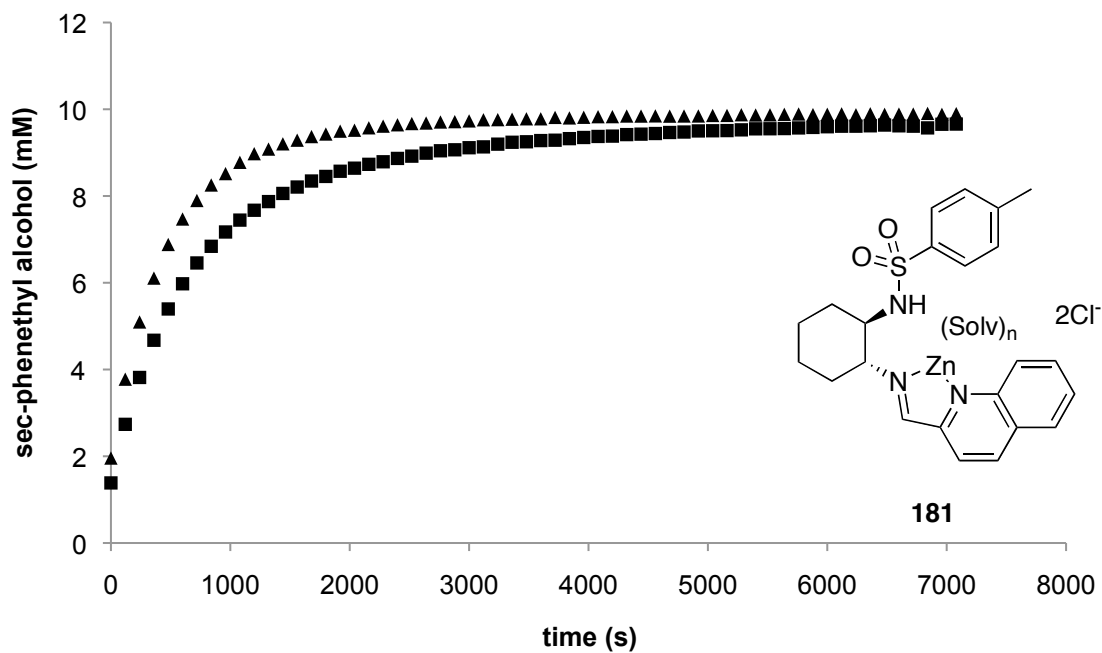


**Figure 153.** $^1$H-NMR-detected methanolysis by **181**. ■, *(S)-176*; ▲, *(R)-176*.
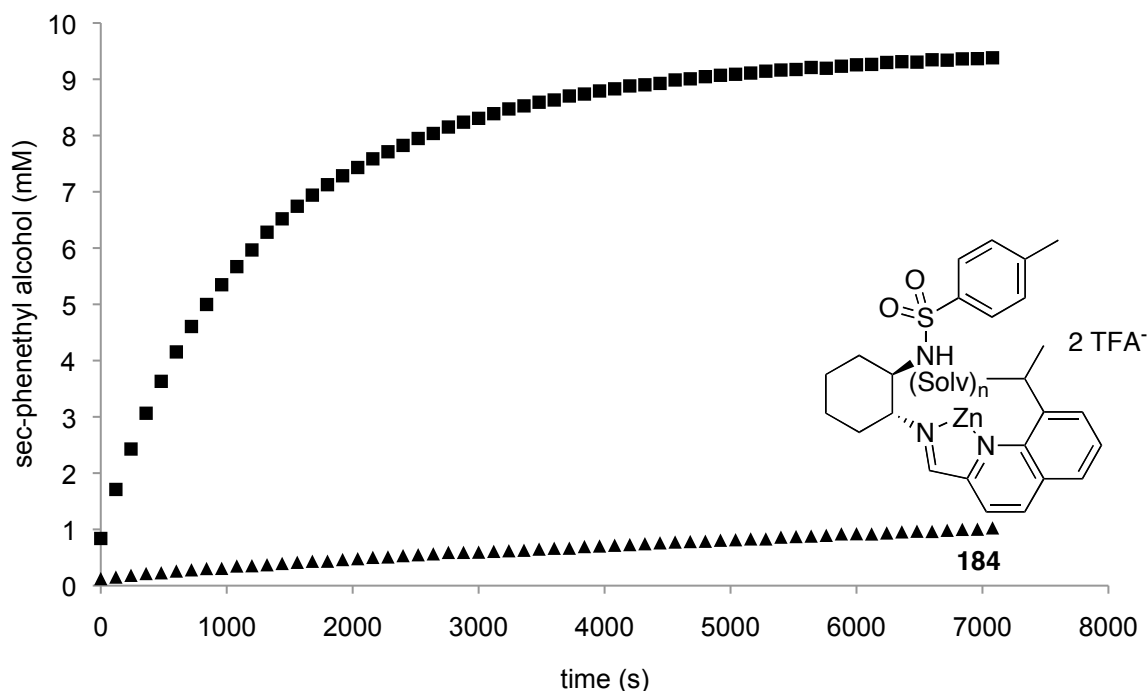
**Figure 154.** $^1$H-NMR-detected methanolysis by **184**. ■, *(S)-176*; ▲, *(R)-176*.

### 4.2.2.3 Attempts at detecting the ternary complex

Attempts were made to detect the ternary complex of ligands, zinc, and TSA by ESI-MS. **183** and *(S)-177* were combined in methanol or acetonitrile (0.1 mM) and analyzed by ES-MS. Although some peaks which could be interpreted as containing TSA *(S)-177* and complex **183** were present, they were not major species, and the analysis was equivocal.

### 4.2.2.4 Discussion

A promising lead for a kinetic resolution catalyst was discovered by screening experiments using NMR kinetics on enantiopure substrates. We believe the high enantioselectivity of **180** is due to the sterically demanding ligand, which places an

174

isopropyl group in the vicinity of the bound substrate. A potential entry into enantioselective catalyst DCL was discovered. Because we now have in hand a series of ligands with varying activity and selectivity, it will be interesting to see how they behave in a dynamic combinatorial library in the presence of TSA **177**. Studies on the formation of a ternary complex from these zinc complexes and TSA **177** are under way.

## 4.3 Conclusion and future work

Several important project goals have yet to be completed to fully take advantage of the opportunity presented by our work with this system. The viability of a true kinetic resolution of pyridylcarboxylate ester catalyzed by **180** is currently being tested. Using racemic substrate, we will observe the production of chiral *sec*-phenethyl alcohol through the use of GC analysis on a chiral stationary phase (CDX-B manufactured by J & W Scientific). The selective catalytic activity of **178** and **180** for the methanolysis of chiral picolinic esters is a promising lead into enantioselective catalyst libraries synthesized and selected by dynamic combinatorial chemistry. We now know where to construct the libraries, how to approach the TSA-based selection, and where to look. The following things need to be accomplished.

First, it is vital to establish unambiguously the nature of the interaction between TSA and catalyst. Dr. Kannappan and myself are attempting to characterize the ternary complexes by ESI-MS and NMR. Second, the dynamic chemistry of these ligands will be investigated. We will carry out DCL experiments based on these ligands templated on chiral TSAs as described in 4.1. The DCLs will be analyzed either by ESI-MS or

borohydride reduction followed by RP-HPLC. Armed with these results, we will be able to further develop a general and useful DCL-based approach to catalyst discovery.

## 4.4 Experimental

**General Spectroscopic Methods.** [1]H, and ^{19}F, and ^{31}P spectra were recorded on a Varian Mercury-300 spectrometer. Mass spectra were acquired on a Finnigan TSQ 700 spectrometer in methanol or acetonitrile solution by ESI. Spectrophotometry was carried out on a Beckman DU 640 spectrophotometer.

### 4.4.1 Materials

1-methyl-2-imidazolecarboxaldehyde, *(S)*-phenylalaninol, *(S)*-tert-leucinol, *(S)*-valinol, *(1R,2R)*-(-) *trans*-1-amino-2-indanol, *(1R,2S)*-(+) *cis*-1-amino-2-indanol, *(R,R)*-(+)-2-amino-1,2-diphenylethanol, and *(1R,2S)*-(-)-2-amino-1,2-diphenylethanol were commercial materials.

1-methyl-benzimidazole-2-carboxaldehyde and 1-methyl-4,5-diphenyl-2-imidazolecarboxaldehyde were synthesized by Deven Estes according to literature procedures.[90,100]

*(S)-Z-Phenylalanine p-nitrophenyl ester* **(S)-163** and *(R)-Z-Phenylalanine p-nitrophenyl ester* **(R)-163** were synthesized by literature procedures.[98] 300 MHz ^{1}H-NMR in CDCl$_3$:

δ ppm 8.25 (2H, d, J = 9 Hz), 7.26-7.37 (10H m), 7.21 (2H, d, J = 9 Hz), 5.06 (2H, s),

4.66 (1H, m), 3.28 (1H, dd, J = 6 Hz, J = 14.1 Hz), 3.14 (1H, dd, J = 8.7 Hz, J = 13.5 Hz).

$[\alpha]_D^{20}$ = − 14.2° (c = 2.0 in ethyl acetate) for *(S)*-**163** (lit. − 14.2°). $[\alpha]_D^{20}$ = + 14.2° (c =

2.0 in ethyl acetate) for *(R)*-**163** (lit. + 14.2°).[101]


(3S)-3-Amino-N-benzyloxycarbonyl-4-phenyl-1,1,1,-trifluorobutan-2-one *(S)*-**164** was

synthesized according to a literature procedure.[99] Compound *(S)*-**164** was a mixture of

ketone and ketone hydrate by $^1$H-NMR. 300 MHz $^1$H-NMR in CDCl$_3$: δ ppm 5.29-5.31

(m, 5H), 4.42-4.48 (2H, m), 3.82-3.86 (1H, m), 3.26-3.30 (1H, m), 2.97-3.02 (1H, m).

$^{19}$F-NMR. δ ppm - 76.2 and - 82.6 (mixture of ketone and ketone hydrate).


Schiff base complexes **178**, **179**, **180, 181**, **182**, **183**, and **184** were prepared by Dr. Ramu

Kannappan. **182, 183,** and **184** were prepared from 8-isopropyl-2-

quinolinecarboxaldehyde synthesized by M. Matsumoto by a literature procedure.[102]


## 4.4.2 Synthesis


### 4.4.2.1 *(S)*-1-phenylethanol picolinic acid ester (*(S)*-**176**)

Picolinic acid (2.05 g, 16.65 mmol) and *(S)*-*sec*-phenethyl alcohol (2.04 g, 16.65 mmol)

were placed in dry pyridine (50 mL) and cooled in an ice bath. DCC (3.44 g, 16.65

mmol) was added. The mixture was stirred in the ice bath and then allowed to warm to

room temperature. The mixture was stirred 24 hours. The reaction mixture was filtered to

remove dicyclohexylurea, and solvent was removed from the filtrate by rotary

evaporator. The resulting crude material was chromatographed on flash silica using 25% ethyl acetate 75% hexanes as eluent, giving 1.33 g (35% yield) of *(S)*-**176**. The compound was stable to chromatography and storage. 300 MHz ^{1}H-NMR in CD$_3$OD: δ 8.67 (1H, d, J = 4.5 Hz), 8.16 (1H, d, J= 8.4Hz), 7.98 (1H, td, J = 7.65 Hz, J = 1.5 Hz), 7.62 (1H, m), 7.47 (1H, d, J = 8.4 Hz), 7.28–7.38 (4H, m), 6.14 (q, J = 6.3 Hz), 1.68 (3H, d, J = 6.6 Hz). 75 MHz ^{13}C-NMR in CD$_3$OD: δ 165.40, 150.81, 149.09, 142.98, 139.41, 129.75, 129.26, 128.94, 127.35, 126.59, 75.66, 22.77.



**Figure 155.** ^{1}H-NMR spectrum of *(S)*-**176**.
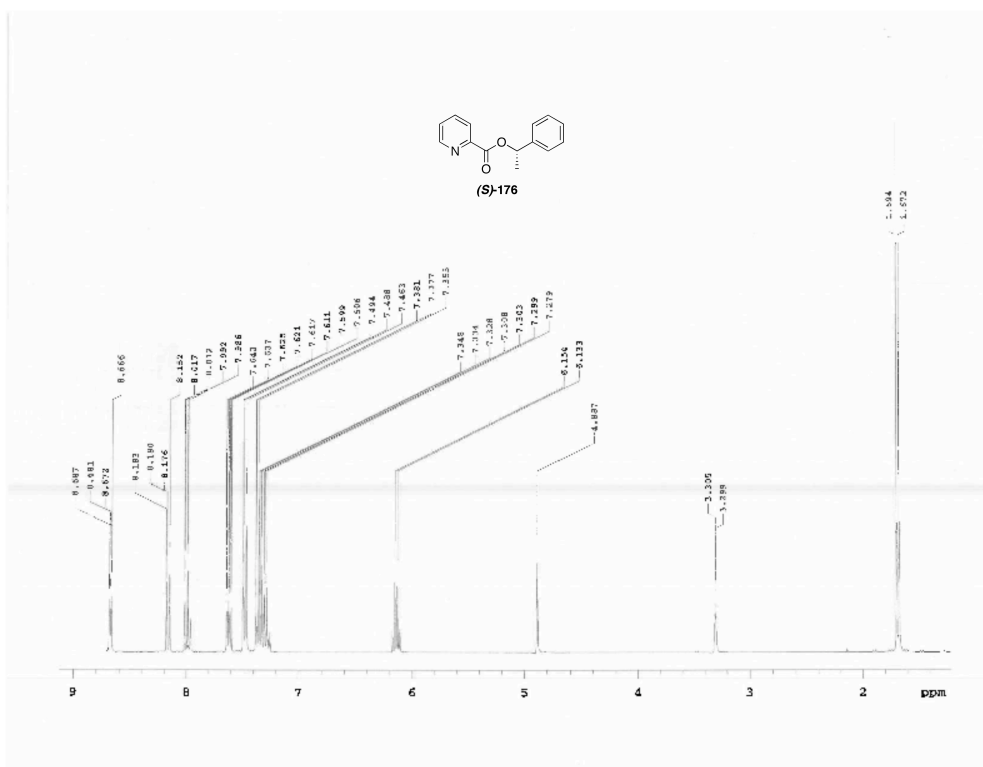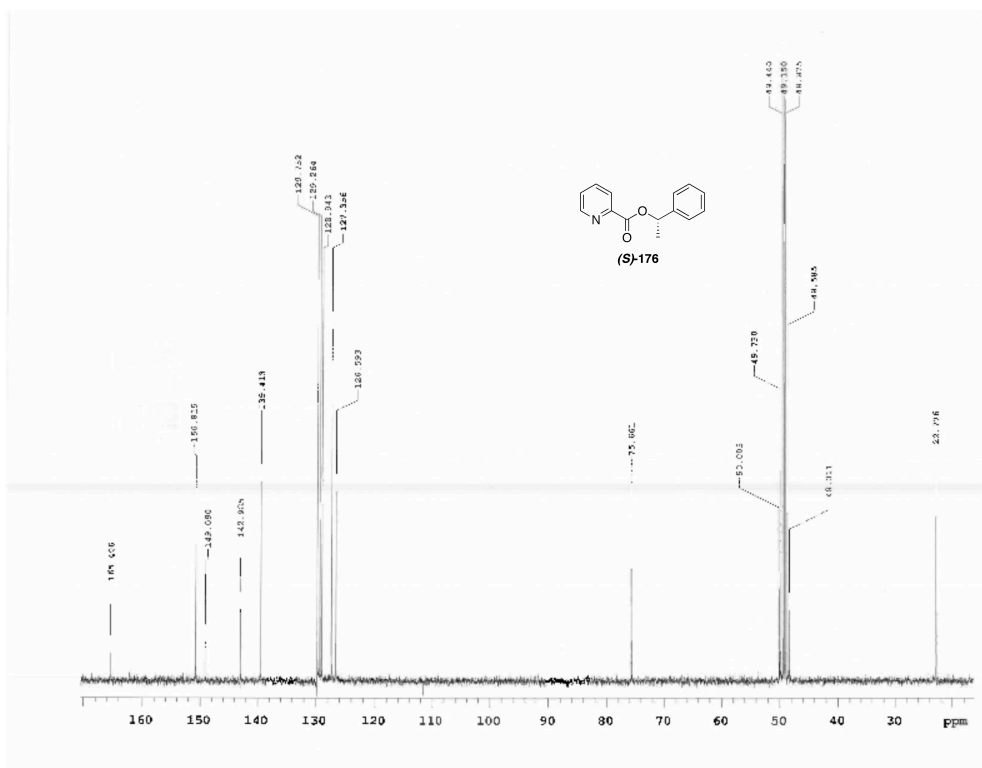
**Figure 156.** $^{13}$C-NMR spectrum of *(S)-176*.

*(R)*-1-phenylethanol picolinic acid ester (*(R)*-**176**)

Prepared in the same way as *(*S*)*-**176** except with *(R)*-*sec*-phenethyl alcohol.

**4.4.2.2** *(S)*-1-phenylethanol pyridinephosphonic acid ester (*(S)*-**177**)

2-Pyridinephosphonic acid (1 g, 6.29 mmol) and *(S)*-*sec*-phenethyl alcohol (0.81 g, 6.33 mmol) were placed in dry pyridine (17 mL) and cooled in an ice bath. DCC (3.16 g, 15 mmol) was added. The mixture was stirred in the ice bath and then allowed to warm to room temperature. After 48 hours, precipitated dicyclohexylurea was removed by filtration. Solvent was removed from the filtrate using a rotary evaporator. The residue was crystallized from ethanol/diethyl ether (0.55 g, 33% yield). 300 MHz $^1$H-NMR in CD$_3$OD: δ 8.52 (1H, d, J = 5.7 Hz), 8.34 (1H, td, J = 5.4 Hz, J = 1.8 Hz), 7.98 (1H, t, J =

7.8 Hz), 7.85 (1H, t, J = 9 Hz), 7.08–7.19 (5H, m), 5.40 (1H, m, J = 6.6 Hz), 1.51 (3H,

d, J = 6.6 Hz). 75 MHz $^{13}$C-NMR in CD$_3$OD: 146.77. 143.77, 143.09, 143.45,

129.53, 128.94, 128.62, 127.32, 111.57, 76.814, 25.34.



**Figure 157.** $^1$H-NMR spectrum of *(S)*-**177**.
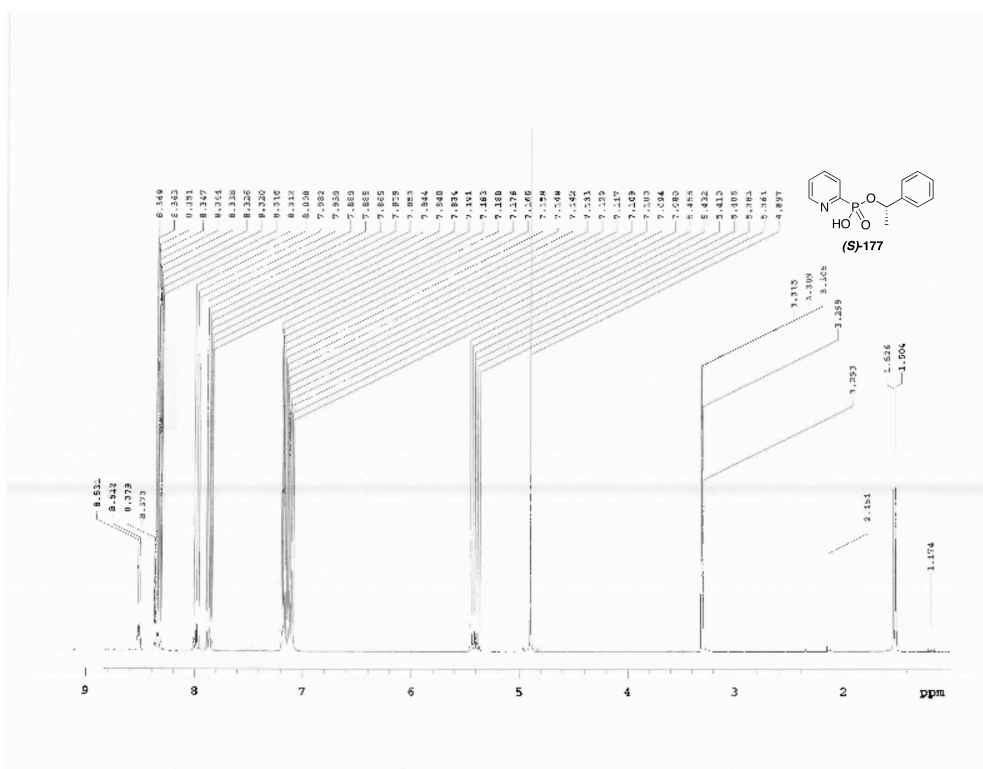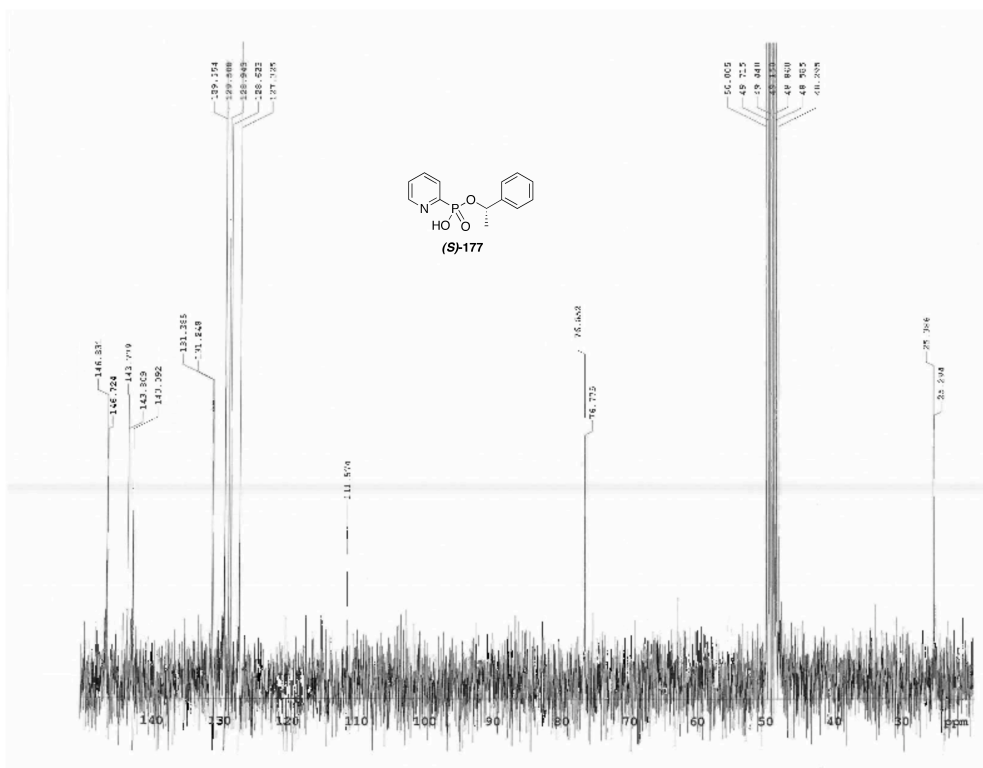
**Figure 155.** $^{13}$C-NMR spectrum of *(S)*-**177**.

*(R)*-1-phenylethanol pyridinphosphonic acid ester (*(R)*-**177**)

Prepared in the same way as *(S)*-**177** except with *(R)*-*sec*-phenethyl alcohol.

### 4.4.3 Kinetics of Z-Phe-ONP (163) methanolysis

Zinc Schiff base complexes **165** – **175** were prepared by mixing the chiral amino alcohol building block, aldehyde, and zinc triflate in methanol at 4 mM concentration and allowing the mixture to equilibrate 48 h. Samples were prepared in a 1 cm quartz cuvette by adding 100 μL of 16.17 mM substrate (**163**) in acetonitrile solution to 860 to 900 μL methanol to which was aliquotted 0 – 40 μL catalyst solution. Each sample therefore was 1.617 mM in substrate and 0 – 0.08 mM in catalyst. Each cuvette was observed at 324 nm

in a Beckman spectrophotometer for 8 minutes at 13 second intervals. A linear portion of the curve was used to calculate initial rate. Rates were plotted against catalyst concentration times substrate concentration to give the second order rate constant. Both enantiomers of **163** were tested in separate experiments for methanolysis by each catalyst.
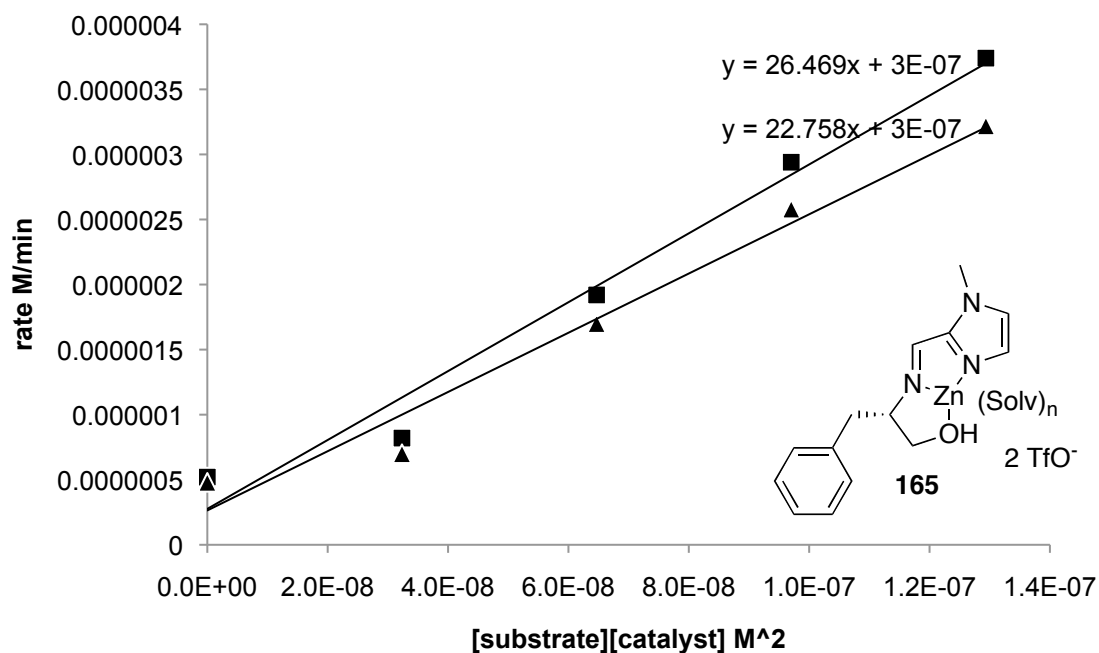


**Figure 159.** Kinetics of methanolysis by **165**. ■, *(S)-***163**; ▲, *(R)-***163**.
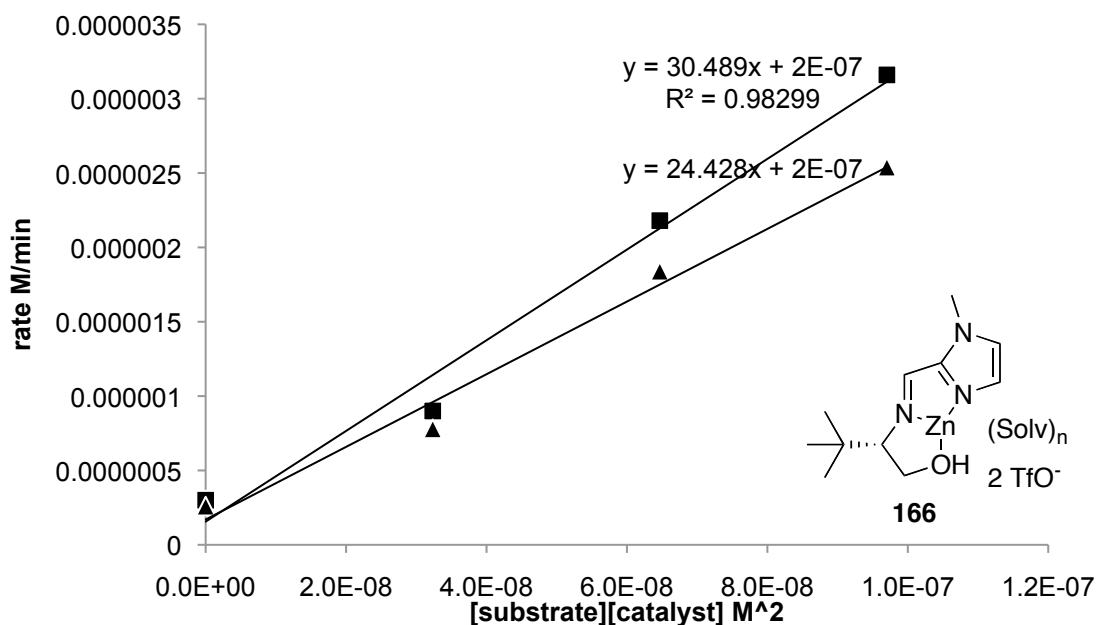
**Figure 160.** Kinetics of methanolysis by **166**. ■, *(S)*-**163**; ▲, *(R)*-**163**.
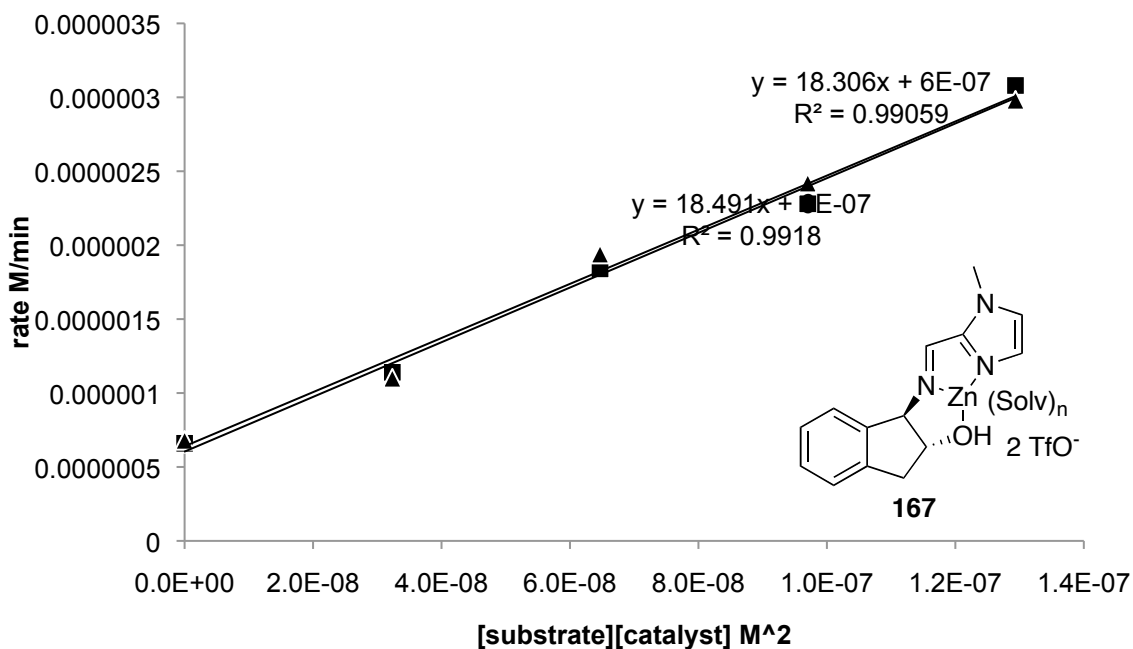


**Figure 161.** Kinetics of methanolysis by **167**. ■, *(S)*-**163**; ▲, *(R)*-**163**.
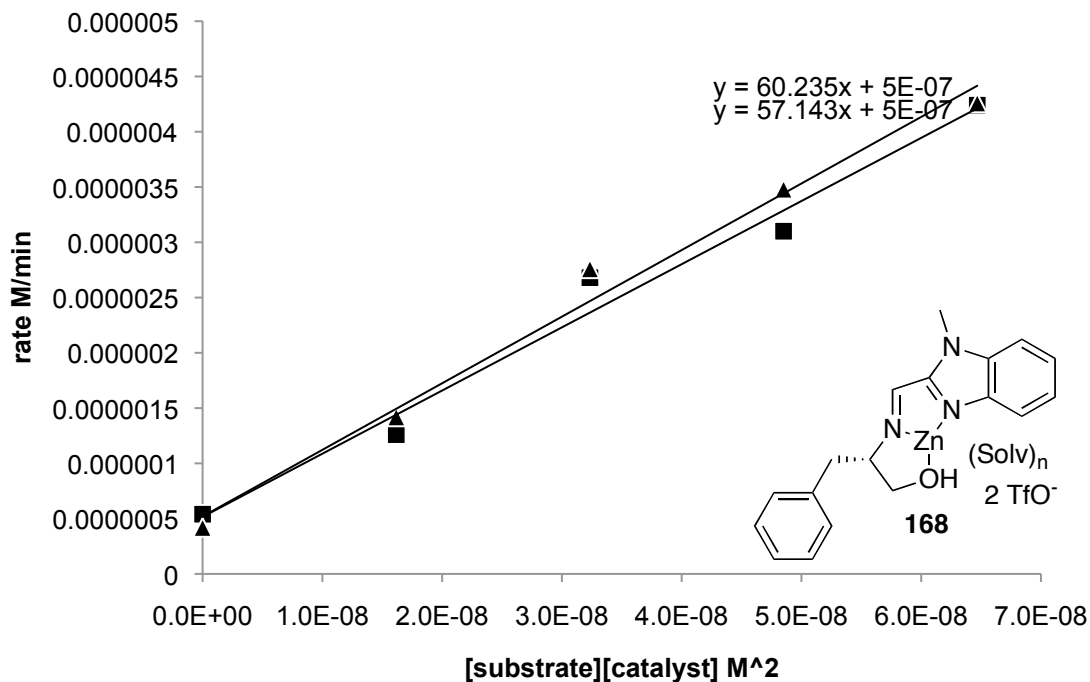
**Figure 162.** Kinetics of methanolysis by **168**. ■, *(S)*-**163**; ▲, *(R)*-**163**.
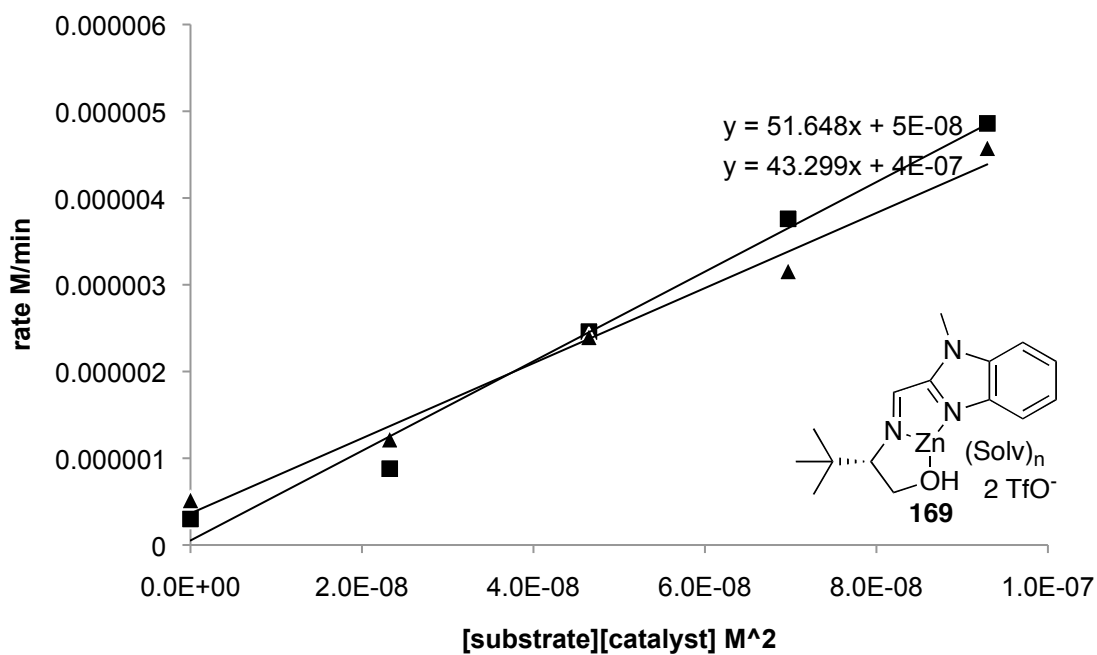


**Figure 163.** Kinetics of methanolysis by **169**. ■, *(S)*-**163**; ▲, *(R)*-**163**.
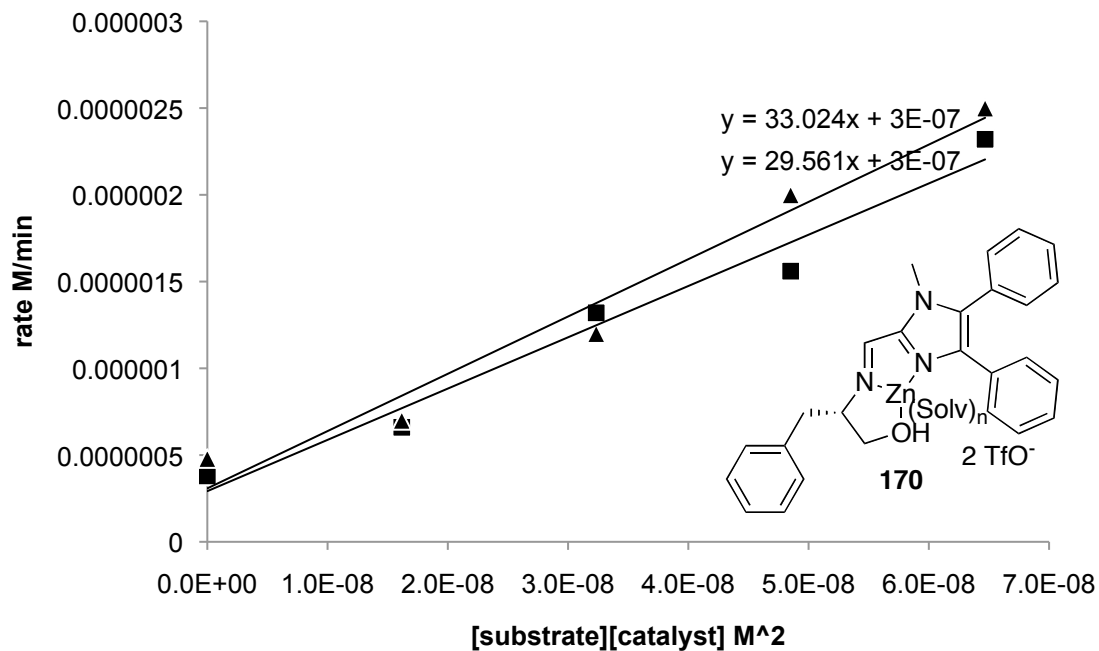
**Figure 164.** Kinetics of methanolysis by **170**. ■, *(S)*-**163**; ▲, *(R)*-**163**.
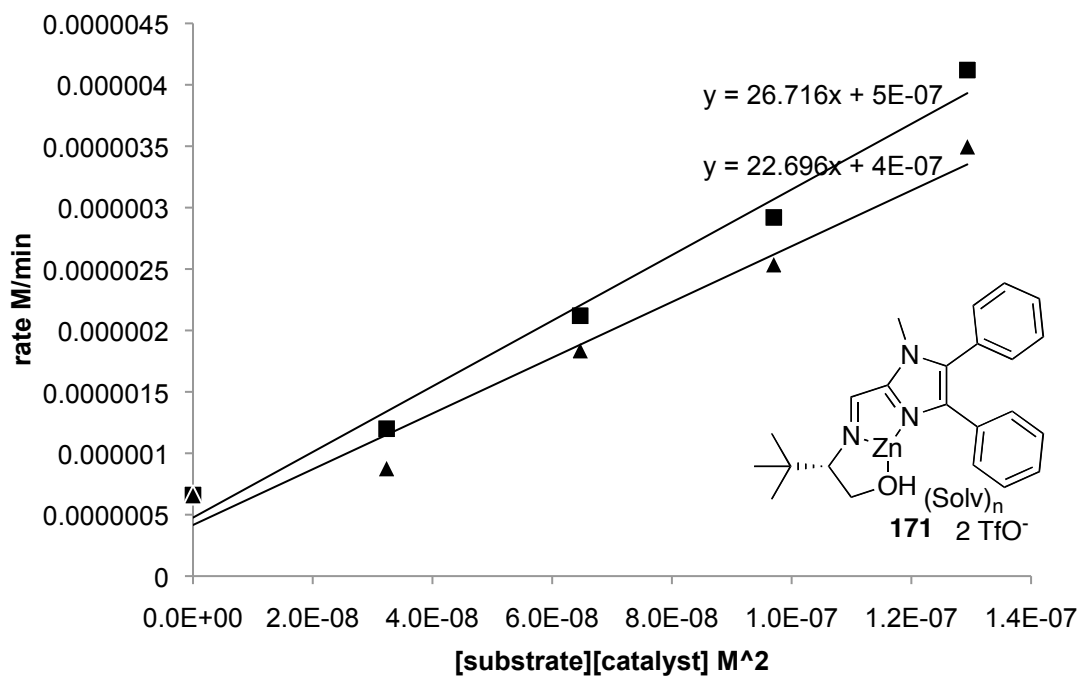


**Figure 165.** Kinetics of methanolysis by **171**. ■, *(S)*-**163**; ▲, *(R)*-**163**.
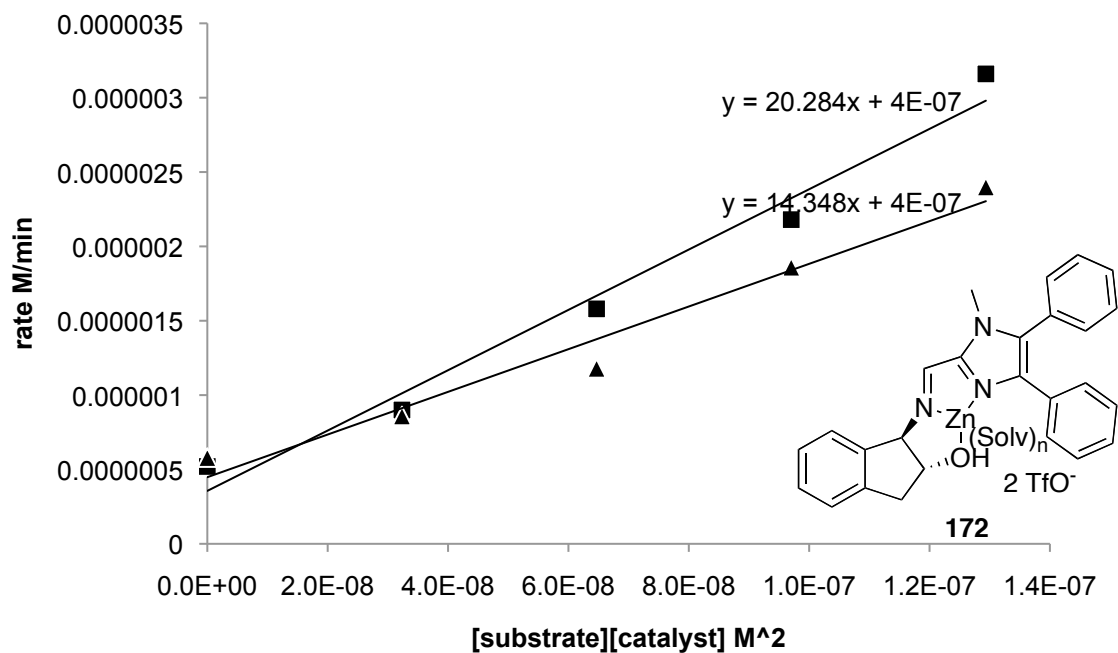
**Figure 166.** Kinetics of methanolysis by **172**. ■, *(S)-163*; ▲, *(R)-163*.
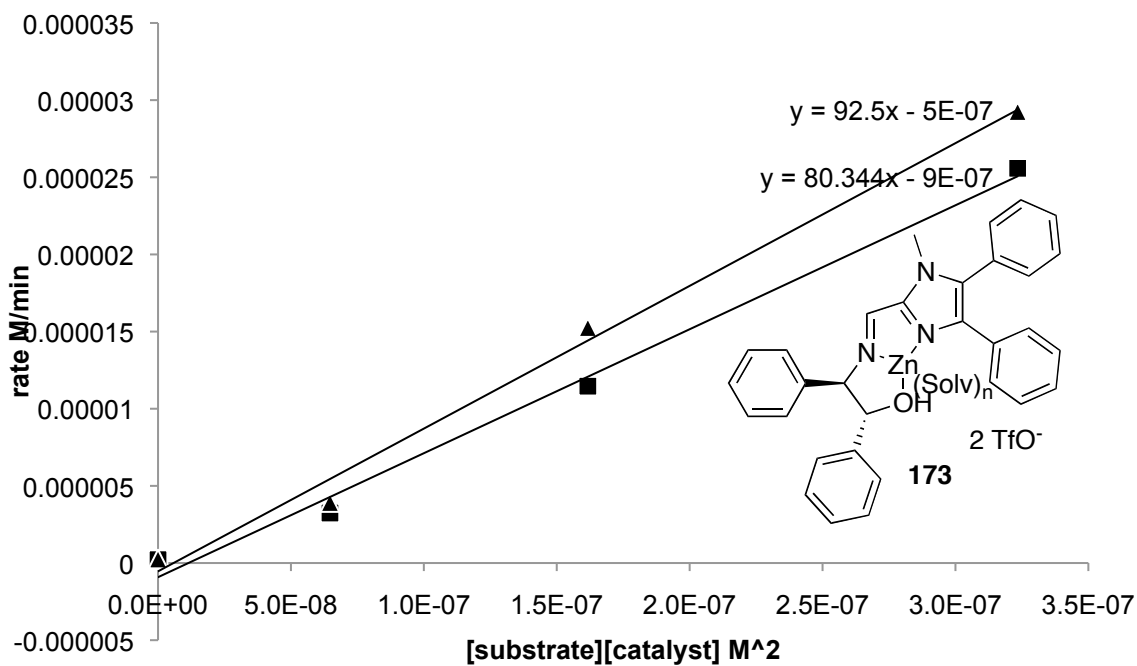


**Figure 167.** Kinetics of methanolysis by **173**. ■, *(S)-163*; ▲, *(R)-163*.
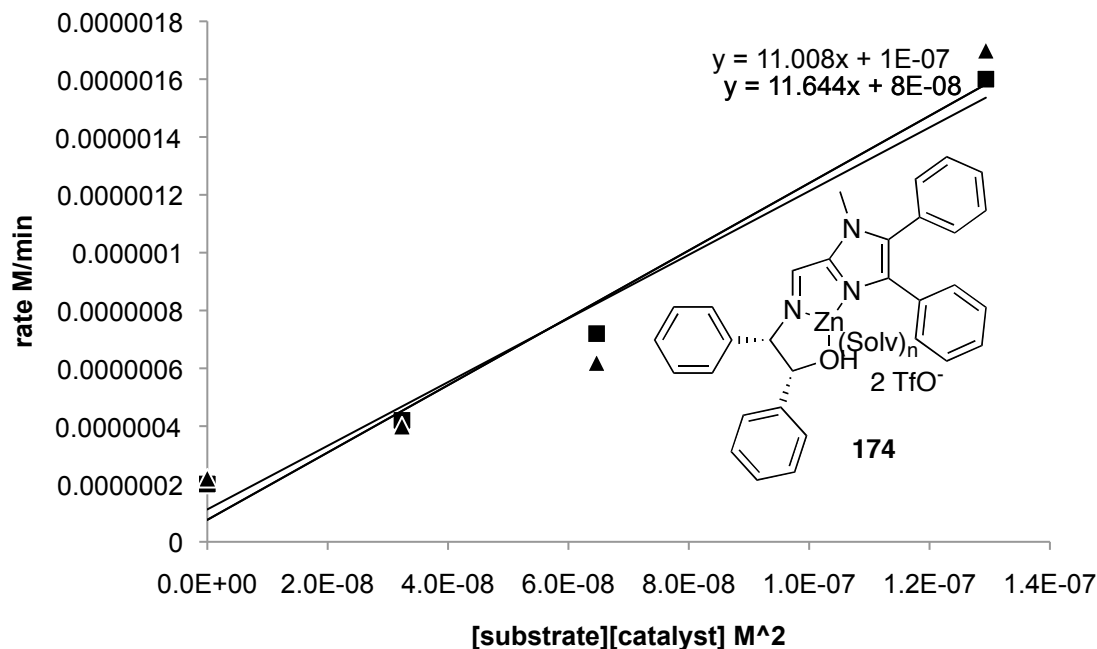
**Figure 168.** Kinetics of methanolysis by **174**. ■, *(S)*-**163**; ▲, *(R)*-**163**.

### 4.4.4 Attempted formation of ternary complexes

Solutions were prepared in 1 mL acetonitrile of 5 mM zinc triflate, 5 mM aldehyde, and 5mM amino alcohol with 5 mM *(S)*-**164**. These solutions were analyzed by ESI-MS in the positive mode. Schiff base Zn complexes **166**, **167**, and **175** were observed but no complexes containing TSA *(S)*-**164** were detected.

### 4.4.5 Kinetics of chiral picolinic ester methanolysis

Solutions of substrate **176** (10 mM) were made in 1 mL 50% $CD_3OD/CD_2Cl_2$. Catalyst stock solution in $CD_3OD/CD_2Cl_2$ was added to the NMR tube to make the sample 0.1 mM (1 mol%) or 1 mM (10 mol%) in catalyst. The reaction was monitored by ^{1}H-NMR over two hours by acquiring 32 transients spectra at an interval of two minutes.

The disappearance of the methyl doublet signal (1.87 ppm) of **176** and the emergence of the methyl doublet (1.61 ppm) of *sec*-phenethyl alcohol were used to monitor the progress of the reaction. Initial rates were approximated by using a linear regression on the first few data points in the run.

## 5. PROJECT SUMMARY AND FUTURE DIRECTIONS

In the first part of the project, a DCL was constructed utilizing histidine as a building block. Although templating behavior was not observed, histidine-based oligomeric macrocycles were generated that exhibited interesting behavior. The cyclic dimer was shown to catalyze NPA hydrolysis. Ultimately, no templating behavior was demonstrated using this system. We suggest several distinct reasons for this. First, it is likely that under the acidic conditions required to effect hydrazone exchange for these particular building blocks, the basic imidazole sidechain of histidine is fully protonated, drastically limiting its availability for metal-binding. Although given the correct choice of metal ion and ligand geometry, it is conceivable that the metal could compete with proton for the ligand, under the conditions of the experiment, this was not observed. It is possible that no such superbly well-suited ligand was possible in our system given the limited choice of monomer metal-binding modes. Second, it is certainly possible that the dimeric species is simultaneously the untemplated thermodynamic minimum *and* the best ligand for the templates we chose, through bis-bidentate imidazole binding. In such a case, since the untemplated and templated libraries would have the same outcome, no equilibrium perturbation would be observed. Third, interactions with anions by the pseudopeptide oligomers was probably severely curtailed by the highly polar (semi-aqueous) solvent mixture in which the experiments were carried out (for solubility reasons). It is known that anions are highly solvated under such conditions, and very rigid and preorganized receptors are usually required in order to bind them with any appreciable affinity in those solvents. Fourth, it is possible that electrostatic repulsion of

189

protonated imidazole-bearing sidechains dominates the energy landscapes of these libraries, completely precluding the higher cyclic oligomers in the equilibrium state.

In the second stage of the project, the feasibility of using TSA-templated DCC to explore the catalytic activity of zinc Schiff-base complexes was demonstrated. First, the use of a phosphonate-derived TSA template to elicit catalysis from a model system consisting of two competing ligands was demonstrated. A benzimidazole-derived Schiff base ligand was amplified in the presence of TSA, at the expense of an imidazole-derived congener. We believe this amplification reflects a change in the population of zinc complexes in the library. We provide evidence for this by demonstrating the formation of the ternary complex and describing the relative binding affinity of TSA for each zinc complex by a competitive NMR titration. The templated amplification of the benzimidazole-derived complex is reflected in the enhanced catalytic activity of the amplified complex.

The use of a trifluoromethylketone hydrate TSA as a template in DCL was demonstrated for the first time. In several model libraries, the trifluoromethylketone TSA was found to amplify zinc complexes with hydroxy-appended ligands that showed the highest esterolytic activity. The TSA adduct of the catalyst zinc complexes was detected by ESI-MS in all relevant cases. With the correct choice of target reaction, exchange chemistry, metal, TSA, and conditions, a correlation was established between DCL amplification and catalysis. This work demonstrates the feasibility of a DCL approach to ligand selection.

In the third stage of the project, we attempted to extend the technique to the development of esterolytic kinetic resolutions of racemic chiral esters. We felt that this

was the next logical move, in that it might simultaneously demonstrate the application of this technology toward a potentially useful method and further establish the dynamic combinatorial evolution of catalysts. Attempts to use amino alcohol-derived Schiff-base zinc complexes to enantiodifferentiate *p*-nitrophenyl esters of Cbz-phenylalanine failed. We also did not detect the adduct of these hydroxy-bearing Schiff base ligands and the phenylalanine-derived trifluoromethylketone hydrate. We believe these results can be rationalized by the fact that neither the substrate nor the TSA in this system is able to form a stable ternary complex with the metal catalyst. The reason for this is that the substrate and TSA lack a coordinating group with which to bind the metal.

More promising results were obtained by using chiral picolinate esters (*(S)*-176 and *(R)*-176) as substrates with chiral diaminocyclohexane-derived zinc complexes **178-184.** With these substrates and catalysts, good rate enhancements and enantioselectivities were obtained. It was discovered by Dr. Ramu Kannapan and myself that the isopropylquinoline-derived Schiff-base zinc complex **184** gave a 26:1 enantiomeric ratio for the methanolysis of chiral picolinic esters in initial screening experiments. Also, quinolinecarboxaldehyde-derived complex **181** gave very rapid esterolysis of the substrate. We believe these results are due to strong interaction between substrate and metal complex, and also TSA and metal complex. Efforts are under way to characterize these interactions, develop this reaction and explore the dynamic chemistry of these ligands. A kinetic resolution based on the racemic ester *rac*-176 and complex **184** is being developed. Templating experiments using TSA *(S)*-177 and *(R)*-177 and an expanded set of ligand building blocks capable of producing several zinc complexes including **184** will be carried out.

We believe there is a pressing need for methods that allow rapid access to novel, structurally complex catalysts with unusual reactivity and high selectivity. The evolutionary approach to catalysis in general and the DCL approach in specific are highly promising strategies for approaching this difficult problem in catalysis. One can imagine large dynamic libraries of complex catalysts templated on TSAs from which unexpected combinations of building blocks will emerge. In practice, catalysts discovery by DCL will be carried out using a two-pronged, iterative process in which rational catalyst design and DCL experimental design will operate simultaneously and synergistically to produce progressively better catalysts and libraries of catalysts. The initial library would be populated using building blocks chosen (designed) for their catalytic properties. The best catalysts from a successful DCL would be used to produce a new library in which subtle variations are introduced to the catalyst structure. DCL should therefore be seen as a powerful massively combinatorial tool for catalyst design, not an end in itself.

Disadvantages of a DCL approach to catalyst discovery include limitations associated with the TSA, practical limits to library size set by analytical techniques, and difficulty of experimental design. Obviously, a fairly accurate stable analog of the transition state of the reaction that is to be studied must exist in order for this approach to work. Unfortunately, the accuracy of TSAs is limited, and there are many reactions for which the transition state structure is not known, and many more for which stable TSAs do not exist. This severely limits the scope of a DCL approach to catalysis. In order for a DCL to be move beyond proof of concept and become truly useful for catalyst discovery, very large libraries will be necessary. The analysis of large libraries presents practical difficulties having to do with the separation of complex mixtures that will require some

innovation to overcome. Finally, a DCL approach to catalysis requires a great deal of experimental design to produce a DCL that yields meaningful and unequivocal results. Paradoxically, DCLs are carefully designed chemical systems. Yet, once the design principles of catalyst discovery via DCL are elucidated (by works like this one), this objection will be rendered less important.

This sets the stage for further exploration of catalyst DCL, developing the concept to include larger libraries, more complex catalyst structures, more diverse building blocks, diverse reactions, counter-substrate-directed chemo-, regio-, or diastereo-selectivities, and high substrate-selectivity targeted at biological targets, leading ultimately to regions of catalyst discovery that cannot now be accessed through normal means.

## REFERENCES

(1)     Rozenman, M. M.; McNaughton, B. R.; Liu, D. R. *Curr. Opin. Chem. Biol.* **2007**, *11*, 259-268.

(2)     Pauling, L. *Chem. Eng. News* **1946**, *161*, 707-709.

(3)     Jencks, W. P. *Catalysis in chemistry and enzymology*; McGraw Hill Book Company: New York, 1969.

(4)     Pollack, S. J.; Jacobs, J. W.; Schultz, P. G. *Science* **1986**, *234*, 1570-1573.

(5)     Jacobs, J. W.; Schultz, D. *J. Am. Chem. Soc.* **1986**, *109*, 2174-2176.

(6)     Tramontano, A.; Janda, K. D.; Lerner, R. A. *Science* **1986**, *234*, 1566-1570.

(7)     Schultz, P. G.; Lerner, R. A. *Science* **1995**, *269*, 1835-1842.

(8)     Brummer, O.; Hoffman, T. Z.; Janda, K. D. *Bioorg. Med. Chem* **2001**, *9*, 2253-2257.

(9)     Fujii, I.; Tanaka, F.; Miyashita, H.; Tanimura, R.; Kinoshita, K. *J. Am. Chem. Soc.* **1995**, *117*, 6199-6209.

(10)    Tsumuraya, T.; Fujii, I. *Bull. Chem. Soc. Jpn.* **2008**, *81*, 1039-1052.

(11)    Takeuchi, T.; Matsui, J. *Acta Polym.* **1996**, *47*, 471-480.

(12)    Robinson, D. K.; Mosbach, K. *Chem. Commun.* **1989**, 969-970.

(13)    Ohkubo, K.; Funakoshi, Y.; Urata, Y.; Hirota, S.; Usui, S.; Sagawa, T. *Chem. Commun.* **1995**, 2143-2144.

(14)    Matsui, J.; Nicholls, I. A.; Karube, I.; Mosbach, K. *J. Org. Chem.* **1996**, *61*, 5414-5417.

(15)     Polborn, K.; Severin, K. *Chem. Commun.* **1999**, 2481-2482.

(16)     Polborn, K.; Severin, K. *Chem. Eur. J.* **2000**, *6*, 4604-4611.

(17)     Liu, J.; Wulff, G. *J. Am. Chem. Soc.* **2004**, *126*, 7452-7453.

(18)     Liu, J.; Wulff, G. *Angew. Chem. Int. Ed.* **2004**, *43*, 1287-1290.

(19)     Corbett, P. T.; Leclaire, J.; Vial, L.; West, K. R.; Wietor, J.-L.; Sanders, J. K. M.; Otto, S. *Chem. Rev.* **2006**, *106*, 3652-3711.

(20)     Rowan, S. J.; Cantrill, S. J.; Cousins, G. R.; Sanders, J. K. M.; Stoddart, J. F. *Angew. Chem. Int. Ed.* **2002**, *41*, 898-952.

(21)     Sanders, J. K. *Pure Appl. Chem.* **2000**, *72*, 2265-2274.

(22)     Sanders, J. K. *Chem. Eur. J.* **1998**, *4*, 1378-1383.

(23)     Furlan, R. L.; Otto, S.; Sanders, J. K. *Proc. Nat. Acad. Sci. U.S.A.* **2002**, *99*, 4701-4804.

(24)     Ladame, S. *Org. Biomol. Chem.* **2008**, *6*, 219-226.

(25)     Godoy-Alcanatar, C.; Yatsimirsky, A., K.; Lehn, J. M. *J. Phys. Org. Chem.* **2005**, *18*, 979-985.

(26)     Lehn, J. M. *Chem. Eur. J.* **1999**, *5*, 2455-2463.

(27)     Huc, I.; Lehn, J. M. *Proc. Nat. Acad. Sci. U.S.A.* **1996**, *94*, 2106-2110.

(28)     Zameo, S.; Vauzeilles, B.; Beau, J.-M. *Angew. Chem. Int. Ed.* **2005**, *44*, 965-969.

(29)     Cousins, G. R.; Poulsen, S. A.; Sanders, J. K. M. *Chem. Commun.* **1999**, 1575-1576.

(30)     Furlan, R. L.; Ng, Y. F.; Otto, S.; Sanders, J. K. M. *J. Am. Chem. Soc.* **2001**, *123*, 8876-8877.

(31)     Furlan, R. L.; Ng, Y. F.; Cousins, G. R.; Redman, J. E.; Sanders, J. K. M. *Tetrahedron* **2002**, *58*, 771-778.

(32)     Kubik, S.; Goddard, R. *J. Org. Chem.* **1999**, *64*, 9475-9486.

(33)     Lam, R. T. S.; Belenguer, A. M.; Roberts, S. L.; Naumann, C.; Jarrosson, T.; Otto, S.; Sanders, J. K. M. *Science* **2005**, *308*, 667-679.

(34)     Corbett, P. T.; Tong, L. H.; Sanders, J. K.; Otto, S. *J. Am. Chem. Soc.* **2005**, *127*, 8902-3.

(35)     Otto, S.; Kubik, S. *J. Am. Chem. Soc.* **2003**, *125*, 7804-5.

(36)     Melson, G. A.; Busch, D. H. *J. Am. Chem. Soc.* **1964**, *86*, 4834-4837.

(37)     Seidel, F.; Dick, W. *Chem. Ber.* **1927**, *60B*, 2018-2023.

(38)     Bamberger, E. *Chem. Ber.* **1927**, *60B*, 314-319.

(39)     Goral, V.; Nelen, M. I.; Eliseev, A. V.; Lehn, J. M. *Proc. Nat. Acad. Sci. U.S.A.* **2001**, *98*, 1347-52.

(40)     Epstein, D. M.; Choudhary, S.; Churchill, M. R.; Keil, K. M.; Eliseev, A. V.; Morrow, J. R. *Inorg. Chem.* **2001**, *40*, 1591-6.

(41)     Choudhary, S.; Morrow, J. R. *Angew. Chem. Int. Ed.* **2002**, *41*, 4096-8.

(42)     Saur, I.; Severin, K. *Chem. Commun.* **2005**, 1471-3.

(43)     Kubota, Y.; Sakamoto, S.; Yamaguchi, K.; Fujita, M. *Proc. Nat. Acad. Sci. U.S.A.* **2002**, *99*, 4854-4856.

(44)     Nitschke, J. R. *Acc. Chem. Res.* **2007**, *40*, 103-112.

(45)    Schultz, D.; Nitschke, J. R. *J. Am. Chem. Soc.* **2006**, *128*, 9887-9892.

(46)    Schultz, D.; Nitschke, J. R. *Angew. Chem. Int. Ed.* **2006**, *45*, 1-5.

(47)    Luning, U. *J. Inclusion Phenom. Macrocyclic Chem.* **2004**, *49*, 81-84.

(48)    Storm, O.; Luning, U. *Chem. Eur. J.* **2002**, *8*, 793-798.

(49)    Gonzalez-Alvarez, A.; Alfonso, I.; Gotor, V. *Chem. Commun.* **2006**, 2224-2226.

(50)    Brisig, B.; Sanders, J. K.; Otto, S. *Angew. Chem. Int. Ed.* **2003**, *42*, 1270-3.

(51)    Vial, L.; Sanders, J. K. M.; Otto, S. *New J. Chem.* **2005**, *29*, 1001-1003.

(52)    Gasparini, G.; Prins, L. J.; Scrimin, P. *Angew. Chem. Int. Ed.* **2008**, *47*, 2475-2479.

(53)    Brooks, D. J.; Fresco, J. R.; Lesk, A. M.; Singh, M. *Molecular Biology and Evolution* **2002**, *19*, 1645-1655.

(54)    Schneider, F. *Angew. Chem. Int. Ed.* **1978**, *17*, 583-592.

(55)    Klinman, J. P. *Chem. Rev.* **1996**, *96*, 2541-2561.

(56)    Costas, M.; Mehn, M.; Jensen, M.; Que, L. *Chem. Rev.* **2003**, *104*, 939-986.

(57)    Abu-Omar, M. M.; Loaiza, A.; Hontzeas, N. *Chem. Rev.* **2005**, *105*, 2227-52.

(58)    Huc, I.; Krische, M. J.; Funeriu, D. P.; Lehn, J. M. *Eur. J. Inorg. Chem.* **1999**, 1415-1420.

(59)    Giuseppone, N.; Lehn, J. M. *J. Am. Chem. Soc.* **2004**, *126*, 11448-9.

(60)    Cacciapaglia, R.; Di Stefano, S.; Mandolini, L. *J. Am. Chem. Soc.* **2005**, *127*, 13666-71.

(61)    Kieran, A. L.; Bond, A. D.; Belenguer, A. M.; Sanders, J. K. *Chem. Commun.* **2003**, 2674-5.

(62)    Stulz, E.; Ng, Y. F.; Scott, S. M.; Sanders, J. K. *Chem. Commun.* **2002**, 524-5.

(63)    Roberts, S. L.; Furlan, R. L.; Otto, S.; Sanders, J. K. *Org. Biomol. Chem.* **2003**, *1*, 1625-33.

(64)    Cousins, G. R.; Furlan, R. L.; Ng, Y. F.; Redman, J. E.; Sanders, J. K. *Angew. Chem. Int. Ed.* **2001**, *40*, 423-428.

(65)    Bornaghi, L. F.; Wilkinson, B. L.; Kiefel, M. J.; Poulsen, S. *Tetrahedron Lett.* **2004**, *45*, 9281-9284.

(66)    Matsumoto, M.; Nicholas, K. M. *J. Org. Chem.* **2007**, *72*, 9308-9313.

(67)    Gelinsky, M.; Vogler, R.; Vahrenkamp, H. *Inorg. Chem.* **2002**, *41*, 2560-2564.

(68)    Spartan '04 for Mac; Wavefunction, Inc.: Irvine, California, 2005.

(69)    Bruice, T. C.; Schmir, G. L. *J. Am. Chem. Soc.* **1957**, *80*, 148.

(70)    Broo, K. S.; Brive, L.; Ahlberg, P.; Baltzer, L. *J. Am. Chem. Soc.* **1997**, *119*, 11362-11372.

(71)    Nicoll, A. J.; Allemann, R. K. *Org. Biomol. Chem.* **2004**, *2*, 2175-2180.

(72)    Jain, R.; Cohen, L. A. *Tetrahedron* **1996**, *52*, 5363-5370.

(73)    Lipscomb, W. N.; Strater, N. *Chem. Rev.* **1996**, *96*, 2375-2433.

(74)    Parkin, G. *Chem. Rev.* **2004**, *104*, 699-767.

(75)    Helm, L.; Merbach, A. E. *Coord. Chem. Rev.* **1999**, *187*, 151-181.

(76)    Matsumoto, M.; Estes, D.; Nicholas, K. M. *Eur. J. Inorg. Chem.* **2010**.

(77)    Chiu, Y.-H.; Gabriel, G. J.; Canary, J. W. *Inorg. Chem.* **2005**, *44*, 40-44.

(78)    Fife, T. H.; Przystas, T. J. *J. Am. Chem. Soc.* **1985**, *107*, 1041-1047.

(79)    Sigman, D. S.; Jorgensen, C. T. *J. Am. Chem. Soc.* **1972**, *94*, 1724-1730.

(80)    Loran, J. S.; Naylor, R. A.; Williams, A. *J. Chem. Soc. Perkin Trans. 2* **1976**, 1444-1447.

(81)    Ziach, K.; Jurczak, J. *Org. Lett.* **2008**, *10*, 5159-5162.

(82)    Fielding, L. *Tetrahedron* **2000**, *56*, 6151-6170.

(83)    Jerez, G.; Kaufman, G.; Prystai, M.; Schenkeveld, S.; Donkor, K. K. *J. Sep. Sci.* **2009**, *32*, 1087.

(84)    Hammock, B. D.; Wing, K. D.; Laughlin, J.; Lovell, V. M.; Sparks, T. C. *Pestic. Biochem. Physiol.* **1982**, *17*, 76.

(85)    Salvador, R. L.; Saucier, M. *Tetrahedron* **1971**, *27*, 1221-1226.

(86)    Eiki, T.; Kawada, S.; Matsushima, K.; Mori, M.; Takagi, W. *Chem. Lett.* **1980**.

(87)    Scrimin, P.; Tecilla, P.; Tonellato, U. *J. Org. Chem.* **1994**, *59*, 18-24.

(88)    Weijnen, J. G.; Koudijs, A.; Schellekens, G. A.; Engbersen, J. F. J. *J. Chem. Soc. Perkin Trans. 2* **1992**, 829-834.

(89)    Martinez-Viturro, C. M.; Dominguez, D. *Tetrahedron Lett.* **2007**, *48*, 1023-1026.

(90)    Katritzky, A. R.; He, H.-Y.; Long, Q.; Cui, X.; Level, J.; Wilcox, A. L. *ARKIVOC* **2000**, *3*, 240-251.

(91)     Keith, J. M.; F., L. J.; Jacobsen, E. N. *Adv. Synth. Catal.* **2000**, *343*, 5-26.

(92)     Tokunaga, M.; Aoyama, H.; Kiyosu, J.; Shirogane, Y.; Iwasawa, T.; Obora, Y.; Tsuji, Y. *J. Organomet. Chem.* **2007**, *692*, 472-480.

(93)     Dro, C.; Bellemin-Laponnaz, S.; Welter, R.; Gade, L. H. *Angew. Chem.* **2004**, *116*, 4579-4582.

(94)     Maxwell, C. I.; Shah, K.; Samuleev, P.; Neverov, A.; Brown, S. A. *Org. Biomol. Chem.* **2008**, *6*, 2796-2803.

(95)     Scrimin, P.; Tecilla, P.; Tonellato, U. *J. Org. Chem.* **1994**, *59*, 4194-4201.

(96)     Weijnen, J. G.; Koudijs, A. *J. Org. Chem.* **1992**, *57*, 7258-7265.

(97)     Chung, M.-K.; Hebling, C. M.; Jorgenson, J. W.; Severin, K.; Lee, S. J.; Gagne, M. R. *J. Am. Chem. Soc.* **2008**, *130*, 11819-11827.

(98)     Bodanszky, M.; du Vigneaud, V. *J. Am. Chem. Soc.* **1959**, *81*, 6072-6075.

(99)     Walter, M. W.; Adlington, R. M.; Baldwin, J. E.; Schofield, C. J. *J. Org. Chem.* **1998**, *63*, 5179-5192.

(100)   LaRonde, F. J.; Brook, M. A. *Inorg. Chim. Acta* **1999**, *296*, 208-221.

(101)   Williams, A. W.; Young, G. T. *J. Chem. Soc., Perkin Trans. 1* **1972**, 1194-1200.

(102)   Prema, D.; Wyznicia, A. V.; Scott, B.; Hilborn, J.; Desper, J.; Levy, C. *Dalton Trans.* **2007**, 4788-4796.